



The influence of fuel molecular structure on particulate
emission investigated with isotope tracing

Thesis submitted in accordance with the requirements of
UCL for the degree of Doctor of Philosophy by

Aaron Eveleigh

October 2015

I, Aaron Eveleigh confirm that the work presented in this thesis is my own. Where information has been derived from other sources, I confirm that this has been indicated in the thesis.

Abstract

This thesis is concerned with the formation of particulate matter, a topic of scientific and practical importance due to the toxicity of particulate emissions from automotive and other combustion sources. At present, fuels are predominantly derived from fossil sources, but as production technology improves, biofuels and synthetic fuels are expected to emerge as scalable long-term sources of liquid fuels. Efforts are being made to ensure that this next-generation of fuels is cleaner burning than the last. In order to inform the production and processing of cleaner burning fuels, more needs to be known about how molecular structure influences the formation of pollutant emissions.

This thesis presents research that has been carried out in order to better understand the role of functional group chemistry on the conversion of carbon atoms in the fuel to the particulate matter (PM). In particular, the propensity of individual molecules or carbon atoms within molecules to form PM is reported quantitatively. To this end, a technique using carbon-13 (^{13}C) *labelled* fuel molecules was used so to track the labelled carbon atoms in the fuel to PM. The technique required only very low levels of ^{13}C enrichment, and isotope ratio mass spectrometry equipment (IRMS) was used as a means of ^{13}C detection.

Samples of particulate matter were formed using a tube reactor, and also in a compression ignition diesel engine. The tube reactor was designed and commissioned in order to study the pyrolysis of various fuel molecules under well-controlled, homogenous conditions.

The contribution to PM of a number of molecules containing various functional groups was assessed, including: alcohols, esters, aromatics, double bonded carbon atoms, a ketone, and a carboxylic acid. Tests were conducted using single-component fuels, and blended in a binary mixture with *n*-heptane. The results show that the contribution of carbon atoms within molecules to PM, is not equal, but depends on the local molecular structure. For example, oxygenated molecules significantly reduced the contribution to PM of the carbon atoms directly attached to oxygen.

The thesis presents one of only a handful of investigations that have been published on the conversion of specific carbon atoms of various molecules to soot and particulate. It advances the field of study by providing data for validation, at the sub-molecular level, for chemical kinetic models of soot formation, and advances fundamental understanding of how fuels convert to soot and particulates.

Acknowledgements

First and foremost, I wish to thank my PhD supervisor, Professor Nicos Ladommatos, for his support and guidance during my PhD. I would also like to thank Dr Rama Balachanran for his support and contributions to the research.

I thank the Department of Mechanical Engineering at UCL for having me, and the financial support from the Engineering and Physical Sciences Research Council (EPSRC).

Thanks is due to Dr Paul Hellier for running the engine tests, and Dr Anne-Lise Jourdan at the Bloomsbury Environmental Isotope Facility (BEIF) for her support with the isotopic analysis. Thanks to Dr Alina Marca (Stable Isotope Laboratory, University of East Anglia), who allowed me the use of the IRMS equipment at UEA, when ours at UCL was out of action, and for her contributions to the development of the isotope tracer technique.

I thank all of my friends and colleagues who I have met during my time at UCL, in particular my friends in the UCL Thermodynamics Lab: Elina, Anne, Baptiste, Mart, Midhat, Aadil, and Taaha. My friendships beyond UCL also deserve thanks, mainly for granting me ‘leave of absence’ for the past few years in order to complete my PhD.

Finally, I wish to say a special thank you to my family. Particularly, my mother, father, brother, and sister for all of their love, encouragement and support.

Contents

Notations	15
1 Introduction	17
1.1 Purpose	17
1.2 Motivation	17
1.2.1 Human health	18
1.2.2 Climate change	20
1.2.3 Legislation	20
1.3 Aims, objectives and overview	21
2 Literature review	24
2.1 Composition and structure of soot	24
2.1.1 Diesel particulate matter	25
2.1.2 Nomenclature of carbonaceous particles	26
2.2 Soot formation	27
2.2.1 Overview	27
2.2.2 Fuel pyrolysis and the formation of the first aromatic ring	27
2.2.3 Aromatic growth	29
2.2.4 Nucleation and surface growth	31
2.2.5 Agglomeration and coalescence	32
2.2.6 Oxidation of soot particles	32
2.2.7 Particulate formation in a direct injection diesel engine	33
2.2.8 Effects of fuel composition on particulate emission in diesel engines	34
Aromatics and PAHs	35
Straight and branched chain	36
Oxygenates	37
2.3 Strategies to reduce particulate emissions	39
2.3.1 Diesel exhaust after treatment technologies	39
2.3.2 Fuel additives	41
2.3.3 Optimisation of the fuel composition	43
2.3.4 Optimisation of combustion conditions	44
2.4 The use of isotopic tracers in pyrolysis and combustion research	46
2.5 Conclusions	54
3 Experimental Systems and Methodology	56
3.1 Flow reactor facility	56
3.1.1 Gas Feed System	57

3.1.2	Liquid Feed System	59
3.1.3	Static mixer	59
3.1.4	Reactor tube	61
3.1.5	Reactor temperature profile	61
3.1.6	Design of thermocouple sheath	63
3.1.7	Gas residence time	64
3.1.8	System control and monitoring	65
3.1.9	Particulate sample collection and storage	65
3.2	Diesel test engine facility	65
3.2.1	Engine specification	65
3.2.2	Ultra low volume fuel system	66
3.2.3	Particulate sample collection and storage	67
3.3	Isotope measurements by Elemental Analysis-Isotope Ratio Mass Spec-	
	trometry (EA-IRMS)	68
3.3.1	Sample preparation	68
3.3.2	Preparation of gaseous CO ₂ samples	69
3.3.3	Sample submission	70
3.3.4	Elemental analysis (EA)	72
3.3.5	Isotope ratio mass spectrometry (IRMS)	73
3.4	Measuring instruments	74
3.4.1	Quantification and Classification of PM	75
3.4.2	Analysis of CO, CO ₂ , O ₂	77
	CO and CO ₂	77
	O ₂	78
3.4.3	Gas Chromatography-Mass Spectroscopy (GC/MS)	78
3.5	Total Hydrocarbon Concentration	80
4	Analytical Methods	81
4.1	Interpretation of isotopic measurements	81
4.1.1	Delta Notation	81
4.1.2	Calibration of results	82
4.1.3	Correction for background carbon	82
4.1.4	Interpretation of the measured $\delta^{13}\text{C}$ values	85
4.1.5	Significance and origins of the applied methodology: Example of	
	calculation to derive the contribution of the labelled carbon atom	
	to the formation of particulate matter	86
4.1.6	Calculation required to isotopically enrich a fuel by a desired amount	90
4.2	Gas composition	91
4.3	The equivalence ratio of combustion experiments	91
4.4	Representation of experimental error	93
5	High-temperature pyrolysis of C₁-C₄ hydrocarbons and C₁-C₅ alcohols	94
5.1	Introduction	94
5.2	Experimental method	97
5.2.1	Apparatus	97
5.2.2	Fuel molecules investigated	97
5.2.3	Calculation of percentage yield	98

5.3	Results and discussion	100
5.3.1	C ₂ fuels	100
5.3.2	C ₃ fuels	105
5.3.3	C ₄ fuels	108
5.3.4	C ₁ -C ₅ alcohols	110
5.3.5	Influence of fuel concentration on the formation of particulates . .	113
5.4	Conclusions	116
6	Tracking the conversion of specific carbon-13 labelled atoms from various fuels to particulate matter under pyrolysis conditions	118
6.1	Introduction	118
6.2	Experimental methods	118
6.2.1	Apparatus	118
6.2.2	Fuel molecules investigated	119
6.2.3	Experimental conditions	119
6.3	Results and discussion	120
6.3.1	Ethanol	121
6.3.2	1-propanol and 2-propanol	124
6.3.3	Pentanol and cyclopentanol	126
6.3.4	Ethyl acetate	128
6.3.5	Toluene	130
6.3.6	Validation of methodology	132
6.4	Further discussion	135
6.5	Conclusions	137
7	Isotopic tracing of labelled atoms in oleic acid and methyl oleate, in a diesel engine and tube reactor	139
7.1	Introduction	139
7.2	Experimental Systems and Methods	142
7.2.1	Fuels	142
7.2.2	Engine experiments	143
7.2.3	Particulate sample collection	144
7.2.4	Tube reactor	145
7.3	Results and discussion	145
7.3.1	Results of the isotope tracer investigation	145
7.3.2	Influence of the formation conditions on the conversion of atoms to PM	149
7.3.3	Emissions analysis: Laminar flow reactor	150
7.3.4	Emissions analysis: diesel engine	151
7.3.5	Conversion of carbon in the ester and carboxylic group to PM . .	154
7.4	Conclusions	155
8	Isotope tracing of labelled atoms in various molecules blended with heptane, in a diesel engine and tube reactor	157
8.1	Introduction	157
8.2	Methods	160
8.2.1	Fuels	160
8.2.2	Apparatus	161

Laminar flow tube reactor	161
Diesel engine	161
8.2.3 EA-IRMS analysis	163
8.2.4 Analytical methods	163
8.3 Results	165
8.3.1 Emissions analysis	165
8.3.2 Ethanol-in-heptane	167
8.3.3 1- or 2-propanol-in-heptane	170
8.3.4 Acetone-in-heptane	174
8.3.5 Ethyl acetate-in-heptane	176
8.3.6 Toluene-in-heptane	176
8.4 Further discussion	179
8.5 Conclusions	181
9 Evaluating the use of GC/C/IRMS for the measurement of PAHs	184
9.1 Introduction	184
9.2 Methods	188
9.2.1 Generation of particulates and sample collection	188
9.2.2 Soxhlet extraction	188
9.2.3 GC/C/IRMS	188
9.3 Results	190
9.3.1 Result and discussion of the GC/MS analysis	190
9.3.2 Result and discussion of the GC/C/IRMS analysis	191
9.4 Conclusions	195
10 Conclusions	196
10.1 Summary of conclusions	196
10.1.1 Influence of molecular structure on the particulate matter formed during pyrolysis of C ₁ to C ₅ Fuels	196
10.1.2 The conversion of labelled carbon atoms from single-component fuels to PM	197
10.1.3 The conversion of oleic acid and methyl oleate to particulate mat- ter in a flow reactor and diesel engine	198
10.1.4 Conversion of labelled carbon atoms in binary mixtures of various hydrocarbon and oxygenate molecules in heptane	198
10.2 A summary of the suitability of carbon-13 as a tracer for combustion research	199
10.3 Recommendations for future work	200
10.3.1 Claims of originality	201
A Supplementary mechanical drawings and images	203
B Supplementary experimental data	212
Bibliography	221

Illustrations

List of Figures

1.1	PM, and hydrocarbon and NO _x emissions limits set as part of European directives.	21
2.1	Artists impression of cooled and diluted diesel particulate matter.	25
2.2	Composition of particulate matter from a heavy-duty diesel engine	25
2.3	Stages involved in the formation of particulates	27
2.4	Acetylene addition to the armchair edge of phenanthrene to yield pyrene. . .	30
2.5	Growth sites of aromatic molecule	30
2.6	Reaction of phenyl with phenanthrene to form benzo-e-pyrene, according to the PAC mechanism	31
2.7	A conceptual scheme for a reacting diesel spray	34
2.8	Measured soot emissions form a diesel engine with oxygenate addition to the fuel.	37
2.9	Diesel particulate trap.	41
2.10	A generic contour plot showing the regions of soot and NO formation as a function of the local formation conditions.	46
2.11	Molecular structure of dibutyl maleate (DBM) and positions of ¹⁴ C labels, and chart showing the relative contributions of the labelled positions to particulate.	50
3.1	Flow reactor general schematic	58
3.2	Gaseous fuel feed system schematic.	58
3.3	Liquid fuel feed system schematic.	60
3.4	Static mixer installed at the reactor inlet	60
3.5	Temperature measured at the center of the reactor at various flow rates of nitrogen	62
3.6	Reactor longitudinal temperature profile	62
3.7	Gas temperatures measured at the center of reactor.	63
3.8	Schematic of probe design for limiting the influence of radiation on thermocouple measurement.	64
3.9	Diesel test engine facility	67
3.10	Schematic of the setup used for conversion of CO and CO ₂ , using Schütze reagent.	70
3.11	Images showing the inlet of an elemental analyser combustion furnace.	72
3.12	Schematic of elemental analyser (EA) configuration.	74
3.13	Schematic diagram of the major components in a typical isotope ratio mass spectrometer.	75
3.14	Schematic showing dilution stages of the DMS500 instrument	76

3.15	DMS 500 classifier column comprised of a corona charger, and 22 classification rings.	77
3.16	NDIR CO/CO ₂ gas analyser schematic.	78
3.17	Horiba FMA-125 oxygen detector schematic.	79
4.1	Example of loading order of samples and standards for IRMS analysis	83
4.2	Example IRMS spectrum	84
4.3	Example IRMS calibration curve using isotopic standards.	84
5.1	Molecular structures of the C ₁ to C ₄ hydrocarbons.	99
5.2	Molecular structures of the C ₁ to C ₅ alcohol molecules.	99
5.3	Number distribution of particulates formed from C ₂ fuels	103
5.4	Analysis of particulate emissions formed from C ₂ fuels in the temperature range 1000-1400 °C	104
5.5	Outlet hydrocarbon concentration from the pyrolysis of C ₂ fuels at an inlet concentration of 8000 ppmv in the temperature range 1000-1400°C	104
5.6	CO and CO ₂ measurements from the pyrolysis of ethanol (8000 ppmv) in the temperature range 1000-1400°C	105
5.7	Analysis of particulate emissions formed from C ₃ fuels in the temperature range of 1000-1400°C	107
5.8	CO and CO ₂ measurements from the pyrolysis of 1-propanol and 2-propanol (8000 ppmv) in the temperature range of 1000-1400°C	108
5.9	A four-center molecular dehydration reaction for 1- and 2-propanol	108
5.10	Particulate emissions formed from the pyrolysis of C ₄ fuels, <i>n</i> - and <i>i</i> -butane.110	
5.11	Particulate formed from the pyrolysis of C ₁ -C ₅ alcohols	112
5.12	CO and CO ₂ products formed from the pyrolysis of C ₁ -C ₅ alcohols	112
5.13	Possible reaction pathways of alkanes, and primary and secondary alcohols. 113	
5.14	Particulate emissions formed from the pyrolysis of ethanol at three concentrations	114
5.15	Particulate percentage yield from the pyrolysis of ethanol at three concentrations	115
5.16	CO and CO ₂ emissions from pyrolysis of ethanol.	115
5.17	Percentage yield of CO formed from the pyrolysis of ethanol at 3000, 6000, and 9000 ppmv	116
6.1	Structure and nomenclature of ¹³ C labelled molecules investigated.	120
6.2	Skeletal structure of ethanol, with ¹³ C labelled atoms assigned (a) ethanol-1- ¹³ C, and (b) ethanol-2- ¹³ C.	121
6.3	Measured delta values for unenriched ethanol, and ethanol enriched with quantities of ethanol-1- ¹³ C (a) or ethanol-2- ¹³ C (b) in the temperature range 1150 to 1450 °C, at 50 °C intervals. Data shown is the mean ± SD (generally, σ >0.15).	122

6.4	Percentage contribution to PM from the labelled position in ethanol-1- ¹³ C (a) and ethanol-2- ¹³ C (b) molecules. Error bars show the influence of the standard deviation on the calculated conversion rate.	122
6.5	Percentage contribution to PM from the labelled position in ethanol-1- ¹³ C (a) and ethanol-2- ¹³ C (b), formed at 1300 °C and at various air-fuel equivalence ratios. Data shown is for single measurements.	124
6.6	Skeletal structure of 1-propanol (left), labelled with ¹³ C at position (c) (1-propanol-1- ¹³ C); and 2-propanol (right), labelled at location (d) (2-propanol-2- ¹³ C).	124
6.7	Measured delta values for unenriched 1-propanol and 2-propanol, and with enriched with quantities of 1-propanol-1- ¹³ C (c) and 2-propanol-2- ¹³ C (d) respectively, in the temperature range 1150 °C to 1450 °C.	125
6.8	Calculated percentage contribution to PM from the labelled positions in 1-propanol-1- ¹³ C (c) and 2-propanol-2- ¹³ C (d) in the temperature range 1150-1450 °C.	126
6.9	Skeletal structure of 1-pentanol (left), labelled with ¹³ C at position ‘e’ (1-pentanol-1- ¹³ C); and 2-pentanol (right), labelled at location ‘f’ (2-pentanol-2- ¹³ C).	126
6.10	Measured $\delta^{13}\text{C}$ values for unenriched fuels 1-pentanol and cyclopentanol, and these with enrichment of 1-pentanol-1- ¹³ C and cyclopentanol-1- ¹³ C.	127
6.11	Calculated percentage conversion of the labelled positions in 1-pentanol-1- ¹³ C and cyclopentanol-1- ¹³ C.	127
6.12	Skeletal structure of ethyl acetate-1- ¹³ C (g), ethyl acetate-2- ¹³ C (h) and ethyl acetate-1,2- ¹³ C (i).	128
6.13	Measured $\delta^{13}\text{C}$ values for unenriched ethyl acetate, and ethyl acetate enriched with ethyl acetate-1- ¹³ C, ethyl acetate-2- ¹³ C, and ethyl acetate-1,2- ¹³ C.	129
6.14	Contribution to PM from tagged groups in ethyl acetate-1- ¹³ C, ethyl acetate-2- ¹³ C, and ethyl acetate-1,2- ¹³ C.	129
6.15	Skeletal structure for toluene showing label locations for toluene-1- ¹³ C (j), toluene- α - ¹³ C (k) and toluene-(phenyl)- ¹³ C ₆ (l).	130
6.16	Measured $\delta^{13}\text{C}$ values for unenriched toluene, and toluene enriched with toluene-1- ¹³ C, toluene- α - ¹³ C, and toluene-(phenyl)- ¹³ C ₆	131
6.17	Percentage contribution to PM from labelled carbon atoms in toluene-1- ¹³ C, toluene- α - ¹³ C and toluene-(phenyl)- ¹³ C ₆	132
6.18	Example of behavior of raw $\delta^{13}\text{C}$ measurements, pyrolysis of ethanol at temperatures in the range of 1150 to 1450°C	134
6.19	Relative conversion rate of ¹³ C labelled atoms in various alcohol molecules calculated for PM formed from a series of alcohols.	137
7.1	Example of a typical transesterification reaction of a triglyceride with methanol.	140
7.2	Structure and nomenclature of ¹³ C-labelled oleic acid and methyl oleate.	143

7.3	Schematic representation of the setup for particulate sample collection from the diesel engine	144
7.4	Flow reactor rig setup for investigating influence of oxygen on pyrolysis products	146
7.5	Percentage composition of PM derived from the labelled carbon atoms in oleic acid-1- ¹³ C, oleic acid-9,10- ¹³ C, and methyl oleate-1- ¹³ C, formed in a flow reactor with varying air-fuel ratios.	147
7.6	Composition of PM derived from ¹³ C labelled carbon atoms, sampled from a diesel engine exhaust gas.	148
7.7	In-cylinder pressure and apparent heat release rates of methyl oleate, oleic acid, and reference diesel at constant injection timing.	150
7.8	Summary of particulate size, number concentration, and total mass characteristics for the pyrolysis of diesel fuel, methyl oleate, and oleic acid in the flow reactor facility	151
7.9	Diesel engine exhaust particulate number and size distributions, and calculated total mass concentration of PM.	153
7.10	Molecular structure of dibutyl maleate (DBM) and tri-propylene glycol methyl ester (TPGME).	154
8.1	General chemical structure of lignin, and schematic for its conversion into mono-aromatic products.	158
8.2	Structure and nomenclature of ¹³ C labelled molecules investigated, which were blended with heptane.	162
8.3	Total particulate mass emissions in the exhaust of the compression ignition engine, from heptane blended with ethanol, 1-propanol, 2-propanol, acetone, ethyl acetate, or toluene.	166
8.4	Particulate size distributions in the exhaust of the compression ignition engine, from heptane blended with ethanol, 1-propanol, 2-propanol, acetone, ethyl acetate, or toluene.	166
8.5	Tracing of ethanol-1- ¹³ C, ethanol-2- ¹³ C, ethanol-1,2- ¹³ C ₂ blended into heptane, to the PM and formed under pyrolysis conditions in a laminar flow tube reactor.	167
8.6	Tracing of ethanol-1- ¹³ C, ethanol-2- ¹³ C, ethanol-1,2- ¹³ C ₂ blended into heptane, to the PM and formed under pyrolysis conditions in a diesel engine.	168
8.7	Locations of the ¹³ C label in 1- and 2-propanol.	171
8.8	Tracing of 1-propanol-1- ¹³ C, 1-propanol- ¹³ C ₃ , 1-propanol-1,3- ¹³ C, 2-propanol-2- ¹³ C, 2-propanol- ¹³ C ₃ and 2-propanol-1,3- ¹³ C ₂ blended into heptane, to the PM and formed under pyrolysis conditions in a laminar flow tube reactor.	172
8.9	Tracing of 1-propanol-1- ¹³ C, 1-propanol- ¹³ C ₃ , 2-propanol-2- ¹³ C, or 2-propanol- ¹³ C blended into heptane, to the PM and formed under pyrolysis conditions in a diesel engine.	173

8.10	Tracing of acetone-2- ¹³ C and acetone- ¹³ C ₃ blended into heptane, to the PM and formed under pyrolysis conditions in a laminar flow tube reactor.	175
8.11	Tracing of acetone-2- ¹³ C, acetone- ¹³ C ₃ blended into heptane, to the PM and formed under pyrolysis conditions in a diesel engine.	176
8.12	The percentage conversion of toluene-in-heptane blends, containing toluene- ¹³ C ₇ , toluene-1- ¹³ C, and toluene-phenyl- ¹³ C ₆ , to PM in a laminar flow reactor.	177
8.13	The percentage conversion of toluene-in-heptane blends, containing toluene- ¹³ C ₇ , toluene-1- ¹³ C, and toluene-phenyl- ¹³ C ₆ , to PM in a diesel engine.	178
8.14	The molecular structure of methylphenanthrene.	179
8.15	The relative conversion rates to PM formed in the flow reactor of the hydroxyl and carbonyl carbon atoms in ethanol, 1-propanol, 2-propanol, acetone, and ethyl acetate.	181
8.16	The relative conversion rates to PM formed in the diesel engine of the hydroxyl and carbonyl carbon atoms in ethanol, 1-propanol, 2-propanol, acetone, and ethyl acetate.	182
9.1	Setup of the GC-IRMS instrument.	189
9.2	Appearance of the soluble extract of PM formed from ethane pyrolysis at 1250 °C (left) and 1150 °C (right).	190
9.3	GC/MS spectra of PAHs extracted from samples of PM, collected from a flow reactor.	192
9.4	GC/MS spectra of PAHs extracted from samples of PM, collected from a flow reactor.	193
9.5	GC/C/IRMS spectrum of a standard mix of 16 PAHs (47930-U Supelco).	194
9.6	GC/C/IRMS spectrum of PAHs extracted from the PM generated from the pyrolysis of ethanol at 1150 °C.	194
A.1	Screenshot of the user interface used to monitor and controll the laminar flow tube reactor (written in NI LabView).	203
A.2	Image of the laminar flow reactor facility.	204
A.3	Outlet of the flow reactor with assembly for collecting particulate matter onto a filter.	204
A.4	Fuel vaporiser and inlet to the reactor.	205
A.5	Image of the EA-IRMS analysis equipment installed in the Bloomsbury Environmental Isotope Facility (BEIF).	205
A.6	Operation of the liquid/gas injection port, installed onto the EA-IRMS.	206
A.7	Setup for soxhlet extraction.	206

List of Tables

3.1	Calculated gas residence time and Reynolds number of nitrogen through the zone of uniform heating in the reactor at a flow rate of 20 l/min (0.6 m length).	64
3.2	Test engine specifications	66
3.3	Conditions employed in the elemental analyser (Thermo Flash EA, 1112 series).	73
4.1	Example of the ppm composition of (a) air composition and (b) a mixture of methane and nitrogen.	92
5.1	Some selected TSI values for various hydrocarbon fuels (values from (Ladomatos et al., 1996)).	96
5.2	Relative FID response factors for a range of hydrocarbon and oxygenated fuels. Relative sensitivity values obtained from Dietz (1967)	100
6.1	$\delta^{13}\text{C}$ measurements of fuel and derived PM (generated at 1300 °C) for ethanol, ethyl acetate, and toluene, at various levels of enrichment.	133
6.2	Measured $\delta^{13}\text{C}$ values for unenriched ethanol with varying delay between capillary transfer and capsule sealing	135
7.1	Fuel properties.	143
7.2	Summary of physical conditions prevailing in the tube reactor and compression ignition engine.	149
7.3	CO and CO ₂ concentrations (ppmv) evolved from the tube reactor pyrolysis of diesel, methyl oleate, and oleic acid.	152
7.4	Calculated the conversion rate of fuel to PM, in the diesel engine	153
7.5	Calculated the conversion rate of ¹³ C labelled atoms in the fuel to PM, in the diesel engine	153
7.6	CO and CO ₂ evolved from the tube reactor pyrolysis of diesel, methyl oleate, and oleic acid.	153
8.1	Mixture of various compounds in heptane at level of 10 mole percent.	161
9.1	Structures, names, and molecular weights of the 16-EPA-PAHs.	187
9.2	Chromatographic Conditions.	189
B.1	Measured $\delta^{13}\text{C}$ values, and calculated parameters for PM formed in a laminar flow reactor at 1300°C.	213
B.2	Measured $\delta^{13}\text{C}$ values, and calculated parameters for PM formed in a diesel engine.	214
B.3	Measured $\delta^{13}\text{C}$ values, and calculated parameters for PM formed from binary mixtures of ethanol-in-heptane, in the flow reactor and diesel engine.	215

B.4	Measured $\delta^{13}\text{C}$ values, and calculated parameters for PM formed from binary mixtures of 1-propanol or 2-propanol-in-heptane, in the flow reactor and diesel engine.	216
B.5	Measured $\delta^{13}\text{C}$ values, and calculated parameters for PM formed from binary mixtures of acetone-in-heptane, in the flow reactor and diesel engine	217
B.6	Measured $\delta^{13}\text{C}$ values, and calculated parameters for PM formed from binary mixtures of ethyl acetate-in-heptane, in the flow reactor and diesel engine. .	218
B.7	Measured $\delta^{13}\text{C}$ values, and calculated parameters for PM formed from binary mixtures of toluene-in-heptane, in the flow reactor and diesel engine.	219
B.8	Engine exhaust emissions, as measured by the Horiba MEXA9100 HEGR instrument.	220

Notations

Abbreviations

ABE	Acetone, butanol, and ethanol
AMS	Accelerator mass spectroscopy
BTDC	Before top-dead-centre
CAD	Crank angle degree
CO	Carbon Monoxide
CO ₂	Carbon dioxide
DCM	Dichloromethane
DICI	Direct injection compression ignition
DMS	Differential mobility spectrometer
DPF	Diesel particulate filter
EA/IRMS	Elemental analysis isotope ratio mass spectrometry
GC/C/IRMS	Gas chromatography combustion isotope ratio mass spectrometry
GC/MS	Gas chromatography mass spectrometry
FAME	Fatty acid methyl ester
FFA	Free fatty acid
fFID	Fast flame ionisation detector
FID	Flame ionisation detector
HACA	Hydrogen abstraction/C ₂ H ₂ addition
HCCI	Homogeneous charge compression ignition
HEPA	High efficiency particulate air filter
HPLC	High performance liquid chromatography
IAEA	International atomic energy agency
IBE	<i>i</i> -propanol, butanol, and ethanol
IMEP	Indicated mean effective pressure
IRMS	Isotope ratio mass spectrometry
MAC	Methyl addition cyclisation
N ₂	Nitrogen
NO _x	Nitrogen oxides
NVOF	Non-volatile organic fraction
O ₂	Oxygen
PAC	Polycyclic aromatic compound

	Phenyl addition/cyclisation
PAH	Polycyclic aromatic hydrocarbon
PM	Particulate matter
PM _{2.5}	Particulate matter up to 2.5 micrometers in size
PM ₁₀	Particulate matter up to 10 micrometers in size
PCCI	Premixed charge compression ignition
PPM	Parts per million
PPMV	Parts per million volume
PID	Proportional integral and derivative
ROS	Reactive oxygen species
SATP	Standard ambient temperature and pressure
SCR	Selective catalytic reduction
SOF	Soluble organic fraction
TCD	Thermal conductivity detector
TDC	Top dead centre
THC	Total hydrocarbons
TSI	Threshold sooting index
UFPs	Ultrafine particles
VOF	Volatile organic fraction

Greek symbols

τ	Residence time
ϕ	Fuel/air equivalence ratio
λ	Air/fuel equivalence ratio
δ	Delta units (isotopic composition)
ρ	Density

Chapter 1

Introduction

1.1 Purpose

The purpose of the body of work presented in this thesis is to examine the effect that the molecular structure of a fuel has on its tendency to form particulate matter. It is important to lower particulate emissions in order to mitigate the harmful effects of combustion-generated particles in the atmosphere. To this end, many studies have investigated how the chemistry of a fuel influences its so-called sooting tendency, but this work is unique in that as well as characterising the overall tendency of a molecule to form particulate matter, the relative tendency of individual carbon atoms within a molecule has also been examined. This provides insight into the behavior and fate of individual carbon atoms during combustion, which is useful in understanding the fundamental physical and chemical mechanisms that govern particulate formation. The influence of a range of fuels, and sub-molecular groups has been assessed in both a flow reactor and a diesel engine.

1.2 Motivation

Particulate matter in the atmosphere arises from a number of sources, including road vehicles, domestic heating, and industrial power generation. In the urban environment the largest contributor is road traffic; it has been estimated that 90% of airborne particles smaller than 10 μm (PM_{10}) in the greater London area are associated with road transport (Harrison, 1996). Of road vehicles, those powered by diesel engines are the most polluting in terms of particulate mass emissions, and a vehicle powered by a diesel engine typically emits 10 to 100 times that of an equivalent vehicle powered by a port fuel-injected gasoline engine (Kittelson, 1998).

Presently, about 80 % of the worlds energy demand is met by the three fossil fuels: oil, coal, and natural gas (Jess, 2010). It is inevitable that these fossil reserves will become depleted if they continue to be consumed at the current rate. Shafiee and Topal (2009) estimated that reserves of oil, coal, and gas could be available until 2040, 2112, and 2042 respectively. In the coming decades it is estimated that the global population

could rise from 7 billion presently, to 9 billion by 2050 (Jess, 2010). Concurrently, the per capita energy demand is rising in line with increasing standards of living in emerging markets, which is increasing the pressure on finding sustainable alternatives.

The sheer number of vehicles on the road raises important issues concerning human health, the environment, energy policy and legislation. These issues are discussed in the following sections, primarily with regard to particulate emissions; although, naturally, in the wider argument, other regulated emissions such as CO₂, NO_x, and unburned hydrocarbons must also be considered.

1.2.1 Human health

The International Agency for Research On Cancer (IARC), a specialised agency of the World Health Organisation, has recently categorised particulate matter as a group 1 carcinogenic agent, therefore satisfying the criteria of *sufficient evidence for carcinogenicity in humans* (IARC, 2013). Epidemiological studies of human exposure to particulate matter have identified correlations between the levels of airborne particulates and adverse health effects, which include respiratory and heart diseases (Davidson et al., 2005). Overall, increased mortality rates are observed and estimates indicate that PM₁₀ emissions are a factor contributing to 37,000 deaths per year in the EU (Fiala et al., 2009). In a 2014 UK government report, based on epidemiological data, it was indicated that in the London Borough of Camden, which has ~160,000 residents, 7.7% of the 1126 deaths in the year 2010 were attributable to anthropogenic PM_{2.5}, of which the life expectancy was shortened by an average of 13 years (Gowers et al., 2014). Put another way, residents of Camden that are aged 25 and above, have a 7.7% chance of having their life expectancy reduced by 13 years due to exposure to airborne particulates.

The aerodynamic diameter of a particle is an important factor for determining its potential health effects, smaller particles (< 1000 nm) are more efficiently transported through the respiratory tract and deposited in the lungs where they can penetrate the pulmonary interstitium (Harrison and Yin, 2000). It has been shown in a number of investigations that there is an association between the atmospheric concentration of ultrafine particles (UFPs), particles that are less than 100nm in diameter, and mortality rate (Pope et al., 1995; Dockery et al., 1993). Atmospheric levels of fine particles was associated with lung cancer as well as cardiopulmonary disease, and less strongly associated with total particulate and NO_x levels. Fine mode particles appear to have considerably higher toxicity per unit mass than larger particles and the toxicity increases as particle diameter decreases. This may be explained by the increasing surface area per unit mass as the particle diameter decreases, and the ability of the particles to penetrate further into the lungs without capture by the human respiratory system defenses (Donaldson et al., 1998). It was pointed out by Kittelson (1998) that this raises the important question of whether emission standards should be introduced to limit the number concentrations of nanoparticles. Indeed, legislators have taken notice of the evidence, in Europe for example, Euro 6 emissions standards limit the number of particulate emitted

from passenger and light commercial vehicles powered by compression ignition engines to 6×10^{11} per kilometer (emissions legislation is discussed in greater detail in Section 1.2.3).

Once a particle has deposited in the lungs there are several characteristics of the particle that could have an influence on its toxicity, including the reactivity of the particle surface and the presence of adsorbed species such as polycyclic aromatic hydrocarbons (PAHs). It is significant that there is little evidence to suggest that acute exposure to elemental carbon results in inflammation; whereas inflammation is associated with more disordered carbon particle surfaces. Frampton et al. exposed healthy asthmatic human volunteers to ultrafine carbon particles that were generated by means of a spark discharge method. No inflammation was observed in the volunteers either at rest or exercising when exposed to particle concentrations 50 to 100 times that of urban environments over a two hour period (Frampton et al., 2004). A study conducted by Oberdörster et al. (2000) which involved exposing rats and mice to UFPs generated by spark discharge over a six hour period also found no evidence of inflammatory response. Black carbon is classified by the IARC as being a group 2B agent, a category of agents that are possibly carcinogenic to humans (IARC, 2013).

Polycyclic aromatic hydrocarbons (PAHs) are formed during combustion and are key precursors to soot, they are also present in the exhaust of diesel and gasoline engines and are predominantly found adsorbed to the surface of soot particles. It has been shown that fresh diesel soot can contain significant quantities of PAHs, including benzo(a)pyrene (BaP) (Zielinska et al., 2004), which is considered to be particularly carcinogenic. It has been shown that PAHs remain bound to the surface of particulates, and samples collected from the urban air also contain significant quantities of adsorbed PAHs (Kawanaka et al., 2004). Particulates can act as effective carriers of the adsorbed organic materials to the human lungs, and *in vivo* desorption of the organic species may result in the cellular uptake. Vogel et al. (2005) found that induction of inflammation in human macrophage cells was primarily due to the soluble organic fraction (SOF) of particulate and not the elemental carbon. Research has also shown that PAHs are toxic and mutagenic, so much so that estimates indicate that up to 1.6% of lung cancer cases in China can be attributed to the inhalation of PAHs from polluted air (Zhang et al., 2009).

Nitrogen or oxygen containing derivatives of PAHs (nitro-PAHs and oxy-PAHs) are direct-acting mutagens, and these are often found to have greater mutagenic potential than their corresponding PAHs due to their ability to produce reactive oxygen species (ROS) (Bolton et al., 2000). Nitro-PAHs and oxy-PAHs can originate directly from combustion and are found in diesel or gasoline engine exhaust, and they can also be formed by the reaction of PAHs in the atmosphere. For example, PAHs can react with hydroxyl radicals (OH) and nitrogen dioxide (NO₂), or nitrate radicals (NO₃) to form nitro-PAHs (Bolton et al., 2000; Busby Jr et al., 1997). There is evidence to suggest that the inflammation observed upon exposure to particulates is caused by oxidative

stress on cells, and ROS are believed to be the cause. ROS such as the hydroxyl radical or hydrogen peroxide are either generated by the particle or generated by the cells in response to the presence of the particle.

It should be mentioned that there is some conflicting evidence regarding the contribution to toxicity of absorbed organic material. Nikula et al. (1995) found that at high concentrations, the tumor forming potential of carbon black and diesel soot were about the same. Whilst Adamson et al. (1999) observed that particulates with soluble material absorbed could induce inflammation, but speculated that observed toxicity could be due to adsorbed metals. Additionally, it has been put forward that unpaired electrons at the surface of soot particles could react with cells or surrounding fluid and result in the observed health effects. Zang et al. (1995) identified semi-quinones to be a primary radical in cigarette tar, and it has since been postulated that this could also be a major cause of the observed health effects in atmospheric particulates. Semi-quinones are a free radical species generated from quinones, which are a class of aromatic molecules that contain an even number of carbonyl groups.

It is clear that in order to inform the legislative and technological efforts to mitigate the health effects of combustion-generated particulates more information is required in order to identify the biochemical mechanism(s) of the observed toxicity. It appears likely that by changing to the composition of PM, particularly to the surface chemistry of ultrafine particles, that it is possible to modify the potential of PM to cause harm to human health.

1.2.2 Climate change

In the literature, CO₂ emissions have received the most attention with regard to global climate change, and there is widespread scientific acceptance that the anthropogenic release of fossil-bound CO₂ contributes to global warming (Zecca and Chiari, 2010). In 2010, the transport sector accounted for 22% of global CO₂ emissions, a total of approximately 6.8 giga-tonnes of CO₂, of which, about 5 giga-tonnes of CO₂ was produced by road transport alone (IEA, 2012).

Although there is a large amount of uncertainty in estimations, some studies suggest that particulate emissions are second only behind CO₂ for its effect on global warming. Particulates precipitate from the atmosphere on a timescale of weeks whereas CO₂ can persist for centuries. This means that efforts to reduce particulate emissions could reap immediate climatic benefits by taking measures to reduce particulate emissions into the atmosphere (Bond et al., 2013).

1.2.3 Legislation

The issues that have already been discussed relating to human health, climate change and energy sustainability are prompting government policies and new legislation that promotes the use of more efficient, clean and renewable technologies. In the EU, legislation limits emissions from numerous sources, including road vehicles. For example,

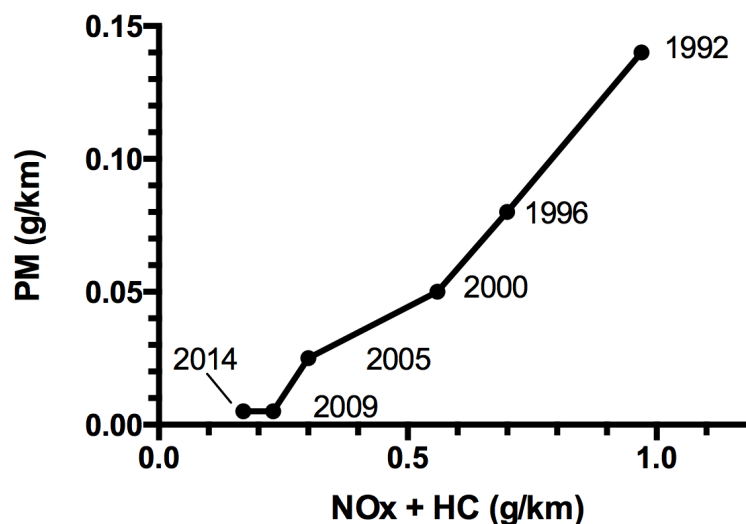


Figure 1.1: PM, and hydrocarbon and NOx emissions limits set for compression ignition engine passenger vehicles, as part of European directives: Euro 1 (1992), Euro 2 (1996), Euro 3 (2000), Euro 4 (2005), Euro 5 (2009), and Euro 6 (2014). The plotted data was acquired from (<http://transportpolicy.net/index.php?title=EU:Light-duty:Emissions> Accessed:17/01/2015).

under Euro 6 emissions standards new diesel powered passenger vehicles sold in the EU must not emit more than 5 milligrams of particulate matter and no more than 6×10^{11} particles per kilometer (EU, 2010). Figure 1.1 shows how emissions standards in the EU have tightened since the introduction of the ‘Euro 1’ emissions standards set in 1992, for compression ignition engine passenger vehicles. The increasingly stringent legislation is projected to continue on its current trajectory putting further pressure on the automotive industry to continually improve emissions performance for the foreseeable future.

Legislation has also been put in place to improve fuel sustainability, security and emissions by requiring that a portion of transport fuel be derived from renewable resources. For example, in the UK, the Renewable Transport Fuels Obligation requires fuel suppliers to ensure that all road transport fuels contain at least 5 per cent (v/v) from sustainable renewable sources (<https://www.gov.uk/renewable-transport-fuels-obligation> accessed:17/01/15). Furthermore in the EU, maximum limits of several components of petrol and diesel fuels is mandated; for example, diesel fuels to be used in compression ignition engines must have an aromatic content of no more than 8% (m/m), and the FAME content is limited to a maximum of 7% (v/v) (Directive 2009/30/EC).

1.3 Aims, objectives and overview

The central aim of this thesis is to provide a holistic analysis of the influence of functional group chemistry on the formation of particulate matter. The approach is described as holistic in the sense that a wide range of fuels have been investigated, and several

experimental systems have been used for generating particulates (e.g. diesel engine, laminar tube reactor). In addition, a number of experimental techniques have been used to characterise the particulates formed. The most notable technique is one that has been used as part of this work and involves the application of carbon-13 (^{13}C) isotope labeling in order to trace specifically labeled carbon atoms from the fuel to particulate matter and gas emissions. This technique allows the identification of the relative probability of specific carbon atoms within a molecule of converting to particulate matter, and it sheds new light on how different molecular functional groups directly influence the conversion of local carbon atoms in a molecule to PM. Overall, the insights gained from this work contribute towards efforts to understand how the chemical structure of fuels influences combustion and emissions characteristics.

The specific objectives of the research were:

1. To characterise the particulate emissions in terms of ‘sooting tendency’, and particle number and size distributions, formed from various fuels of different molecular structure under pyrolysis conditions in a tube reactor.
2. Use a ^{13}C labelling technique to identify the extent of particulate formation from different ‘sub-molecular’ carbon atoms in a range of single-component fuels with different functional group chemistry. For example, in ethanol, identify the extent of the contribution to PM from the carbon atom that is directly bonded to the hydroxyl functional group, compared to the methyl carbon atom; and
3. Test a series of functional groups within various fuels molecules including alcohols, ketones, carboxylic acids, methyl esters, aromatic rings, and double bonded carbon atoms.
4. Identify if/how the conversion to PM of specific ‘sub-molecular’ carbon atoms in the fuel is influenced by the formation conditions prevailing (e.g. temperature, and availability of oxygen).
5. Investigate the extent of the contribution to PM of a component in a binary mixture with heptane, using ^{13}C to label one of the molecules to assess the extent to which it produces particulate matter.
6. Assess the conversion of individually labelled carbon atoms under different formation conditions, in the well-controlled conditions of a tube reactor, and also in a modern compression ignition diesel engine.

A range of molecules were investigated in terms of their overall propensity to form particulate matter by pyrolysis in a tube reactor (Chapter 5), and the ^{13}C isotope labeling technique has been applied to track specific sub-molecular groups from within those fuels to PM (Chapter 6). Further investigation, using the biofuels oleic acid and methyl oleate, compared the particulate matter formed in a tube reactor to a compression ignition engine (Chapter 7). The labeling technique was also applied to binary mixtures

of heptane with small amounts of added ethanol, propanol, acetone, ethyl acetate, or toluene, tested in both the reactor and diesel engine, with a view to evaluate individual carbon atom contributions as part of the mixture (Chapter 8). Finally, a preliminary investigation was carried out to investigate the presence of PAH compounds on the surface of particulates formed in the tube reactor (Chapter 9).

Modifying fuels in order to yield more desirable emissions and combustion characteristics is a promising avenue for meeting future legislative demands, and, most importantly, for mitigating damage to the environment and climate. Traditional fossil diesel fuel that has been used for the past century has been comprised of a large mixture of hydrocarbon molecules, typically with several hundred chemically distinct hydrocarbon molecules. Future fuels, such as those derived from biological feedstock, are likely to have a more uniform composition, depending on material from which they are formed and the biological, chemical or physical processes which they are subjected to. This means that there is an opportunity to make targeted improvements to the molecular structure of fuels. In order to make such targeted improvements, it is important to understand the fundamental mechanisms of how the chemical composition of a fuel influences its combustion and emissions properties.

Chapter 2

Literature review

This thesis is concerned with the fundamental understanding of how the molecular structure of a fuel influences particulate formation. It also considers a promising new diagnostic technique based on ^{13}C isotope tracing. The literature reviewed here therefore describes the processes that result in particulate formation, discusses some common strategies to reduce particulate emissions, and provides a comprehensive background of the use of isotope tracers in combustion science. It was discussed in the introduction that the emissions from road vehicles are particularly problematic to human health and the environment, and diesel engines are the most polluting in terms of particulate and NOx emissions. Therefore, where relevant, much of the commentary in this review is focussed on diesel engine particulate emissions and how they may be reduced.

2.1 Composition and structure of soot

Soot particles are predominantly comprised of carbon, and to a lesser extent hydrogen. Soot formed in a diesel engine typically has a carbon to hydrogen (C/H) ratio of 8:1 (Heywood, 1988). Nascent particles usually have a C/H ratio of ~ 1 , and the hydrogen fraction reduces as the particle matures. The density of soot formed in a premixed flame has been reported to be $1.84 \pm 0.1\text{g}$ (Choi et al., 1994), and similar values are reported for particles formed in a diesel engine.

Viewed by electron microscope, soot particles appear as chain-like or clustered structures that consist of agglomerated spherical particles. These clustered structures may be comprised of as many as 4000 individual spheres which are often referred to as spherules (or primary particles). Each spherule is around 5-50 nm in size, and the clustered aggregates are generally sized between 50 and 220 nm. Spherules consist of graphene sheets that are wrapped around the center of the sphere, forming onion-like layers. X-ray diffraction analysis shows that at an atomic level carbon atoms are arranged as a planar lattice with a regular hexagonal pattern (Heywood, 1988). The layers of the lattice are bonded to parallel planes with a mean spacing between the layers of 0.355 nm, which is slightly larger than the interlayer spacing in graphite (0.354 nm). These small graphite-like units are commonly referred to as platelets, and 2 to

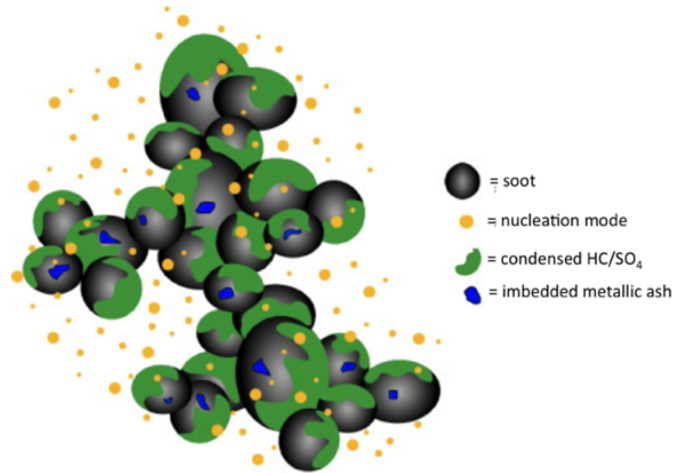


Figure 2.1: Artists impression of cooled and diluted diesel particulate matter. Reproduced from (Matti Maricq, 2007), with permission of the publisher (Elsevier).

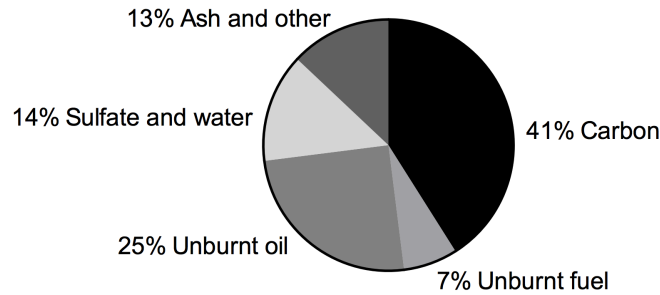


Figure 2.2: Composition of particulate matter from a heavy-duty diesel engine, tested in a transient cycle, figure recast from data of (Kittelson, 1998). It should be noted that the composition of the PM is heavily dependent on the engine design, operating conditions, and the composition of the fuel.

5 platelets stack to form larger units known as crystallites. It is the crystallites that arrange in concentric layers and are observable by transmission electron microscopy; spherules are comprised of approximately 1000 crystallites. It has been shown that the arrangement of crystallites in spherules becomes more well-ordered at higher formation temperatures with a greater similarity to graphite, when produced in a laminar flow reactor (Ruiz et al., 2007b).

2.1.1 Diesel particulate matter

Engine exhaust is composed of mainly nitrogen, oxygen, CO₂, CO, unburnt hydrocarbons, water vapor, and PM. Diesel particulate matter is typically composed of two types of particles: (i) agglomerates of carbonaceous primary particles of soot (each 15 to 30nm in diameter) containing trace amounts of metallic ash, where the agglomerated soot particles are covered in condensed organic compounds and sulfate; and (ii) nucleation mode particles, condensed particles, and sulfate (Matti Maricq, 2007). An artists conception

of diesel particulate matter is shown in Figure 2.1. As an example, the chart in Figure 2.2 shows the composition of particulate matter collected from a heavy-duty diesel engine, measured over a transient cycle (Kittelson, 1998).

Due to the volatility of many of the components of the PM, the conditions employed to sample PM in the engine exhaust influences the composition of the PM that is collected onto a filter. Depending on the conditions, the volatile fraction may: remain in the gas phase; condense onto the surface of solid particles; or, nucleate to form new particles. In addition, there is potential for water condensation to occur as the exhaust temperature cools. Therefore, engine tests that are carried out for the purpose of regulatory compliance must be carried out under prescribed conditions. For example, in Europe, the Euro 5 and Euro 6 legislation determines that PM mass emissions measurements to be carried out using a method, which was developed under the UN/ECE Particulate Measurement Programme (PMP); using a similar method that was introduced in the USA in 2007 (CFR, 2007). In European legislation PM mass emissions measurements must be made through a dilution tunnel, where the engine exhaust is diluted into filtered air, under temperature and humidity controlled conditions; for example, the temperature of the sampling line and the filter housing must be kept at a constant $47\text{ }^{\circ}\text{C} \pm 5\text{ }^{\circ}\text{C}$, to ensure a filter face temperature of $47\text{ }^{\circ}\text{C} \pm 5\text{ }^{\circ}\text{C}$. Specific measurement details are available in references (CFR, 2007) and (Anderson et al., 2007).

2.1.2 Nomenclature of carbonaceous particles

There is a wide range of terms available for referring to carbonaceous particles, for example: soot, particulate matter (PM), PM_{10} , $\text{PM}_{2.5}$, black carbon, carbon black (distinct from black carbon), brown carbon, and ‘elemental carbon’. Each terms is distinct in its definition, and the particles may be defined on the basis of their size, morphology, chemical composition, source, light absorbing properties, and so on. However, in literature, some of these terms are often used interchangeably. The importance of the precise classification of such particles is highlighted in a publication by Andreae and Gelencsér (2006).

Soot, as described above, although not clearly definable, is comprised of solid carbon particles formed by combustion, which may have hydrocarbons and heteroatoms bound at its surface (Tree and Svensson, 2007). Particulate (or particulate matter), as described in the previous section, is generally defined as the combination of solid and liquid phase matter that is present in the engine exhaust.

In this thesis, carbonaceous matter has been collected at a wide variety of operating conditions from a tube reactor and also a diesel engine; therefore the morphology and composition of the material varied widely. In the interest of accuracy and consistency, all of the soot-like material that was generated for analysis in this work is referred to as particulate matter (or particulate); however, where reference to the work of others is made the terminology of the source has been adopted.

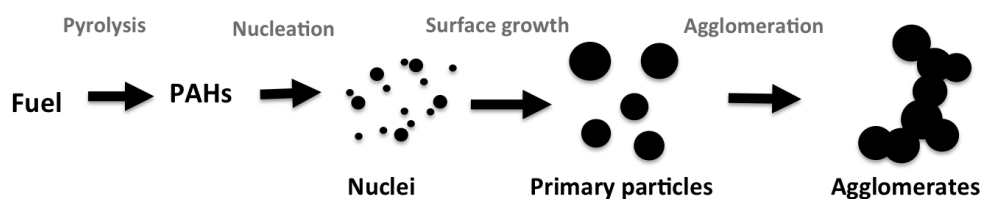


Figure 2.3: Stages involved in the formation of particulates. Figure based on that of (Tree and Svensson, 2007)

2.2 Soot formation

Particulate matter and unburned hydrocarbons, including PAHs, are undesirable products that are formed due to incomplete combustion. Many factors can influence the conversion of fuel to particulate matter or species that are precursors to PM, including: the availability of oxygen, residence time, temperature, pressure, and the molecular structure of the fuel.

The process of soot formation involves the conversion of small hydrocarbon molecules in the gas-phase to spherical solid particles, and this is a complex process that takes only a few milliseconds behind shockwaves or tens of milliseconds in flames. During the combustion of a hydrocarbon, many parallel reactions occur that involve a large number of species, for example a widely cited mechanism for n-heptane oxidation reported by Curran et al. (1998), lists 2450 reactions and 550 chemical species. In the following section some of the major chemical pathways to soot are described. It should be noted that some of these chemical pathways are dependent on the formation conditions prevailing (temperature, pressure, concentration) and also on the composition of the fuel being burned. For this reason the following review serves to give the reader a generalised overview of the processes involved in the formation of soot.

2.2.1 Overview

The process of particulate formation is generally described as having five distinct stages, involving: (i) Fuel pyrolysis, (ii) particle inception (nucleation), (iii) particle growth, (iv) surface growth, and (v) coalescence and the formation of agglomerates. Figure 2.3 summarises the stages involved in formation of soot particles. Soot particles or their precursors may also be partially or completely oxidised during any stage of their formation, depending on the availability of oxygen. For example, in diffusion flames soot oxidation occurs at the flame front, whereas oxidation and formation occur simultaneously in a premixed environment.

2.2.2 Fuel pyrolysis and the formation of the first aromatic ring

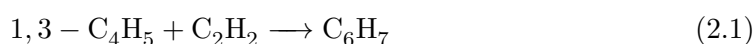
Pyrolysis occurs when organic molecules are heated to high temperatures but do not undergo oxidation, under these conditions the molecules fragment; hydrocarbons and

oxygenated molecules begin to fragment even at relatively mild temperatures, for example, the catalytic cracking of palm oil at 450°C yields light gaseous hydrocarbons (Sang, 2003). In a laminar diffusion flame, at temperatures in the range of 1500 to 2500 K, typical pyrolysis products include various unsaturated hydrocarbons including acetylene (C_2H_2), polyacetylenes (i.e. $C_{2n}H_2$), and PAHs (Tree and Svensson, 2007). Haynes and Wagner (1981) listed C_2H_2 , C_2H_4 , CH_4 , C_3H_6 , and benzene (C_6H_6) as typical pyrolysis products of paraffin and olefin combustion in laminar diffusion flames; the products are broadly similar regardless of the structure of initial fuel. Many of the pyrolysis products are closely associated with soot formation, and in the literature acetylene has received particular attention as a soot precursor.

The generation of large polycyclic aromatic hydrocarbon (PAH) molecules is a prerequisite for soot formation, and the growth process of initial aromatic rings to larger ring structures is common for all fuels. The formation of the first aromatic ring is therefore a key step in the pathway to soot formation from fuels that do not contain aromatic molecules. This means that the rate of formation of the initial ring structures largely determines the propensity of a molecule to form soot.

A number of mechanisms have been put forward to describe the formation of benzene from precursor species, many of which are described in the review article of Richter and Howard (2000). Reactions involving radical species have been shown to be more important than reactions of stable species in the formation of aromatics.

Cole et al. (1984) put forward that aromatic compounds are formed by the addition of a 1,3-butadienyl radical species to acetylene followed by ring closure and hydrogen loss, as described by the following reaction schemes:



The mechanism appeared to be consistent with the rate of formation of benzene in 1,3-butadiene and also in acetylene flames, Cole et al. also stated that in other aliphatic flames butadiene radicals might form by vinyl radical (C_2H_3) addition to acetylene. The involvement of similar species has also been pointed out by other commentators, for example $n-C_4H_4$, formed by the dehydrogenation of the butadiene radical, and the subsequent reaction with acetylene to form a phenyl ring (Frenklach, 2002). Frenklach stated that the reaction of $n-C_4H_5$ is more significant at lower temperatures. These mechanisms discussed so far are termed carbon-even pathways due to the fact that they involve reactants with an even number of carbon atoms.

A popular mechanism developed by Miller and Melius (1992) involves a ‘carbon-odd pathway’, and it was demonstrated that the formation of the first aromatic rings in flames is likely to proceed by the self reaction of a propargyl radical species to form benzene, as follows:



Or



The propargyl species are a resonantly stabilised free radical, which makes it particularly stable. Miller discussed the formation of the propargyl radical in acetylene flames and suggested the following reaction:



Other carbon-odd pathways include a cyclopentadiene radical ($c\text{-C}_5\text{H}_5$), which can react with a methyl radical to form benzene; or self-react which can form the polycyclic aromatic naphthalene directly, bypassing the formation of benzene (Frenklach, 2002).

Overall, the relative contributions of the above mechanisms are not well understood for all conditions and fuels; the most frequently cited mechanisms involving C_3H_3 , C_4H_3 or C_4H_5 are likely to be highly dependent on the formation conditions (Richter and Howard, 2000).

2.2.3 Aromatic growth

In the literature a large number of mechanisms have been put forward to describe the growth of aromatic molecules (Celnik et al., 2008). The most widely-cited mechanism for the growth of aromatics is the so-called HACA mechanism. HACA was originally an acronym for H-abstraction- C_2H_2 -addition, and was developed by Frenklach and Wang (1991). In the literature, however, the term HACA is sometimes used in a more general sense and applied to other growth species. The mechanism proceeds by a repetitive reaction sequence consisting of two steps. Firstly a hydrogen atom is abstracted from the surface of the reacting PAH molecule by a gaseous H atom resulting in a radical PAH species, as follows:



Followed by a second step where gaseous acetylene is added to the radical site, as follows:



Equation (2.7) and 2.8 use the same nomenclature as Frenklach and Wang, where A_i represents an aromatic molecule with i peri-condensed rings, and A_{i-} is the resulting radical. Naturally, there are many parallel reactions that could also give rise to such a radical A_{i-} species, but under typical conditions prevailing in a flame it is found that hydrogen abstraction is predominantly initiated by gaseous atomic hydrogen. Shukla and

Koshi (2010) argue that the HACA mechanism is only efficient at a so-called armchair-edge site, for example the acetylene addition to an armchair edge of phenanthrene, as follows in Figure 2.4:

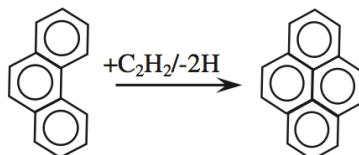


Figure 2.4: Acetylene addition to the armchair edge of phenanthrene to yield pyrene. Reproduced from Shukla and Koshi (2011).

Although several mechanisms involving reactions at other sites at the edges of aromatic molecules have been identified as having a role in aromatic growth (Celnik et al., 2008), and Figure 2.5 shows the sites and the nomenclature of the sites where aromatic growth may occur.

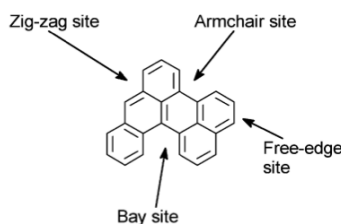


Figure 2.5: Growth sites of aromatic molecules. Reproduced from Celnik et al. (2008).

It is important to point out the reversibility of the HACA mechanism. Firstly, the radical A_{i-} species may react with gaseous atomic or molecular hydrogen pushing the reaction in the reverse direction. Secondly, the reverse reaction of the acetylene addition step is often favorable due to the loss of entropy associated with acetylene addition, although some entropy can be recovered with the formation of a hydrogen atom product. Frenklach argues that the reaction only becomes irreversible when there is low thermodynamic resistance (of reaction reversibility) and when the decrease in energy is large enough (Frenklach, 1989). The formation of particularly stable aromatics, sometimes referred to as stabilomers (Stein and Fahr, 1985) is significant, as it was described in the previous section (Section 2.2.2) the high temperatures that facilitate soot formation also cause hydrocarbons to fragment. The resistance of stabilomers to fragmentation is therefore critical to the formation of soot. Temperature is therefore important factor in determining the rate of molecular growth and also the fragmentation rate.

Various commentators, however, indicate that the HACA mechanism is slow, relative to the fast formation of PAHs and soot observed experimentally (Böhm et al., 1998); the HACA process is limited largely due to the dependence of the mechanism on

the availability of armchair edge sites. Another, more efficient mechanism of aromatic growth is phenyl-addition/cyclisation, known by its acronym PAC, and this was put forward by Shukla and Koshi (2011). PAC involves the addition of a phenyl radical at any fusing site on an aromatic, for example in the reaction of phenanthrene with phenyl to form benzo[e]-pyrene, as follows in Figure 2.6:

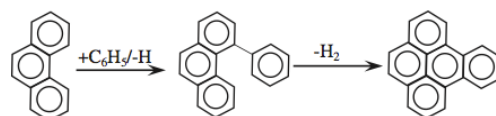


Figure 2.6: Reaction of phenyl with phenanthrene to form benzo-e-pyrene, according to the PAC mechanism. Reproduced from Shukla and Koshi (2011)

HACA and PAC appear to be the dominant mechanisms under most conditions, however other contributing reactions have been put forward, such as methyl addition/-cyclisation (MAC). MAC involves the addition of successive methyl radicals, and ends with a dehydrocyclisation reaction, which results in a fused cyclopenta/tetra or benzenoid structure (Shukla et al., 2010). The reader is reminded that the pathways of PAH formation and growth are likely to be governed to a large extent by the fuel and the local formation conditions prevailing.

2.2.4 Nucleation and surface growth

Nucleation is defined as the formation of particles from gas-phase reactants. Generally, it is understood that nucleation occurs by the coalescence of moderately sized PAHs into stacked clusters. Such a process involving the dimerization of PAHs is supported by experimental evidence, for example the observed bimodal distribution of sizes of nascent soot particles (Wang, 2011). Herdman and Miller (2008) proposed that electrostatic and dispersion forces were sufficient to allow binding of moderately sized PAHs even at flame temperatures, and others suggest chemical coalescence into cross-linked structures (Wang, 2011). The size of observable solid particles in flames is reportedly in the range of 1.5 to 2 nm (Bartok and Sarofim, 1991), and particle inception temperatures vary from 1300 to 1600 K, depending on the fuel. Clearly, the mass of the small nascent nucleated particles do not contribute appreciably to the overall mass of the soot, but by virtue of their large number they do significantly impact on how much mass is added later due to surface growth.

Surface growth is defined as the addition of mass to the surface of the nucleated particles, and is the process whereby the bulk of solid phase material of soot is generated. In reality the nucleation and surface growth occur simultaneously, and there is no clear distinction between the end of the overall nucleation and the onset of the surface growth process. Surface growth involves the addition of gas phase hydrocarbons to the surface of the nucleated particle, and appears to proceed mainly by the addition of acetylene to the surface by the HACA mechanism (described previously). In combustion it is

estimated that 80% of the soot mass is added in surface growth (Haynes and Wagner, 1981). Given that surface growth is responsible for the majority of mass addition, the residence time of the growing particle has a large influence on the total mass of soot formed.

2.2.5 Agglomeration and coalescence

Both agglomeration and coalescence are processes that involve the collision and combining of two particles, where the combined mass of the particles remains unchanged but results in a decrease in the total number of particles. Agglomeration involves the sticking of primary particles with one another to form clusters or chains; where there is no change to the structure of the individual primary particles (or spherules). Coalescence on the other hand involves the collision of spherical particles that give rise to a single spherical particle. Soot particles that are present in diesel engine exhaust are observed to be agglomerated structures of primary particles typically arranged as chains (Tree and Svensson, 2007). The sizes of primary particles are usually reported to be around 20 to 50 nm, and contain in the order of 10^5 to 10^6 carbon atoms (Heywood, 1988).

2.2.6 Oxidation of soot particles

Oxidation is a competing and parallel process to the soot formation pathways; oxidation results in the conversion of carbon and hydrocarbons to combustion products. There are several oxidising species that may oxidise soot, these are: O, O₂, OH, and CO₂. Oxidation can occur at any stage in the pathway of soot formation, from the initial fuel through to a mature agglomerated particle. There is evidence to show that the OH radical is the principle oxidising agent for soot particles (Neoh et al., 1985), and in the region of 10-20% of OH collision with soot are successful at oxidising soot (Haynes and Wagner, 1981). Oxidation prevents carbon from proceeding to soot formation and it appears it is most effective when oxidation occurs at earlier stages of soot formation, before the formation of aromatic rings. Under certain conditions, however, the addition of small amounts of oxygen can increase soot formation by stimulating radical formation, specifically H atoms which promotes HACA. For example, the addition of small amounts of oxygen to acetylene in shock-tube experiments results in increased soot formation at lower temperatures and retarded soot formation at higher temperatures (Frenklach et al., 1985).

Whilst the OH radical is believed to be mainly responsible for the oxidation of soot particles, Frenklach put forward that in laminar premixed flames the dominant species for oxidation of aromatic radicals was O₂, and oxidation by OH occurred only to a minor extent (Frenklach, 2002). The mechanism of aromatic oxidation has been suggested from numerical simulations, although overall the process is not fully understood.

The presence of CO₂ has also been shown to reduce soot formation, partially as a diluent and through thermal effects (lowering pyrolysis temperature) on soot formation (Liu et al., 2001), but also by promoting hydroxyl formation by the reaction

$\text{CO}_2 + \text{H} \longrightarrow \text{CO} + \text{OH}$ (Vandooren et al., 1998). It should be noted that once carbon is oxidised to CO it is no longer able to form soot, even under fuel-rich conditions.

2.2.7 Particulate formation in a direct injection diesel engine

A conceptual model of particulate formation in a diesel engine was developed by Dec (1997) and forms the basis of current understanding of the processes that lead to soot formation in direct injection compression ignition engines during the quasi-steady phase of combustion. Figure 2.7 shows a schematic of the conceptual model of a diesel jet as fuel is injected into the engine cylinder (from left to right). The fuel jet forms a cone-shaped spray of fuel droplets as it issues from injector nozzle (A). Downstream of the fuel injector a flame stabilises (B), and the distance from the injector to the location of flame stabilisation is defined as the lift-off length (LL). The velocity of the jet largely determines how far from the nozzle the diffusion flame is located, which follows the perimeter of the plume where the fuel/air mixture is stoichiometric. In the premixed reaction zone, indicated as the pale blue region in Figure 2.7 (D), combustion of some of the vaporised fuel occurs, which results in a temperature rise within the reacting jet. Soot begins to form in fuel-rich premixed regions of vaporised fuel (C) where air-to-fuel ratios (ϕ) are typically in the range of 2 to 4, and small soot particles are observed in this section of the jet. Increasing soot number and mass concentrations are observed continuing through the jet (E), with the largest concentrations found at the periphery of the jet. This is due to the fact that beyond the flame lift-off length, oxygen-deficient combustion gasses are entrained into the jet, and not fresh cylinder gas, which is prevented from entering the jet zone by being consumed in the diffusion flame at the plume periphery. There is therefore little oxygen available within the flame envelope to oxidise the fuel, and the high temperature conditions prevailing (due to conduction, convection and radiation from the flame) provide an environment conducive to soot formation. The mixture fraction (ratio of fuel mass to mixture mass) decreases in axial and radial directions; there becomes a point where the oxygen and fuel mixture is stoichiometric, and this is the location of the diffusion flame (F). Soot burnout occurs at the flame, where the soot particles are oxidised by OH radicals (discussed in Section 2.2.6). In the axial direction the mixture fraction diminishes to a point where the flame closes off, and this is referred to as the flame length. The soot number concentration and particle mass therefore increase down the jet and reach a maximum at the head vortex (G), while those particles upstream remain of a similar size and number throughout the combustion event.

The flame lift-off length has been shown to be an important parameter for determining the conditions prevailing in the premixed burn phase and ultimately the final soot emissions in the exhaust (Higgins and Siebers, 2001; Siebers and Higgins, 2001). An increased lift-off length results in increased oxygen entrainment into the premixed phase, which results in greater fuel consumption and ultimately lower particulate emissions. In a direct injection diesel engine, typical lift-off length is in the order of 10-15 mm.

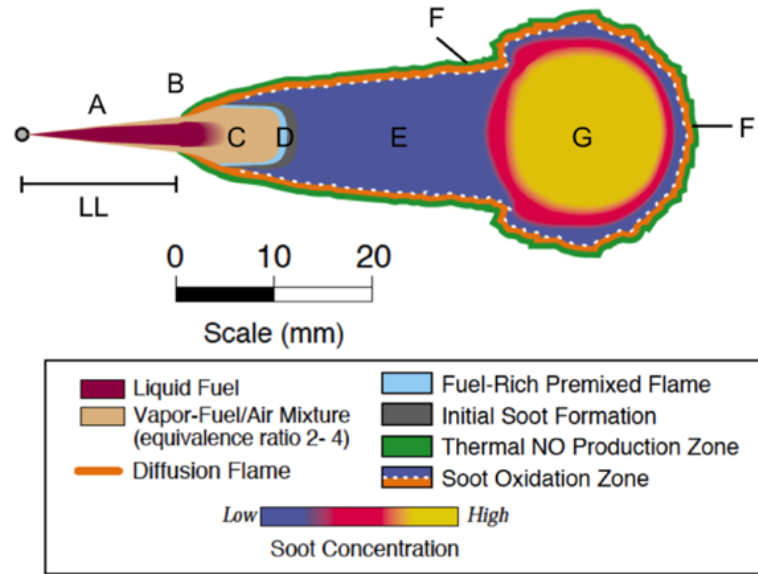


Figure 2.7: A conceptual scheme for a reacting diesel spray. From (Dec, 1997), reproduced with permission of the publisher (SAE international).

2.2.8 Effects of fuel composition on particulate emission in diesel engines

The question of whether the composition and molecular structure of a fuel affects its propensity to form soot, is one that has been studied extensively. The role of fuel composition in soot and particulate matter formation has been investigated most extensively in laboratory flames (e.g. Botero et al., 2014; Ladommatos et al., 1996), and to a lesser extent in practical combustion systems including such as gas turbine engines (Gülder et al., 1990), gasoline engines (Gu et al., 2012), and diesel engines (Tree and Svensson, 2007). The effects of fuel structure and composition on soot and particulate emissions in diesel engines is reviewed in this section; the reader is also referred to Chapter 5, which presents the results of experimental work concerning the influence of fuel molecular structure on soot formation in a tube reactor.

It should be noted that in engines it is generally difficult to separate fuel composition effects from changes in temperature, air-fuel equivalence ratio, lift-off length, and pressure. Therefore, most engine experiments focus on the affect of changing a fuel component on the exhaust particulate mass and number concentrations. Given that a change in the fuel composition directly influences a number of other combustion parameters, a fair comparison would require engines that are optimised for the specific test fuels. It is therefore a challenge to separate fuel effects form those related to the engine geometry (Tree and Svensson, 2007).

Aromatics and PAHs

Most of the research that has been carried out to determine the role of fuel composition on diesel particulate emissions has been related to the role of aromatics in the fuel. Aromatic molecules, that may be present in the fuel or pyrosynthesised during combustion from other non-aromatic molecules, have an important role in the formation of larger PAHs and soot (as discussed Section 2.2). It is well known that increasing fuel aromaticity is associated with higher soot formation in laboratory flames (see for example Ladommatos et al., 1996), but their influence on the formation of particulate in engines is less clear.

Miyamoto et al. (1994) investigated the effect of fuel aromatic content using mixtures of two base fuels, normal paraffin (n-tetradecane), and iso-paraffin (heptamethylnonane), with one of five mono-aromatic, di-aromatic and non-aromatic cyclic compounds added (tetralin, dipentene, decalin, methyl naphthalene, and alkyl benzene). The aromatic content was varied from 0 to 60 % volume for the mono-aromatic fuels and 0 to 40 % volume for the di-aromatics. The fuel mixtures were tested in both an a DI (direct injection) engine and an IDI (indirect injection) engine. Similar results were obtained from both engines, and showed that regardless of the molecular structure of the fuel, the particulate and NO_x emission increased linearly with C/H ratio of the fuel under constant ignition delay. The increase in particulate emission with C/H of the fuel was due to an increase in the mass of dry soot of the particulate.

Bryce et al. (1999) reported that there was a trend of increased soot emission from a diffusion flame and CFR IDI (Co-operative Fuel Research indirect injection) diesel engine with increasing aromatic content. It was suggested that the increased density and viscosity of the fuel could increase soot emission due to changes in the injection, vapourisation and penetration. Further work was carried out using the CFR IDI engine and diffusion flame, where binary mixtures of heptane and increasing proportions of toluene were investigated by holding constant the start of injection (SOI), start of combustion (SOC), and ignition delay (Ladommatos et al., 1997). In the engine, measurement of the dry soot mass was shown to increase with increasing toluene fuel content, although the total particulate mass was insensitive. In the laboratory flame, the difference was much more marked, and the formation of soot was very sensitive to addition of the aromatic compound, and when the aromatic content was increased beyond 10 % volume further increases of the aromatic proportion had no significant effect. The contrast of the two results, in the engine and laboratory flame, suggested that the enhanced air-fuel mixing in the engine offsets the influence of fuel effects on particulate formation.

Williams et al. (1986) investigated the the influence of PAH content in five diesel fuels on the PAHs found in the soluble organic fraction (SOF) of the PM in diesel engine exhaust. The main PAHs that were present in the diesel fuels were naphthalene, fluorene and phenanthrene and their alkylated derivatives. GC/MS analysis showed that the PAHs of the particulate were similar to those present in the fuel. Williams et al. (1986) concluded that the 2 to 4 ring PAH molecules in the particulate were primarily

unburnt fuel components, and that between 0.2 and 1% weight of the fuel PAH survive combustion. Further work by Andrews et al. (1998) involved GC/MS speciation of the PM SOF in diesel engine exhaust, using three fuels with varying aromatic content. Fuel 'a' was a diesel fuel composed of 37 % 1-3 ring aromatics, and 12 % PAH. This initial fuel was processed to remove 2 and 3 ring PAHs, resulting in test fuel 'b'. Fuel 'c' was a mixture composed of 60 % fuel 'a' and 40 % fuel 'b'. The results showed that the fuel with negligible PAH content (fuel 'b') showed very low PAH emissions compared the fuel with high PAH content (fuel 'a'); the authors concluded that unburnt fuel dominates the PAH emissions from the engine. Five pyrosynthesised PAHs were detected in the SOF of the PM, that were not present in the fuel, these were: anthracene, benzo(a)pyrene, benze(e)pyrene, chrysene, and carbazole. This pyrosynthesis was very low (0.06 to 0.02 $\text{mg}_{\text{soot}}/\text{kg}_{\text{fuel}}$) for the fuel with low PAH content, and up to 15 times larger for the fuel with high PAH content. Therefore, it was theorized that the main route to PAH pyrosynthesis in diesel engine combustion is from other PAH molecules. This theory was supported by the results of Abbass et al. (1988), who found that the diesel engine combustion of a single-component fuel hexadecane, an alkane, produced particulate with considerably lower PAH emissions than a reference diesel, indicating that pyrosynthesis of PAHs from alkanes only occurs to a minor extent. Furthermore, and with particular relevance to future fuels, single-component biofuels, including 100 % methyl ester derived from waste cooking oils, and 100 % rapeseed oil, were combusted in a EURO 2 compliant diesel engine (Lea-Langton et al., 2008). Analysis of the VOF fraction of the particulate showed that both biofuels emitted PM containing PAHs, but to a much lower extent compared to a typical diesel fuel; the most abundant PAHs identified in the PM were: phenanthrene, fluoranthene and pyrene.

The 'survivability' of PAH molecules during combustion, compared to non-aromatics, is likely to be a factor contributing to their apparent higher conversion rate to PM. The 'survivability' of PAHs in diesel engine combustion was been correlated with the lowest unoccupied molecular orbital (LUMO) of various PAHs (Tancell et al., 1995); this suggests that it is the chemical kinetics of the reactions occurring in the combustion chamber, rather than the thermodynamic stabilities of the PAH molecules, that determines their survival.

Straight and branched chain

Nakakita et al. (1998) tested three different diesel fuels with near identical combustion characteristics in a single cylinder optical research engine. Test fuel 'a' produced more particulate matter than fuel 'b', despite the fact that fuel 'a' lower aromatic content of fuel, distillation temperatures, sulfur content, and density; all factors which they expected to reduce particulate emissions. Test fuel 'a' contained 50 to 70 % more branched hydrocarbons, and twice amount of naphthenes. They concluded that a chemical effect of the branched structures in the paraffin fraction and naphthenes was likely to have influenced the PM emissions. Further work by Takatori et al. (1998) used isomers of

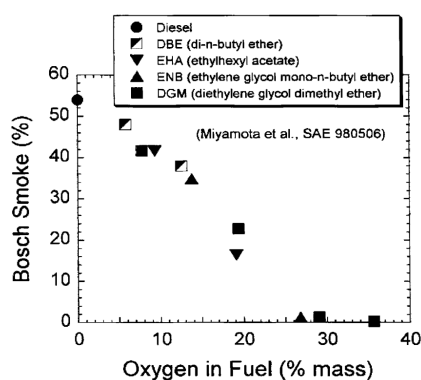


Figure 2.8: Measured soot emissions from a diesel engine with oxygenate addition to the fuel (Miyamoto et al., 1998).

hexane and octane in a tube reactor in the temperature range of 1000 to 1300K, to determine the sooting tendencies of the molecules. The order of sooting tendency was determined to be n-paraffin < 1-branched paraffin < 2-branched paraffin < cycloparaffin.

For further information on the effects of structural isomerism on soot formation, the reader is referred to Chapter 5, which summarises literature and experimental results relating to isomers of butane.

Oxygenates

It has been demonstrated that oxygenated fuels can be used to reduce soot emissions from diesel engines. For example, Miyamoto et al. (1998) showed that soot emissions from diesel engines were reduced when oxygenated molecules were blended with regular diesel fuel. The oxygenate molecules tested were: diethylene glycol dimethyl ether and di-*n*-butyl ether, which contained ether groups (-O-); ethylene glycol mono-*n*-butyl ether, which contained an ether and an alcohol group (-O- and -OH); and ethylhexyl acetate, which contained an acetate group (-O(C=O)-). The amount of soot reduction depended on the percentage oxygen in the fuel blend, and each of the molecules tested were all approximately equally effective at reducing the soot emissions (in terms of percentage oxygen added to the fuel), see Figure 2.8. Based on their smoke meter measurements, particulate emissions decreased in a linear manner, and when the oxygen in the fuel reached 25 to 30% by mass virtually all particulate emissions had been reduced to zero. Similarly, Tsurutani et al. (1995) found that oxygenates reduced particulate emissions, particularly the soot component exhaust PM, and observed that the PM emissions seemed to be more affected by the oxygen content, rather than by its molecular structure, boiling point and cetane number.

It was believed for some years that only the amount of oxygen added to the fuel, and not the type of oxygenated molecule (e.g. alcohol, ester, ketone, etc.), influenced the reduction, and the work by Miyamoto et al. (1998) was widely cited as evidence. Cheng (2002) plotted the results of a number of studies that reported numerical data

on the influence of oxygenate addition to diesel on PM emissions, and there was a broad correlation with oxygen content. However, a number of other experimental results do indicate that different types of oxygenated molecules influence PM emissions to differing extents. Earlier work by Miyamoto et al. (1996) investigated eight types of oxygenated molecule, and although particulate emissions decreased linearly with every fuel, there did appear to be small differences between the different oxygenated fuels. In particular, the reduction in PM emission tended to be greater for lower boiling point oxygenates. Similarly, McCormick et al. (1997) found differences between the ability of oxygenated molecules to reduce particulate emissions. They studied the particulate emissions from heavy-duty diesel engines, using blends of the oxygenated molecules octanol, methyl soyate, and decanoic acid added into diesel fuel to 1 or 2 % of oxygen by mass. Emissions were measured during the hot-start portion of the U.S. heavy-duty transient test, in both a 2-stroke and 4-stroke engine. It was shown that 1 % blends of octanol, methyl soyate, and decanoic acid resulted in a PM emissions reductions of 17.2 %, 15.4 % and 12.7 %, respectively. Whilst, 2 % blends of octanol and methyl soyate reduced PM emissions by 11.6 % and 20.4 %, respectively (McCormick et al., 1997).

Theoretical work also supports the notion that molecules with different oxygenate functional groups should influence soot formation to differing extents, and that some oxygenated molecules use their oxygen more efficiently than others to reduce soot formation. Kinetic modelling by Westbrook et al. (2006) indicates that the structure of the oxygenate molecule is important in determining the ability of oxygen to prevent soot formation, which is particularly in the case of the ester moiety. The ester functional group contains two oxygen atoms bonded to a single carbon atom, the modelling predicted that under conditions where the ester moiety directly produces CO₂, the oxygen is therefore less efficient at preventing soot formation from the pool of carbon atoms available to produce soot. Detailed kinetic modelling, supported by experimental work that utilised radiocarbon (¹⁴C) to track the conversion of specific carbon atoms to soot, indicated that in the ester moieties of di-butyl maleate, 30 % of the oxygen is effectively ‘wasted’ due to direct CO₂ formation (Mueller et al., 2003; Buchholz et al., 2004). In addition the reader is referred to the results of Chapter 7 which show that for ester (R-CO₂-R’) and acid (-COOH) functional groups, the carbon atom which is directly attached to the functional group was not found to form soot.

In the literature, ethanol has received a lot of attention due to it being a renewable fuel that contains oxygen, and its potential to reduce particulate emissions in diesel blends has been explored extensively. The energy content of ethanol-diesel blends decreases by 2 % for each 5 % volume of ethanol added; and an increase in fuel consumption of approximately equivalent to the reduction in energy content of the fuel can be expected when using ethanoldiesel blends (Hansen et al., 2005). A number of compression-ignition engine tests have been reported which have confirmed that blending ethanol into diesel significantly reduces PM emission (see for example Kass et al., 2001; Cheng et al., 2002; Schaus et al., 2000). The results of Kass et al. (2001), for example,

showed that diesel fuel blends of 10 to 15 % volume resulted in a reduction of particulate emissions by 20 % and 30 % respectively; however, despite lowering PM emission, and having no noticeable influence on NO_x emissions, there were small increases of CO and HC (of 140 % and 175 % respectively, compared to the reference diesel). It was shown in an isotopic tracer study by Buchholz et al. (2002), diesel engine combustion of an ethanol-in-diesel blend containing 5.7 % (by carbon mass) ethanol, only 2.4 % carbon mass of the PM was derived from the ethanol component; i.e. the mass fraction of carbon derived from ethanol in the PM was only 42 % of the carbon mass fraction that the ethanol accounted for in the fuel. Therefore, it appears that at least in part, the reduction in PM emissions by blending ethanol with conventional diesel fuel would appear to be due to a direct reduction in the conversion of ethanol to PM relative to the non-oxygenated diesel fuel.

Overall, the literature shows that oxygenated diesel blends invariably result in a reduction in PM emissions from diesel engines, with only little or no changes in NO_x emissions. One explanation for the reduced levels of soot formation from oxygenated fuels, is due to changes in the soot structure and morphology. Song et al. (2006) investigated the effect of fuel composition on the structure and reactivity of soot, they showed that soot derived from neat biodiesel fuel was far more reactive to oxidation than a neat Fischer-Tropsch fuel. This was explained as due to the incorporation of surface oxygen functionality in the soot formed from the oxygenated biodiesel fuel, the surface oxygen groups could induce changes during attack by air, which resulted in more rapid oxidation.

2.3 Strategies to reduce particulate emissions

As it was discussed in the introduction, increasingly stringent emissions legislation is motivating a number of strategies to reduce particulate and other emissions. The vision is to engineer practical combustion systems that do not emit soot at all. The work undertaken in this thesis seeks to better understand the fundamentals of particulate formation from fuels of different molecular structures, with the ultimate aim of improving the composition of the fuel to yield cleaner burning properties. There are other popular strategies to reduce particulate emissions, which include the use of exhaust after-treatment technologies, development of alternative low-emission combustion regimes, and the addition of additives to fuels. Each strategy is reviewed in this section.

2.3.1 Diesel exhaust after treatment technologies

Polluting emissions emanating from combustion processes and present in the exhaust may be converted to less harmful products after they have been formed using exhaust treatment technologies. For diesel engines, emissions of CO and hydrocarbons are relatively low and most efforts focus on reducing particulate and NO_x emissions. Since these

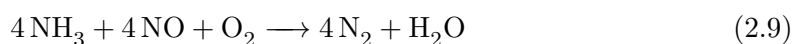
emissions are subject to trade-offs (see section 2.3.4, and Figure 2.10), it is instructive to discuss both particulate and NOx emission reduction technologies.

There are three classes of diesel particulate filter (DPF): (i) non-catalytic filter based systems; (ii) catalytic filters that consist of filters with a catalytic coating; (iii) non-filter based catalytic systems. Particulate filters are commonly referred to as ‘particulate traps’. The so-called wall flow monolith type is the most commonly applied, and is based on a simple method of filtering particulates from exhaust gas. The filters are comprised of a ceramic structure (e.g. cordierite) with parallel channels. Half of the channels are blocked with ceramic plugs at the upstream end in a checkerboard arrangement, and the opposite half are blocked at the downstream end, Figure 2.9 shows a schematic representation. The particulates are therefore forced to flow through the porous walls of the filter where they deposit (Neeft et al., 1996). The filtration efficiency of the DPF is dependent on the wall thickness and the pore size, which are typically between 0.3 and 0.6 mm, and 10 to 40 μm respectively. Despite the relatively large pore size (10 to 40 μm) the trap is able to retain smaller particles by thermophoresis, which causes the particles to deposit onto the filter walls.

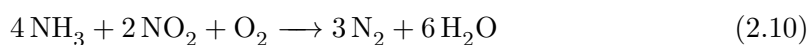
Whilst diesel particulate filters are effective at limiting particulate exhaust emissions, there is evidence that the secondary combustion of particulates in DPFs can give rise to the formation of new pollutants. For example, Heeb et al. (2008) studied the secondary combustion of particulates and PAHs in a monolithic, wall flow cordierite DPF. Emission of a number of 4–6 ring PAHs were reduced by 40–90%, and detoxified particulates in terms of total aryl hydrocarbons. However, 1– and 2–nitronphtalene increased by 20–100%, additionally, 9-nitrophenanthracene and 9-nitroanthracene were only detected after the DPF (Heeb et al., 2008).

Electrostatic precipitation of particulates is an alternative method that has been proposed to collect particles. For example, corona discharge can be used to charge the particles and increase their agglomeration rate. Agglomerated particles larger than 1 μm can then be removed by means of a cyclone (Kittelson et al., 1991). This method has not been applied in practice presumably due to the high voltages required, additional fuel requirement needed to power a corona discharge, and the need to regularly empty the cyclone (especially in vehicle-borne applications).

Selective Catalytic Reduction (SCR), is widely used to reduce NOx emissions from heavy-duty diesel engines (Koebel et al., 2000). SCR is based on the addition of ammonia to the NOx-containing exhaust gas, which react in the presence of a selective catalyst (e.g. $\text{TiO}_2\text{-WO}_3\text{-V}_2\text{O}_5$) to form water and nitrogen. NOx in diesel exhaust is usually composed of NO (>90%) and NO_2 and react by the following schemes:



and



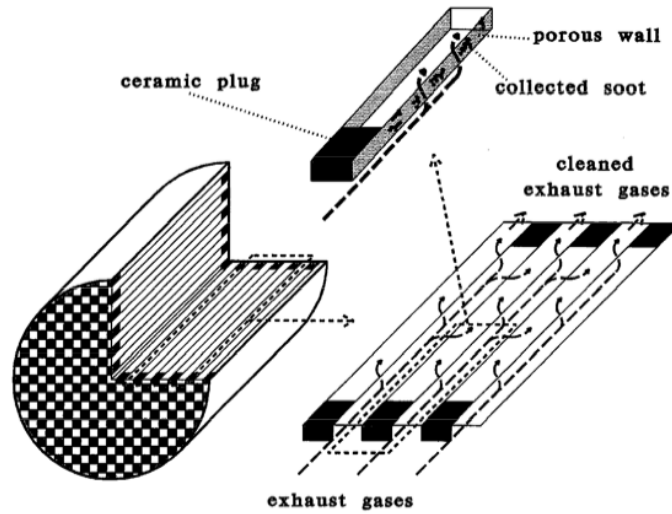


Figure 2.9: Diesel particulate trap. Reproduced with permission of the publisher (Elsevier).

In mobile SCR applications, urea (marketed as AdBlue) is generally used instead of ammonia for safety and toxicity reasons, and the urea solution decomposes to ammonia when it is atomised into the hot exhaust gas. The advantage of SCR is that it is applicable to diesel engine exhaust which contains significant quantities of O_2 (unlike three-way catalysts).

2.3.2 Fuel additives

The hardware-based emissions technologies that have been discussed so far can be expensive to implement, with emission reduction technologies accounting for around 10% of the cost of a new light-duty diesel vehicle (ICCT, 2012). Fuel-based solutions could offer an economical alternative whilst improving emissions from older vehicles without the need for retrofitting hardware technologies. Fuel additives are routinely added to fuels to improve a number of characteristics such as lubricity, freezing point, anti-foaming properties, anti-knock, and emissions. A number of additives have been shown to suppress particulate emissions from diesel engines, including: metallic, organometallic, and non-metallic compounds.

Metal-based additives can reduce particulate emissions by two mechanisms: (i) reaction with water to produce OH radicals which oxidise soot, or (ii) lowering the oxidation temperature of soot by direct reaction with carbon. It has been described in the previous section that diesel particulate filters are a ubiquitous technology used for the reduction of tailpipe particulate emissions, but over time these filters can become obstructed by carbonaceous deposits. Regeneration of particulate filters to remove accumulated particulate requires temperatures of $550 - 600^\circ\text{C}$ and 5% oxygen concentration in the exhaust gas, which can make *in situ* regeneration impractical without catalysis. A variety of transition and noble metals have been shown to reduce the oxidation

temperature of soot, for example, organometallic compounds based on Cu, Mn, and Ce have been shown to reduce the ignition temperature of particulates to around 150°C. Therefore, catalytic regeneration of particulate filters is commonplace and deployed in the form of either a fuel additive or filter surface coating. Ce compounds are reported to be the most effective and non-toxic (Simon, 1986).

The emission of PAHs is unregulated, but is important due to their mutagenicity, which has been discussed previously in Chapter 1. It was shown by Matter and Siegmann (1997) that the addition of 400 mg/kg of Manganese-based additive to diesel fuel reduced particulate and PAH emissions by 32%, indicating that Mn catalyses particulate and PAH oxidation. However, the fraction of particulates smaller than 50 nm did increase, but no elemental carbon or PAHs were detectable in this fraction, instead it was mainly comprised of metal oxides stemming from the additive. Similarly, a commercial diesel additive Envirox contains nanoparticles of cerium oxide (CeO₂), and has been shown to increase fuel efficiency (due to reducing of filter back-pressure) and to reduce CO₂, CO, various PAHs, and total particulate mass emissions (Zhang et al., 2013a). Zhang et al. (2013a) pointed out that reduced particulate mass concentrations does not necessarily equate to a reduction in the toxicity of the emitted particles. They showed that the use of Envirox results in higher number concentrations of smaller diameter particulates, which could possibly be more damaging for human health. The deployment of fuel additives therefore raises important health questions, and further investigations are required to comprehensively characterise emissions from additised fuels and to carry out accurate risks/ benefits analysis.

Addition of oxygenates to fossil fuels has been studied intensively. It has been found that the combustion characteristics of oxygenated fuels depend on the molecular structure and the amount of oxygen present in the spray core. Coda Zabetta et al. (2006) showed that particulate emissions from seed-derived oil and blends with fossil diesel could lower the ignition temperature of particulates, thereby aiding particulate trap regeneration. Additional benefits are associated with the use of some oxygenated additives (including ethanol and N-octyl nitramine), which form a lubricating film that reduces wear.

Emulsions of water-in-diesel, usually stabilised by a surfactant or emulsifier, have been shown to significantly reduce particulate matter and NO_x emissions from diesel engines in addition to improving combustion efficiency (Abu-Zaid, 2004). Typically, the percentage reduction in soot emissions is higher than for NO_x, and the reduction in soot emissions is usually around twice the percentage mass of the water-in-fuel. Water-in-diesel emulsions result in longer ignition delays which increase the premixed burn fraction and reduce soot formation; in addition, longer spray lift-off lengths increase the amount of oxygen that is entrained into the jet, creating leaner spray-core conditions (Song et al., 2000). Aquazole is an example of a commercial diesel-water emulsion that was marketed by Elf in the 1990s, but was later withdrawn due to its instability (the emulsion had a lifetime of ~ 3 weeks) (Barnaud et al., 2000).

2.3.3 Optimisation of the fuel composition

A large amount of experimental and modelling research has been conducted with the aim of exploring how the molecular structure of a fuel influences its combustion characteristics and emissions formation. It is well known that the molecular structure of a fuel directly influences its fate during combustion or pyrolysis (Ladommatos et al., 1996; Botero et al., 2014; Ruiz et al., 2007a), and the reader is referred to Chapter 5, which gives a detailed analysis of the how molecular functional groups influence soot formation under well-controlled formation conditions. In practical systems, such as a gasoline or diesel engine, soot formation is complex, because not only chemical effects influence combustion and soot formation but physical properties also play an important role (Leach et al., 2013; Schönborn et al., 2009a). Due to the fact that in engines it is difficult to observe how molecular structure affects local temperature, local equivalence ratio, and so on, most engine experiments focus on how the fuel influences exhaust particulates concentration.

One of the main effects of fuel composition that influences the formation of particulates in diesel combustion is the presence of oxygen in the fuel. As the oxygen content of a fuel is increased the particulate mass emissions are reduced, and can also improve or maintain other regulated emissions such as NO_x, CO, CO₂, and unburned hydrocarbons (Cheng et al., 2002). Significantly, it appears that when the percentage mass of oxygen in the fuel is increased to 27-35%, near complete elimination of soot is observed. Some studies show that particulate emissions decrease in a linear way with increasing oxygen mass in the fuel, independent of the identity of the structure of the oxygenate functional group. However, other research shows that the ability to reduce PM emissions is different for the various oxygenate functional groups, with the molecular structure of oxygenated groups being identified as being responsible for these differences (Buchholz et al., 2004; Mueller et al., 2003; Eveleigh et al., 2014). The reader is referred to Section 2.2.8 above for further information on the influence of oxygenated molecules on diesel engine PM emissions.

The understanding of how molecular structure influences combustion and particulate formation is likely to become particularly useful for developing cleaner burning bio-fuels. The industrial-scale production of bio-ethanol by the fermentation of sugars is a process that has been carried out for decades for the purpose of fuel production (Rosillo-Calle and Walter, 2006). Bio-diesel production by the transesterification of biologically derived triglycerides to fatty acid esters is another common route to biofuel production, where the molecular structure of such fatty acid esters may be influenced by the feedstock used or the synthetic pathway (Schönborn et al., 2009a). Understanding how fuel molecular structure impacts on combustion and particulate formation can be used to inform improvements to fuel production. An example of how this can be achieved in practice is given in a publication by Hellier et al. (2013a). Hellier et al. showed the combustion characteristics of four different terpine molecules, which could potentially be produced from cyanobacteria. The terpinenes were all molecules that could

be derived by means of metabolic engineering from geraniol, the most abundant and easily produced terpene in cyanobacteria. The combustion characteristics were assessed in a diesel and spark ignition engine, and the terpenes were tested as single-component fuels and blended with diesel. One significant finding was that single component fuels geraniol and farnesene were found to combust well in a diesel engine, and were suitable for blending with fossil diesel fuel up to 20% (wt./wt.). The exploration of such novel biofuel production methods that investigate new synthetic pathways are still in their infancy but have potential to greatly improve the overall viability and efficiency of some fuel production routes.

2.3.4 Optimisation of combustion conditions

Diesel engine NO_x and soot formation are known to depend heavily on both temperature and fuel-air equivalence ratio. Figure 2.10 shows a typical ϕ - T contour plot, of the type first introduced by Kamimoto and Bae (1988), which shows the engine equivalence ratio and temperature conditions that give rise to high levels of soot and NO. The soot contours are shown in terms yield of soot as a percentage of the fuel carbon, this analysis shows that soot may be avoided at either: low temperatures (<1500 K), high temperatures (>2500 K), or low fuel-to-air equivalence ratios and lower temperatures ($\phi < 2$, and <2200 K). Soot formation may be avoided at high temperatures due to an increase in the rate of soot oxidation; although this has not been demonstrated in an engine, and support for this is only through results obtained by modelling and in premixed shock-tubes, and may not apply in diesel-like fuel jets (Tree and Svensson, 2007). The region of high NO_x formation is at high temperatures and low equivalence ratios (bottom right of the plot, Figure 2.10). The majority of the NO_x emissions from a diesel engine is in the form of nitric oxide (NO), and is formed by the oxidation of atmospheric nitrogen (N₂) via the *thermal* or *Zeldovich* mechanism, as follows Bowman (1975):



The reaction of nitrogen with OH radicals was also suggested to contribute, particularly at near stoichiometric and fuel-rich conditions Lavoie et al. (1970):



Equation (2.11) above is the rate limiting step in the formation of NO, and is strongly temperature dependent; therefore, the amount of NO formed in diesel engines is largely determined by peak combustion temperatures and availability of O₂. Under fuel-rich conditions, NO is reduced to N₂, which means that NO emissions are reduced with increasing equivalence ratio. In a diesel combustion jet (see Figure 2.7 for schematic),

the centre of the jet is at the conditions of the high soot contours in Figure 2.7, whilst the flame envelope surrounding the fuel spray is at the conditions of high NO formation.

It can be seen that for the reasons described above, combustion conditions that lower NO_x emissions generally tend to increase PM levels and *vice versa*, the NO_x-PM tradeoff makes it difficult to simultaneously reduce both emissions from engines. In conventional (current) DI diesel engines there are high levels of soot and high NO_x formation. However, low temperature flameless combustion regimes have received a lot of attention in the literature due to the possibility of simultaneous reductions of NO_x and particulate emissions (Gan et al., 2011). In homogenous combustion strategies combustion occurs in a similar way to the premixed burn phase in a direct injection compression ignition engine (DICI), and soot is not formed when the mixture is sufficiently lean. Low temperature homogenous charge compression ignition (HCCI) is an approach to eliminate both soot and NO_x formation, where fuel is injected into the air intake plenum allowing the homogenous mixing of fuel and air mixture before compression ignition. Another strategy is termed premixed charge compression ignition (PCCI), where the in-cylinder fuel injection timing occurs either early or late in the cycle in order to promote the local mixing of the spray with air (Tree and Svensson, 2007). Both HCCI and PCCI are flameless and occur at low temperature to avoid soot and NO_x. Tree and Svensson (2007) point out that reducing residence time required for soot formation and mixing fuel with the air are competing variables in a low-temperature system. Therefore there is also a need to explore the role of the fuel molecular structure, which may influence the residence times required to form soot. For example, a volatile fuel, but resistant to soot formation, could be a favorable fuel for PCCI/HCCI combustion, although other requirements apply also (i.e. resistance to early ignition, slower premixed combustion).

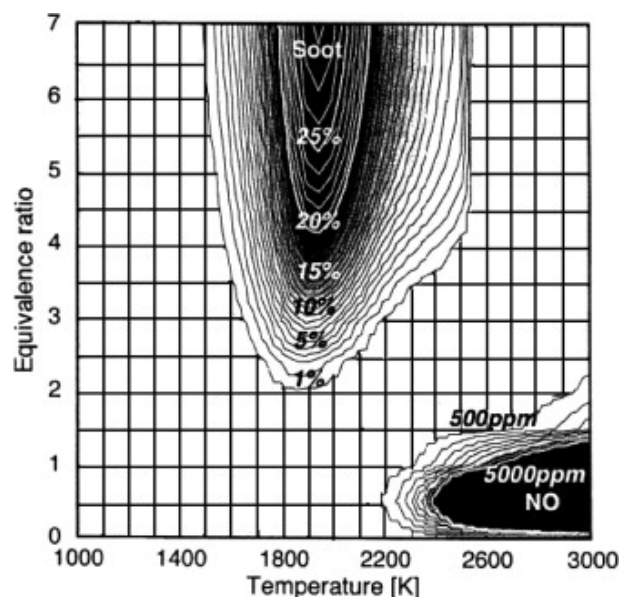


Figure 2.10: A generic contour plot showing the regions of soot and NO formation as a function of the local formation conditions. Reprinted from (Gan et al., 2011), used with permission of the publisher (Elsevier).

2.4 The use of isotopic tracers in pyrolysis and combustion research

The isotopic ratios of a number of elements are routinely measured by isotope ratio mass spectrometry (IRMS), including carbon ($^{13}\text{C}/^{12}\text{C}$), nitrogen ($^{15}\text{N}/^{14}\text{N}$), oxygen ($^{18}\text{O}/^{16}\text{O}$), sulphur ($^{34}\text{S}/^{32}\text{S}$) and hydrogen ($\text{D}/^1\text{H}$). The ability to precisely measure the isotopic abundance of samples has a wide variety of applications, including: dating, metabolic pathway analysis, chemical mechanism analysis, geochemical tracer studies, and medical diagnostic tests. As an example of a routine medical application, a urea breath test is a standard method to diagnose individuals suspected of hosting *Helicobacter pylori* stomach infection; for this test the patient ingests urea labelled with ^{13}C . If the *Helicobacter pylori* is present in the gut, the bacteria metabolises the urea to CO_2 . As a result, CO_2 with enriched levels of ^{13}C is detectable in the breath of those suffering with the infection (Graham and Klein, 2000).

In a further and very relevant example, Oberdörster et al. (2004) investigated the *in vivo* translocation of inhaled ultrafine particles (UFPs) to the brain. Rats were exposed to ultrafine particles composed of ^{13}C (generated by spark discharge of a ^{13}C graphite rod), at a concentration of $160 \mu\text{g}/\text{m}^3$ for a period of 6 hours. The lungs, cerebrum, cerebellum and olfactory bulbs were removed at 1, 3, 5 and 7 days following exposure, and ^{13}C concentrations in the organs were determined by means of IRMS. Using ^{13}C as a tracer, it was shown that at one day after exposure to ^{13}C containing UFPs, the mass of ^{13}C detected in the lung was significantly above background levels, and the ^{13}C level was found to decline over the 7 day period. Enhanced ^{13}C levels were

Box 2.1. Definitions and additional background information relating to isotopes of carbon

AMS, Accelerator mass spectrometry.

Isotope, variants of particular chemical element that differ in the number of neutrons, but have the same number of protons. E.g. ^{12}C , ^{13}C and ^{14}C are all *isotopes* of carbon.

IRMS, Isotope ratio mass spectrometry.

Isotopic fractionation, is a process which results in partitioning of a sample into two (or more) parts that have different isotopic compositions.

Isotopologue, is a molecule that is distinguishable by its isotopic composition, for example, a molecule of water with one hydrogen atom substituted for deuterium (HDO) is an *isotopologue*, distinct from $^1\text{H}_2\text{O}$.

Nuclide, is the term used to refer to a specific type of atom, with a specified number of protons and neutrons, e.g. $^{14}_7\text{C}$.

In nature there are three isotopes of carbon, these are ^{12}C , ^{13}C and ^{14}C , and their natural abundances are around 98.89%, 1.11% and 0.0000000001% respectively. The atomic nucleus of ^{12}C is comprised of six protons and six neutrons, ^{13}C and ^{14}C are composed the same number of protons, but contain seven and eight neutrons respectively. ^{12}C and ^{13}C are both stable isotopes, which means that they do not undergo radioactive decay. ^{14}C , however, is a radioactive nuclide and undergoes radioactive beta decay, a process where a neutron decays to a proton, therefore yielding the stable isotope of nitrogen (^{14}N) and emitting an electron and an antineutrino. ^{14}C decays with a half life of 5730 years; the half-life is the time taken for the radioactivity of a sample to fall to half of its original value. Despite these differences, the isotopes are practically identical in terms of their chemistry, particularly at high temperatures.

subsequently detectable in the cerebrum, cerebellum and olfactory bulbs, demonstrating the translocation of UFPs to the brain.

Despite the evident widespread application of isotope labelling techniques in physiology and more generally, they have not been widely used as diagnostic tools in combustion and pyrolysis research. A relatively small number of studies have been found in the literature, and these usually involve the tracing of isotopes of carbon (either the stable isotope ^{13}C or radioactive ^{14}C) from the fuel, oil, or additive to the combustion products, including CO, CO₂ and particulate matter. A literature survey of those studies involving isotope tracing that have been applied in the field of combustion is summarised below, the reader is also referred to Box 2.1 which provides some definitions and additional background information relating to carbon isotopes.

The earliest example identified of the use of isotope labelling in combustion was by Ferguson (1957), and used a ^{13}C labelling technique. The aim of the study was to identify whether a two-carbon fragment of propane was responsible for soot formation during propane combustion. It was initially put forward that fragmentation of propane

during combustion could result in scission of a carbon atom from the end of the three-carbon propane chain, therefore leaving a two carbon atom fragment to form soot by a mechanism involving acetylene as an intermediate. If this were the case, then the central carbon atom would preferentially be converted to soot with respect to the two carbon atoms at the ends of the chain. Combustion of propane in a combustion vessel was carried out, and soot and CO₂ samples were collected for isotope ratio analysis, by means of mass spectrometry. Propane was labelled at its central carbon with ¹³C, and two test samples were combusted with levels of enrichment at ~21 and ~62 mole percent. Analysis of the ¹³C/¹²C ratios indicated that the three carbon atoms contributed equally to soot formation. Prior to the work reported in this thesis, Ferguson's research is the only example identified in literature that employs ¹³C as a tracer with application to the bulk analysis particulate matter.

The majority of articles in the literature involve the use of ¹⁴C as a tracer, and two different detection methods have been used for detecting ¹⁴C. Due to the fact that ¹⁴C is radioactive, one detection method involved counting the rate of decay of a sample as a measure of the ¹⁴C/C rate in the sample; the second method involved counting individual ¹⁴C atoms. Lieb and Roblee Jr (1970) published work that described a ¹⁴C tagging experiment, which used decay counting to quantify the conversion of carbon atoms in ethanol to soot. In turn, ethanol-1-¹⁴C (where the carbon atom next to the hydroxyl group was ¹⁴C labelled) and ethanol-2-¹⁴C (where the methyl carbon contained ¹⁴C) were combusted in a diffusion flame and soot was extracted from the flame using a probe. It was concluded that the methyl carbon contributed the majority of carbon to the soot, and a conversion ratio of 2:1, methyl-to-hydroxyl carbon was identified. Expanding on this work, Schmieder (1985) investigated a wider range of hydrocarbons specifically labelled with ¹⁴C, to determine the carbon atom conversion probability to soot in a diffusion flame. Schmieder used the decay counting method, and employed a scintillation counter to measure the rate of decay. Toluene, benzoic acid, and 1-butanol were assessed in terms of carbon conversion to soot. Additionally, benzene and cycloheptane were tested, and in these molecules each of the carbon atoms is in a chemically equivalent environment, that is to say that due to the symmetry of the molecules all of the carbon atoms are 'the same'. It was found that the level of ¹⁴C enrichment of the fuel for benzene and cycloheptane mirrored the enrichment in the PM derived from those fuels, thereby verifying the effectiveness of the method. Similar work, using the decay counting technique has also been reported by Sorek et al. (1984); Sorek and Anderson (1986).

The disadvantage of using decay counting as a technique is that it is inefficient at detecting small changes in the ¹⁴C abundance. Short-lived radioisotopes can be efficiently detected by decay counting, but longer-lived radioisotopes are not, and ¹⁴C has a half-life of 5730 years. During the time available to carry out an experiment only a small number of the ¹⁴C atoms will decay; Buchholz et al. (2002) point out that in order to measure 0.1% of the decay of a sample containing ¹⁴C, it would require uninterrupted

sampling for 8.3 years. In order to compensate for the poor sensitivity at low levels of ^{14}C enrichment, relatively high concentrations of molecules with enriched levels of ^{14}C are required to improve resolution of the decay counting method. As a result, large quantities of ^{14}C containing molecules must be synthesised or acquired from commercial suppliers in order to carry out these investigations, and doing so can be prohibitively expensive. Furthermore, due to the high levels of ^{14}C required, precautionary measures must be implemented to work with materials that have levels of radioactivity in excess of the natural background, and disposal of the radioactive waste that is produced is a further restriction of the use of the technique.

The second isotope ratio measurement technique that has been used to measure ^{14}C abundance is accelerator mass spectrometry (AMS). AMS is a highly sensitive technique which involves the counting individual nuclei, rather than relying on radioactive decay. AMS was developed during the 1970s for the purpose of carbon dating, which has been used extensively in the earth sciences and archaeology. Due to the fact that AMS is much more sensitive, Buchholz et al. (2002) introduced a tracer method which does not require enriching a test sample with molecules that are artificially enriched with ^{14}C . Instead, the method relies on the natural variation of ^{14}C rate in different sources, to trace a specific component through combustion. ^{14}C is formed in the atmosphere, and occurs when cosmic rays collide with nitrogen. The newly formed carbon-14 is quickly oxidised to CO_2 , where it enters the carbon cycle and therefore becomes incorporated into plants and animals, this means that living things are composed of about 1.2 parts of ^{14}C per 10^{12} C atoms. Biologically derived fuels are formed from processes that incorporate atmospheric CO_2 , and as a result contain atmospheric levels of radiocarbon. Fossil fuels, however, are essentially ^{14}C free since they have been isolated underground for >60,000 years, a period of >10 half-lives. The relative absence of ^{14}C in fossil fuels means that there is a very low ^{14}C background, and bio-fuels have around three orders of magnitude more ^{14}C . This means that biofuels are naturally ^{14}C 'labelled' relative to fossil fuels. Buchholz et al. (2002) made use of this 'natural label' by adding biologically derived fuel to fossil fuel and the elevation of ^{14}C arising from the biofuel was sufficient to trace the fate of 'labelled' fuel through combustion to the emissions, using AMS as the detection method. In one investigation, 9.5 % bio-ethanol (v/v) was blended into fossil diesel using an emulsifier, the fuel was combusted in a diesel engine and the contribution of ethanol to PM, CO, and CO_2 was assessed (Buchholz et al., 2002). It was identified that the particulate was composed of only 2.4 % by carbon mass derived from the ethanol component, but ethanol constituted 5.7 % of the carbon mass in the fuel. This means that relative to fossil diesel, carbon atoms in ethanol were found to convert to particulate matter at a much lower rate. In addition, it was showed that of the particulate collected, which is comprised of a non-volatile organic fraction (NVOF) and an absorbed volatile organic fraction (VOF), carbon from the ethanol was more likely to end up in the VOF than the NVOF. Carbon from the ethanol comprised 3.4 % of the VOF.

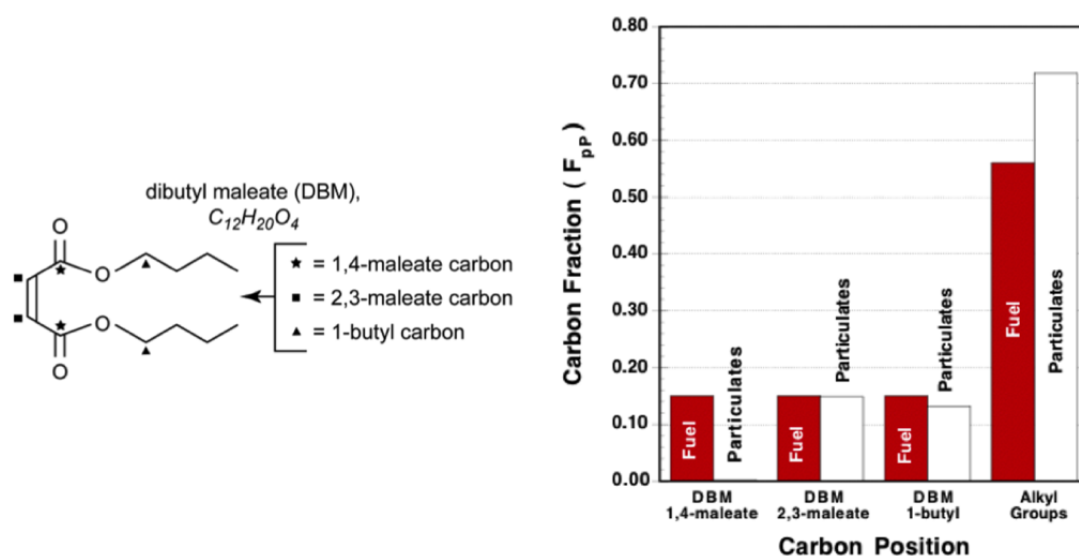


Figure 2.11: Molecular structure of dibutyl maleate (DBM) and positions of ^{14}C labels, and chart showing the relative contributions of the labelled positions to particulate. Reprinted from (Buchholz et al., 2004).

Further work by the same group, expanded the concept by using compounds synthetically enriched with ^{14}C at specific molecular positions to investigate the relative contribution of individual atoms within a molecule to PM (Buchholz et al., 2004). They selected dibutyl maleate (DBM), which has a number of interesting molecular features, such as a double bond, ester groups and alkyl chains. Specific carbon atoms involved in the various functional groups were selectively ^{14}C labelled at the positions indicated in Figure 2.11. Even though the investigation involved the addition of synthetically enriched ^{14}C molecules, the level of enrichment did not exceed the natural abundance range, and therefore was not 'radioactive'. The isotopologues of DBM were combusted in turn in a diesel engine and their relative conversion rates to both the NVOF and VOF fractions of exhaust PM and in-cylinder deposits were assessed. Figure 2.11 shows the fraction of carbon in the initial fuel at the indicated molecular locations, and the fraction carbon in the PM derived from those locations. Significantly, it was shown that the carbon atom attached to the two oxygen atoms (1,4-maleate position) in DBM did not contribute to PM emissions or in-cylinder deposits. It was also found that doubly bonded carbon (2,3-maleate carbon) did not contribute more than the average carbon atom in the DBM molecule to the NVOF and VOF emissions; higher levels of conversion might have been expected, since numerical simulations indicated that double bonded carbons would be more prone to forming acetylene and subsequently PM.

The ability to track the contribution of a labelled component in the fuel to a combustion product has also proved useful for quantifying the extent of engine oil contribution to particulate emissions, which may only be possible using isotope tracing. Mayer et al. (1980) developed a technique based on ^{14}C labelling to identify conversion

of engine oil to particulate. Using the same technique, Hilden and Mayer (1984) published further work on the contribution of engine oil; they examined the contribution of the oil to total particulate emissions and soluble fraction of the particulate, carried out in a range of light-duty diesel engines and using a range of oil formulations. They identified that the oil contributed in the range of 7 – 14% of the total particulate emissions. Between 14 and 26% of the total particulate mass in the exhaust was extractable by solvent extraction, of which between 30 and 50% of the extractable fraction was derived from the engine oil. They showed that, generally, there were only minor effects of engine design and oil formulation on the observed oil contribution to PM. The fact that the majority of the oil derived contribution to PM was in the solvent extractable fraction demonstrated that the engine oil had little to do with the early formation and growth process of soot particles. This indicates that the oil does not undergo pyrolysis to the point that it is available to be incorporated into nascent particles. It was recognised that the oil adsorption onto the particle surface could occur in the exhaust, or even as an artifact of filter-based particulate sample collection as oil vapor passes through the filter.

Using the more efficient AMS detection method Buchholz et al. (2003) investigated the contribution of engine oil to PM in a direct injection diesel engine run on 100 per cent biofuel (with natural ^{14}C levels) and conventional lubrication oil (^{14}C depleted). They estimated the oil contribution based on the depression in the ^{14}C level in the soot with respect to the biofuel, since the engine oil was derived from fossil sources with ^{14}C levels three orders of magnitude lower than the biofuel. It was estimated that 4% of carbon in the non-volatile fraction of the particulate matter originated from the engine oil. In similar work, a group at the University of British Columbia, Jones et al. (2005) in collaboration with Buchholz published work that identified the sources of particulate emissions formed from a heavy-duty diesel engine fuelled by pilot-ignited natural gas.

The isotope tracer work discussed so far has focussed on how individual carbon atoms or whole molecules convert to particulate matter for the purpose of source apportionment. There is a smaller group of experiments have applied isotopic techniques in the literature that involved tracking various isotopes to other combustion-generated species. For instance, a series of experiments by Katoh and colleagues have applied a laser technique, which they called isotope shift/ planar laser induced fluorescence spectroscopy (IS/PLIF), to visualise the distribution of various isotopes in flames. For example, the OH radical species has a distinct excitation wavelength, which is different to its deuterated analogue OD. When steam produced from deuterated water is added to flames, OH radicals are formed by the dissociation of water (e.g. $\text{H}_2\text{O} \rightarrow \text{OH} + \text{H}$). Katoh demonstrated that it was possible to distinguish and visualise the difference between OH radicals formed by combustion reactions and those formed by dissociation from steam generated from deuterated water (Katoh et al., 2006c). This has given some useful insights into the observed behavior of steam addition to flames, which can be useful to suppress formation of NO_x. Other such examples published by the same research

group can be found in the following references (Katoh et al., 2006b; Kajimoto et al., 2013; Katoh et al., 2006a).

Lombaert et al. (2006) investigated whether the presence of PAHs in fuel promoted the formation of PAHs, that were identified in the particulate matter formed from a diesel engine. To assess the direct influence of naphthalene ($C_{10}H_8$) addition to fuel, deuterated naphthalene ($C_{10}D_8$) was added as a tracer at 1000ppm levels to the fuel. Particulate was collected from the exhaust onto a filter, and PAHs were removed from the particulate by solvent extraction. The solvent containing the PAHs was analysed by GC/MS in order to identify the presence of the PAHs and their deuterated equivalents. The presence of naphthalene did not have an appreciable influence on the total particulate mass, or quantity of the soluble fraction (which accounted for $\sim 14\%$ of total mass). Analysis of the mass spectra showed, somewhat surprisingly, that only deuterated and semi-deuterated pyrene and phenanthrene, and residual deuterated naphthalene were detectable in the soluble extract. It should be noted that this method (involving GC/MS) was only used to detect the presence of deuterated PAHs, but the method could not be used to quantify the amount detected.

In a related study Lea-Langton et al. (2013) used ^{13}C labelling to determine the pyrolysis products of a methylated-PAH, methylphenanthrene, which is present in diesel fuel. Methylphenanthrene was labelled on the methyl carbon atom with an isotopic enrichment at that location of 99%. Pyrolysis was carried out in a cell-flow reactor with helium as a carrier gas at temperatures of 800 and 900°C. Following pyrolysis, GC/MS was used to analyse the PAHs present in the effluent gas. Substantial amounts of unreacted 9- ^{13}C -methylphenanthrene were observed in the product gas, and the major product was found to be the parent PAH, phenanthrene (not containing ^{13}C), which confirmed that dealkylation is a dominant pyrolytic reaction. A number of other methylated-PAHs were detectable including 1- ^{13}C - and 2- ^{13}C -methylnaphthalenes, and the ^{13}C label was shown to reside in the methyl position, which suggested that re-alkylation of pyrolysis-formed PAHs occurred.

The usefulness of isotope tracing is clear, particularly for the purpose of source apportionment of particulates, for elucidating mechanistic details of PAH pyrolysis, and can provide valuable input and verification to computational models of particulate formation. From the literature reviewed in this section it has been shown that a range of isotope techniques have been exploited by a number of different research groups since the 1950s. Still, overall, only a relatively small number of investigations have been reported and no single method has emerged dominant. There are a number of factors that may have prevented isotope techniques being more widely used. Firstly, as it has already been discussed, ^{14}C tracing experiments are expensive to carry out if used at high enough levels of enrichment for decay counting to be used as a detection technique. Additionally at high enrichment levels safety issues relating to the use of radiocarbon need to be considered, the safety precautions can be both expensive and impractical to implement. The more recent implementation of ^{14}C tagging that has employed AMS detection has

greatly improved the economic and practical viability of such ^{14}C studies, especially as it reduces or eliminates the need to acquire ^{14}C enriched compounds. Globally there are a number of laboratories that have AMS capability, for instance in the UK there are 4 such facilities registered in a directory kept by the journal *Radiocarbon*, (*Radiocarbon*, 2014). However, the cost of AMS analysis itself, and acquiring even small quantities of site specifically enriched ^{14}C compounds, at low enrichment levels are still expensive to synthesise or source. The examples of ^{14}C labelling that have been discussed have generally been conducted at well-resourced national laboratories; for isotope labelling techniques to become more widely used in combustion science, both cost-effectiveness and availability of measuring equipment is essential.

The examples of ^{13}C labelling that have been discussed so far have used GC/MS as a detection technique. GC/MS is a sensitive analytical technique, but still requires significant levels of ^{13}C enrichment for detection and quantification, for example the investigation by Lea-Langton and colleagues used 99% ^{13}C enrichment at the specifically labelled site. Such high levels of enrichment are not particularly restrictive in some experiments, for example pyrolysis experiments carried out in a flow reactor can yield large quantities of particulates, and only require a few millilitres of fuel. However, to run a flame experiment or diesel engine for long enough to generate a sufficient quantity of sample for analysis requires significantly more fuel, since the majority of fuel is efficiently combusted to CO_2 . The high levels of ^{13}C enrichment required for GC/MS analysis is therefore likely to have been a factor preventing its use for the bulk analysis of PM for the purpose of source apportionment; although, it should be noted that due to the ‘survivability’ of compounds such as PAHs during pyrolysis, GC/MS can be used efficiently trace specific compounds in the fuel to specific components of the particulate (e.g. Lombaert et al., 2006).

The ^{13}C tagging technique detailed in this thesis, provides a practical alternative, which requires only low levels of ^{13}C enrichment, at volumes typically less than 0.2% v/v. Detection of ^{13}C by IRMS is much cheaper to conduct than AMS; AMS is generally 50 to 100 times more expensive than IRMS measurements (Eveleigh et al., 2014). The high precision of IRMS, and the technique itself (which reports relative differences between a sample of interest and a known standard reference material) make it suitable for tracer studies. The level of ^{13}C enrichment used in the experiments reported here do not exceed the range of natural abundance on Earth ($\sim 1\%$). The low levels of ^{13}C enrichment that have been used mean that the combustion experiments are cost-effective, but also give adequate resolution owing to the precision of IRMS. In any case, laboratories that measure ^{13}C abundances by IRMS are generally reluctant to measure samples highly enriched with ^{13}C , greatly in excess of natural abundance, since this would pose a risk of contamination to the highly sensitive equipment.

Broadly similar work that has employed IRMS was that of Corso and Brenna (Corso and Brenna, 1997; Corso et al., 1998; Corso and Brenna, 1999). They induced the fragmentation of a number of hydrocarbons in an open tube furnace, and determined

the isotopic composition of the resulting fragments by online GC/IRMS. For example, methyl palmitate and methyl palmitate-1- ^{13}C (labelled at the carboxyl position) were tested separately and the isotopic ratio of the carbon atom in the labelled position was determined in the both the unlabelled and labelled variant (Corso and Brenna, 1997). In doing so they demonstrated that they could accurately determine the ^{13}C composition at the specifically labelled position, since their calculated dilution of methyl palmitate-1- ^{13}C into its unlabelled equivalent was consistent with the measured and back-calculated value. It appears that the main aim of their work was to develop an automated instrument for the position-specific isotope analysis of carbon, and their work was published in more generalist analytical chemistry journals. It was not the aim of their work to express the isotopic data reported in terms of the conversion probability for a specific atom converting to a product such as soot, but rather as an absolute measure of the ^{13}C composition at a specific locality or fragment. These factors may have meant that the potential usefulness of the IRMS technique was not picked-up by the combustion community.

The relatively low cost of routine isotope measurements by IRMS, and the availability of off-the-shelf commercially provided ^{13}C labelled compounds, used at low levels of enrichment, thus provides a high-precision yet relatively economical means of tracking ^{13}C . This could mean that the use of ^{13}C labelling, as demonstrated in this thesis, could become more widely used as a diagnostic tool in combustion research.

2.5 Conclusions

The literature on the fundamentals of particulate formation shows that whilst many of the processes involved in soot formation have been described there is still much that is not fully understood. Particularly, the dependence of certain reaction pathways on the initial fuel and formation conditions appears to be an area that requires further work.

In the reviewed literature there are a number of commonly reported strategies to reduce particulate emissions. Reducing emissions by making improvements to the fuel blend has a number of distinct advantages, including:

- Can be implemented for the current fleet; and
- Does not require the fitting of expensive emissions technology;
- Many alternative fuels have been shown to drastically reduce emissions; and
- The possibility to engineer biofuels by metabolic engineering, or by making changes to the processing of fuels to yield cleaner burning characteristics.

Considering the literature on the use of isotopic tracers in combustion research the following conclusions may be drawn:

- The attempts of isotope tracing techniques in the past demonstrate their potential usefulness, particularly for the purpose of particulate source apportionment;

- However, isotope tracing has not become widely used in combustion, probably due a number of reasons including cost, practicality, safety surrounding use of radioactive materials, and access to measuring equipment;
- There is a need for a cost effective, practical, safe, method that utilises a ubiquitous measurement technique.
- Many of the investigations in the literature only apply the tracer technique to one or a few molecules, there is a need for more comprehensive investigations using a range of labelled compounds.

Therefore, it can be seen that understanding the fundamentals of how different molecular structures behave during combustion are important for exploring and informing how fuels might be better designed. In order for this to happen more experimental data is required in order to provide both phenomenological understanding of how the conversion process to soot occurs, and also supply input and comparison for numerical models. The usefulness of isotope tracing is apparent, for providing additional insights into how individual molecules or atoms convert to soot. The ^{13}C labelling technique that was developed and applied as part of the work presented in this thesis could therefore become a standard method for tracing a labelled hydrocarbon component in fuel to combustion products including PM, or indeed intermediate species.

Chapter 3

Experimental Systems and Methodology

This chapter describes the experimental apparatus and measuring equipment used to conduct the experiments carried out as part of this thesis. The flow reactor facility and the numerous associated components that are detailed in this chapter were designed, commissioned, assembled, and characterised as part of this work. Furthermore, the isotope technique applied to particulate matter is entirely novel and the methodology for processing samples and interpreting the isotopic data has been developed to support this technique. The development of the experimental rig and analytical methodology represent a substantial portion of the work presented herein.

3.1 Flow reactor facility

There have been a number of investigations into the combustion and emissions characteristics of both single-component fuels and fuel blends, many of these studies have been carried out in practical combustion systems such as spark-ignition or compression-ignition engines (Hellier et al., 2013b, 2011). Generally, the combustion characteristics of fuels are governed by the chemical composition of the fuel, and also its physical properties, such as volatility and viscosity. In order to investigate the chemical effect of fuels on emissions characteristics while limiting the influence physical properties, a number approaches have been used in the literature that employ well-controlled conditions: in flames (Botero et al., 2014), shock tubes (Noorani et al., 2010a; Yasunaga et al., 2012), rapid compression machines (Curran et al., 1998), jet stirred reactors (Dagaut et al., 2009; Togbé et al., 2010), plug flow reactors, and laminar flow reactors (Esarte et al., 2009; Peg et al., 2007; Roesler, 1998).

In this investigation, a laminar flow reactor facility has been developed in order to investigate the thermal decomposition products of a variety of liquid and gaseous fuels over a range of temperatures in both inert and oxygen-containing atmospheres. Pyrolysis was generally carried out in the temperature range of 1100 to 1450 °C in the tube reactor, and the resulting PM was collected. The conditions employed in the

tube reactor were intended to resemble, in a general sense, the conditions prevailing in the core of a diesel spray; where the conditions are oxygen-deficient and at high temperatures. High temperatures and fuel-rich conditions promote soot formation in diesel engines, the reader is referred to the discussion in Section 2.3.4 and particularly Figure 2.10. As opposed to diesel engines, however, there are several notable differences in the characteristics and composition of the particles formed in the reactor; the particles evolved from the reactor are principally composed of ‘dry’ soot. For further information on the distinction between the diesel particulate matter and the soot formed in the reactor, the reader is referred to Section 2.1.

The reactor was installed in Experiment room B.09 in the Thermodynamics Laboratory, within the Department of Mechanical Engineering at UCL. Figure 3.1 gives a schematic representation of the general setup. This consisted of a nitrogen carrier gas system (components 1–3), a gas and liquid fuel feed system (4–6), a static mixer (7), a tube reactor (9, 10), and sample collection and analysis systems (11–14). The following sections describe the various components of the flow reactor rig in more detail in terms of its design and characterisation. The description of the rig follows the route of the carrier gas and fuel through the system. Two fuel feed systems were developed for introducing either gaseous or liquid fuels, and for clarity these have been described separately in the following sections. The reader is also referred to Appendix A for images of the experimental setup.

3.1.1 Gas Feed System

Figure 3.2 shows a schematic of the setup used to meter and introduce gaseous fuels into the reactor. In all experiments oxygen-free nitrogen (supplied by BOC) was used as an inert carrier gas. The flow of nitrogen was metered by means of a mass flow controller (Bronkhorst EL BASE), which was monitored and controlled by a PC via an RS-232 connection. This type of mass flow controller meters the gas flow rate on a principle of heat transfer, and operates by sensing the temperature change of the gas in a heated section of capillary within the instrument (Jouwsma, 1993). After the nitrogen flow rate had been precisely metered the nitrogen then passed through a 750W air process heater (RS 200-2531), that heated the nitrogen up to a maximum temperature of 400°C. The temperature of the nitrogen that was heated by the process heater was controlled by a PID controller (Tempatron, TL4800, temperature controller), a type-K thermocouple (TC-1) was positioned immediately after the heater to provide feedback to the PID controller. As a safety feature, a flow switch was located upstream of the process heater in order to cut power to the heater in case an insufficient flow of nitrogen was detected, which may otherwise have caused damage to the heater. Downstream of the process heater the nitrogen flow passed through a check-valve (Swagelok, SS-58S12), which was positioned directly after the heater in order to prevent the reverse flow of flammable gasses into the heater.

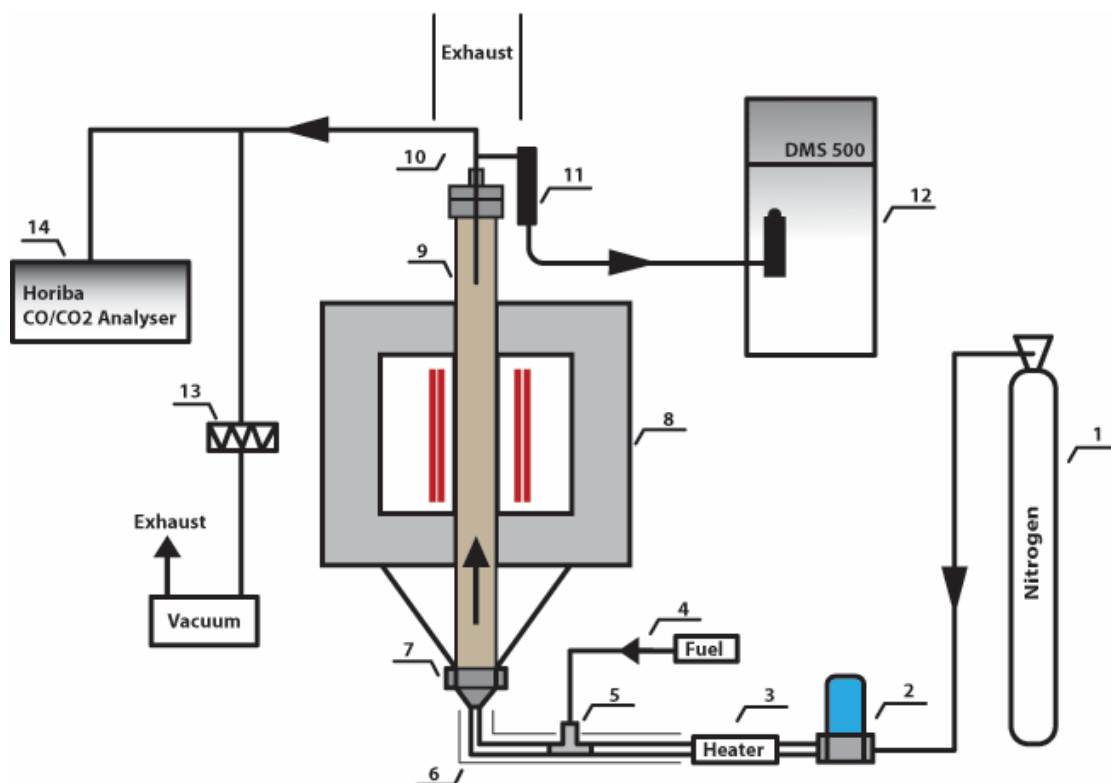


Figure 3.1: Flow reactor general schematic. (1) Nitrogen carrier gas cylinder. (2) Nitrogen mass flow controller. (3) Air process heater. (4) Fuel feed system. (5) Vaporiser. (6) Heated and insulated section. (7) Static mixer. (8) Nabertherm high-temperature electric oven. (9) Alumina reactor tube. (10) Stainless steel sample tube. (11) Remote dilution cyclone. (12) DMS500 instrument. (13) Filter housing. (14) Horiba exhaust gas analyser

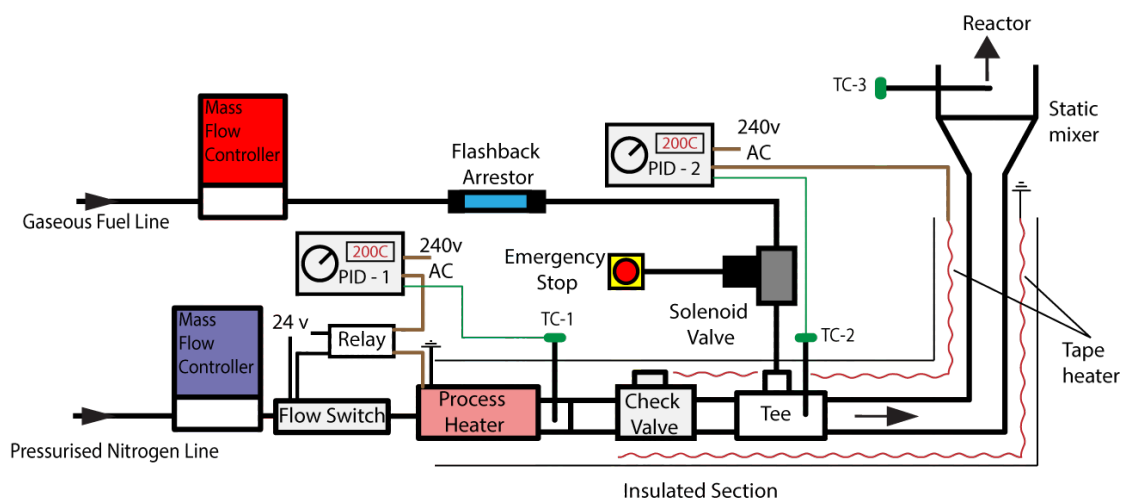


Figure 3.2: Gaseous fuel feed system schematic.

The introduction of gaseous fuels into the nitrogen stream was also metered by a mass flow controller (Bronkhorst, EL Flow Select), the controller was calibrated with acetylene in the range of 0.01 to 2 l/min. FLUIDAT software, supplied by Bronkhorst, was used to calculate conversion factors in order to use the flow meter with gasses other than acetylene (e.g. ethane, ethylene, propane, etc.), and the calibration curves were uploaded to the instrument using FlowTune software (Bronkhorst).

As a safety precaution, a flashback arrestor was positioned in the fuel line, to protect against the event of a flame propagating along the pipe, although this was in reality highly unlikely, as air-fuel ratios used in this system were below the flammability limit of the fuels used. As an additional safety measure, a solenoid valve (normally closed) connected to an emergency stop button was positioned immediately before the tee fitting where the flammable gasses were introduced into the nitrogen stream. The tube leading to the reactor was made of stainless steel (18mm o.d.) that was wrapped with a tape heater and glass-fibre insulating material. The temperature of the tape heater was controlled by a separate PID controller (PID-2), which was also a Tempatron, TL4800. For experiments, heating of the gas feed system was to the same temperature as for liquid fuels, so that the conditions of entry to the reactor were the same for both types of fuels.

3.1.2 Liquid Feed System

Figure 3.3 provides a schematic of the system for use with fuels that were liquid under ambient conditions, in order to vaporise those fuels and introduce the vapor to the reactor. A mechanical syringe pump (Chemyx, Fusion 100 Touch) was used to meter the volumetric flow rate of liquid fuels into the vaporiser. A stainless steel capillary tube (1 mm outer diameter \times 0.7 mm internal diameter) was used to connect the syringe to the vaporiser. A luer-lock connection was made at one end on the capillary for connection to the syringe, and a specially adapted Swagelok fitting was made on the other end for connection to the vaporiser. The capillary issued into the vaporiser, which was constructed by means of a stainless steel tee fitting (18mm) that was packed with 3mm borosilicate glass beads. The glass beads were intended to provide some inertia against temperature fluctuations, and also to prevent Leidenfrost effects from disturbing the efficient vaporisation of fuels. As fuels were fed into the vaporiser they were entrained into a stream of nitrogen carrier gas. Nitrogen carrier gas was fed using the same setup described above (3.1.1 Gas Feed System).

3.1.3 Static mixer

In order to ensure that a homogenous mixture of fuel and carrier gas was passed into the reactor, a static mixer was designed, and positioned at the inlet of the reactor tube (see the schematic in Figure 3.2, and an image of the mixer in Figure 3.3). Since the mixer was positioned at the inlet of the reactor the mixer also served as an adapter, connecting the 18 mm stainless steel tube of the fuel/carrier gas feed system and the

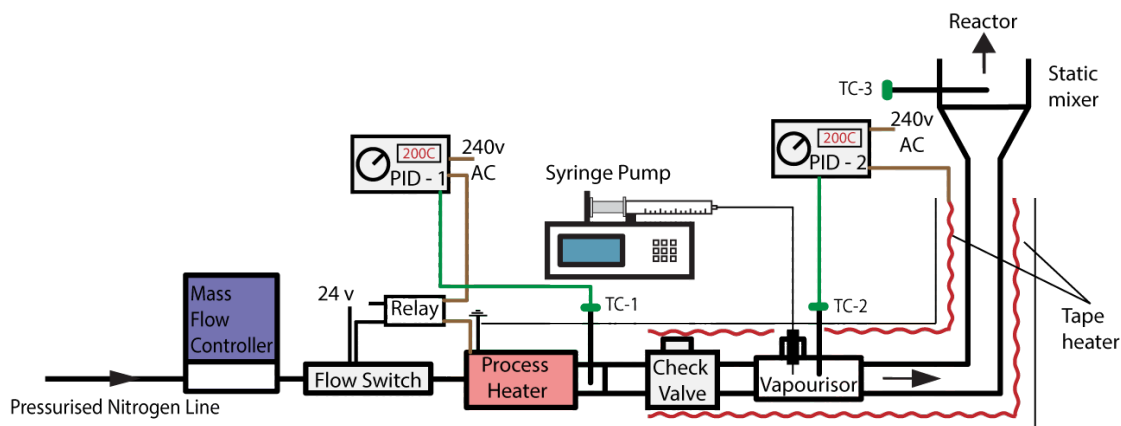


Figure 3.3: Liquid fuel feed system schematic.

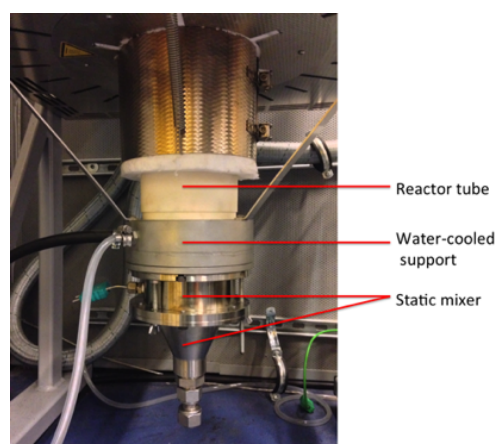


Figure 3.4: Static mixer installed at the reactor inlet

104 mm alumina reactor tube. With consideration to the range of temperatures and corrosive properties of some of the fuels used the mixer was constructed from stainless steel (316). Mixing was achieved by packing the upstream part of the mixer with 8mm stainless steel ball bearings. A second compartment of the mixer was located following the stainless steel ball bearings and was initially intended to be packed with stainless steel wool, however sufficient mixing was obtained with only the first compartment. The two compartments were separated with 1mm thick perforated stainless steel sheet (RS, 340-6186). Figure 3.4 shows the static mixer installed at the inlet to the reactor. The mixer was designed to be easily removed for cleaning and maintenance, and could be lowered from its position by removing the wing nuts that held it in place. The mixer was suspended from the water-cooled reactor support, by a flange that was specially designed and fabricated for this purpose; to seal the connection, an ‘O’-ring was compressed between the mixer and the flange.

The effectiveness of the static mixer was verified by radial sampling with a Combustion Fast Flame Ionisation Detector (FFID), which showed homogeneity across the diameter of the mixer with various gaseous and liquid fuels.

3.1.4 Reactor tube

The reactor was used in order to study the thermal decomposition of fuels, and this involved the characterisation of product species, sampled at the reactor outlet. A high-temperature electrically heated oven was procured (manufactured by Nabertherm, model RHTV 120-600) and was used for heating the reactor tube to a maximum temperature of 1800°C. The oven was fitted with the alumina reactor tube (grade C799, recrystallized alumina) which had the dimensions 120 o.d. × 104 i.d. × 1440 mm length, and was orientated vertically in the oven. In the literature, both alumina and quartz reactors have been used and are shown to produce similar results regardless of the reactor material (Skjøth-Rasmussen et al., 2004). A 600 mm length of the reactor tube was heated uniformly by the high-temperature heating elements of the oven, with the elements being constructed from molybdenum disilicide (MoSi_2).

Due to the high temperatures the reactor operated at, stainless steel water-cooled flanges were supplied by Nabertherm, and fitted at the reactor inlet and outlet in order to support the tube. Due to the cooling, particulates were found to deposit on the tube reactor wall towards the outlet of the tube as a result of thermophoresis; to overcome this, a conical stainless steel section was designed and positioned at the reactor outlet in order to direct product gasses out of the reactor and aid cleaning of the reactor.

Samples were extracted from the reactor using a stainless steel sample probe (6mm o.d.) that was positioned inside the tube 200 mm from the reactor outlet. Instruments such as the DMS500 particle spectrometer or Horiba emissions analyser withdrew samples for analysis using vacuum pumps integral to these instruments.

3.1.5 Reactor temperature profile

The heated cavity electric oven, surrounding the reactor tube was controlled by a PID system. The PID used a type-B thermocouple, which was positioned within the oven cavity. Therefore, the set temperature of the electric oven represented the cavity temperature and not the temperature of the gas flowing through the reactor. In order to characterise how the set temperature of the oven related to the actual reactor centerline temperature a series of temperature measurements were carried out, using a type K thermocouple that was surrounded by a sheath (the design of which is detailed in the following section). Figure 3.5 shows that the temperature of the nitrogen carrier gas, as measured in the middle of the reactor along the central axis, was insensitive to the flow rate of nitrogen carrier gas in the range of 0 to 25 l/min.

All of the experiments that were conducted using the reactor in this body of work were carried out using 20 l/min (SATP) of nitrogen carrier gas. Figure 3.6 shows the temperature along the length of the reactor, as measured along the centerline of the reactor, at 8 set temperatures, and at a flow rate of nitrogen of 20 l/min. This profile is typical for a tube reactor (Skjøth-Rasmussen et al., 2004), and in this case it had an almost uniform temperature along a length of approximately 0.5m at the center of the reactor tube.

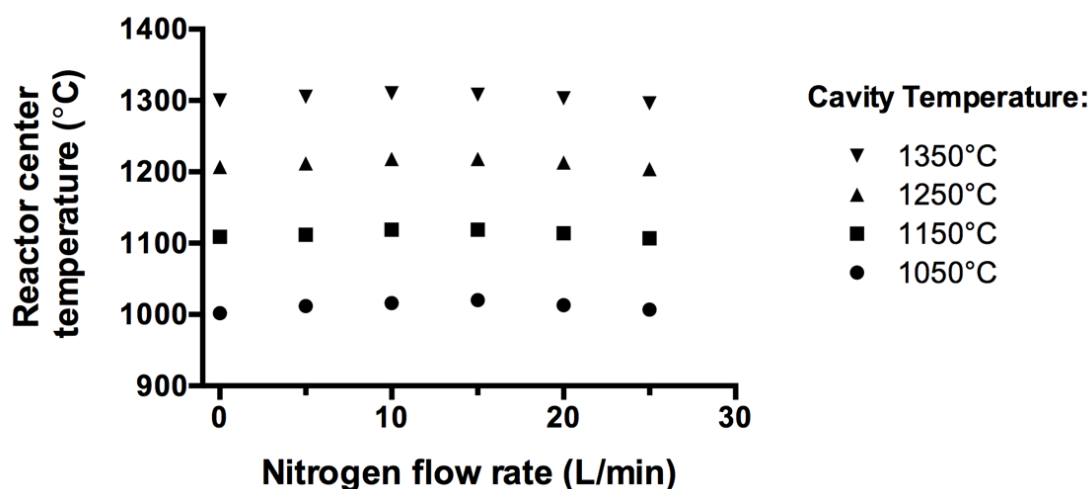


Figure 3.5: Temperature measured at the center of the reactor (700mm from inlet), at the centerline, with varying nitrogen flow rates. Measured with a K type thermocouple (with sheath).

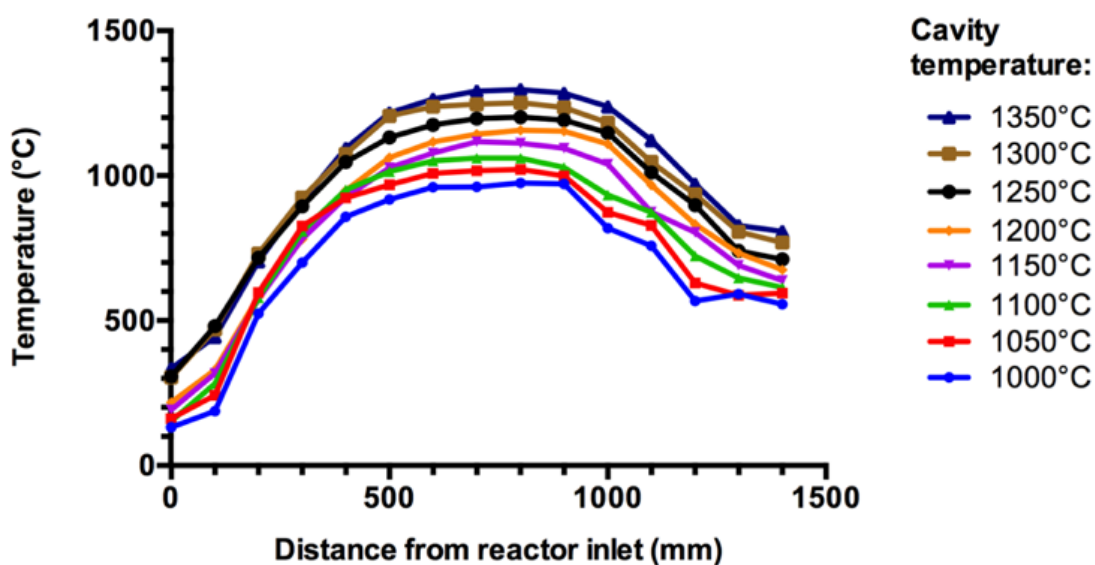


Figure 3.6: Reactor longitudinal temperature profile, measured at the reactor centerline; with 20 l/min nitrogen flow pre-heated to 150°C. Measured by a type K thermocouple (with sheath).

Figure 3.7 shows that there is a linear relationship between the temperature at the center of the reactor and the heated cavity, and this calibration was used to estimate the carrier gas temperature. The temperatures quoted in this thesis refer to the estimated gas temperatures using the calibration and not the cavity temperature.

It should be noted that part of the reason the fuels were highly diluted in an inert carrier gas (nitrogen) was to reduce any effects of endothermicity or exothermicity of pyrolysis or oxidation reactions on local temperatures within the reactor. The fuel

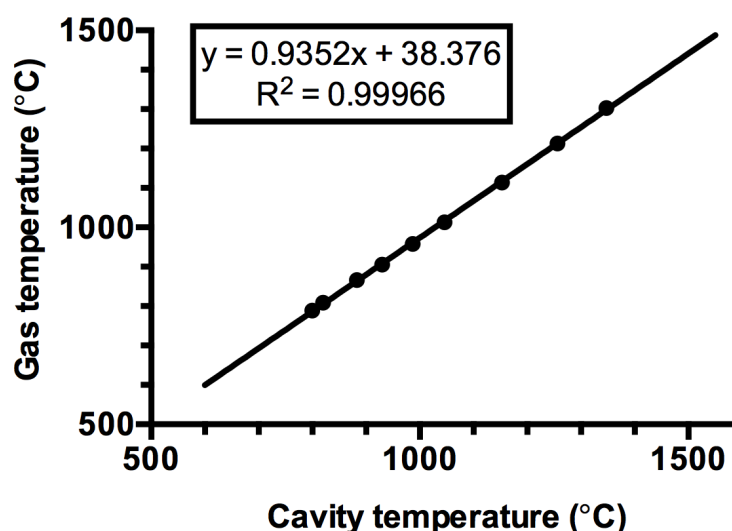


Figure 3.7: Gas temperatures measured at the center of reactor by a sheathed type K thermocouple, at various cavity temperatures. Carried out at an inlet nitrogen flow rate of 20 l/min (SATP) and nitrogen pre-heated to 150°C.

concentration introduced to the reactor was typically in the region of 5,000 parts per million (ppmv), and the bulk was comprised of the nitrogen carrier.

3.1.6 Design of thermocouple sheath

When a thermocouple is used to measure the local temperature of a stream of gas through a heated tube, the indicated temperature of the thermocouple is determined by the balance of heat transfer to and from the thermocouple junction. The thermocouple junction gains heat from the surrounding gas by convection, and heat is lost by conduction along the thermocouple wire. Depending on the conditions prevailing, the thermocouple can also either lose or gain heat by radiation to or from the wall of the reactor tube (Rogers et al., 1992).

In order to better estimate the temperature of the gas flowing in the reactor, practical measures needed to be implemented to remove as far as possible the influence of radiation on the gas temperature readings. To this end, a concentric shield around the thermocouple junction was devised, as shown in Figure 3.8, to reduce radiation from the reactor wall and increase the rate of convection to the thermocouple tip. The shield consisted of a 200 mm section of 3 mm thick stainless steel tube (70 mm diameter), a stainless steel rod was secured across the diameter of the tube and held the thermocouple in place with a setscrew. The rod positioned across the diameter also aided with centering of the probe in the reactor. A 6mm stainless steel tube, which was attached to a vacuum pump, was positioned to increase the velocity of gas over an exposed junction thermocouple tip (at 5 l/min).

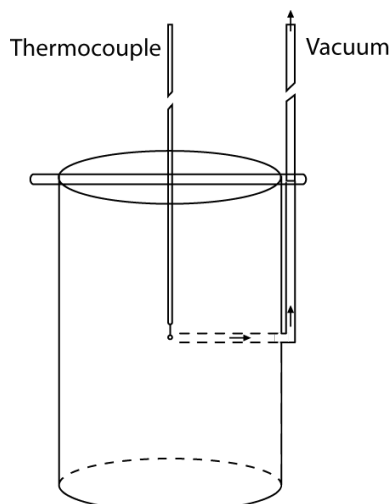


Figure 3.8: Schematic of probe design for limiting the influence of radiation on thermocouple measurement.

Temperature measurements were made by quickly lowering the shielded thermocouple into the furnace, and recording the temperature of the thermocouple as soon as the temperature had stabilised. The rate of heating of the 0.5 mm thermocouple tip was assisted by heat transfer from the gas drawn by the vacuum. Due to the fast response of the exposed junction thermocouple, aided by extra convection, the temperatures of the shield was much lower than that of the reactor wall and the thermocouple junction, therefore heat gain by radiation transfer to the thermocouple tip was minimised.

3.1.7 Gas residence time

The residence time (τ) of gas in the reactor is defined as the ratio of the reactor volume, V , and the gas flow rate through the reactor, Q .

$$\tau = V/Q \quad (3.1)$$

Table 3.1 supplies the gas residence time of nitrogen through the reactor zone of uniform heating at various temperatures, when supplied with nitrogen at a flow rate of 20 l/min.

Table 3.1: Calculated gas residence time and Reynolds number of nitrogen through the zone of uniform heating in the reactor at a flow rate of 20 l/min (0.6 m length).

Gas temperature (°C)	Residence time (s)	Reynolds number
1000	1.40	243.6
1100	1.30	232.8
1200	1.21	222.3
1300	1.13	212.9
1400	1.06	204.4

3.1.8 System control and monitoring

A PC program with user interface was developed in LabView in order to monitor and control various conditions in the system. K-type thermocouples positioned at the static mixer and vapouriser fed back to a National Instruments USB-6210 data acquisition card (DAQ), in order to alert the user in case temperature or pressure deviated outside an accepted range. The syringe pump and mass flow controllers were also controllable from the program. In order to shut-off the supply of gaseous fuels to the reactor a solenoid valve was also fitted, which was controllable from the program. A screenshot of the program is shown in Appendix A.

3.1.9 Particulate sample collection and storage

Samples of particulate matter for isotopic analysis were collected by thermophoretic deposition onto a borosilicate glass plate, which was positioned at the reactor outlet. The samples of particulate matter were removed from the glass with a stainless steel spatula and transferred into a borosilicate glass vial. The vials were labelled and stored in a gridded sample tray at -20°C in a deep freezer, until required for analysis.

Particulate samples that were collected for soxhlet extraction (Chapter 9) were sampled from inside the reactor through a stainless steel probe, which was positioned at the reactor centerline, 200 mm from the tube outlet. The sample was extracted using a vacuum pump, and soot was collected onto glass fibre filters (Fisherbrand, Microfibre filter MF300) that were placed in a stainless steel filter housing positioned between the probe inlet and the vacuum pump.

3.2 Diesel test engine facility

All engine tests that were conducted as part of this work were carried out in a purpose built laboratory equipped with an engine-dynamometer test bed located in an engine test cell, which was operated from an engine control room. The laboratory and test rig have been described and characterised previously by Hellier (2013) and Schönborn (2009), and a summary is provided below.

3.2.1 Engine specification

All engine experiments in which exhaust gas particulates were collected were conducted on a modern direct-injection compression-ignition engine, converted and instrumented to run as a single cylinder research engine. The engine was equipped with an ultra low volume fuel system (described in Section 3.2.2), and was normally-aspirated with air drawn into the engine at atmospheric temperature and pressure for all experiments. Given in Table 3.2 are some technical details of the engine and the conditions employed, and Figure 3.9 shows a general schematic of the experimental setup.

Table 3.2: Test engine specifications

Engine head model	Ford Duratorq
Engine bottom end model	Ricardo Hydra
Number of cylinders	1
Cylinder bore	86 mm
Crankshaft stroke	86 mm
Swept volume	499.46 cc
Compression ratio	18:1
Maximum cylinder pressure	150
Peak motoring pressure at test conditions	43 bar
Injectors	6-hole solenoid (DELPHI DF1 1.3)
Electronic fuel injection system	EMTRONIX EC-GEN 500 (1 μ s accuracy)
Piston design	Central ω -bowl in piston
Oil temperature	80 \pm 2.5°C
Water temperature	80 \pm 2.5°C

The engine cylinder gas pressure was measured at every 0.2 CAD using a piezoelectric pressure transducer (Kistler 6056AU38) and charge amplifier (Kistler 5011), and the data was recorded by a National Instruments DAQ connected to a PC. At bottom-dead-center (BDC) of every combustion cycle, the cylinder pressure was pegged by the DAQ using a piezoresistive pressure transducer (Druck PTX 7517- 3257) positioned in the intake manifold, 160 mm upstream of the inlet valves. Type-K thermocouples were positioned at numerous locations throughout the system and logged with the DAQ system.

The engine exhaust gas composition was determined by continuous sampling at approximately 180 mm downstream of the engine exhaust valves and analysed by a gas analyser system (Horiba MEXA9100 HEGR) and a fast particulate spectrometer (Cambustion DMS 500). Sampling of exhaust gases for particulate measurements was made via a heated line with a dilution cyclone at the connection between the exhaust and heated line. Exhaust gases were diluted with air at this point by 4:1, and a second air dilution of 100:1 was applied upon entry to the analyser. The heated line and the dilution cyclones was heated to a constant temperature of 55°C.

All engine tests were conducted at the engine speed of 1200 rpm, fuel injection pressure of 450 bar and a start of fuel injection of 5 crank angle degrees (CAD) before top-dead-center (BTDC). For all tests, the injection duration was varied between 648 μ s and 770 μ s so as to maintain a constant engine IMEP of 4 bar.

3.2.2 Ultra low volume fuel system

The experiments that were conducted in this thesis have involved the use of high-assay fuels and fuels enriched with labelled ^{13}C molecules. A typical diesel commonrail system usually requires several litres of fuel to operate, which would be prohibitively expensive, considering the cost of the fuels; for this reason, use was made of an ultra low volume fuel system. The system, first developed by Schönborn (2009) and developed further

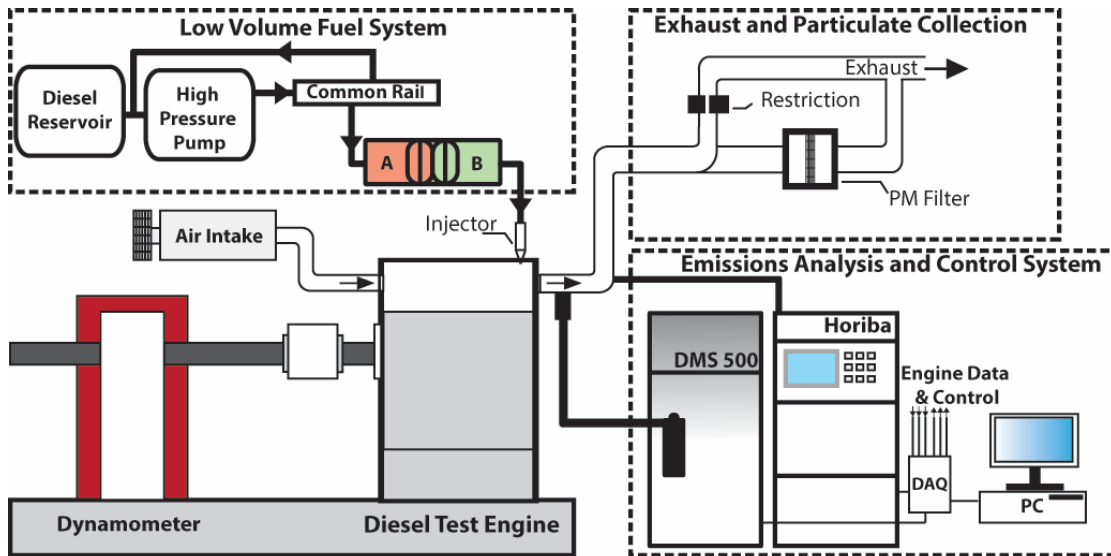


Figure 3.9: Diesel test engine facility. Showing the engine test bed and periphery systems, including: low volume fuel system; emissions analysis and control system; and exhaust and particulate collection system.

by Hellier (2013), utilises fossil diesel as a hydraulic fluid, pressurised to fuel injection pressures by a conventional common rail fuel circuit, to pressurise test fuels for high pressure direct injection. The schematic representation of the entire engine-dyno test rig in Figure 3.9 shows the fuel system where diesel fuel (A) is used to pressurise a low volume of test fuel (B). The low volume fuel system can operate with sample fuel volumes of between 100 and 250 ml and can be heated in the case of high melting point or high viscosity fuels. In this work the low volume fuel system was held at a constant temperature of 40 ± 2.5 °C.

In addition to reducing the volume of fuel required for each engine test, there are several other notable advantages of the fuel system, including:

- Reduced time spent cleaning, that would be required for a larger conventional diesel system to remove any residual fuel between each test run; and
- The ability to use fuels with physical or chemical properties that would otherwise be detrimental or impractical for use in a conventional diesel fuel system (e.g. high melting point, low lubricity, or corrosive properties).

3.2.3 Particulate sample collection and storage

Samples of particulate matter from the engine exhaust gases for ^{13}C isotope analysis were collected onto glass fibre filters (Fisherbrand, Microfibre filter MF300) with a pore size of $0.22 \mu\text{m}$. The engine exhaust gas flow was split and diverted through the glass fibre filter approximately 700 mm downstream of engine exhaust valves, with the main exhaust path partially restricted to ensure a sufficient flow through the filters. Figure 3.9

shows the exhaust sampling arrangement in schematic form. The method allowed the collection of both volatile and non-volatile PM, and subsequent baking of the filter (or part of the filter) allowed the volatile PM to be baked-off, allowing the subsequent analysis of only the non-volatile fraction.

3.3 Isotope measurements by Elemental Analysis-Isotope Ratio Mass Spectrometry (EA-IRMS)

The objective of the isotopic analysis carried out in this work was to determine the relative rate or likelihood of specific carbon atoms in various fuel molecules becoming soot. This required calculation of the fraction of the particulate matter that was derived from carbon atoms that had been specifically ^{13}C labelled. In order to calculate this, isotopic measurements were necessary of the PM and of the fuel that the PM was derived from.

Isotope ratio mass spectrometry (IRMS) was used to make precise measurements of isotopic abundance ($^{13}\text{C}/^{12}\text{C}$ ratio). In the course of the research presented in this thesis, several different spectrometers were used to determine relative $^{13}\text{C}/^{12}\text{C}$ ratios. The operating principle is common to all of the equipment used in this thesis for EA-IRMS; IRMS measurements are reported relative to standard material of known isotopic composition. This ensures that isotopic measurements are replicable between laboratories. The process for determining isotopic composition, and calculations to determine the fraction of PM derived from the labelled component are described in detail in Chapter 4.

The following description of the stages involved in the measurement processes starts with preparation of samples and follows the sample and its derivatives through the EA-IRMS.

3.3.1 Sample preparation

The standard method of introducing material into an elemental analyser (EA) for the subsequent isotopic analysis by an IRMS instrument is by enclosing the sample in small tin capsules and submitting them for analysis using an automated sample carousel. It is important that the capsules are loaded with similar quantities of the element of interest, in this case carbon, since sample size can have a small influence on the outcome of the measurement. Tin capsules (Elemental Microanalysis, D1000) were loaded with the equivalent of $70\ \mu\text{g} \pm 5$ of carbon, weighed using a Mettler Toledo XP6 micro-balance. Solid samples and associated standard reference materials were generally prepared in batches of 50 or 100.

Liquid samples generally required more sensitive handling than solid samples, due to the possibility of sample evaporation, which could result in isotopic fractionation prior to measurement. It became apparent that two different methods were required to introduce liquid samples to the EA in this work; one that was generally more suitable

for non-volatile high boiling point single- or multicomponent fuels, and another method for single- or multicomponent samples that are volatile.

Samples of non-volatile liquid fuels were collected from the surface of a sample vial using a short length of Pyrex glass capillary (~ 3 mm length, 0.5 mm i.d.). Using stainless steel tweezers the capillary was transferred to a smooth walled tin capsule (Elemental Microanalysis, D4001) and enclosed using a capsule sealing press. Once the samples were enclosed the sample was transferred to the sampling carousel for immediate analysis. This technique was adequate for the majority of liquid samples tested, particularly high boiling point single-component fuels; tests showed little variability between measurements. However, in tests where binary mixtures of fuels that had at least one volatile component (e.g. a binary mixture of heptane and ethanol), a large variability in measurements was observed. Following a detailed investigation, the problem was identified as the loss of the volatile fuel either during the sample preparation or whilst in the sample carousel awaiting analysis. To overcome this issue an injection port was designed to allow samples to be directly injected into the EA using a syringe; therefore, eliminating the need to use the autosampler, and minimised the potential for fuel evaporation. The section relating to sample submission methods (Section 3.3.3) details the injection port innovation that was developed to improve the process of measuring liquid samples.

3.3.2 Preparation of gaseous CO₂ samples

Pyrolysis of alcohols at temperatures upwards of about 1100°C yields soot and PAHs, but also generates a mixture of lighter hydrocarbons, and some carbon monoxide (CO) and carbon dioxide (CO₂) (Peg et al., 2007). In the case of oxygenated molecules, and hydrocarbon molecules that undergo pyrolysis in the presence of small amounts of oxygen, as well as identifying how specific carbon atoms convert to PM it was also of interest to determine whether specific carbon atoms were more ‘predisposed’ to becoming CO or CO₂. In order to make this determination the bulk isotopic composition of CO and CO₂ was analysed, which required a process of converting CO to CO₂, due to the fact that IRMS measurements involve the detection of CO₂. Schütze reagent (iodine pentoxide, I₂O₅) is an oxidising agent, and was used for the oxidation of CO to CO₂, according to the following reaction:

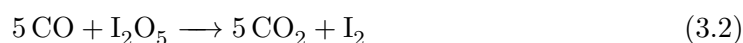


Figure 3.10 shows the setup, which was used to perform the conversion of CO to CO₂ at room temperature. Samples of reactor gasses, containing a mixture of hydrocarbons as well as CO and some CO₂, were collected in a 10 litre Tedlar bag from the reactor outlet. The conversion of CO to CO₂ was carried out by emptying the Tedlar bag into the oxidation line at a rate of approximately 1 l/min. The oxidation line consisted of an assembly of tubing for passing the effluent gas through the Schütze reagent, whilst

trapping unwanted reactants such as the unburned hydrocarbons. The $\frac{1}{4}$ " stainless steel tube of the oxidation line, first passed through cold trap '1', set at -50 °C, the purpose of this first trap was to remove any light hydrocarbons ($> C_3$) and PAHs by condensation, but not the gasses CO and CO₂ (boiling points -192 and -57 °C respectively). Following the trap a 12 mm Pyrex glass tube was connected, using a Swagelok compression fitting with PTFE ferrules, the glass tube was packed with a 6 cm length of Schütze reagent (Leco Corporation, 761-747), which was plugged at either end with glass wool. The oxidised gas then passed into the second cold trap, also set to -50 °C; this trap was to remove any iodine (I₂) which was produced by Reaction Equation (3.2). Finally, the sample gasses were then passed into a 1 l sample bag for IRMS analysis. At the inlet and outlet of the line a 'tee' fitting with a valve was installed to allow the line to be purged with nitrogen between samples, to flush the system and exclude atmospheric contamination. The method described was suggested by A. Marca (personal communication, Feb 2014), and similar methods are reported in literature (Santrock and Hayes, 1987; de Groot, 2008).

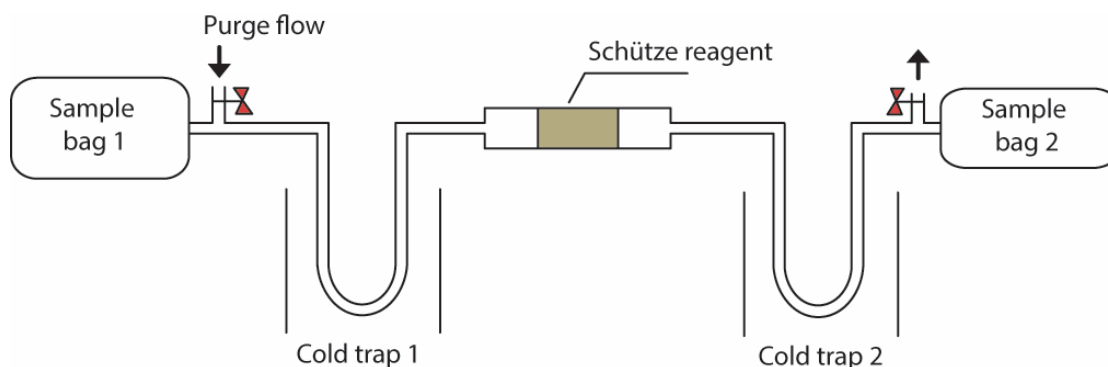


Figure 3.10: Schematic of the setup used for conversion of CO and CO₂, using Schütze reagent.

The temperature of a dry ice bath can be fixed to a desired temperature between -17 °C and -78 °C depending on the mixing ratios of ethylene glycol and ethanol (Jensen and Lee, 2000). A dry ice slush with 50% ethylene glycol and 50% ethanol by volume was used to chill trap '1' and '2' to -52 °C, and the temperature was monitored using a type-K thermocouple.

3.3.3 Sample submission

An automated sample carousel was used to introduce all solid PM samples and associated standard reference materials into the elemental analyser, in batches of 50 or 100 samples depending on the capacity of carousel installed. This is the standard means of submitting samples in tin capsules, and individual tin capsule samples were submitted at regular intervals, controlled by software (*IsoDat*) that synchronises the process with the EA-IRMS. During analysis of the liquid samples that were collected in a glass capillary and enclosed in a tin capsule it was found that the measurement of binary mixtures of fuels

was not repeatable due to the evaporation of the more volatile component in the samples before they could be submitted to the EA. As a result, a number of approaches were investigated, and the procedure evolved during the course of this research.

For liquids submitted using the ‘zero blank’ style autosampler carousel, shown in Figure 3.11(a), it was discovered that liquid samples of volatile fuels partially or completely evaporated prior to introduction to the EA. This was even observed in the case of 1-pentanol which has a boiling point $\sim 139^\circ\text{C}$. The design of the ‘zero blank’ autosampler requires all samples to be sealed in an air-tight carousel and to be purged with helium prior to analysis; this process being necessary so as to exclude atmospheric contamination. This process took approximately 15 minutes to complete before samples could be passed individually to the EA. During this time some or all of the liquid was lost, despite being sealed in a smooth-walled tin capsule. Overall, this type of sample system was found to be an unreliable method in terms of sample loss. Even in the cases where sample test results were detectable the result was highly variable as a result of isotopic fractionation. The zero blank style carousel is therefore not recommended for use with volatile or semi-volatile fuels.

A semi-open carousel, such as the one pictured in Figure 3.11(b), was also trailed. The sample wells in this style carousel are not sealed from atmosphere, instead only one sample is purged at a time in a small chamber immediately before the EA (Colombo and Tosi, 1982); therefore, from the time of a sample being loaded into the chamber, only about 1 minute elapses before the sample is passed to the combustion furnace of the EA. By preparing liquid samples immediately before analysis and using the semi-open style carousel it was found that repeatable results could be obtained for all of the single-component compounds measured, including ethanol, the most volatile of these.

However, measurements of binary mixtures of fuels with dissimilar boiling points (particularly mixtures of heptane and ethanol) produced results with large variability using the capillary collection method and submission by the semi-open style carousel. It is believed that the observed variability was due to differential evaporation of the more volatile component during sample preparation or whilst waiting for submission in the carousel. Many methods were tried to improve the technique to no avail, including: flame sealing one end of the capillary, to reduce surface area for evaporation; enclosure of capillary into larger tin capsules, so as to reduce the concentration gradient to the atmosphere; and double encapsulation of the capillary into two tin capsules, one inside the other.

To overcome this issue, binary mixtures of fuels were injected directly into the EA, using a manual injection port that was designed specifically for this purpose, and fabricated in-house, as shown in Figure 3.11(d). The stainless steel injection port allowed the introduction of liquids and gasses by syringe injection through a high-temperature septum (Agilent, 5183-4757). The septum was compressed by a lid, which was threaded to attach to the main body of the injector. On the inside of the injector directly beneath the septum, a carrier flow of helium was introduced to carry the sample through

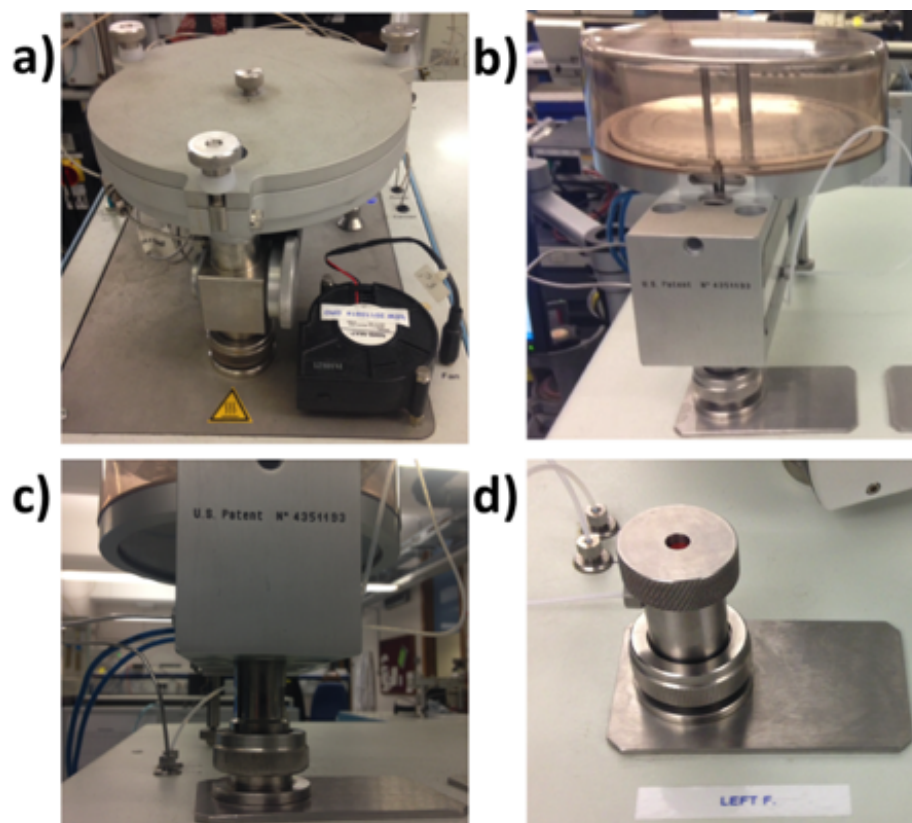


Figure 3.11: Images showing the inlet of the elemental analyser combustion furnace, fitted with: (a) Zero blank carousel. (b) Semi-open carousel. (c) Carousel connection to EA. (d) Manual liquid/gas injection port.

the system. Further mechanical drawings of the injection port design can be found in Appendix A under the title ‘injector block and lid’. The manual injection method required precise timing of the syringe injection into the EA, in order to correspond to the timing of the oxygen that was introduced automatically into the EA. Using a countdown timer the injections were made at a regular interval following initiation of the instrument measurement sequence.

3.3.4 Elemental analysis (EA)

Analysis of carbon $^{13}\text{C}/^{12}\text{C}$ isotope composition by IRMS involves the detection of isotopically resolved beams of CO_2 , and in order to convert the carbon-containing samples to CO_2 an element analyser (Thermo Flash EA, 1112 series) was used. The overall technique is therefore referred to as EA-IRMS, and is a bulk measurement technique that gives an average isotopic composition of the entire sample. Elemental analysis is a useful technique in its own right and is also routinely used to measure elemental concentrations of C, H, N, O and S, using a TCD detector for quantification. The EA, shown by a schematic representation in Figure 3.12, was comprised of an oxidation furnace,

Table 3.3: Conditions employed in the elemental analyser (Thermo Flash EA, 1112 series).

Combustion furnace temperature	1020 °C
Reduction furnace temperature	680 °C
Reaction tube material	Transparent silica
Helium flow rate	100 ml/min
Oxygen flow rate	175 ml/min
GC temperature	50 °C
GC column	Porapak (3 m)

a reduction furnace, a water trap, GC column, and reference gas pneumatic control system.

The oxidation reactor (left furnace, Figure 3.12) was constructed of silica and heated to 1020°C for all of the samples analysed. The centre of the reactor was packed with chromium oxide (Cr_2O_3), which served as a secondary oxygen source to aid the combustion of samples. Following the section packed with chromium oxide the oxidation reactor was filled with silvered cobaltic oxide in order to remove halogens and sulphur from the combusted gasses. The specifications of the EA and conditions that were employed are listed in Table 3.3.

When the organic sample is dropped by the autosampler into the oxidation reactor of the EA, it is combusted under a flow of oxygen to carbon dioxide (CO_2) and water (H_2O); in addition N_2 , NO , NO_2 , excess O_2 are usually present. The combusted sample was then carried under a helium flow to a reduction chamber (labelled ‘right furnace’ in Figure 3.12), where excess oxygen was removed and oxides of nitrogen were converted to N_2 . The flow then passed through a chemical trap to remove water and the gas then passed into a GC column where N_2 and CO_2 were separated. The gas issuing from the GC column then passed through a TCD detector before being carried to the IRMS for isotopic analysis.

It should be noted that, as well as an EA instrument, there are other instruments that may be interfaced to an IRMS, including a gas chromatography system (GC), or liquid chromatography system (LC). Gas chromatography combustion isotope ratio mass spectrometry (GC/C/IRMS) is a technique that has been probed in this work and is described in some more detail in Chapter 9.

3.3.5 Isotope ratio mass spectrometry (IRMS)

Two isotope ratio mass spectrometers have been used in this present work, a Thermo Finnigan, Delta V, and a Thermo Fischer Delta XP. Isotope ratio mass spectrometry is routinely used to detect the isotopic abundances of a range of stable isotopes including: carbon, nitrogen, oxygen, and hydrogen. IRMS instruments are usually used for resolving small differences in the isotopic compositions of samples at around natural abundance levels. The abundance of ^{13}C in nature is $\sim 1.1\%$, and the resolution of the IRMS instruments used in this work was in the region of 1 ^{13}C atom in 10,000 C atoms

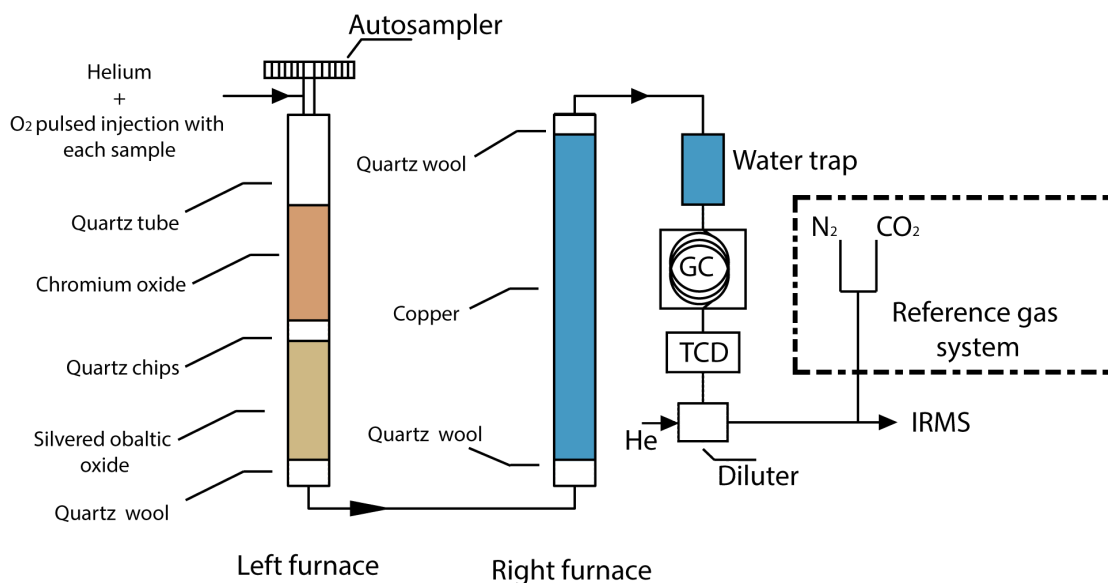


Figure 3.12: Schematic of elemental analyser (EA) configuration. The setup shown here was employed for all EA-IRMS experiments.

(or 0.1 $\delta^{13}\text{C}$). The description here is mainly focussed on CO_2 detection and follows the path of the molecules through the instrument. Regardless of the species of interest the IRMS instrument is invariably comprised of three basic components: a source, analyser, and collector. A source is used to generate ions of CO_2 ; in the case of the Delta V and XP instruments, ions are generated by electron impact ionisation, induced by a thermionic cathode. The ions are then accelerated into the flight tube by charged plates, where collimating plates and electronic lenses define the beam shape and path. The ion beam passes into the analyser, where a magnetic field, generated by an electromagnet, deflects the ion beam into separate beams of distinct isotopic components, based on molecular mass. For carbon analysis, CO_2 ions with masses 44, 45, and 46 are usually measured, where the main isotopologues of interest are: $^{12}\text{C}^{16}\text{O}_2$, mass 44; and $^{13}\text{C}^{16}\text{O}_2$, mass 45. Corrections are applied for minor abundances of isotopologues arising from oxygen ^{17}O nuclides. The separated ion beams are electronically compared at the collector. Figure 3.13 shows a schematic of how these components are arranged in a typical isotope ratio mass spectrometer; the basic design of this type of mass spectrometer was pioneered by Nier (1947) and was used to determine isotopic composition of a number of gasses including CO_2 .

3.4 Measuring instruments

A number of further analytical techniques have been used in order to characterise and quantify a range of gaseous species and particulate matter. The following sections explain the use of the analytical instruments and their operating principles.

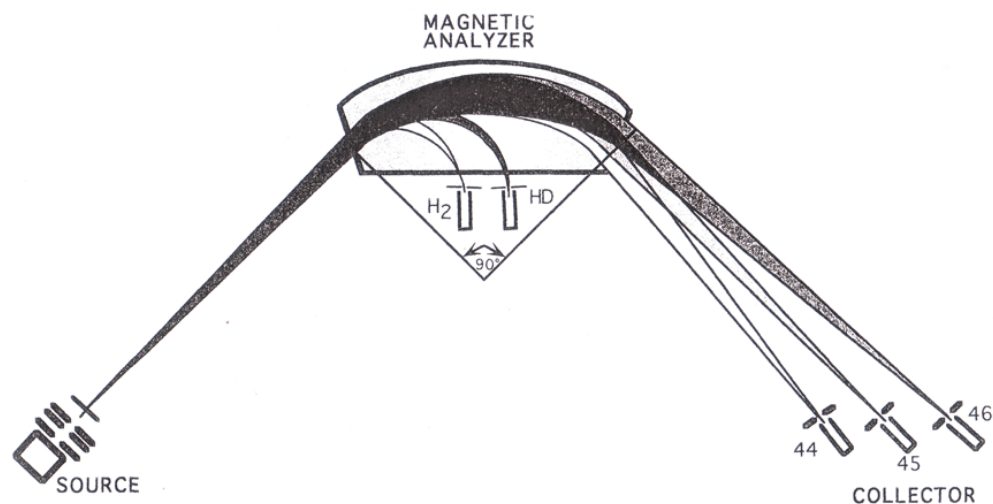


Figure 3.13: Schematic diagram of the major components in a typical isotope ratio mass spectrometer (MAT 252 mass spectrometer), showing: source, analyser and collector. Reproduced from (Criss, 1999).

3.4.1 Quantification and Classification of PM

A fast particulate spectrometer (Cambustion DMS500) has been used to determine size and number distributions of particulates in the range of 5 to 1000 nm, as sampled from both the flow reactor, and from the diesel engine exhaust. The broad dynamic range of the instrument means that it is suited for sampling PM at concentrations ranging from atmospheric levels to the high concentrations that can be generated in a flow reactor.

A stainless steel tube (6 mm diameter), approximately 500 mm in length, was used to collect sample from inside the reactor, along the centreline and positioned 200 mm from the outlet. From here, the sample passed into the remote sampling head of the DMS500 shown in Figure 3.14, where the flow was diluted with a metered flow of compressed air. For samples collected from the reactor a dilution ratio of 6:1 was applied at this point. The application of dilution before the sample was passed along the heated sampling line towards the analyser was in order to prevent agglomeration or deposition of particles within the sample line. Following the primary dilution, the flow passed into the heated cyclone of the remote sampling head, where particles larger than 1000 nm were separated from the smaller particles by impaction; particles smaller than 1000 nm are generally of greatest interest in terms of human health effects and current legislature (EU, 2010; Endo, 2003). The sample flow then passed through an orifice (1.10 mm), which limited the sample flow rate, and the pressure downstream of the orifice was reduced to about 250 mbar, the sample was transported along the 5-meter long PTFE sample line which was maintained at a constant 80 °C. When the sample reached inside the main enclosure of the DMS500 instrument, a secondary air dilution was applied to the sample flow by means of a rotating disc diluter (Figure 3.14, shown as stage '3') which could apply a dilution ranging from 10-500:1. Dilution was

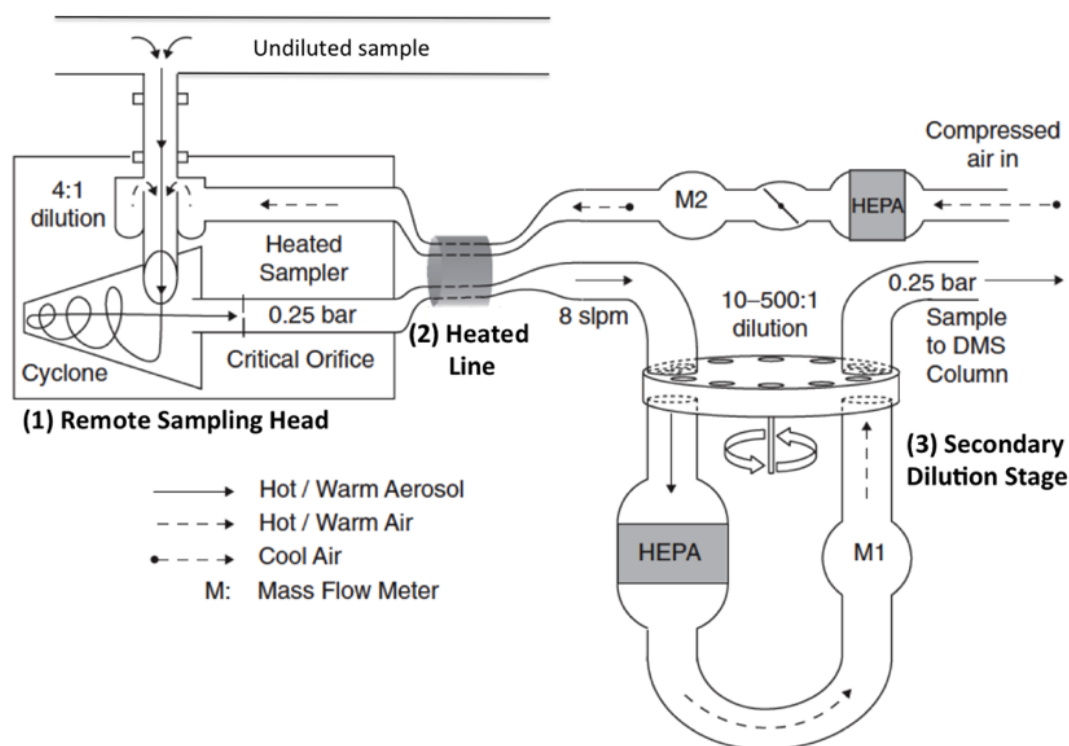


Figure 3.14: Schematic showing dilution stages, and the heated sample line of the Cambustion DMS500 instrument: (1) remote cyclone, (2) heated sample line (5 m), and (3) Secondary diluter. High efficiency particulate air filter (HEPA). (M) Mass flow controller. Figure adapted from (Symonds et al., 2007).

achieved by filtering a portion of the sample flow with a high efficiency particulate air filter (HEPA), an undiluted portion of the sample flow bypassed the HEPA by a rotating disc; the filtered sample gas was mixed with the unfiltered sample gas to complete the dilution. For experiments conducted in the reactor, a dilution factor of 200 was applied at the secondary stage resulting in a total dilution factor of 1200.

The sample then entered a corona discharge charger, where particulates were negatively charged, shown in Figure 3.15. The charged aerosol then passed to the classifier column, where it was introduced to a laminar flow of HEPA filtered air that acted as sheath flow. A high voltage electrode positioned along the central axis of the cylindrical classifier column deflected the negatively charged particles through the sheath flow of air towards electrometer detector rings, which were positioned around the electrode. The instrument had 22 detector rings located at different positions along the classifier column. The location of impaction of the charged particles onto the rings was dependent on their aerodynamic drag to charge ratio. Therefore, the particles were classified by their relative mobility in the column, which was based on the charge and drag of the particle, and ultimately on the particles size. When a particle impacted upon one of

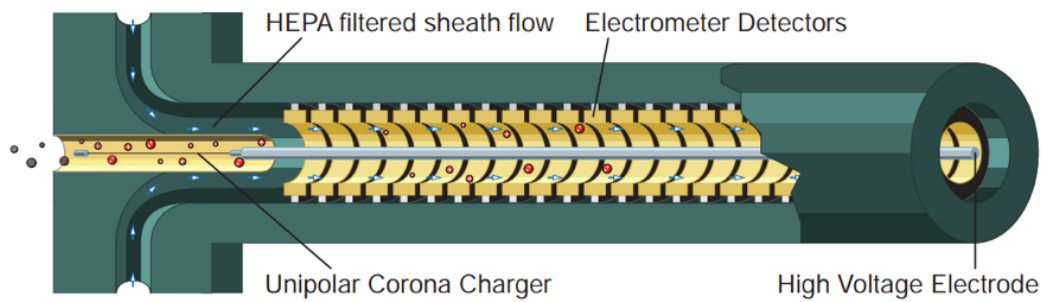


Figure 3.15: DMS 500 classifier column comprised of a corona charger, and 22 classification rings. Cambustion (2010).

the grounded detection rings it discharged and the magnitude of the charge was measured. The mass of particulates at any given fraction was calculated by assuming the density of the particles, the total mass of particulates was calculated using the software provided with the DMS500 (DMS Utilities Macro). In the literature it has been found that good estimates of particulate mass can be obtained for particulates sampled from a diesel engine exhaust using the DMS500 instrument, and these are in agreement with filter-based measurements (Symonds et al., 2007).

3.4.2 Analysis of CO, CO₂, O₂

CO and CO₂

A Horiba-AIA-120 was used to determine concentrations of CO and CO₂. The detector utilised non-dispersive infrared absorption, which operates on a principle of wavelength-specific absorption of infrared energy.

Figure 3.16 shows a schematic diagram of a single detector system, where two cells are placed in parallel. Through one cell flows a reference gas that does not absorb infrared energy, and sample gas flows through the other cell. An infrared beam, controlled by a light chopper, is passed through both cells simultaneously, it then exits and the relative beam intensities are detected. If CO or CO₂ are present in the sample gas, the two infrared beams reaching the detector cells will have different intensities due to partial absorption of the infrared beam. The extent of the absorption is proportional to the concentration of the absorbing species, according to Beer's law, which can be written as:

$$a_{\lambda} = 1 - e^{(-c_i Q_{\lambda} L)} \quad (3.3)$$

where C_i is the concentration of the species, Q_{λ} is the absorption efficiency and L is the optical path. The beam then passes to the detector cell, which is comprised of a sealed cell filled with the gas of interest (i.e. CO or CO₂). The remaining infrared energy is absorbed at the detector cell, resulting in a temperature and pressure rise, which

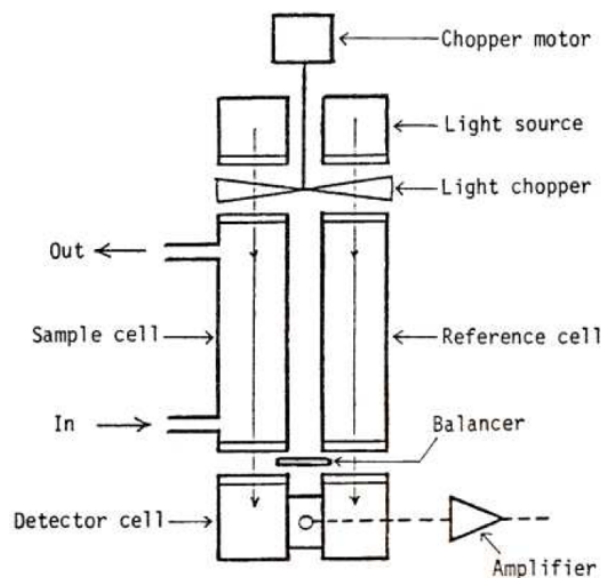


Figure 3.16: NDIR CO/CO₂ gas analyser schematic.

causes expansion of the gas via a flexible metallic membrane. A capacitive sensor on the membrane measures the deflection and produces an electrical output. The reference beam and sample beam are compared yielding a compound signal that can be translated into an absolute concentration.

O₂

Measurements to determine oxygen concentrations have been carried out using a magneto-pneumatic analyser (Horiba FMA-125). The O₂ detector has principally been used to ensure that the flow reactor rig was free of leaks and purged of oxygen for pyrolysis experiments. Molecular oxygen has a much higher paramagnetic susceptibility compared to many other gasses present in exhaust, and oxygen is drawn to magnetised poles within the analyser. Figure 3.17 shows a schematic of the detector, which has two magnetic poles that are alternately magnetised. Oxygen is drawn towards the magnetised pole, which blocks nitrogen from an orifice located within that pole, while the nitrogen flow is unobstructed on the opposite side. This causes a pressure differential downstream and results in the deflection of a metallic membrane positioned between the two nitrogen streams, the membrane produces an electrical output that is proportional to the amount of oxygen in the sample.

3.4.3 Gas Chromatography-Mass Spectroscopy (GC/MS)

GC/MS is an analytical technique that combines Gas Chromatography (GC) and Mass Spectroscopy (MS), and allows the identification of wide range of compounds that can be quantified using analytical standards.

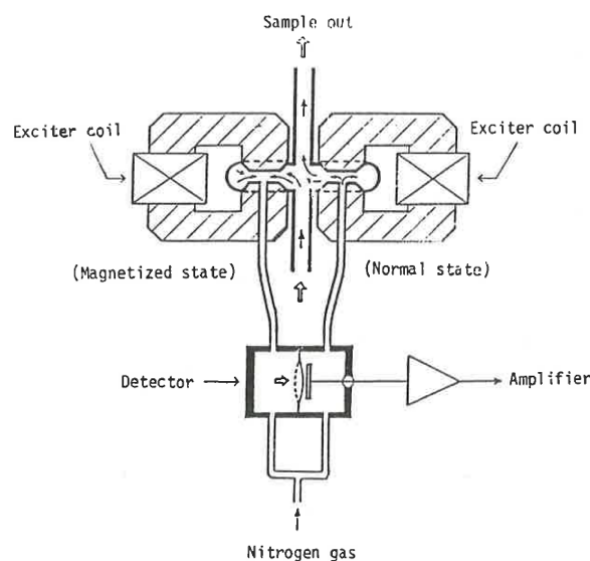


Figure 3.17: Horiba FMA-125 oxygen detector schematic.

GC is a technique that is used to separate a mixture of compounds present in a sample. A sample is injected onto the column, and a helium carrier sweeps the constituent compounds of the sample through the column. The column is lined with a coating on its inner wall, referred to as the ‘stationary phase’, which is typically a high boiling-point polymer. The time any given molecule spends travelling through the column, its ‘retention time’, is determined by its chemical and physical properties and its interaction with the stationary phase. The process primarily separates molecules based on their boiling points (or vapor pressure), but characteristics such as solubility in the stationary phase and polarity of the molecule can also influence retention time.

Once the separated sample elutes from the column it is passed to the MS for detection. The operating principle is broadly similar to that of the more specific type of mass spectrometry IRMS (Section 3.3.5). The process involves four main stages (i) ionisation, (ii) acceleration, (iii) deflection, and detection (iv). Firstly, ions are generated by electron ionisation (EI) of the sample, and as soon as the ions are generated they are accelerated out of the ionisation chamber. Ions are deflected by a magnetic field according to their mass-to-charge ratio, and are detected. A mass spectrum for any compound can be compared against a database (e.g. NIST mass spectral library) for identification.

In this present work an Agilent 7890B GC coupled to a 5977A MS system was used, and was installed in the same laboratory as the flow reactor rig. The GC was also fitted with a second channel that was connected to a TCD and FID detector. The column installed in the GC and conditions employed were dependent on the species of interest (e.g. see Chapter 9).

3.5 Total Hydrocarbon Concentration

Total hydrocarbon concentrations have been measured using a flame ionisation detector (FID). The principle of FID is that when a hydrocarbon is burned it forms ions; the number of ions in the flame is approximately proportional to the total number of carbon atoms present. In flames not involving hydrocarbons, for example a hydrogen or carbon monoxide flame, the formation of ions is limited and equilibrium values for ions is very small. If a hydrocarbon sample is added to the flame a significant number of ions are formed, which are detectable.

A fast flame ionisation detector (fFID), Cambustion HFR 400, was used to measure hydrocarbon concentrations in the reactor. The fFID was designed to give a fast response and high frequency measurements of hydrocarbon concentrations, which was only limited by the small dispersion effects in the sample capillary and flame. Fast response sampling capability has been useful in this work, particularly for the radial measurements at the reactor inlet, as mentioned in Section 3.1.3. It should be noted that not all hydrocarbon molecules give an equal response in the FID, for example oxygenated molecules are found to have somewhat suppressed FID signals with respect to their hydrocarbon analogues. Where appropriate, response factors have been subsequently applied to correct FID signals, a comprehensive list of response factors for different molecules is supplied in reference (Dietz, 1967).

Chapter 4

Analytical Methods

4.1 Interpretation of isotopic measurements

4.1.1 Delta Notation

Isotope ratio mass spectrometry (IRMS) is most commonly used for resolving small variations in isotopic composition at around natural abundance levels. In nature, the carbon isotope ratio $^{13}\text{C}/^{12}\text{C}$ is usually ~ 0.011 ; in other words, just over 1% of the carbon atoms are ^{13}C and the rest predominantly ^{12}C . The variation of ^{13}C around the natural abundance levels is usually reported relative to the ^{13}C abundance in an international standard. This means that the measurements of isotopic abundance are not made as absolute measurements, because they are a lot more difficult to measure accurately in absolute terms. For the above reasons, the isotopic composition of a sample is reported in terms of difference of the $^{13}\text{C}/^{12}\text{C}$ ratio relative to an international standard, Equation (4.1), as follows:

$$\delta^{13}\text{C} = \left(\frac{\frac{^{13}\text{C}}{^{12}\text{C}}_{\text{Sample}}}{\frac{^{13}\text{C}}{^{12}\text{C}}_{\text{Standard}}} - 1 \right) \times 1000 \quad (4.1)$$

where the factor 1000 is used to convert the dimensionless δ -values (delta-values) to delta per mille (‰). In plain terms, the value essentially means that for every 1000 carbon-13 atoms in the standard reference material the sample differs by a number of carbon-13 atoms equal to δ . For example, a sample value of $+16 \delta^{13}\text{C}$ means that the sample has 1,016 ^{13}C atoms for every 1,000 ^{13}C atoms contained in the standard reference material. Similarly, a sample $\delta^{13}\text{C}$ value of -26 means that the sample had 974 ^{13}C atoms for every 1000 ^{13}C atoms in the reference material.

For carbon the most commonly used standard is Vienna Pee Dee Belemnite (VPDB), and will, of course, have a $\delta^{13}\text{C}$ value of 0. Originally PDB was a marine fossil, but the supply of the material has now been exhausted. In order to continue using the standard, the International Atomic Energy Agency (IAEA, based in Vienna) supply a number of reference materials that are calibrated against the original PDB. PDB had

an unusually high $^{13}\text{C}/^{12}\text{C}$, which means that measurements of most natural materials have a negative $\delta^{13}\text{C}_{VPDB}$ value.

4.1.2 Calibration of results

Samples and associated standards have generally been measured in batches of 50 or 100 samples, depending on the size of the autosampler carousel fitted to the elemental analyser (EA). At the beginning and end of every batch, two of each of the following standards were run: IAEA-CH-7 (polyethylene, $-32.15 \delta^{13}\text{C}$), IAEA-C6 (sucrose, $-10.80 \delta^{13}\text{C}$), USGS-24 (graphite, $-16.05 \delta^{13}\text{C}$), and USGS-40 (L-glutamic acid, $-26.39 \delta^{13}\text{C}$). After about every 10 samples analysed two USGS-24 standards were run in order to identify and correct for instrument artifacts if necessary. USGS-24 was selected for this purpose because its structure and morphology is most similar to that of the particulate matter samples, and its $\delta^{13}\text{C}$ was generally in the middle of the range of values that have been measured. A further two standards ‘WF’ (wheat flour) and ‘CF’ (corn flour) were used as a measure of the error associated with the measurement, and also used by the isotope laboratory to monitor the long-term behavior of the instrument. An annotated example of a typical batch of samples is shown in Figure 4.1.

Immediately before each sample or standard is measured by IRMS, two separate pulses of CO_2 reference gas are passed into the spectrometer in order to ‘zero’ the instrument. This means that initially the $\delta^{13}\text{C}$ that is reported for a sample or standard reference material is a value relative to the CO_2 reference gas. The CO_2 gas cylinder did not have a specifically isotopically certified composition for this purpose, and had an uncharacterised $\delta^{13}\text{C}_{VPDB}$ value. However, since any given cylinder of reference CO_2 has a homogenous isotopic composition, it provides a highly repeatable ‘zero’. An example EA-IRMS spectrum is shown in Figure 4.2, which shows the two peaks of reference CO_2 at 27 and 67 seconds respectively, followed by a sample peak at approximately 200 seconds. The three traces plotted in the CO_2 spectrum of Figure 4.2 show the detected CO_2 of masses 44, 45, and 46, which predominantly correspond to $^{12}\text{C}^{16}\text{O}_2$, $^{13}\text{C}^{16}\text{O}_2$, and $^{13}\text{C}^{17}\text{O}^{16}\text{O}$ respectively.

In order to convert to $\delta^{13}\text{C}_{VPDB}$, the measured values of the standards (relative to reference CO_2) were plotted against their certified values, and a linear fit was applied (in the case of all batches analysed for experiments in this thesis $R^2 \geq 0.994$). Figure 4.3 shows an example of this linear calibration; and using this calibration, $\delta^{13}\text{C}_{VPDB}$ of the samples was predicted.

4.1.3 Correction for background carbon

The blank smooth-walled tin capsules used for hydrocarbon liquid measurements were found to produce a very low intensity CO_2 peak when combusted on their own (empty) in the elemental analyser. Therefore, it was necessary to apply corrections to the results that were obtained using these capsules. For any given sample, the amplitude of the response from the sample can be calculated by subtracting the area of the peak

LOADING ORDER EXAMPLE (UEA FEB 2014)

Batch 11			17/02/2014 Tray: AARON5
Number	Tray ID	Sample Name	Weight (ug)
1	A1	IAEA-CH7	68
2	A2	IAEA-CH7	74
3	A3	IAEA-C6	100 uL
4	A4	IAEA-C6	100 uL
5	A5	USGS-24	77
6	A6	USGS-24	66
7	A7	USGS-40	100 uL
8	A8	USGS-40	100 uL
9	A9	Engine_Base_Diesel_Start_1	207
10	A10	Engine_Base_Diesel_Start_2	194
11	A11	Engine_Base_Diesel_Start_3	196
12	A12	Engine_Oleic_Acid_Nat_4	194
13	B1	WF	159
14	B2	CF	152
15	B3	Engine_Oleic_Acid_Nat_5	208
16	B4	Engine_Oleic_Acid_Nat_6	205
17	B5	Engine_Oleic_Acid-9,10_13C_7	198
18	B6	USGS-24	76
19	B7	USGS-24	77
20	B8	Engine_Oleic_Acid_13C18_10	199
21	B9	Engine_Oleic_Acid_13C18_11	201
22	B10	Engine_Oleic_Acid_13C18_12	205
23	B11	Engine_Oleic_Acid-1-13C_CON!_13	203
24	B12	WF	157
25	C1	CF	147
26	C2	Engine_Oleic_Acid-9,10_13C_8	205
27	C3	Engine_Oleic_Acid-9,10_13C_9	206
28	C4	Engine_Base_Diesel_End_14	194
29	C5	Engine_Base_Diesel_End_15	190
30	C6	Engine_Base_Diesel_End_16	200
31	C7	IAEA-CH7	73
32	C8	IAEA-CH7	68
33	C9	IAEA-C6	100 uL
34	C10	IAEA-C6	100 uL
35	C11	USGS-24	67
36	C12	USGS-24	73
37	D1	USGS-40	100 uL
38	D2	USGS-40	100 uL

Figure 4.1: Example of loading order of samples and standards for IRMS analysis. Where (a) are the standard reference materials, and (b) are the standards WF (wheat flour) and CF (corn flour) which are not used in the calibration, but used to check accuracy of the calibration and estimate the error associated with the measurement.

recorded for the blank capsule from that of the measured sample and capsule together, Equation (4.2). Likewise, the isotopic ratio measured is influenced by the $\delta^{13}\text{C}$ of the blank capsule. Thus using the mass balance Equation (4.3) the $\delta^{13}\text{C}$ of the sample is calculated in Equation (4.4):

$$Area_{sample} = Area_{measured} - Area_{blank} \quad (4.2)$$

$$\delta_{measured} \times Area_{measured} = \delta_{sample} \times Area_{sample} + \delta_{blank} \times Area_{blank} \quad (4.3)$$

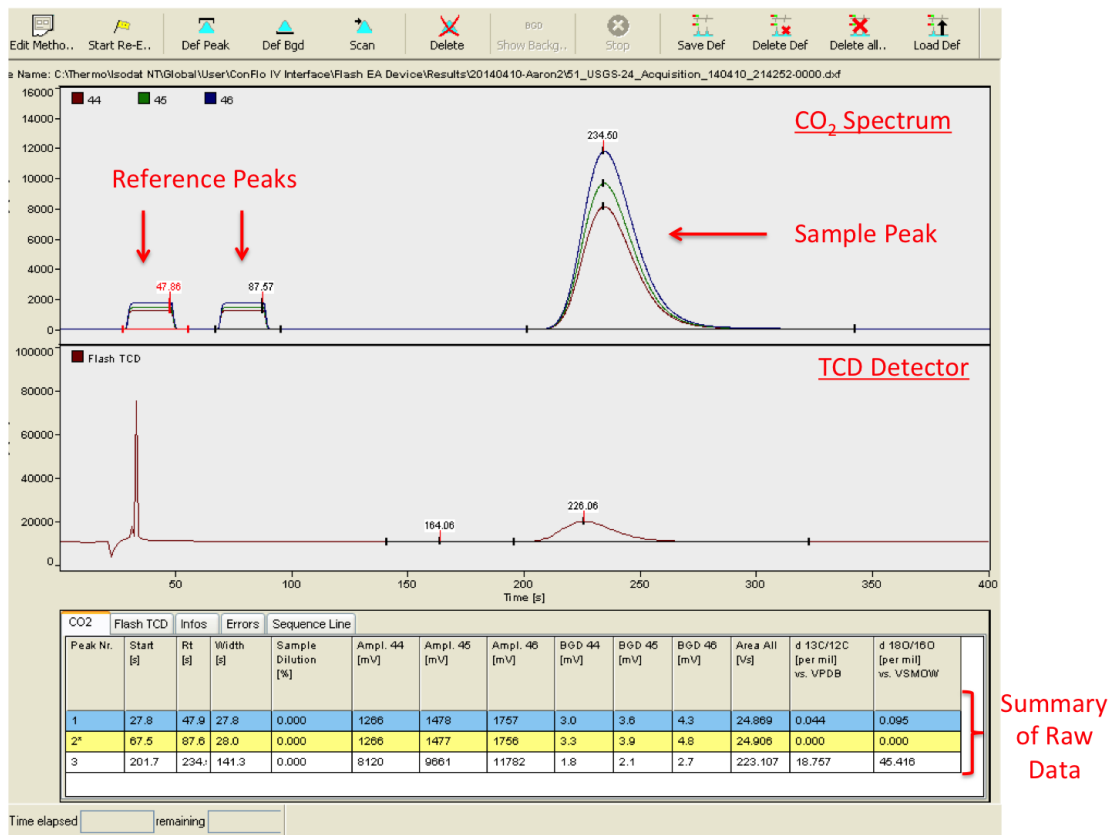


Figure 4.2: An example of a CO₂ isotopic spectrum measured by an IRMS instrument, shown in *Isodat 3.0* gas isotope ratio MS software. IRMS spectrum (top), TCD trace (middle), tabulated summary of IRMS peak interpretation (bottom).

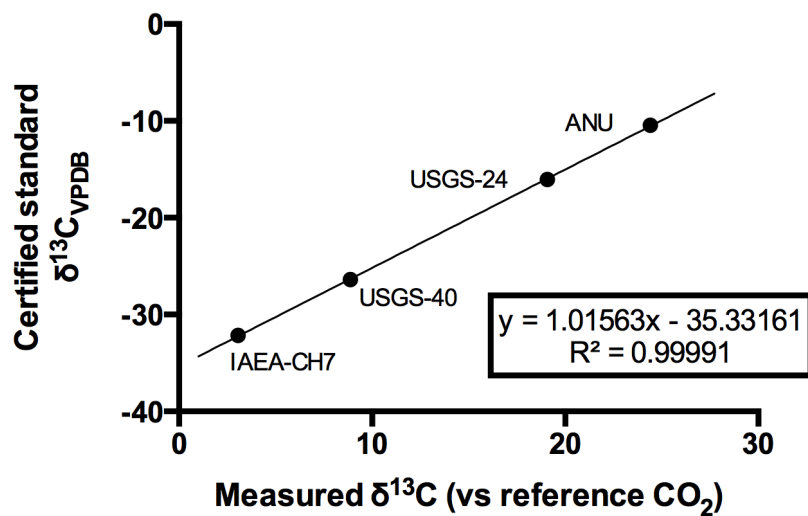


Figure 4.3: Example IRMS calibration curve using the isotopic standards USGS-24, IAEA-CH7, ANU (or IAEA-C6), and USGS-40.

Box 4.1. Definitions of the different fuel types.

- **Enriched fuel**, refers to a version of the fuel comprising of the unenriched fuel with a small amount of the labelled fuel added. Typically the enriched fuel had an enrichment of ~ 30 $\delta^{13}\text{C}$ with respect to the unenriched fuel.
- **Labelled fuel**, the undiluted isotopically tagged fuel containing ^{13}C at specific sub-molecular location(s), typically this fuel was of a purity of 99% and contained a ^{13}C on each of the molecules.
- **Unenriched fuel**, the standard laboratory-grade chemical ($\sim 99\%$ purity) containing the natural abundance of ^{13}C .

$$\delta_{\text{sample}} = \frac{\delta_{\text{measured}} \times \text{Area}_{\text{measured}} - \text{Area}_{\text{blank}} \times \delta_{\text{blank}}}{\text{Area}_{\text{sample}}} \quad (4.4)$$

4.1.4 Interpretation of the measured $\delta^{13}\text{C}$ values

As described in the sections above, samples were measured and the isotopic composition was reported in terms of $\delta^{13}\text{C}$. However, in this work it was mainly of interest to interpret these measurements in terms of the relative probability of a specific carbon atom within a molecule converting to particulate matter. To the best of the author's knowledge there is no standard methodology for calculating the relative contribution of labelled atoms converting to a product species; the methodology presented here has been developed specifically for this task. In order to clarify some of the terms relating to the different versions of the fuel (i.e. *enriched*, *unenriched*, *labelled*), the reader is referred to Box.4.1.

The reader is reminded that the purchased unenriched liquids, containing ^{13}C at natural abundance levels, were subsequently enriched with only small amounts of labelled compounds. For example, typically the equivalent of $45 \mu\text{L}$ of labelled ethanol- $1\text{-}^{13}\text{C}$ was used to enrich 100 mL of unenriched ethanol. The enrichment of the mixture was so small that the ^{13}C levels was still within the natural variability limits, in fact the vast majority of ^{13}C in the combined mixture (enriched fuel) originated from naturally occurring ^{13}C in the unenriched ethanol and not from the added labelled compound. Despite the relatively high background levels of ^{13}C the high precision measurements of the IRMS overcame this.

Isotopic measurements of all unenriched (or 'native') and labelled fuels ($\delta^{13}\text{C}_F$) and the particulate matter derived from them ($\delta^{13}\text{C}_{PM}$) were required. For each fuel and derived PM, a calculation was made of the difference in isotopic composition between the unenriched and enriched versions called Δ_F and Δ_{PM} as follows:

$$\Delta_{(F)} = \delta^{13}\text{C}_F^* - \delta^{13}\text{C}_F^n \quad (4.5)$$

$$\Delta_{(PM)} = \delta^{13}C_{PM}^* - \delta^{13}C_{PM}^n \quad (4.6)$$

where the (*) refers to the enriched fuel or the PM derived from it, and the (n) refers to the unenriched (or ‘native’) fuel or PM derived from it. Also calculated were the parameters Δ_{max} and $F_{labelled}$ according to Equation (4.7) and 4.8 as follows:

$$\Delta_{max} = \frac{\Delta_F}{n_{labelled}} \times n_{total} \quad (4.7)$$

$$F_{(labelled)} = \frac{\Delta_{PM}}{\Delta_{max}} \quad (4.8)$$

where $n_{labelled}$ represents the number of carbon atoms labelled and n_{total} represents the total number of carbon atoms (sum of ^{12}C and ^{13}C atoms) within the chemical compound used as fuel. The parameter Δ_{max} represents the maximum enrichment that could be reached by the chemical compound used as fuel if all its carbon atoms were ^{13}C . The parameter $F_{labelled}$ represents the contribution to PM, as a fraction of the total PM carbon, of the labelled carbon positions in the fuel. The product $F_{labelled} \times 100$ gives the % contribution of the labelled ^{13}C atom to PM. Despite the apparent simplicity of the calculation, the origin and significance of the parameters described in this section are more complex, and are described in greater detail in the following section.

4.1.5 Significance and origins of the applied methodology: Example of calculation to derive the contribution of the labelled carbon atom to the formation of particulate matter

For simplicity the calculation protocol is described here in more detail for the case of ethanol used as a single-component fuel. For all other molecules the protocol is identical, and the molecules are treated as being made of two components: the labelled carbon atom location(s) being one component and all the other carbon atom location(s) being the second component.

Ethanol is a molecule containing two carbon atoms. In this molecule C_1 is the carbon atom bonded to the hydroxyl functional group (OH) and C_2 is the methyl carbon atom. When adding a small amount of ^{13}C labelled ethanol 100% labelled at one carbon atom to unenriched ethanol, in the resulting mixture only one carbon atom in the resulting fuel will be isotopically enriched in ^{13}C , and the enriched site is appropriately named. When calculating the contribution of a carbon atom from the fuel (in this example the fuel is ethanol) to particulate matter, it has to be compared to the behavior of an enriched fuel with the unenriched (‘native’) counterpart. For the unenriched (‘native’) ethanol fuel (before the addition of a labelled compound) measurements determined the overall $\delta^{13}C_{E_n}$ to be -27.8 per mille, and it is assumed that the isotopic composition (delta values) of the individual carbon atoms in this fuel is identical to the overall composition of this fuel (i.e. $\delta^{13}C_{E_n} = (\delta^{13}C_{C_1}) = (\delta^{13}C_{C_2}) = -27.8$ per mille).

In reality, the two carbon atoms in the ethanol molecule probably have slightly different isotopic compositions, but these cannot be measured. Thus, the best assumption one can make is that both carbon atoms have the same isotopic composition, and are equal to the overall composition of this compound.

For the case of the ethanol enriched to an overall delta value of $\delta^{13}C_{E_l} = -6.1$ per mille and labelled at C_2 , the delta value of C_2 can be calculated using Equation (4.9), as follows:

$$\delta^{13}C_{E_l} = [(\delta^{13}C_{C_1}) \times (0.5)] + [(\delta^{13}C_{C_2}) \times (0.5)] \quad (4.9)$$

Knowing that each carbon atom contributes equally to the bulk (overall) isotopic composition of this labelled fuel and assuming that C_1 has an isotopic signature equal to -27.8 per mille.

Next, the isotopic composition of the C_2 position was calculated, knowing that this labelled ethanol has a bulk isotopic composition of $\delta^{13}C_{E_l} = -6.1$ per mille and that each carbon atom contributes equally to its bulk isotopic composition. For simplicity, the unenriched ethanol is called E_n and the labelled ethanol that was mentioned above is E_l . Following this calculation a delta value for the C_2 position in this labelled ethanol was determined to be $\delta^{13}C_{C_2} = +15.6$ per mille. Using the isotopic delta values for the individual carbon atoms in E_n and E_l , and knowing the isotopic compositions of the particulate matter derived from these two ethanol sources, a calculation was made of the contributions of each carbon atom (C_1 and C_2) from the ethanol molecule to the PM formation. It is not expected that the isotopic signatures of the carbon atoms in the fuels to transfer to the particulate matter without being altered by potential fractionation paths. Therefore, fractionation factors are taken into account when calculating the isotopic signatures of C_1 and C_2 that gets incorporated into the PM (this means that the isotopic signatures of C_1 and C_2 that form PM might not be identical to their original signatures in the ethanol fuel, but they will be proportional to the signatures in the starting fuel). The fractionation factors, describing the partitioning of an isotopic species between the starting and the end material, in this case ethanol and PM derived from it, for C_1 and C_2 are:

$$\alpha_{C_1} = \frac{1000 + (\delta^{13}C_{C_1})_{E_n}}{1000 + (\delta^{13}C_{C_1})_{PM_n}} \quad (4.10)$$

and

$$\alpha_{C_2} = \frac{1000 + (\delta^{13}C_{C_2})_{E_n}}{1000 + (\delta^{13}C_{C_2})_{PM_n}} \quad (4.11)$$

From Equation (4.10) and (4.11) the $(\delta^{13}C_{C_1})_{PM_n}$ and $(\delta^{13}C_{C_2})_{PM_n}$ are calculated as a function of the fractionation factor and use these isotopic signatures in the mass balance equation that can be written for the PM derived from the E_n , Equation (4.12). The same fractionation factors can be written for the case of the ^{13}C labelled ethanol and derived PM, from which $(\delta^{13}C_{C_1})_{PM_l}$ and $(\delta^{13}C_{C_2})_{PM_l}$ are calculated and used

in the mass balance equation that can be written for the PM derived from the E_l , Equation (4.13). For the PM derived from E_n the isotopic signature is calculated as follows:

$$\delta^{13}C_{PM_n} = a \times \left(\frac{1000 + (\delta^{13}C_{C_1})_{E_n} - 1000}{\alpha_{C_1}} \right) + b \times \left(\frac{1000 + (\delta^{13}C_{C_2})_{E_n} - 1000}{\alpha_{C_2}} \right) \quad (4.12)$$

For the PM derived from E_l the isotopic signature is calculated as follows:

$$\delta^{13}C_{PM_l} = a \times \left(\frac{1000 + (\delta^{13}C_{C_1})_{E_l} - 1000}{\alpha_{C_1}} \right) + b \times \left(\frac{1000 + (\delta^{13}C_{C_2})_{E_l} - 1000}{\alpha_{C_2}} \right) \quad (4.13)$$

In Equation (4.10) to Equation (4.13) the following notations were used:

$\delta^{13}C_{PM_n}$ and $\delta^{13}C_{PM_l}$ = the measured delta values for the PM derived from E_n and E_l respectively (continuing the example of ethanol, these values are -31 permil and -1.5 per mille respectively).

$\delta^{13}C_{E_n}$ and $\delta^{13}C_{E_l}$ = the measured delta values for the unenriched ('native') and enriched ethanol (for the ethanol example, these values are -27.8 permil and -6.1 permil respectively).

a and b are the contributions of C_1 and C_2 to the PM formation. Note that regardless from which ethanol fuel PM is derived, the proportions in which C_1 and C_2 contribute to PM are the same. Also $a+b=1$, i.e. the total mass of the PM formed from any ethanol fuel is made up of contributions from C_1 and C_2 .

α_{C_1} = the fractionation factor describing the distribution of ^{13}C for C_1 between the starting and the ethanol and PM derived from it.

α_{C_2} = same as above but for C_2 .

$(\delta^{13}C_{C_1})_{E_n}$ and $(\delta^{13}C_{C_1})_{E_l}$ = the delta value of C_1 in the E_n and E_l respectively (both equal to -27.8 permil, as the tracer was added to C_2 in E_l).

$(\delta^{13}C_{C_2})_{E_n}$ and $(\delta^{13}C_{C_2})_{E_l}$ = same as above for C_2 (equal to -27.8 permil and +15.6 permil respectively, as mentioned above).

$(\delta^{13}C_{C_1})_{PM_n}$ and $(\delta^{13}C_{C_1})_{PM_l}$ = the delta value of C_1 in the PM derived from E_n and E_l respectively.

$(\delta^{13}C_{C_2})_{PM_n}$ and $(\delta^{13}C_{C_2})_{PM_l}$ = the delta value of C_2 in the PM derived from E_n and E_l respectively.

Using Equation (4.12) and (4.13) the difference between isotopic signatures of the PM formed from the unenriched and enriched fuels is calculated as follows:

$$\Delta_{(PM)} = \delta^{13}C_{PM_l} - \delta^{13}C_{PM_n} \quad (4.14)$$

from which a and b were calculated. This is possible because it is known that (i) $a + b = 1$, (ii) the fractionation factors α_{C_1} and α_{C_2} are the same for the formation of PM from E_n and from E_l , (iii) $(\delta^{13}C_{C_1})_{E_n} = (\delta^{13}C_{C_1})_{E_l} = -27.8$ permil (C_1 isotopic composition is unaffected by the addition of the ^{13}C label at C_2 in E_l), (iv) the term

containing α_{C_1} cancels out while solving this equation, (v) α_{C_2} can be assumed as equal to 1, at temperatures above 1000°C and (vi) $(\delta^{13}C_{C_2})_{E_i} = +15.6$ per mille and $(\delta^{13}C_{C_2})_{E_n} = -27.8$ per mille, as mentioned above.

From solving Equation (4.14), b can be calculated as follows:

$$b = \frac{\Delta_{PM}}{(\delta^{13}C_{C_2})_{E_i} - (\delta^{13}C_{C_2})_{E_n}}$$

For the example discussed so far, the value for $b = 0.68$. This means that C_2 (the labelled carbon atom in this example) has a 68% contribution to the formation of PM when ethanol is used as a fuel.

The same approach can be applied for any of the single-component fuels considered in this thesis, and in doing so it was noticed that the denominator in the calculation of b is equal to the maximum enrichment one could expect if all the carbon positions in the fuel molecule are enriched to the same amount. This also means that one does not have to calculate the isotopic composition of the enriched position in any given molecule used as fuel; thus for simplicity, the term Δ_{max} has been calculated as follows:

$$\Delta_{max} = \frac{\Delta_F}{n_{labelled}} \times n_{total} \quad (4.15)$$

where $n_{labelled}$ represents the number of labelled carbon atoms of the organic compound used as fuel, n_{total} represents the total number of carbon atoms in the molecule of the compound used as fuel and Δ_F represents the difference in the isotopic composition of the labelled compound ($\delta^{13}C_{F_i}$) used as fuel and the same compound prior to the addition of the ^{13}C tracer ($\delta^{13}C_{F_i}$), thus:

$$\Delta_F = \delta^{13}C_{F_i} - \delta^{13}C_{F_n} \quad (4.16)$$

Generalising from the example considered for the case of ethanol, F is calculated, which is defined as the fractional contribution to the PM of the labelled carbon atom location(s) in the fuel molecule, as follows:

$$F = \frac{\Delta_{PM}}{\Delta_{max}} \quad (4.17)$$

The contribution to the formation of PM for the rest of the unlabelled carbons is equal to $1 - F$. It should be noted that from the above explanation it appears necessary to assume that $\delta^{13}C$ of the local carbon atoms in the native (unenriched) ethanol is equal to the overall composition of the mixture (i.e. $\delta^{13}C_{E_n} = \delta^{13}C_{C_1} = \delta^{13}C_{C_2}$). In reality, it is possible that the local $\delta^{13}C$ of the two carbon atoms in ethanol may not be equal, since the ethanol that has been used throughout this work was derived from yeast fermentation of agricultural substrates, a process that could result in the preferential incorporation of isotopic carbon into a specific molecular locality. Even in the case that $\delta^{13}C$ of the two atoms was vastly different in nature, it would have no influence on the outcome of the calculation. The only assumption that is required is that the overall

conversion rate to PM of a molecule containing carbon-13 is at the same rate as that of carbon-12. Supporting this assumption, it was observed that when a molecule is labelled with ^{13}C at every carbon atom, the isotopic enrichment of the fuel was equal to the enrichment observed in the PM (i.e. $\Delta_{(F)} = \Delta_{(PM)}$), which shows that ^{12}C and ^{13}C convert at the same rate. Data supporting this point is supplied and discussed in Chapter 6.

4.1.6 Calculation required to isotopically enrich a fuel by a desired amount

In this work, unenriched fuels have been enriched with small amounts high-assay ^{13}C fuels. For example, 45 μL of ethanol-1- ^{13}C was added into 100 mL of unenriched ethanol and it resulted in an increase in the ^{13}C rate from about $-27 \delta^{13}\text{C}$ to $-7 \delta^{13}\text{C}$, an increase of 20 δ . It was desirable to enrich the fuel by precise amounts for several reasons. Firstly, as it has been discussed above (Section 4.1.2), the IRMS instrument was calibrated with a range of standard reference materials, and it was therefore desirable that the isotopic signature of the samples were around the calibrated range. Secondly, fuels needed to be isotopically enriched by just enough to give sufficient resolution but not too much that the experiment became prohibitively expensive. In order to enrich any given fuel with its labelled counterpart to a desired level, simple molar calculations were used.

First, the $^{13}\text{C}/^{12}\text{C}$ isotope ratio of the labelled fuel ($R_{labelled}$) was obtained as follows:

$$R_{labelled} = \frac{n_{labelled}}{n_{total} - n_{labelled}} \quad (4.18)$$

where $n_{labelled}$ is number of labelled carbon atoms in the molecule and n_{total} is the total number of carbon atoms. For example, take ethanol-1- ^{13}C where one carbon atom out of the two is ^{13}C labelled, the $^{13}\text{C}/^{12}\text{C}$ in this case is clearly 1, and this value is obtained from Equation (4.18).

The next step was to calculate the theoretical $\delta^{13}\text{C}$ of the undiluted labelled fuel ($\delta^{13}\text{C}_{labelled}$), using $R_{labelled}$ calculated in Equation (4.18). For this calculation it was necessary to assume an absolute $^{13}\text{C}/^{12}\text{C}$ for 0 $\delta^{13}\text{C}_{PDB}$, and here a ratio of 0.01124 is assumed, as reported by Craig (1957).

$$\delta^{13}\text{C}_{labelled} = \left(\frac{R_{labelled}}{0.01124} - 1 \right) \times 1000 \quad (4.19)$$

When the undiluted labelled fuel was added in small quantity to the unlabelled fuel, the resulting mixture had a delta value ($\delta^{13}\text{C}_{mixture}$) that was influenced by the isotopic composition and quantities of the two components, as follows:

$$\delta^{13}\text{C}_{mixture} = [a \times (\delta^{13}\text{C}_{unlabelled})] + [b \times (\delta^{13}\text{C}_{labelled})] \quad (4.20)$$

where a and b are the molar quantities of $\delta^{13}\text{C}_{unlabelled}$ and $\delta^{13}\text{C}_{labelled}$ respectively.

The molar ratio (a:b) required to enrich the unlabelled fuel to a desired level ($\delta^{13}\text{C}_{mixture}$) can be calculated by solving for b, as follows:

$$b = \frac{(\delta^{13}\text{C}_{mixture}) - a \times (\delta^{13}\text{C}_{unlabelled})}{(\delta^{13}\text{C}_{labelled})} \quad (4.21)$$

4.2 Gas composition

In the experimental work carried out in the laminar flow reactor it was necessary to define the composition of gasses, for example the concentration of fuel in nitrogen at the inlet of the reactor, or the exhaust gas composition at the reactor outlet. In this thesis the abundance of gaseous components has usually been expressed in terms of parts per million volume (ppmv). As an example Table 4.1 gives the composition of air and an example mixture containing 10,000 ppmv of methane in nitrogen. It has been of interest to define and fix inlet flow rates in terms of ppm due to the fact that the focus of the work has mainly involved exploring molecular effects of fuel on the pyrolysis products. For example, in Chapter 5 comparisons between propane and propanol are made; it was therefore of interest to fix the molecular concentration at the reactor inlet of the two C_3 fuels, rather than on a fixed mass or volumetric flow rate basis.

In this thesis, the inlet flow rate of a given hydrocarbon (hc) in a nitrogen carrier gas was set in terms of ppmv, defined as follows:

$$ppmv_{hc} = \frac{\dot{n}_{hc}}{\dot{n}_{hc} + \dot{n}_{N_2}} \times 1,000,000 \quad (4.22)$$

where $ppmv_{hc}$ is the inlet molar concentration of a given hydrocarbon (hc), \dot{n} is the molar flow rate of the hydrocarbon (hc), or nitrogen (N_2). As long as the ratio of the molar flow rates of the hydrocarbon and nitrogen ($n_{hc} : n_{N_2}$) is conserved the ppmv concentration is unchanged.

The molar flow rate may be converted to a mass flow rate as follows:

$$\dot{m}_{hc} = \dot{n}_{hc} \times \bar{M}_{hc} \quad (4.23)$$

where \dot{m} is the mass flow rate, and \bar{M}_{hc} is the molecular weight of the hydrocarbon.

4.3 The equivalence ratio of combustion experiments

Under the theoretical conditions where there is just the right amount of air to fully oxidise the fuel, the mixture is said to be *stoichiometric*. For example, Equation (4.24) shows the overall complete combustion equation for a general hydrocarbon fuel (C_aH_b) in air under stoichiometric conditions.

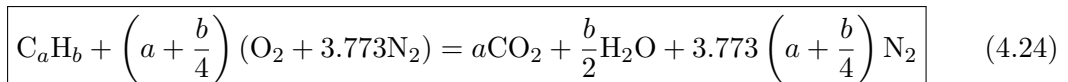


Table 4.1: Example of the ppm composition of (a) air composition and (b) a mixture of methane and nitrogen.

Gas	ppmv	Molecular weight	Mole fraction	Molar ratio
Composition of dry air				
O ₂	209,500	31.998	0.2095	1
N ₂	780,900	28.012	0.7905	3.773
A	9,300	38.948		
CO ₂	300	40.009		
Air	1,000,000	28.962	1.000	4.773
CH₄ at 10,000 ppmv in Nitrogen				
CH ₄	10,000	16.04	0.01	1
N ₂	999,000	28.012	0.99	99

It should be noted that only the molar ratios (numbers in front of the chemical symbol) are defined in this equation, therefore the fuel composition could have been written as CH_y where $y = b/a$. For the purposes of the pyrolysis experiments conducted in this thesis, it was assumed that nitrogen, which is present in air and used as a carrier gas in the pyrolysis experiments, emerges unreacted. Equation (4.24) describes the theoretical conditions where there is just enough air to fully oxidise the fuel. At conditions where there is excess air the mixture is deemed to be fuel lean, or where there is less air than required the mixture is determined to be fuel rich (Heywood, 1988).

In this work, experiments were conducted using various air/fuel mixtures, and the mass flow rates for inlet fuel (\dot{m}_f) and air (\dot{m}_a) have been measured. The ratio of these two flow rates is useful for defining the conditions, as follows:

$$\text{Air/fuel ratio}(A/F) = \frac{\dot{m}_a}{\dot{m}_f} \quad (4.25)$$

or

$$\text{Fuel/air ratio}(F/A) = \frac{\dot{m}_f}{\dot{m}_a} \quad (4.26)$$

In order to set the equivalence ratio (the ratio of fuel and air, (F/A) , relative to the stoichiometric ratio $(F/A)_s$) of a combustion or pyrolysis experiment an equation for the complete combustion of fuel under stoichiometric fuel-to-air ratios is first determined. The stoichiometric air/fuel or fuel/air ratio is dependent on the composition of the fuel being burned and can be calculated using Equation (4.24), and the molecular weights of oxygen (32), nitrogen (28.16), carbon (12.011), and hydrogen (1.008), as follows:

$$\left(\frac{A}{F}\right)_s = \left(\frac{F}{A}\right)_s^{-1} = \frac{(1 + y/4)(32 + 3.773 \times 28.16)}{12.011 + 1.008y} = \frac{34.56(4 + y)}{12.011 + 1.008y} \quad (4.27)$$

Due to the fact that the stoichiometric fuel/air ratio depends on the molecular composition of the fuel, the ratio of the actual fuel/air ratio of the experiment to the

fuel/air ratio stoichiometric conditions is a more useful parameter. This is commonly expressed as the *fuel/air equivalence ratio* (ϕ), as follows:

$$\phi = \frac{(F/A)_{actual}}{(F/A)_s} \quad (4.28)$$

or the inverse, the air/fuel equivalence ratio (λ), as follows

$$\lambda = \phi^{-1} = \frac{(A/F)_{actual}}{(A/F)_s} \quad (4.29)$$

In this thesis the air-to-fuel ratio (λ) has generally been used throughout, the conditions employed in the reactor were generally fuel-rich ($\lambda < 1$) in order to generate sufficient sample of particulate matter for collection. It should be noted that the air and fuel flow rates were highly diluted with nitrogen at the entry of the flow reactor.

4.4 Representation of experimental error

Throughout this thesis, where error bars are indicated on figures, the error bars show plus and minus one standard deviation from the mean value, where the mean value was obtained from experimental repeats. In some instances, for example where particulate matter has been collected from the engine for isotopic analysis, only one experimental run was possible due to the high cost associated with the fuel, in these cases the standard deviation has been obtained from the repeat IRMS measurements of the collected sample.

Chapter 5

High-temperature pyrolysis of C₁-C₄ hydrocarbons and C₁-C₅ alcohols

In this chapter a number of C₂ to C₄ hydrocarbons, as well as C₁ to C₅ alcohols have been analysed to determine their relative tendency to form soot in a laminar flow tube reactor, at temperatures in the range of 1000 to 1400 °C. A range of fuel molecules including alkanes and alkenes, and primary and secondary alcohols have been assessed; this has given insights into the influence of the molecular structure of the fuel on its tendency to form soot under the well-controlled pyrolysis conditions of a laminar flow tube reactor.

5.1 Introduction

It is well established that the conversion of fuel to emissions during combustion or pyrolysis is influenced by the molecular structure of the fuel being burned, and this has been the subject of a number of studies over the years (e.g. Hunt, 1953; Calcote and Manos, 1983; Ladommatos et al., 1996). A number of studies have investigated the propensity of individual molecules or ‘single-component fuels’ to form particulates, and a variety of methods have been reported in the literature to make such determinations. From about the 1930s smoke point tests have been used to determine the quality of a fuel, originally the test was used to determine the quality of kerosene in producing soot for illumination, and similar tests have since been used to assess the tendency of various fuels to form soot. In a diffusion-type flame, soot is formed in an oxygen deficient environment at the core of the flame by pyrolytic reactions. The soot is subsequently oxidised as it passes through the reaction zone of the flame, and at low fuel flow rates all of the soot formed within the flame is consumed as it passes through the flame envelope. If the rate at which fuel is supplied to the flame is progressively increased, at a certain flame height the soot formation rate exceeds the oxidation rate and soot will begin to

emerge from the tip of the flame, and this is called the sooting height or smoke point. The smoke point is the most prevalent method for determining the propensity of a fuel to form soot. Due to the fact that the smoke point or the sooting height is also a function of the experimental apparatus, several normalisation methods have been introduced over the years (Watson et al., 2013). The most commonly used metric for qualitatively assessing the relative ‘sooting tendency’ of a fuel is the threshold sooting index (TSI), which was defined by Calcote and Manos (1983), as follows

$$\text{TSI} = a \left(\frac{M}{h} \right) + b \quad (5.1)$$

where h is the sooting height, M is the molecular weight, and the parameters a and b are specific to the experimental equipment. The TSI has a scale from 1 to 100, a value of 0 was assigned to ethane and value of 100 to naphthalene; where the higher value indicates an increased tendency to form soot. It is seen from Equation (5.1) that the TSI is proportional to the molecular weight, and inversely proportional to the sooting height.

Ladommatos et al. (1996) investigated the sooting tendency of a range of single hydrocarbons including alkanes, alkenes, alkynes, branched, cyclic, and aromatic molecules in a laboratory diffusion flame. Table 5.1 presents some selected TSI values for various hydrocarbon molecules, and it can be seen that more unsaturated molecules tend to have higher sooting tendencies, and cyclic and aromatic molecules are the most prolific for forming soot. It is generally accepted that hydrocarbon molecules have increasing sooting tendencies in the order: paraffins < iso-paraffins < mono-olefins < alkynes < aromatics < polyaromatics.

It has been reported that in diffusion flames, binary and ternary mixtures of hydrocarbons tend to blend linearly (Gill and Olson, 1984), described in the following equation

$$\text{TSI}_{blend} = \sum x_f \text{TSI}_{pure} \quad (5.2)$$

However, it should be noted that fuel blends do not all necessarily have a sooting tendency that is simply the weighted sum of its components. A number of studies have reported that synergistic effects occur under certain conditions when specific fuels are blended (for example, Yoon et al., 2008; Roesler et al., 2003; Roesler and De Tessian, 2000; Wang et al., 2013). Roesler et al. (2003) conducted experiments in a flow reactor at 1340 K, with fuel mixtures of ethylene and methane, highly diluted in nitrogen and at a constant carbon atom flow rate. It was reported that replacing the ethylene content with methane up to the maximum of 50% of the total carbon resulted in an increase in the production of PAHs (precursors to soot) by a factor of 2.5 compared to ethylene only pyrolysis. Given that the sooting tendency of methane is known to be less than that of ethylene, it might have been expected that the gradual replacement of ethylene with methane would have reduced the soot yield. However, this synergistic effect was

Table 5.1: Some selected TSI values for various hydrocarbon fuels (values from (Ladommatos et al., 1996)).

Fuel	Formula	TSI
Ethane	C ₂ H ₆	0.00
Ethene	C ₂ H ₄	1.30
Ethyne	C ₂ H ₂	3.70
Benzene	C ₆ H ₆	31.00
Butane	C ₄ H ₁₀	1.40
Cyclohexane	C ₆ H ₁₂	3.20
Heptane	C ₇ H ₁₆	2.70
Hexane	C ₆ H ₁₄	2.50
Naphthalene	C ₁₀ H ₈	100.00
Propane	C ₃ H ₈	0.60

attributed to the production of methyl radicals from the methane, which promoted aromatic formation through ‘carbon-odd’ reaction channels (e.g. C₃H₃, as discussed in Chapter 2).

The main benefits of tests using smoke point lamps to determine the sooting propensity is that the TSI is widely used and many fuels have been characterised, the experiments are practical and easy to carry out, moreover, the sooting propensities from smoke point tests well predict the soot forming tendencies of fuels in real engines (Yang et al., 2007). However, it should be mentioned that there are several disadvantages, and despite efforts to clearly define smoke point, there is inherently an element of subjectivity to the tests. Recently it has been pointed out by Li and Sunderland (2012) that a flaw in the TSI is in the use of the molecular weight (M) in the equation as a measure of the stoichiometric ratio. The flaw is evident when fuels exhibit a similar smoke point but have a very different molecular weight. The result is that a higher sooting propensity will be assigned to the higher molecular weight fuel even when they exhibit nearly identical flame lengths and at equal mass flow rates.

The classic smoke point tests that utilise a diffusion-type burner indicates the overall tendency of a fuel to form soot in a flame; the extent that a hydrocarbon decomposes in the pyrolysis region of a diffusion flame is also a function of the temperature, and the molecular diffusivity influences the flame shape. So a question which arises is: when the conditions such as temperature and physical effects are well controlled, what is the *natural* influence of the molecular structure of the fuel on the pyrolysis products?

A number of examples in the literature have employed a flow reactor for the pyrolysis of fuels in order to determine the tendency of molecules to convert to soot and various other emissions (e.g. Esarte et al., 2009; Ruiz et al., 2007b). The benefit of using apparatus such as a flow reactor or jet-stirred reactor for such determinations is that the conditions such as temperature, fuel flow rate, and pressure can be tightly controlled. The pyrolysis studies that are reported usually involve determining the particulate mass evolved from a flow reactor by means of filter-based particulate collection. In this chapter, a differential mobility particle spectrometer instrument (Cambustion DMS500) has

been used to determine the total mass concentrations of soot evolved from the tube reactor, and in addition, the size and mass distributions of particulates (smaller than 1000 nm) are also reported. The overall sooting propensity of a fuel is an important parameter, but so too is the particle size distribution, due to the fact that smaller size particles (< 100 nm) are more harmful as they can reach the human lungs and stay airborne for much longer periods of time. Such studies can provide valuable insights as to the overall influence that functional group chemistry has on the generation of particulate. It is intended that this work will contribute to the description of how the molecular structure of a fuel influences the conversion of carbon to soot, and eventually towards the development of models which will be able to predict sooting tendency and particle size distribution for a variety of fuels.

5.2 Experimental method

5.2.1 Apparatus

The experiments conducted in this chapter have been using the flow reactor facility and measuring equipment described in Chapter 3. Testes were conducted at atmospheric pressure, and the temperature of the fuel vapouriser was set at 200°C for all experiments.

Where the fast flame ionisation detector (fFID) was used to profile the inlet or outlet hydrocarbon concentrations at the reactor tube centreline, measurements were made over a 40 second window and the results represent the average measurement. Due to the design of the fFID instrument, which draws sample through a capillary, measurements made under sooting conditions required a filter to be placed before the sampling probe of the fFID to prevent blocking the capillary sampling tube, which could reduce sample flow and therefore influence the FID response. The filter was changed at regular intervals to ensure that filter plugging by soot did not influence the sample flow. Additionally calibration gas (4000 ppmv methane in nitrogen) was used to check instrument calibration immediately before and after each measurement.

The Cambustion DMS500 was operated at the sampling conditions described in Chapter 3.

5.2.2 Fuel molecules investigated

A number of oxygenated and hydrocarbon molecules have been studied in terms of their conversion to PM and CO and CO₂ in a laminar flow reactor. These molecules are discussed as four separate homologous series: C₂, C₃, and C₄ molecules, Figure 5.1; and C₁ to C₅ alcohols, Figure 5.2. The selection of these homologous molecules will allow the influence of the following molecular structures to be assessed:

C₂ series:

- The influence of the presence of oxygen in the molecule, in the form of an hydroxyl group -OH (comparing ethanol to ethane).
- The effect of a carbon-carbon double bond (C=C), compared to a single bond (C-C), by comparing ethane to ethylene.

C₃ series:

- The influence of the presence of the alcohol group in a carbon chain (comparing particulate emissions of 1-propanol and 2-propanol to that of propane)
- The influence of moving the alcohol group from the end of the chain in 1-propanol to the middle of the chain in 2-propanol.
- Whether the carbon-carbon double bond which is present in propene has an impact on the conversion of carbon to PM with respect to that of propane.

C₄ series:

- The influence on going from a straight-chained alkene (butane) to a branched alkane (*i*-butane).

Series of C₁-C₅ alcohols:

- The effect of increasing carbon chain length (comparing methanol, ethanol, 1-propanol, 1-pentane).
- The influence of going from a primary alcohol (1-propanol) to a secondary alcohol (2-propanol).
- The effect of going from a straight-chained alcohol (1-pentane) to a cyclic alcohol (cyclopentanol).

5.2.3 Calculation of percentage yield

In this chapter the percentage soot and gas yields from different fuels is reported. The percentage carbon content of the soot relative to the total amount of carbon fed into the reactor, has been defined as follows:

$$\text{Soot yield(\%)} = \frac{C_{\text{soot}}}{C_{\text{inletgases}}} \times 100 \quad (5.3)$$

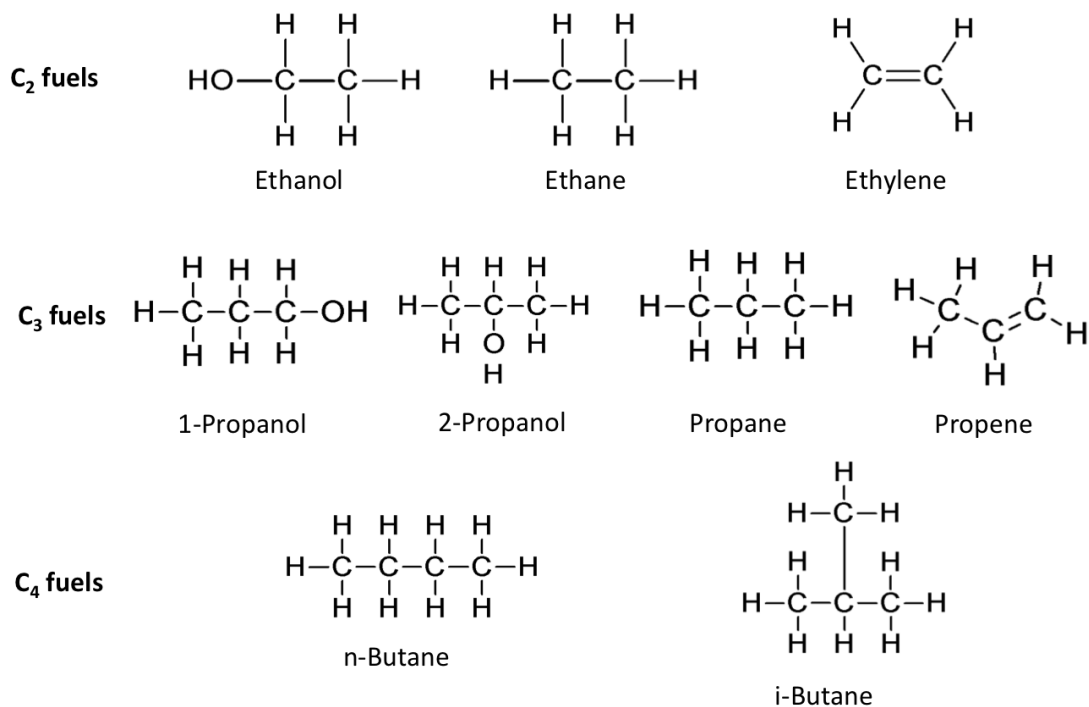


Figure 5.1: Molecular structures of the C₁ to C₄ hydrocarbons.

Series of C₁-C₅ Alcohols

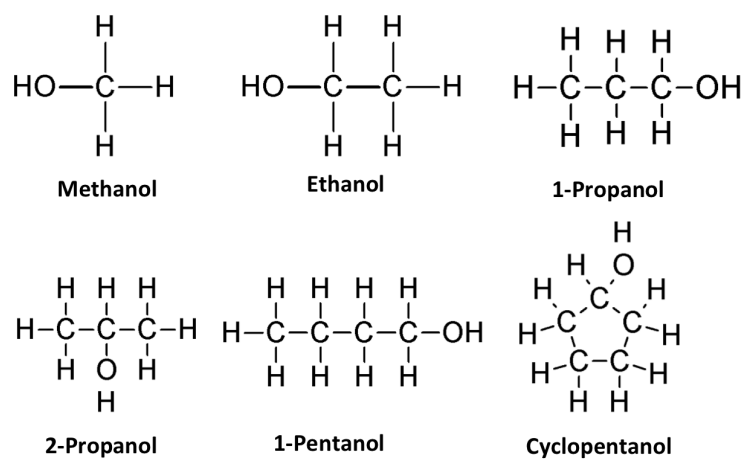


Figure 5.2: Molecular structures of the C₁ to C₅ alcohol molecules.

Likewise, the percentage carbon content of the gaseous products, relative to the total amount of carbon fed into the reactor, has been defined as follows:

$$\text{Gas yield(\%)} = \frac{C_{\text{outletgases}}}{C_{\text{inletgases}}} \times 100 \quad (5.4)$$

These percentage yields refer to the amount of carbon in the soot (C_{soot}), or in the effluent gas ($C_{\text{outletgas}}$), in relation to the amount of carbon fed into the reactor ($C_{\text{inletgases}}$).

Some caution should be heeded due to the fact that the experimental results indicated that the sum of the soot and gas yield was not 100%; the percentage yield was, therefore, generally used simply as an indication of the fate of carbon during pyrolysis. A number of factors contributed to this apparent imbalance of outlet/inlet carbon, including the production of tars and other pyrolysis products that are not measured by the FID or DMS500 due to their build-up in the reactor and in the instrument sampling lines. Additionally, the experimental systems used are subject to some overlap, where some of the smallest particles measured by the DMS (in the 5-20nm range) may also be picked up by the FID.

Finally, the response of the flame ionisation detector to carbon concentration may not be equal for all hydrocarbons and can be particularly suppressed for oxygenated molecules, see Table 5.2 for some of the response factors of the molecules tested. These FID response factors were used in order to verify the inlet concentration of the molecules under investigation. Due to the fact that the precise composition of the effluent gas was unknown, FID response factors were not applied to the results obtained from the analysis of the effluent gas at the reactor outlet.

Table 5.2: Relative FID response factors for a range of hydrocarbon and oxygenated fuels. Relative sensitivity values obtained from Dietz (1967)

Fuel	Relative sensitivity
Ethane	0.97
Ethylene	1.02
Propane	0.89
Butane	1.09
Methanol	0.23
Ethanol	0.46
<i>n</i> -Propanol	0.60
<i>i</i> -Propanol	0.53

5.3 Results and discussion

5.3.1 C₂ fuels

Figure 5.3 and 5.4 shows a summary of the characteristics of particulates formed during the pyrolysis of ethane, ethylene and ethanol, at an inlet concentration of 8,000 ppmv

(0.8% v). As an example, the the size and number spectra for the particulate matter formed from ethanol, ethane, and ethylene are supplied in Figure 5.3 (a) to (c) respectively. It can be seen in these spectra that for each of the three C₂ molecules there is a shift towards larger size particles with increasing formation temperatures. For example, in the case of ethanol pyrolysis, pyrolysis at 1200 °C resulted in particulates mainly in the size range of 100–400 nm, whereas at a higher temperature of 1400 °C, the particulates were generally distributed in the 100–700 nm range. This shift is also shown in Figure 5.4(c), which displays the median diameter of particle in terms of number concentration ¹. Shown in Figure 5.3(d) is an example mass spectrum for the pyrolysis ethanol pyrolysis, and corresponds to the ethanol number spectrum in Figure 5.3(a).

From the total number concentration of particulates evolved from the reactor, Figure 5.4(a), it is seen that high number concentrations of small diameter particles are formed at lower temperatures (around 1000 to 1200 °C). At higher temperatures (upwards of about 1200 °C), the number concentration falls and becomes constant as the median particle diameter increases, Figure 5.4(c). For example, it is seen that ethanol does not start to form particulates with a significant total mass until upwards of about 1100 °C, however high number concentrations nascent particles are still formed at lower temperatures, Figure 5.4(a). Figure 5.4(c) shows that there is a steep increase in the median particle diameter of PM formed from ethane and ethylene from about 50 nm at 1100 °C to about 150 nm at 1150 °C. This finding of rapidly increasing particle diameter coupled with a decreasing total particle number concentration is consistent with the agglomeration of spherical primary particles (of about 50 nm), to agglomerated structures composed of clusters of primary particles that are several hundred nm in size (Heywood, 1988).

Figure 5.4(b) shows the total mass concentration of particulates formed at various pyrolysis temperatures. In the case of all of the fuels tested it is observed that higher formation temperatures result in greater mass concentrations of particulates evolved from the reactor. It is seen that the presence of the alcohol group in ethanol has a large impact on the overall tendency of the molecule to form particulate matter, for example at 1250 °C ethanol formed a total of just 1.43 μg/cc of particulate, which compared to 3.21 μg/cc from ethane. By comparing the total mass of particulates formed from ethane and ethylene pyrolysis it is observed that ethylene appears to form higher mass concentrations of soot, particularly at higher temperatures; at the lower temperatures of 1000, 1050 and 1100 °C the total mass concentration of PM formed from ethane and ethylene is indistinguishable. Figure 5.4(b) also shows the particulate emissions in terms of percentage carbon yield, pyrolysis of ethanol at 1400 °C yielded 10% PM, and this compared to 35% for ethane, and 40% yield for ethylene; whilst a significant portion of the balance of the carbon is present in the effluent gas as unburned hydrocarbons, see Figure 5.5.

¹It should be noted that the particulate matter measured has a lognormal distribution of particulates, i.e. the log of the particle distribution is symmetrical, exemplified in Figure 5.3 (a) to (c). So therefore the median and mean of the lognormal distribution are equal.

In comparable work to that reported here, Ruiz et al. (2007a) investigated the pyrolysis of ethylene (C₂H₄) and acetylene (C₂H₂) in the temperature range of 1000 to 1200 °C, using a similar laminar flow reactor facility. In their experiments an inlet concentration of 15,000 ppmv was used, and a residence time of 1706/*k*(s) (equivalent to ~ 1.4s at 1200 °C). They observed increasing particulate yield at increasing reaction temperatures, and acetylene pyrolysis resulted in greater yields at all temperatures, with the greatest difference at low temperatures. This is in general agreement with this present work that the less saturated C₂ hydrocarbon tended to yield higher soot concentrations. It was found by Ruiz et al. (2007a) that pyrolysis of both acetylene and ethylene at 1200 °C, yielded about 40% soot; this compared to about a ~ 20% yield in this present work, although the inlet concentration was roughly half of that used by Ruiz.

In the literature, the most commonly cited reaction mechanism to soot involves the addition of acetylene (C₂H₂) to the edges of polycyclic aromatic hydrocarbons and at the edges of nascent soot particles by the so-called HACA mechanism (hydrogen abstraction C₂H₂ addition), and acetylene is therefore assumed to be an important species for soot formation (e.g. Frenklach, 2002). Therefore, it follows that if acetylene is indeed an important growth species, the formation conditions including temperature, inlet concentration, and the residence time of acetylene in the reactor will largely determine the soot yield. In the case of ethylene pyrolysis, acetylene is an intermediate product which must first be formed before undergoing HACA; the yield of soot is therefore dependent on the residence time of the acetylene following its formation from ethylene. In the series ethane (C-C bond), ethylene (C=C bond), and acetylene (C≡C bond), the molecules are progressively less saturated, and the mechanistic route for acetylene formation from ethylene is shorter than from ethane. In other words, in the series ethane, ethylene, and acetylene, mechanistically acetylene has a ‘head start’ in forming soot over ethylene, and ethylene has a ‘head start’ over ethane.

Naturally, it is expected that less soot would be formed from ethanol with respect to ethane, due to the oxygen content. The oxygen promotes the formation of carbon monoxide (CO), which reduces the concentration of carbon available for soot formation. Figure 5.6 shows the measured CO and CO₂ evolved from ethanol pyrolysis. It is observed that CO is formed in relatively high concentrations at all temperatures; whilst negligible amounts of CO₂ are produced. For example, at 1000 °C ethanol pyrolysis resulted in the evolution of 3000 ppmv CO, which accounted for approximately 20% of the carbon balance.

Previous work involving the pyrolysis of ethanol conducted by Peg et al. (2007), showed that pyrolysis of 50,000 ppmv ethanol in the temperature range of 800 to 1200 °C resulted in CO concentrations of ~25,000 ppmv at all temperatures; 25,000 ppmv would equate to ~25% carbon yield, similar to that obtained here, although the research conducted by Peg et al. was carried out at a much higher concentration. Additionally, they also observed small amounts (less than 2% yield) of CO₂ over the same range of

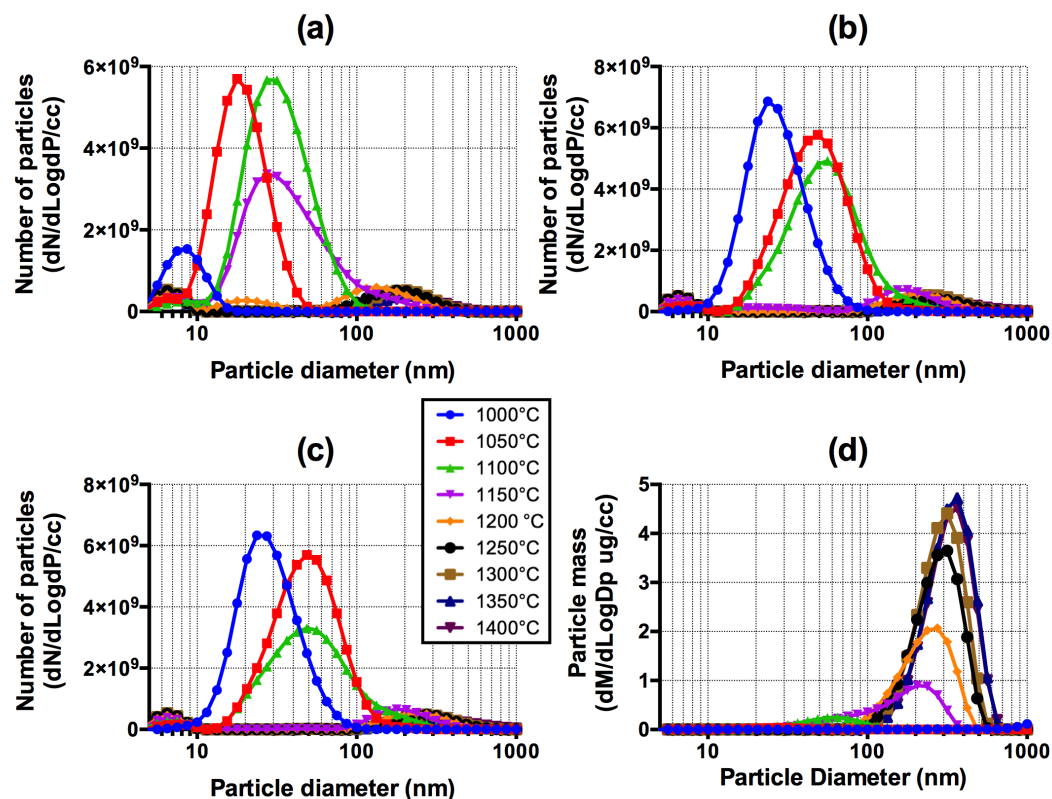


Figure 5.3: Number distribution of particulates formed from C_2 fuels: (a) ethanol, (b) ethane, and (c) ethylene. (d) shows an example of the size and mass spectra of ethanol pyrolysis at various temperatures.

temperatures. Other comparable research by Li et al. (2001) investigated the pyrolysis of ethanol in a variable pressure flow reactor, and characterised the outlet gases using fourier transform infrared (FTIR) spectrometry. At 3 bar, and 3000 ppmv inlet concentration it was seen that as well as CO there were significant concentrations of oxygen containing molecules including water (H_2O), ethanol (CH_3CH_2OH), acetaldehyde (CH_3HCO) and formaldehyde (CH_2O). In this work, it is assumed that any oxygen did not evolve from the reactor in the form of CO or CO_2 , was evolved as principally H_2O but also significant quantities of acetaldehyde and formaldehyde could be expected. It should be noted that hydrocarbon concentration measured by FID has reduced sensitivity to oxygen containing molecules (see for example Table 5.2); and this should be noted when interpreting the balance of carbon.

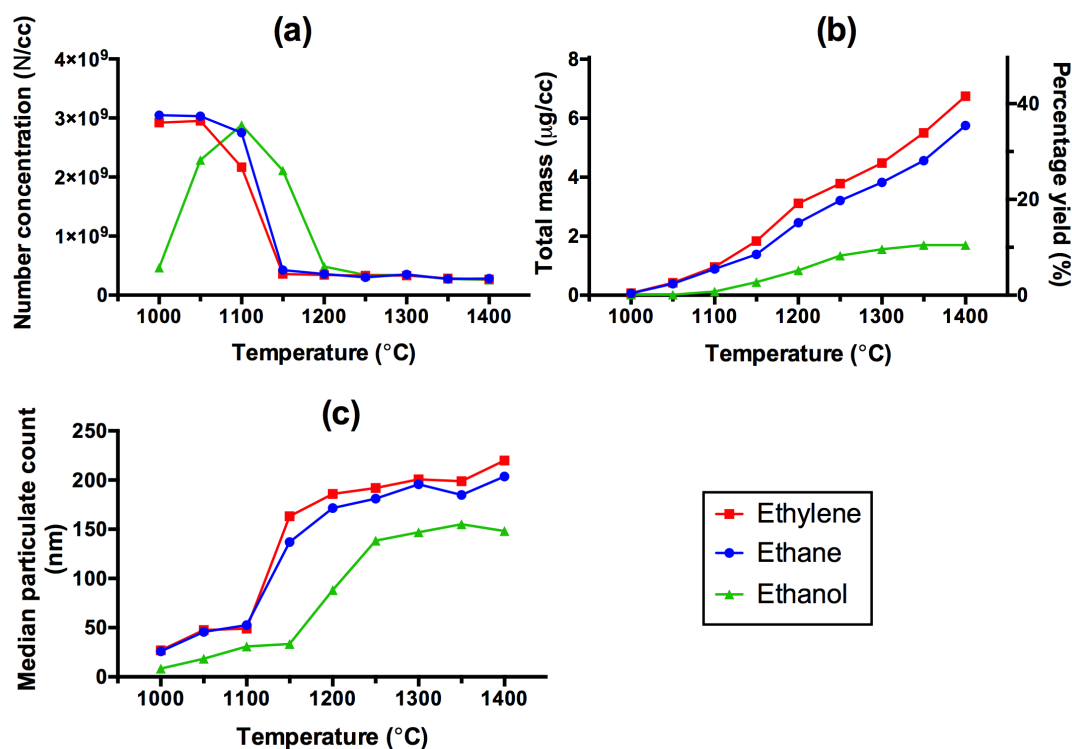


Figure 5.4: Analysis of particulate emissions formed from C_2 fuels in the temperature range 1000-1400 °C, showing: (a) the total number concentration of particulates (N/cc), (b) total mass of particulates, and (c) median particulate count.

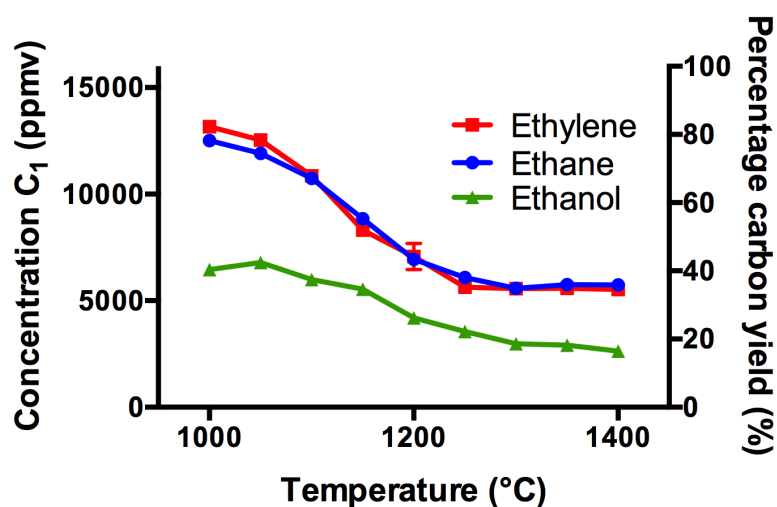


Figure 5.5: Outlet C_1 concentration from the pyrolysis of C_2 fuels in the temperature range of 1000 to 1400 °C, as measured by the fFID. Data shown is the average value measured over 30s \pm standard deviation

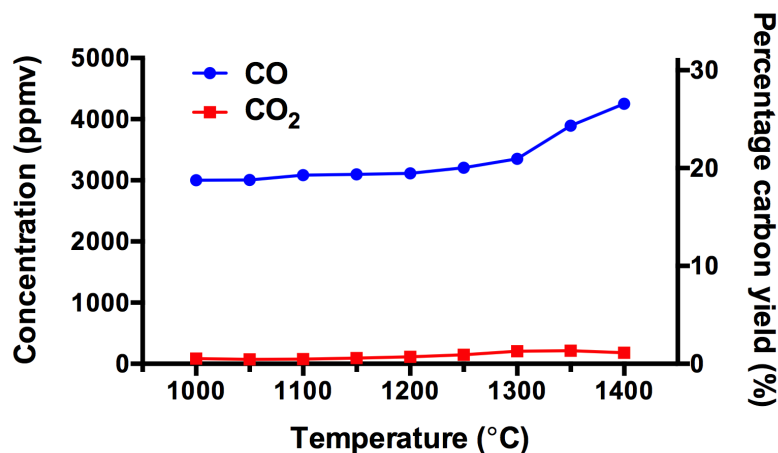


Figure 5.6: CO and CO₂ measurements from the pyrolysis of ethanol (8000 ppmv) in the temperature range 1000-1400°C.

5.3.2 C₃ fuels

This section presents the results of the pyrolysis of the homologous series of C₃ fuels, including the simplest pair of alcohol isomers 1-propanol and 2-propanol (which both have the empirical formula C₂H₈O), their alkane equivalent propane, and the alkene propene.

Figure 5.7 shows an overall summary of the particulate formed from the pyrolysis of the C₃ fuels. Figure 5.7(a) shows the total number concentration (N/cc) of particulates evolved from the reactor. Figure 5.7(b) shows the total mass of particulates and it is apparent that the general tendency to form soot in this series is: 1-propanol < 2-propanol < propane < propene. There are significant differences in the conversion rate of carbon between the molecules. At the highest pyrolysis temperature (1400 °C) the difference between the conversion rates to PM of the fuels was most marked, for example, for 1-propanol 20% of the inlet carbon converted to PM, which compared to 26% for 2-propanol. The hydrocarbon molecules converted to PM at higher rates than the oxygenates, for example at 1400 °C 45% of the inlet carbon of propane ended up as particulate matter, and 58% for propene. The finding that the alcohol molecules converted to soot at much lower rates than hydrocarbon molecules was not surprising, but the extent of the difference between the two propanol isomers was significant. It should also be noted from Figure 5.8 that the carbon monoxide (CO) evolved from the reactor was also lower for 2-propanol than that of 1-propanol at all of the temperatures investigated; only comparatively minor concentrations of carbon dioxide (CO₂) were observed.

The average diameter of particles weighted by number is reported in Figure 5.7(c), and also average particle diameter in mass terms is given in Figure 5.7(d). This is useful for demonstrating that whilst smaller diameter particles might dominate in terms of number, much of the mass of the particulates is accounted for by less numerous but

larger diameter particles. The total number concentration of particulates formed in the reactor is relatively high for each fuel at lower temperatures (<1150 °C) and decreases to a constant concentration at higher temperatures. The total number concentration is closely related to the average particle size (shown in Figure 5.7(c)), it is seen that as the average particle size increases, the number concentration decreases. Similarly to what was observed for the C₂ fuels in the previous section, it is seen that there was a shift from high concentrations of small primary particles produced at lower temperatures, to lower number concentrations of larger agglomerated molecules upwards of about 1100 to 1150 °C.

Previous research on the sooting tendencies of propanol isomers has reached different conclusions. For example, Kasper et al. (2009) studied the combustion of 1-propanol, 2-propanol and propane in low-pressure, fuel-rich, premixed flat flames. The mole fraction profile of intermediate hydrocarbon species was found to be similar for each of the propanol fuels, which included the soot growth species benzene and its precursors propargyl and acetylene. Due to the fact that the concentrations of these species was found to be similar, it indicated that the sooting tendencies of the fuels would also be similar.

However, Veloo and Egolfopoulos (2011) conducted experimental and computational analysis of 1-propanol, 2-propanol, and propane flames, and predicted the sooting propensity of these fuels in both premixed and non-premixed flames. It was found that in freely propagating propane/air, 1-propanol/air, and 2-propanol/air flames ($\phi = 1.5$), the maximum mass fraction of the propargyl radical species (C₃H₃) for 2-propanol and propane was predicted to be twice that of 1-propanol. The finding that there was a similar maximum level of propargyl formation in propane and 2-propanol, was somewhat surprising due to the presence of oxygen in 2-propanol. The pyrolysis results reported here appear to agree with the prediction of Veloo and Egolfopoulos (2011) with regard to the sooting tendency, and it is seen in Figure 5.7(b) that 2-propanol and propane do indeed have a similar sooting tendency (in terms of total particulate mass) at temperatures less than 1200 °C; at temperatures greater than 1200 °C propane was found to have a significantly higher sooting tendency.

Norton and Dryer (1990) studied the oxidation of propanol isomers in a atmospheric flow reactor, and observed that the intermediate hydrocarbon species included, methane, ethane, ethylene, propene, acetaldehyde, acetylene, and formaldehyde. Frassoldati et al. (2010), developed a kinetic model to describe the combustion of the propanol isomers, and compared the modelling results to those obtained by Norton and Dryer (1990). It was reported that there were increased maximum concentrations of propene (C₃H₃) observed in the case of 2-propanol combustion, compared to 1-propanol. This was attributed to a four-center molecular dehydration reaction (shown in Figure 5.9), that was predicted to occur to a greater extent in 2-propanol. The reaction is more prevalent in 2-propanol combustion and pyrolysis due to the greater number of β C–H sites in comparison to 1-propanol. The formation of C₃H₃ and water

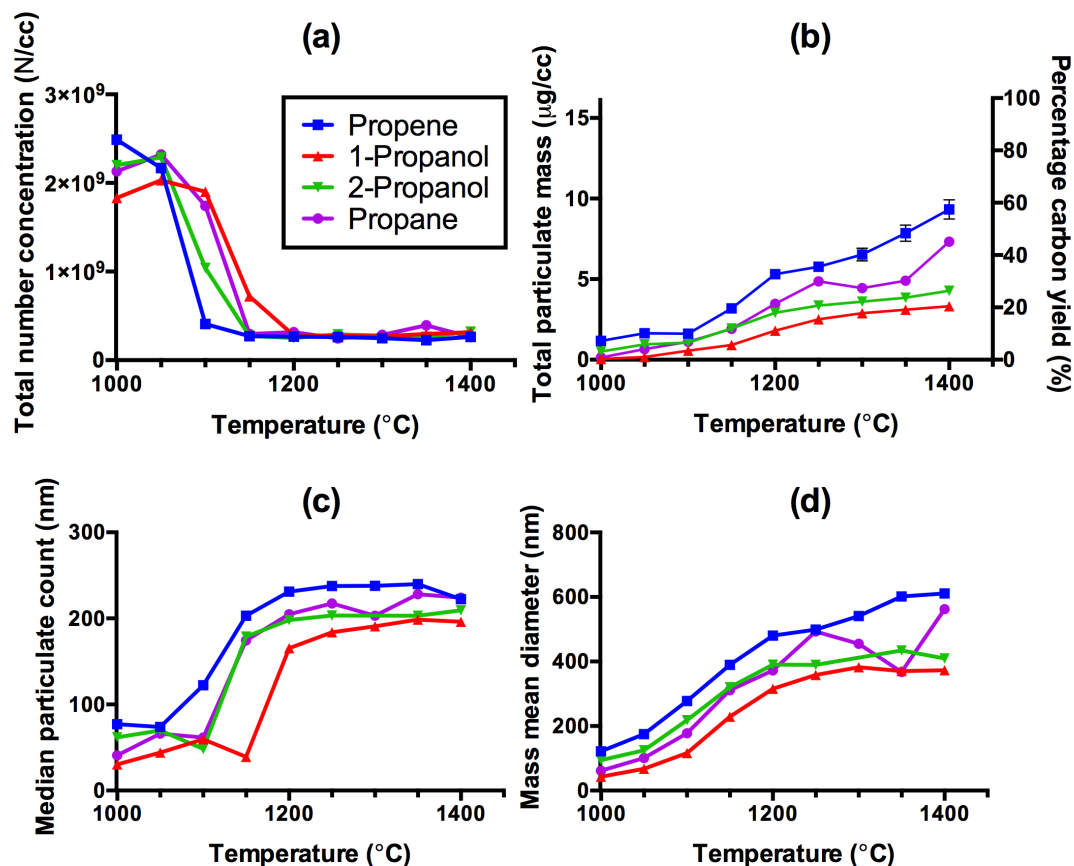


Figure 5.7: Analysis of particulate emissions formed from C_3 fuels in the temperature range of 1000-1400°C. (a) Total particulate mass. (b) Total number concentration. (c) Median particulate count (nm), weighted by number concentration. (d) Mass mean diameter.

may also explain the observed reduced CO formation in the case of 2-propanol at lower temperatures (Figure 5.8) due to oxygen used for the formation of H_2O .

Some additional analysis of the behavior of primary and secondary alcohols on the formation of particulate, CO and CO_2 emissions is covered in Section 5.3.4.

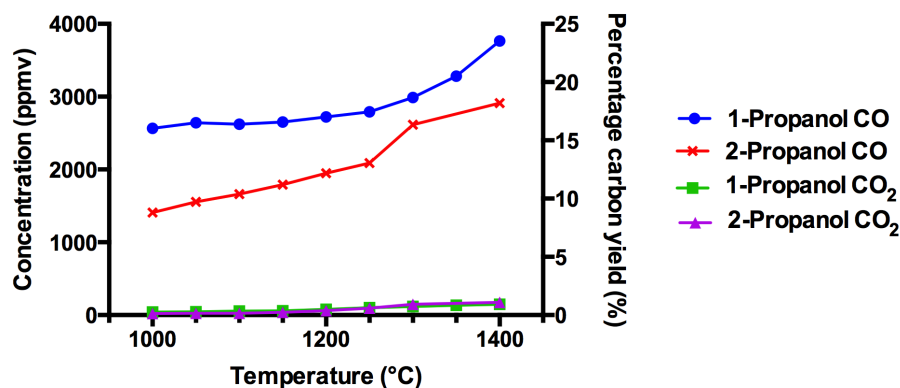


Figure 5.8: CO and CO₂ measurements from the pyrolysis of 1-propanol and 2-propanol (8000 ppmv) in the temperature range of 1000-1400°C.

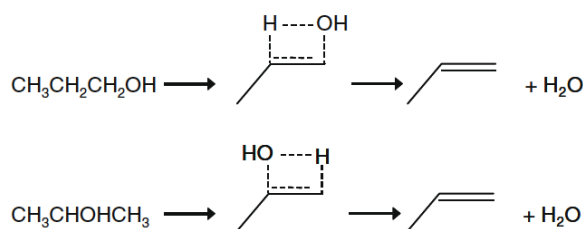


Figure 5.9: Reaction scheme for a four-center molecular dehydration reaction, for 1- and 2-propanol. Reprinted from reference Frassoldati et al. (2010), with permission from Elsevier.

5.3.3 C₄ fuels

Pyrolysis of the pair of isomers *n*-butane and *i*-butane was carried out at temperatures from 1000 to 1400°C, at an inlet concentration of 4000 ppmv. The particulate emissions were measured by the DMS500 instrument, and a summary of the particle characteristics are shown in Figure 5.10. The total mass of soot produced was shown to gradually increase with temperature for both fuels, and the particulate emissions for both fuels were similar at all temperatures. At the lowest temperature of 1000°C, only 1% conversion of *n*-butane to soot was seen, but at 1400°C the majority of the carbon (60%) was converted to soot during pyrolysis. From Figure 5.10(c) it is evident that in the case of both *n*- and *i*-butane there is a step shift from the formation of high number concentrations of small particles, to lower number concentrations of larger agglomerated particles at higher temperatures. This change occurs between 1100 and 1150°C, for example for *n*-butane at 1100°C particles with an average diameter of 60 nm were formed, and at a formation temperature of only 50°C higher, at 1150°C the average diameter was 204 nm.

n-butane and *i*-butane have received a significant amount of interest in the literature (e.g. Oehlschlaeger et al., 2004), although head-to-head studies of the combustion and pyrolysis of these isomers under identical conditions are more scarce. Oßwald

et al. (2011) investigated both *n*-butane and *i*-butane in fuel-rich (ϕ 1.71) laminar flat flames. They measured and modelled the formation some typical soot precursor species including C₃H₃, C₃H₄, C₆H₆, and C₇H₈ at various locations in the flame. In the case of *n*-butane decomposition there was a strong tendency of decomposition resulting in C₂ species. On the other hand, it was observed that the influence of C₃ intermediates appeared to be more dominant in the *i*-butane flame, which was almost exclusively allene (C₃H₄). As a result, the ‘typical’ soot formation species were found to be twice as high in *i*-butane flames as opposed to *n*-butane flames. Although other species, for example acetylene and polyacetylenes in the exhaust, are typically similar for both fuels.

Other research has also reported that *i*-butane has a greater tendency to form aromatics than *n*-butane at lower temperatures, due to its increased tendency to form benzene precursors such as the propargyl radical (Zhang et al., 2013b). Indeed, it was generally found in the literature that *iso*-alkanes were reported to have an increased tendency to form soot or soot-precursors than their corresponding *n*-alkanes. For example research by Takatori et al. (1998) showed that the flow reactor pyrolysis of *iso*-octane tended to form significantly higher concentrations of benzene and toluene in the temperature range 850 to 1000°C. However, the preferential formation of soot precursors at lower temperatures does not appear to influence the overall sooting tendency at higher temperatures under pyrolysis conditions as the results in this section show. Overall, it can be said that despite the differences that have been reported in the literature regarding the decomposition pathways of the butane isomers, there was no discernible difference in the characteristics of the soot particles formed from either *n*-butane and *i*-butane under the conditions tested here.

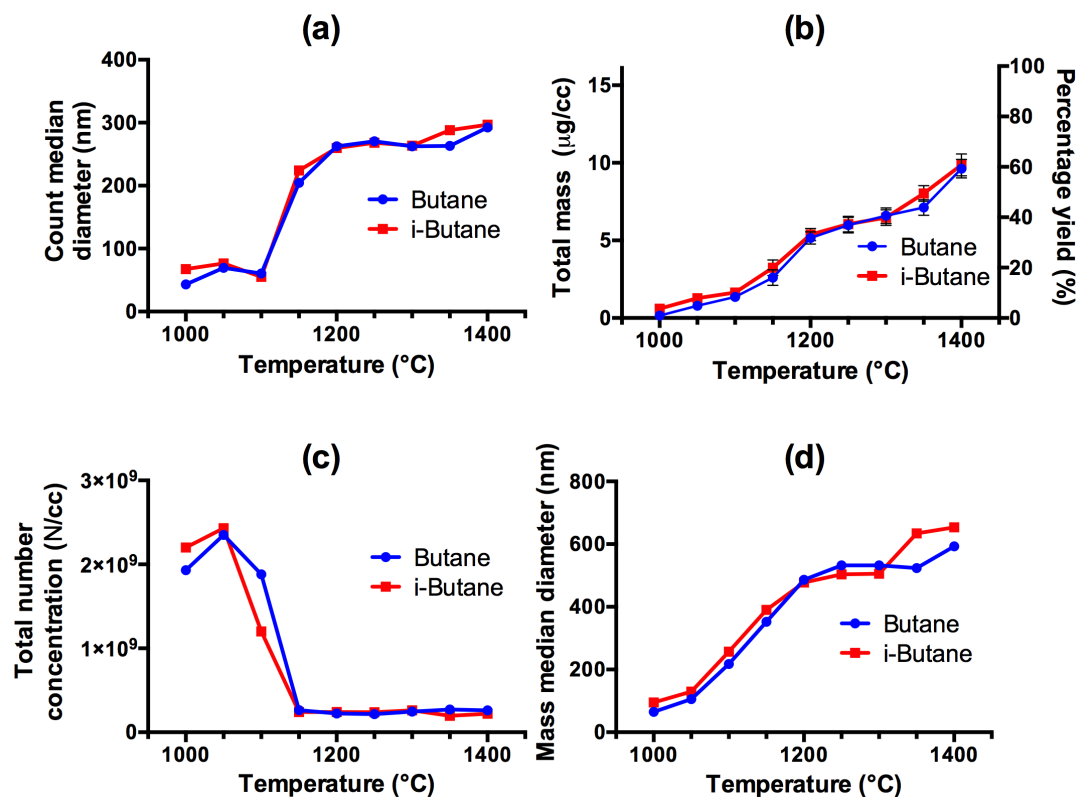


Figure 5.10: Particulate emissions formed from the pyrolysis of C_4 fuels, n - and i -butane: (a) total mass concentration. (b) total number concentration. (c) count median diameter (nm). (d) mass median diameter (nm).

5.3.4 C_1 - C_5 alcohols

Studies of the combustion products of methanol and ethanol in the literature are well documented; however, fundamental studies of higher alcohols, and including isomers of propanol and pentanol are more scarce (Sarathy et al., 2014). Here, the results of the pyrolysis of a homologous series of C_1 to C_5 alcohols is presented, including: methanol, ethanol, 1-propanol, 2-propanol, 1-pentanol, and cyclopentanol. The fuels were fed into the reactor at a constant carbon atom flow rate of 5,000 ppm on a C_1 basis (i.e. the molecular inlet concentration for methanol was 5000 ppmv, but for 1-pentanol it was 1000 ppmv).

Figure 5.11 shows the characteristics of the particulate matter formed by pyrolysis of the alcohols at various temperatures. The overall order of sooting tendency was found to be: methanol \ll ethanol $<$ 1-propanol $<$ 1-pentanol $<$ 2-propanol $<$ cyclopentanol. Cyclopentanol was found to produce by far the highest yields of soot across all temperatures, for example at 1200 °C there was 31% soot yield (or 1.55 $\mu\text{g}/\text{cc}$) formed from cyclopentanol. The next highest sooting molecule was 2-propanol, another secondary alcohol, which converted to PM at a rate of 13% (1.18 $\mu\text{g}/\text{cc}$). Primary alcohols (where the hydroxyl group is located at the end of the carbon chain) formed significantly less

soot; whilst methanol was not found to form soot at all, pyrolysis of ethanol, 1-propanol, and 1-pentanol at 1200 °C yielded 2%, 5% and 7% respectively.

Figure 5.12(a) shows the CO evolved from the pyrolysis of the various alcohols, whilst (b) shows the CO₂ emissions. It can be seen that the majority of carbon-bound oxygen in the fuel was evolved from the reactor in the form of CO, and only low concentrations of CO₂ were produced. It can be seen from the plot that the CO emissions from the reactor were in the order of: methanol > ethanol > 1-propanol > 1-pentanol > 2-propanol > cyclopentanol. This general order that the smaller-chain alcohols tended to form more CO is not particularly surprising, due to the fact that fuel inlet concentrations into the reactor were fixed based on the carbon flow rate, meaning that as the carbon chain length of the molecule under investigation increased, lower amounts of oxygen were fed into the reactor. For methanol, for example, the O:C ratio was 1, whereas in ethanol it was 0.5, and 0.2 for pentanol. Methanol produced predominantly CO under all conditions with approximately 70% CO yield; a result which was consistent with the research of Aronowitz et al. (1977) which found that flow reactor pyrolysis of methanol produced predominantly CO and H₂, and no more complex hydrocarbon molecules beyond acetylene.

It should be noted that the bond strengths in alcohol molecules are typically in the order of: O-H > C-H > C-O > C-C, and the C-O bond strength (92-93 Kcal) is similar for all alcohol molecules including primary and secondary alcohols. The main chemical difference between alcohol molecules and their corresponding alkane is the reduced symmetry of the molecule, which increases the number of decomposition pathways (see Figure 5.13), and the reduced C-H bond energy in carbon atoms neighboring the alcohol moiety (Norton and Dryer, 1990). The finding that the primary alcohols tested tended to evolve greater amounts of CO and less soot from the reactor can be attributed to the different reaction pathways that primary and secondary alcohols undergo during pyrolysis. Figure 5.13 highlights some of the main differences in the pyrolysis of primary and secondary alcohols compared to alkanes, where the initial decomposition pathways occur by dehydrogenation or dehydration reactions. Figure 5.9 shows the dehydration reaction, which occurs via a cyclic 4-member intermediate species and is an important reaction in determining differences in the intermediate species produced from the two isomers. The dehydration reaction pathway is more prevalent than dehydrogenation in a secondary alcohol due to the increased number of neighboring C-H groups (α C-H), and due to the relative weakness of the α C-H bonds which is induced by the alcohol group; this results in secondary alcohols producing more alkenes than ketones. Primary alcohols (e.g. methanol, ethanol, 1-propanol) on the other hand produce more aldehydes than alkenes (Norton and Dryer, 1990). The overall result of this is that secondary alcohols tend to behave more like alkenes in terms of sooting tendency under pyrolysis conditions than primary alcohols, due to the production of deoxygenated C₂ and C₃ intermediates which are known soot precursors.

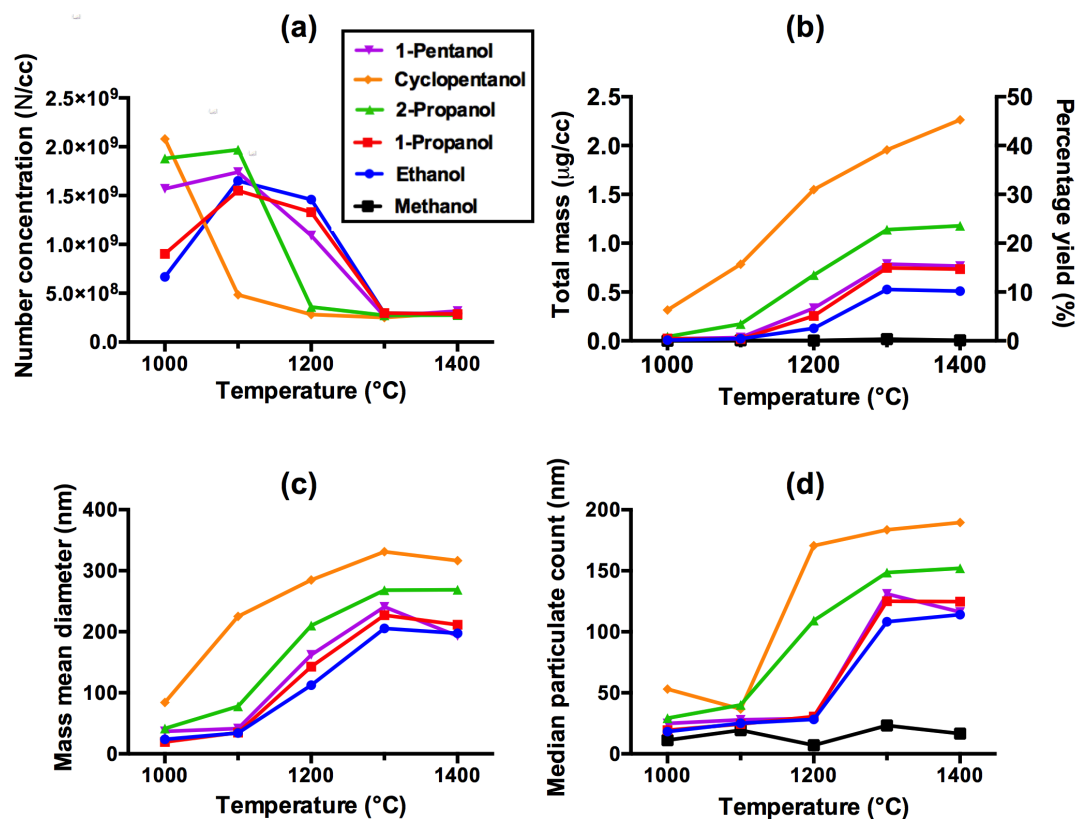


Figure 5.11: Particulate formed from the pyrolysis of C_1 - C_5 alcohols, as measured by a Cambustion DMS500 instrument. (a) total mass concentration. (b) total number concentration. (c) mass median diameter (nm). (d) count median diameter (nm).

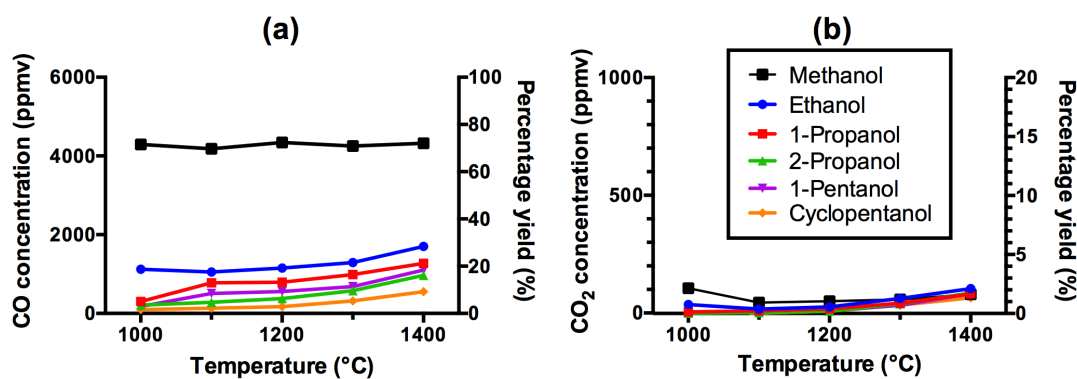


Figure 5.12: CO and CO₂ products formed from the pyrolysis of C_1 - C_5 alcohols: (a) CO concentration. (b) CO₂ concentration.

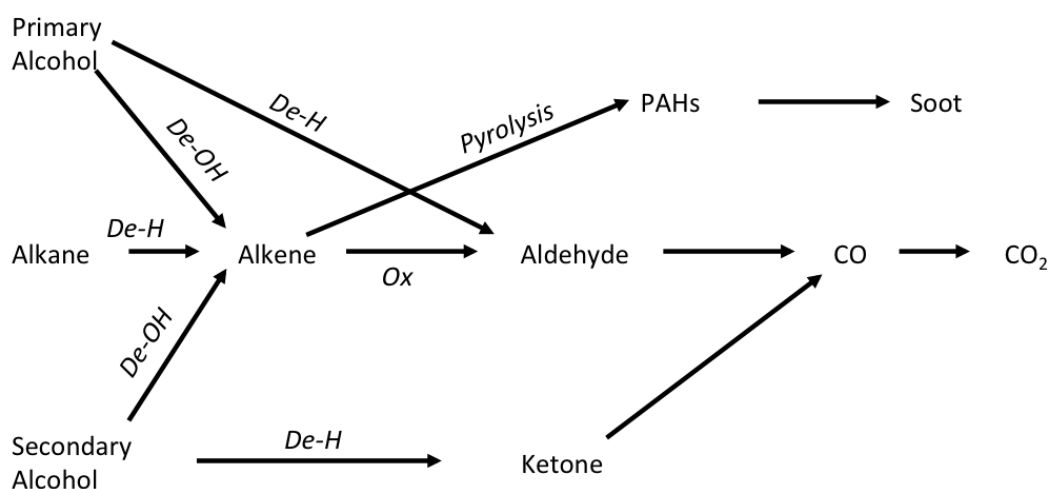


Figure 5.13: Possible reaction pathways of alkanes, and primary and secondary alcohols. Including dehydrogenation ($De-H$), dehydration ($De-OH$), and (Ox oxidation).

5.3.5 Influence of fuel concentration on the formation of particulates

Three concentrations of ethanol (1250, 2500, and 3750 ppmv) have been tested in order to understand the influence of the initial fuel concentration on the yield and particle characteristic of the soot formed.

Figure 5.14 shows the particle characteristics of the particles evolved in the reactor effluent gas from the pyrolysis of the various concentrations of ethanol. Figure 5.15 shows the percentage yield of particulate matter relative to the carbon at the reactor inlet. It is shown that all of the concentrations of ethanol investigated produced generally similar particulate yields, although higher ethanol inlet concentrations resulted in slightly higher particulate yields. For example, at 1200 °C 3000 ppmv of ethanol produced 2% particulate matter, whilst a concentration of 9000 ppmv produced a 6% yield. The finding that the percentage soot yield increases with inlet concentration, is in agreement with the research of Ruiz et al. (2007c), on the effect of varying acetylene concentration and residence time for flow reactor pyrolysis.

It has been noted from the results presented in the preceding sections that at lower pyrolysis temperatures (~ 1000 °C) high number concentrations of particles are formed, whilst lower concentrations of larger agglomerated particles are produced at higher temperatures. This phenomenological observation is also captured well in this present section, because at low inlet carbon concentrations and at the lowest temperatures investigated soot formation was not observed, soot only began to form at higher temperatures. For example, at an inlet concentration of 1250 ppmv and at 1000 °C no soot particles were formed, at the higher temperature of 1100 °C only very low concentrations of nascent particles were produced, by 1200 °C very high concentrations were present. At temperatures upwards of 1300 °C lower concentrations of agglomerated

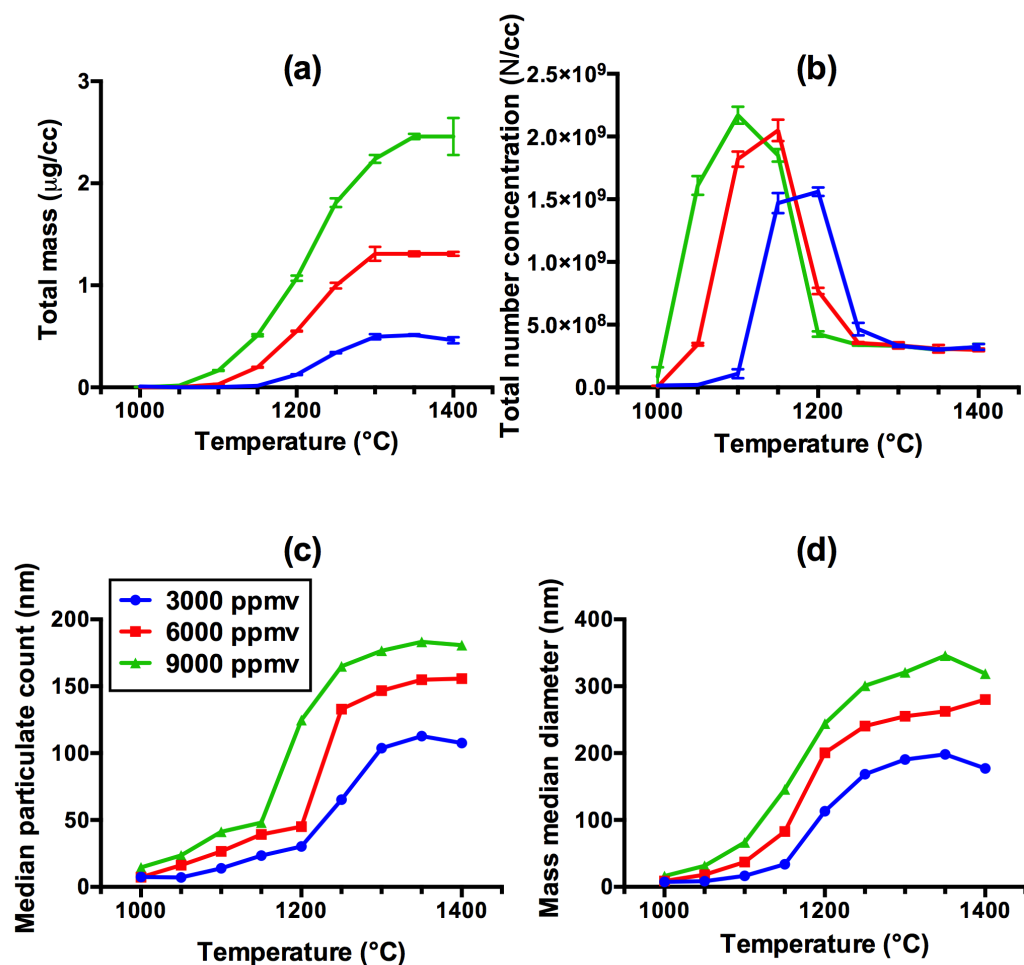


Figure 5.14: Particulate emissions formed from the pyrolysis of ethanol at 3000, 6000, and 9000 ppmv: (a) total particulate mass concentration. (b) total number concentration. (c) count median diameter (nm). (d) mass median diameter (nm).

particles are produced, shown in Figure 5.14(b); in this plot the entire process of the particle evolution is captured.

Finally, a proportional increase in the effluent CO and CO₂ concentrations was observed in Figure 5.17, and this resulted in a constant percentage yield as shown in Figure 5.15.

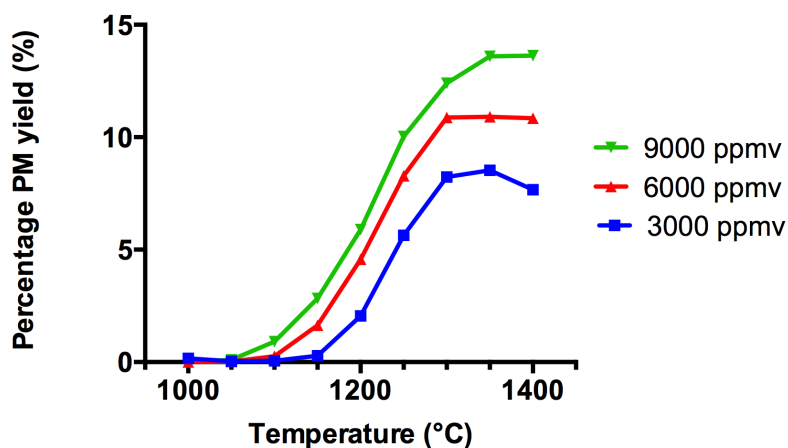


Figure 5.15: Particulate percentage yield from the pyrolysis of ethanol at three concentrations; 3000, 6000 and 9000 ppmv.

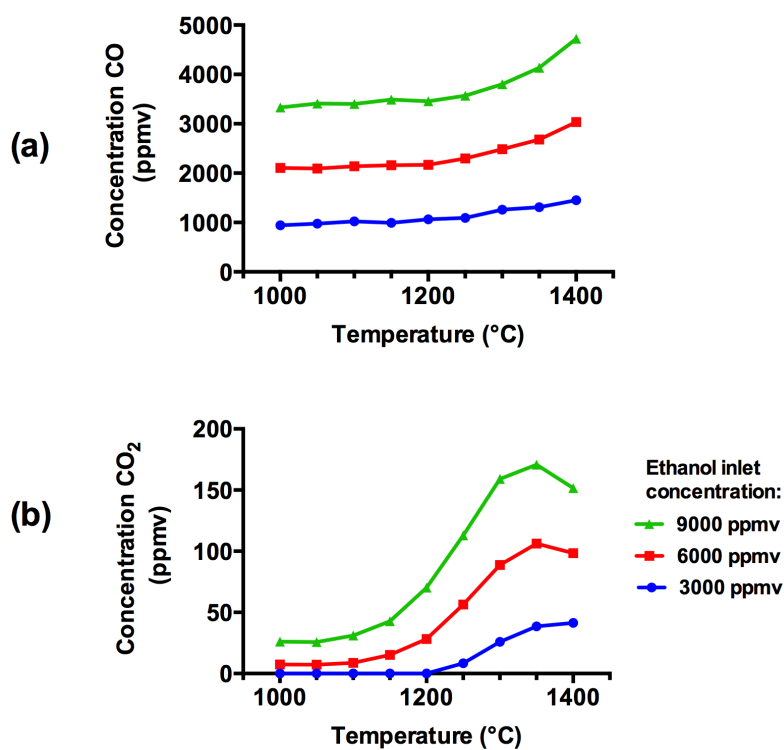


Figure 5.16: CO and CO_2 emissions formed from the pyrolysis of ethanol at three concentrations 3000, 6000, and 9000 ppmv (a) CO. (b) CO_2 .

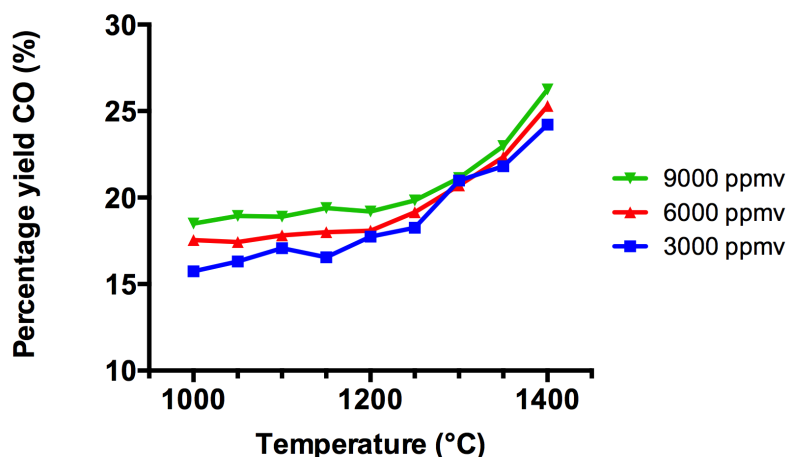


Figure 5.17: Percentage yield of CO formed from the pyrolysis of ethanol at 3000, 6000, and 9000 ppmv inlet concentrations.

5.4 Conclusions

The results in this chapter have shown that under the homogenous pyrolysis conditions employed in the reactor, considerable differences in the conversion of carbon from different molecules was observed. The most significant results from the experimental work described in this chapter are as follows:

- For all fuels tested, higher pyrolysis temperatures (in the range 1000 to 1400°C) yielded higher particulate mass concentrations, and higher soot yields.
- The C₂ series of fuels tested showed that the tendency of the fuels to form soot was in the order ethanol < ethane < ethylene.
- In the case of the C₃ series the order of soot forming tendency was 1-propanol < 2-propanol < propane < propene;
- It was found that secondary alcohols had a higher tendency to form PM, this was explained as due to a dehydration reaction, which is more prevalent in secondary alcohols compared to primary alcohols.
- There was no discernible difference between the ‘sooting tendency’ of *n*- and *i*-butane under the conditions employed in the reactor.
- It was generally observed that at lower pyrolysis temperatures, higher number concentrations of primary particles (~50nm) were formed;
- At higher temperatures the primary particles cluster to form agglomerated structures, which tended to increase the particle size and reduce and the total number concentration of particulates.

The novelty and importance of the work that has been described in this chapter is that relatively few experiments of soot formation are available in literature which have been conducted under such well-controlled conditions; and for such a wide range of molecules. Where there is overlap with the literature, it has been shown that the results of the DMS instrument were consistent with the published results, confirming the effectiveness of the methodology.

It has been shown in this work and in the literature that the molecular structure of a fuel has an influence on its conversion to particulate matter. A question that arises from this work is: *how* does functional group chemistry influence the conversion of carbon to soot? And, does a given functional group impact only on the carbon atoms which are directly bonded, or is there a global influence? The following chapter explores these questions by the application of a novel isotope labelling technique to identify the fate of individually *labelled* carbon atoms during pyrolysis.

Chapter 6

Tracking the conversion of specific carbon-13 labelled atoms from various fuels to particulate matter under pyrolysis conditions

6.1 Introduction

The influence of functional group chemistry on the conversion organic molecules to particulate matter and other emissions has been the subject of numerous studies. As the previous chapter introduced, many of the studies that have been reported investigate how simple changes to chemical functional groups influence the overall propensity of single-component hydrocarbon molecules to form PM and other emissions. In order to understand in greater detail the direct influence of functional group chemistry on the fate of specific carbon atoms through a combustion or pyrolysis process, a ^{13}C labelling technique has been used.

In this Chapter, the results of experimental work are presented, which involved oxygen-free pyrolysis of a number of ^{13}C labelled molecules (ethanol, propanol, pentanol, ethyl acetate, and toluene). Pyrolysis was carried out in the temperature range of 1100 to 1450 °C in the tube reactor, and the resulting PM was collected. The formation conditions of PM in the tube reactor were intended to resemble, in a broad sense, the conditions in the core of a diesel spray; in that, the conditions were oxygen-deficient and at high temperatures.

6.2 Experimental methods

6.2.1 Apparatus

The pyrolysis experiments described in this chapter were performed using the flow reactor rig described previously in Chapter 3. Samples of PM were collected directly by

deposition onto a borosilicate glass plate, by thermophoresis. Following collection of a sufficient quantity of PM, the sample was removed from the glass plate using a stainless steel spatula and transferred into a borosilicate glass vial, which was frozen at $-20\text{ }^{\circ}\text{C}$ until it was required for EA-IRMS analysis.

6.2.2 Fuel molecules investigated

Figure 6.1 shows the skeletal structure and nomenclature of the ^{13}C labelled compounds investigated in this chapter. Particular attention has been given to oxygenated molecules, so-called first-generation bio-fuels such as ethanol have been used extensively as fuels for vehicles for helping to reduce regulated emissions (Johnson et al., 2009; Noorani et al., 2010b).

The systematic changes in molecular structures of the molecules studied here allows for the influences of the following features to be assessed:

- Whether the presence of a hydroxyl group (-OH) reduces the contribution to PM formation of the carbon atom that it is attached to (groups 1,2,3);
- The influence on PM formation of increasing chain length of a primary alcohol (by comparing groups 1,2,3);
- The influence on PM of moving an alcohol group from the end of a hydrocarbon chain to a mid-chain position (group 2);
- The contribution to PM from the hydroxyl carbon in straight-chained primary alcohols, secondary aliphatic alcohols, and an alicyclic secondary alcohol (groups 1,2,3);
- Whether the carbon atom in the ester functional group ($\text{R-CO}_2\text{-R}'$) of ethyl acetate forms PM to a lesser extent than its neighboring 'methyl' carbon atom (group 4);
- Whether the carbon atoms in the phenyl group of toluene contribute to PM at the same rate as the methyl group, and whether the α -position (toluene- α - ^{13}C) contributes to PM at a the same rate as the other carbon atoms contained in the ring of toluene (group 5).

6.2.3 Experimental conditions

PM was collected at 50°C intervals in the temperature range 1100 to 1450°C . The following conditions were used for the generation of PM for all of the molecules investigated:

- The nitrogen carrier gas flow rate used in all experiments was 20 l/min ;
- The temperature of the nitrogen carrier, heated by the air-process-heater, was maintained at $200\text{ }^{\circ}\text{C}$, controlled by a PID;

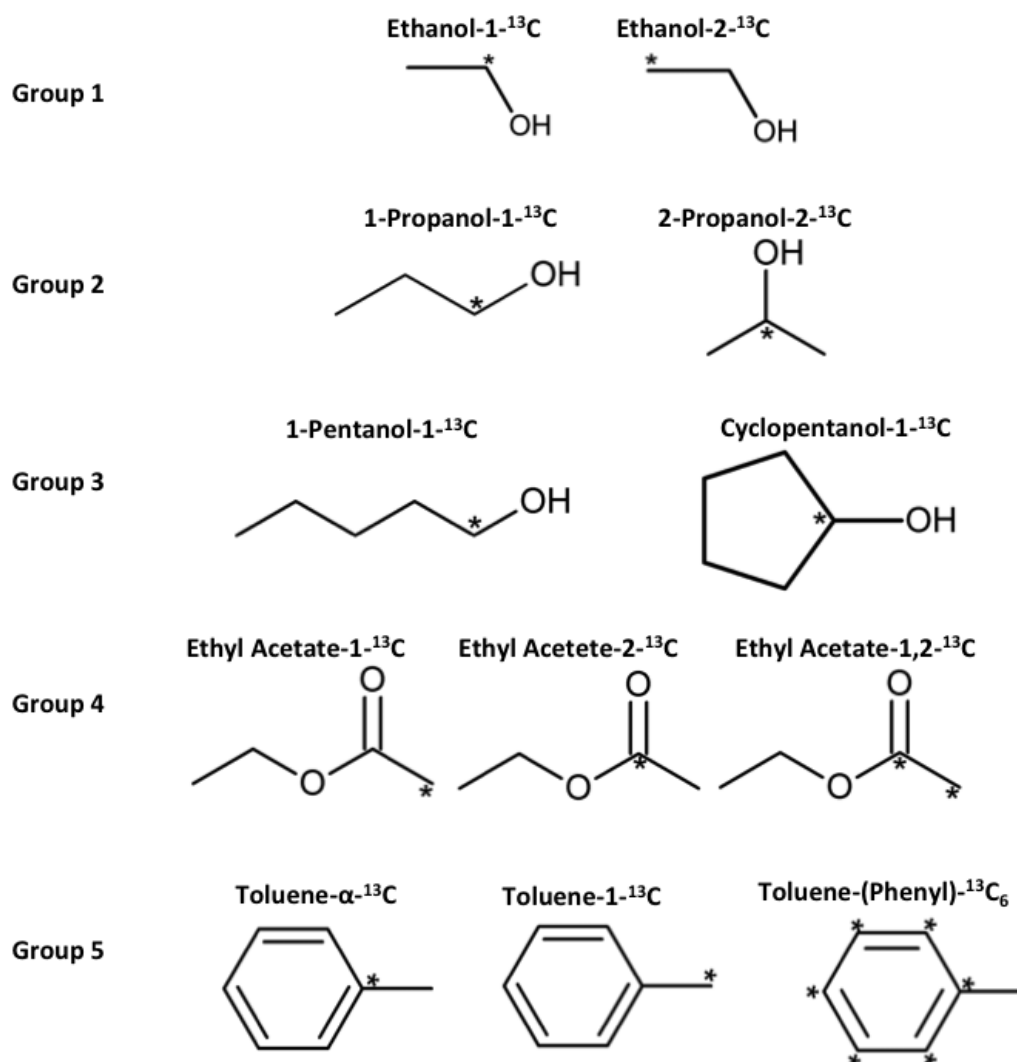


Figure 6.1: Structure and nomenclature of ^{13}C labelled molecules investigated. * shows the location of ^{13}C labelled atom.

- The vaporiser and stainless steel tubing was maintained at a constant temperature of $200\text{ }^{\circ}\text{C}$, controlled by a PID;
- The temperature of the static mixer was monitored to ensure the temperature was above $180\text{ }^{\circ}\text{C}$;
- The flow rate of the liquid fuels was fixed so as to obtain a fuel concentration in nitrogen of 10,000 ppmv.

6.3 Results and discussion

In addition to the results displayed in the figures in the following sections, Appendix B contains measured data, and subsequently calculated parameters are presented in a

tabulated form. The units of measure used in this section, particularly $\delta^{13}\text{C}_{VPDB}$, and calculations to derive the percentage contribution of individual atoms to PM have been set-out previously in Chapter 4.

6.3.1 Ethanol

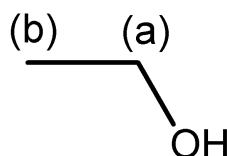


Figure 6.2: Skeletal structure of ethanol, with ^{13}C labelled atoms assigned (a) ethanol-1- ^{13}C , and (b) ethanol-2- ^{13}C .

In order to aid explanation throughout this chapter carbon atoms within molecules have been assigned letters where the ^{13}C label was located. For ethanol, each of the two carbon atoms was ^{13}C labelled in turn, in two separate experiments, and Figure 6.2 shows that the carbon atom directly bound to the hydroxyl group has been labelled ‘a’, and the methyl carbon has been labelled ‘b’.

It was described previously in Chapter 4 that, in order to calculate the relative probability of specifically labelled carbon atoms converting to PM, measurements were required of the unenriched and enriched variants of PM, as well as the fuel from which the PM was derived. For example, in the case of ethanol, it was necessary to measure the unenriched ethanol fuel and ethanol fuel that was enriched with small quantities of either ethanol-1- ^{13}C (where carbon ‘a’ was ^{13}C labelled), or with ethanol-2- ^{13}C (where carbon ‘b’ was ^{13}C labelled); furthermore, the PM derived from these two fuels was also measured.

Unlabelled ethanol, which was measured to be $-27.8 \delta^{13}\text{C}$, was enriched in two separate batches: with ethanol labelled at position ‘a’ to $-6 \delta^{13}\text{C}$, and at position ‘b’ to $-6.1 \delta^{13}\text{C}$. Figure 6.3 shows the measured delta values ($\delta^{13}\text{C}$) for the PM derived from these two enriched fuels in the labelling experiment; the reader is reminded that the higher delta value the greater the amount of ^{13}C there is in a given sample. Figure 6.3 shows that despite being enriched to approximately the same level in the fuel, the resulting PM derived from the labelled fuels had very different isotopic signatures. The relative ^{13}C abundance of PM formed from ethanol labelled at ‘b’, was greater (^{13}C ‘heavier’) than the PM formed from ethanol labelled at ‘a’, indicating that the carbon from the methyl position formed PM in greater quantities than the carbon atom neighboring the hydroxyl group.

In Figure 6.3 it is shown that the relative ^{13}C abundance in PM formed from the unenriched stock ethanol was relatively unaffected by changing the formation temperature; this is significant as this indicates that the conversion of ^{13}C to PM is uninfluenced

by temperature in the range tested. This point and its implications is discussed further in Section 6.3.6.

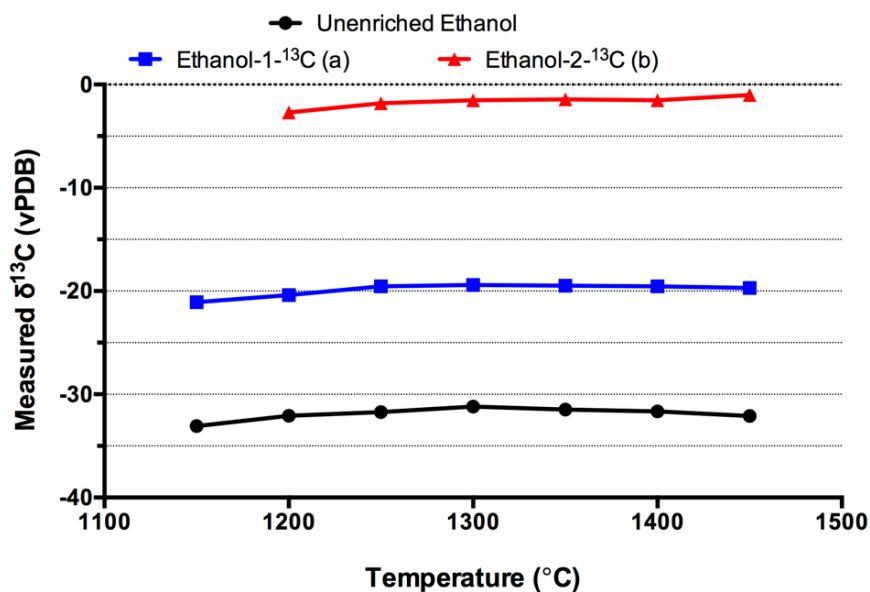


Figure 6.3: Measured delta values for unenriched ethanol, and ethanol enriched with quantities of ethanol-1- ^{13}C (a) or ethanol-2- ^{13}C (b) in the temperature range 1150 to 1450 $^{\circ}\text{C}$, at 50 $^{\circ}\text{C}$ intervals. Data shown is the mean \pm SD (generally, $\sigma > 0.15$).

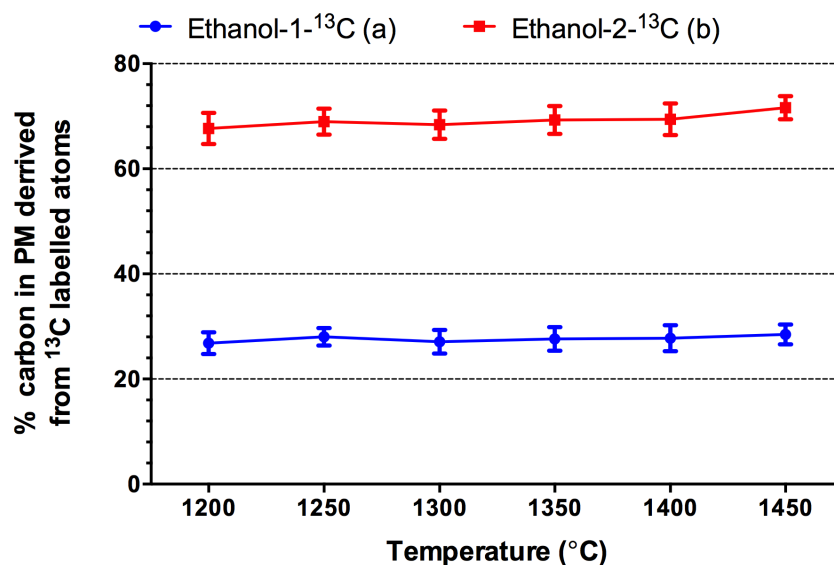


Figure 6.4: Percentage contribution to PM from the labelled position in ethanol-1- ^{13}C (a) and ethanol-2- ^{13}C (b) molecules. Error bars show the influence of the standard deviation on the calculated conversion rate.

From the raw results presented in Figure 6.3 it is a simple matter to conclude that the methyl carbon (b) in ethanol contributes more to PM than its neighboring hydroxyl carbon (a). This is a result one might expect *a priori* since it is reasonable that a carbon

atom already attached to an oxygen atom may stay attached throughout the pyrolysis process and may be evolved as CO or CO₂, rather than converted to soot. Figure 6.4 shows the percentage of carbon atoms in the PM that were derived from atoms ‘a’ or ‘b’, in the temperature range 1150-1450 °C. Take the result at 1300 °C for example, it is seen that the methyl carbon (b) contributes approximately 68% to the PM, and the contribution of the hydroxyl carbon (a) is 27%. The results corroborate since the two independent measurements total close to 100%, with small experimental error bars.

The influence of the addition of small amounts of oxygen during the pyrolysis of ethanol was also investigated. Pyrolysis of ethanol at 1300 °C at air-fuel equivalence ratios (λ) of 0.05, 0.10, and 0.2 was carried out. Figure 6.5 shows that the conversion ratios to PM of the two carbon atoms in ethanol are broadly conserved, even with the addition of small amounts of oxygen. It is shown that similar conversion rates are observed regardless of the presence of added oxygen, which indicates that the relative contributions of the two carbon atoms in ethanol to PM is conserved over a range of formation conditions. It should be noted that the set of tests carried out to determine the influence of oxygen addition, only single measurements were taken; for all other series, triplicate measurements were obtained.

Similar results have been obtained by other researchers, for example, research published by Lieb and Roblee Jr (1970) used the radioisotope ^{14}C as a tracer and labelled ethanol-1- ^{14}C and ethanol-2- ^{14}C was burned at various air-fuel mixtures. Samples were collected from a Bunsen flame (maximum flame temperature of 1360 °C), using a sampling probe and detection of the ^{14}C rate was carried out by means of a radioactive decay counting method. A conversion ratio of 2:1, hydroxyl-to-methyl carbon was reported (Lieb and Roblee Jr, 1970), which is similar to the 68:27 ratio found in the study presented in this thesis. Based on the observations of Lieb and Roblee Jr (1970), Homan and Robbins (1986) put forward the hypothesis that the process of making the growth species from the fuel is independent of the process of making soot from the growth species.

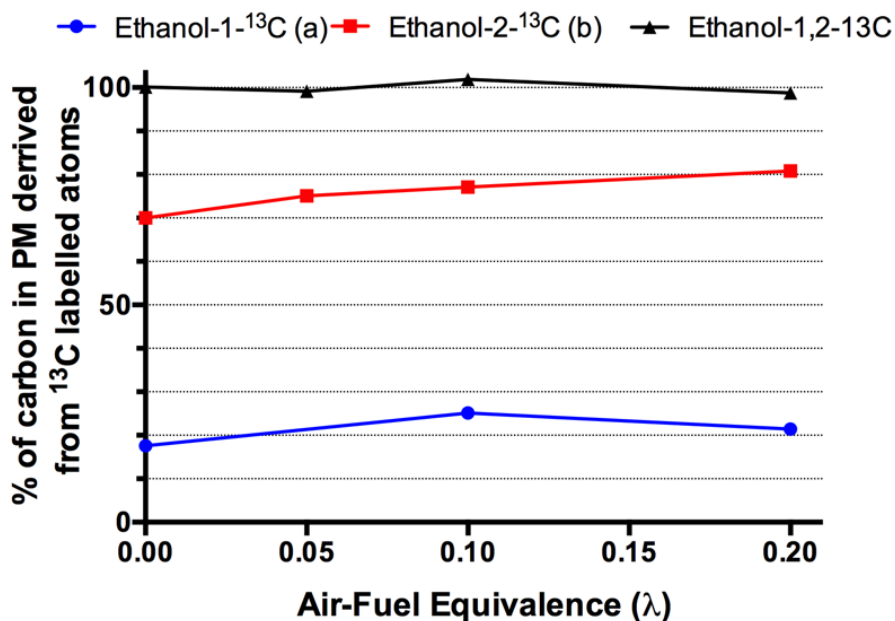


Figure 6.5: Percentage contribution to PM from the labelled position in ethanol-1- ^{13}C (a) and ethanol-2- ^{13}C (b), formed at 1300 °C and at various air-fuel equivalence ratios. Data shown is for single measurements.

6.3.2 1-propanol and 2-propanol

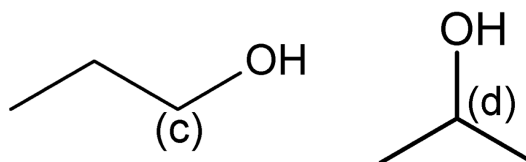


Figure 6.6: Skeletal structure of 1-propanol (left), labelled with ^{13}C at position (c) (1-propanol-1- ^{13}C); and 2-propanol (right), labelled at location (d) (2-propanol-2- ^{13}C).

Figure 6.6 shows the locations of the selectively labelled ^{13}C atoms in 1-propanol and 2-propanol; in both cases the ^{13}C label was located on the carbon atom that is directly attached to the hydroxyl group (-OH). 1-propanol was enriched from -30.80 to -7.20 $\delta^{13}\text{C}$; and 2-propanol was enriched from -28.06 to -4.50 $\delta^{13}\text{C}$.

Figure 6.7 shows the measured $\delta^{13}\text{C}$ values of the PM formed from the labelled and unlabeled versions of the fuel. The implications of this raw result is initially less obvious than that observed for ethanol (above), but it is clear that there are significant contributions to the PM from atoms 'c' and 'd', since enhanced levels of ^{13}C were found in the PM formed from the labelled fuels. Figure 6.8 shows that for all temperatures tested, the labelled atoms in 1-propanol-1- ^{13}C (c) and 2-propanol-2- ^{13}C (d) contribute to PM at a rate less than the average carbon atom in the molecule (which would be

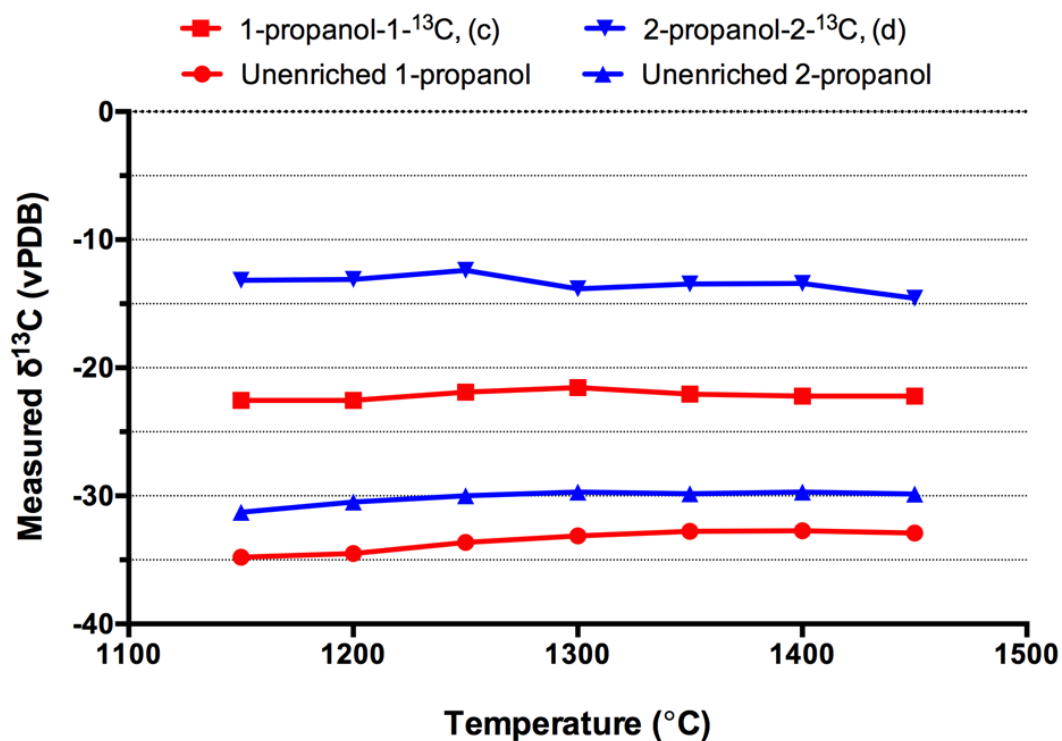


Figure 6.7: Measured delta values for unenriched 1-propanol and 2-propanol, and with enriched with quantities of 1-propanol-1- ^{13}C (c) and 2-propanol-2- ^{13}C (d) respectively, in the temperature range 1150 °C to 1450 °C.

33% if each carbon atom contributed equally). Similar to the result for ethanol, the hydroxylated carbon atoms in both of the propanol isomers, also contribute to PM to a lesser extent than atoms that are not directly bonded to an oxygen atom. Furthermore, it appears that when the hydroxyl (-OH) group is moved from the end of the 3-carbon atom chain to the middle carbon there is an increased contribution to PM from the carbon it is attached to. For example, at 1300°C the labelled carbon in 1-propanol- ^{13}C (c) was estimated to contribute 16% of the total carbon in the PM, whereas 2-propanol- ^{13}C (d) carbon contributed 22%.

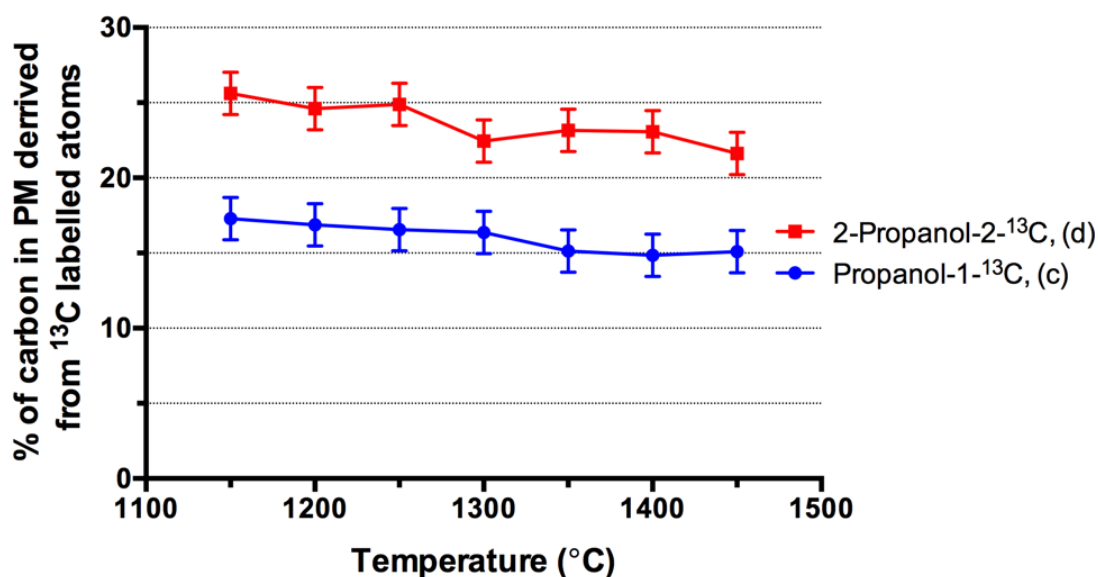


Figure 6.8: Calculated percentage contribution to PM from the labelled positions in 1-propanol-1- ^{13}C and 2-propanol-2- ^{13}C in the temperature range 1150-1450 $^{\circ}\text{C}$.

6.3.3 Pentanol and cyclopentanol

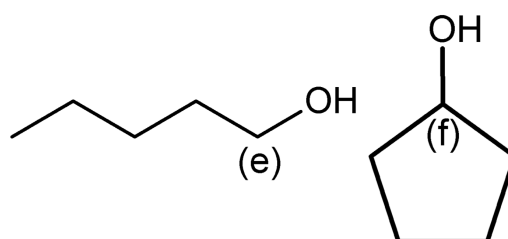


Figure 6.9: Skeletal structure of 1-pentanol (left), labelled with ^{13}C at position 'e' (1-pentanol-1- ^{13}C); and 2-pentanol (right), labelled at location 'f' (2-pentanol-2- ^{13}C).

Two isomers of pentanol were tested, 1-pentanol and cyclopentanol, shown in Figure 6.9. Figure 6.11 shows the percentage conversion rates of the *hydroxyl* carbon atoms ('e' and 'f'). It is observed that the hydroxylated carbon atom contributes to PM formation to a reduced extent with respect to the average carbon atom in the molecule. Given that the pentanol molecules contain five carbon atoms, if each converted to PM at an equal rate each would contribute 20%. However, at 1300 $^{\circ}\text{C}$ the labelled carbon in 1-propanol and cyclopentanol contributes approximately 10% and 16% respectively (Figure 6.11). The reader is reminded of the results in the previous sections, where the *hydroxyl* carbon in the primary alcohol 1-propanol contributed less to PM than the secondary alcohol 2-propanol; the same is observed here with the primary alcohol 1-pentanol contributing less from its hydroxyl carbon than the alicyclic secondary alcohol cyclopentanol.

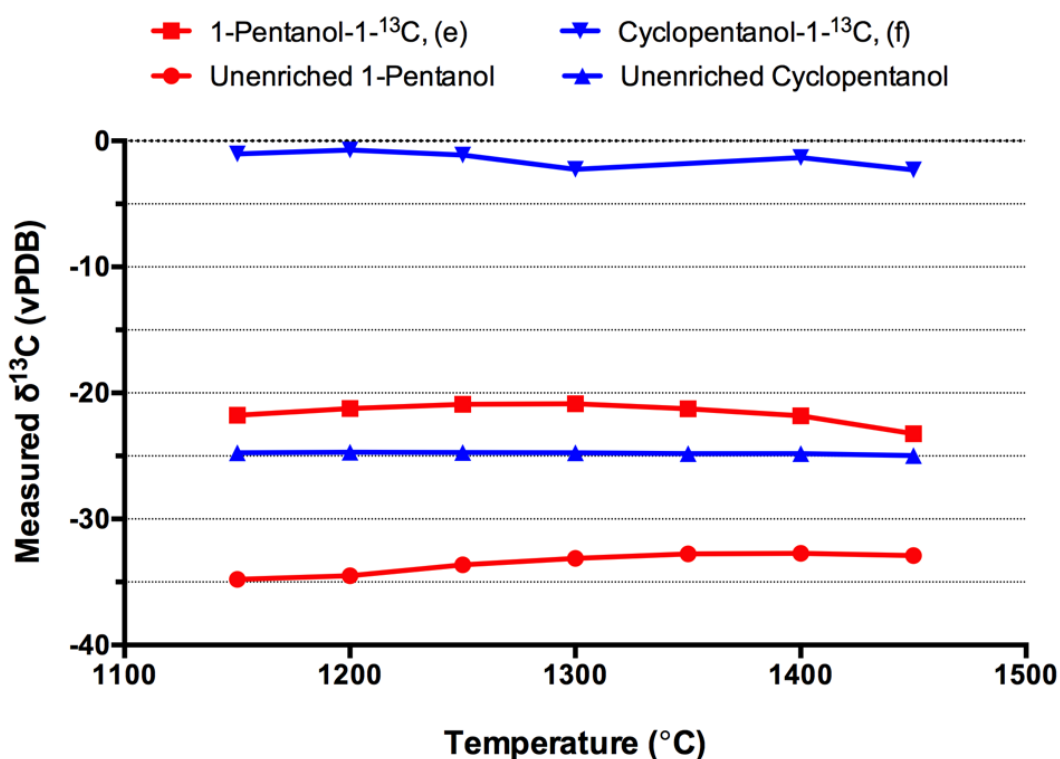


Figure 6.10: Measured $\delta^{13}\text{C}$ values for unenriched fuels 1-pentanol and cyclopentanol, and these with enrichment of 1-pentanol-1- ^{13}C (e) and cyclopentanol-1- ^{13}C (f) (enriched to $\delta^{13}\text{C}$ -7.20 and +4.30 respectively), in the temperature range 1150 to 1450°C, at 50°C intervals. Note that capsules of cyclopentanol-1- ^{13}C at 1350°C were lost during the measurement process, due to an error with the autosampler.

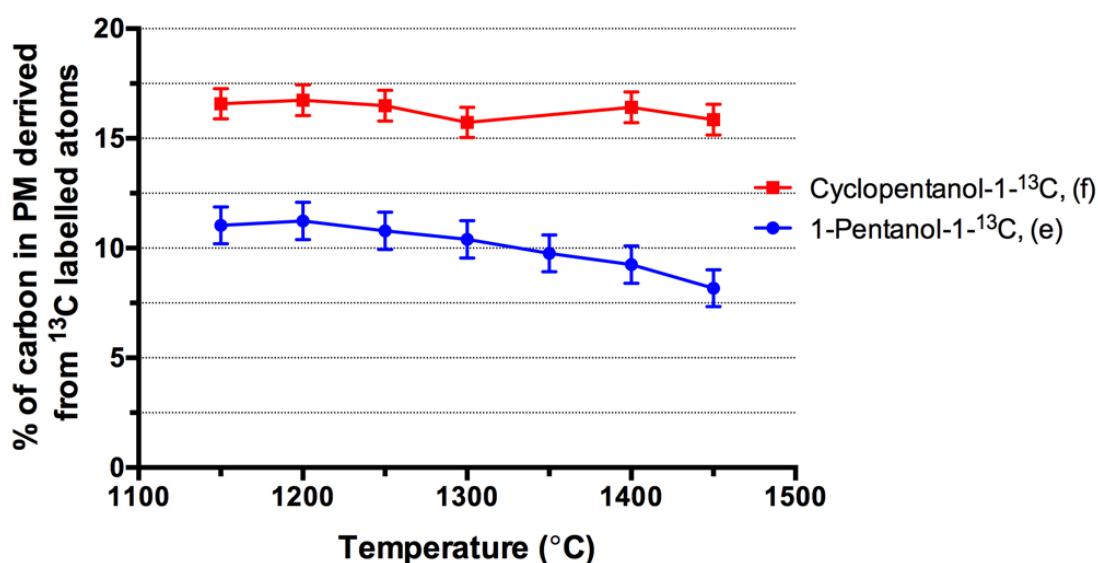


Figure 6.11: Calculated percentage conversion of the labelled positions in 1-pentanol-1- ^{13}C (e) and cyclopentanol-1- ^{13}C (f).

6.3.4 Ethyl acetate

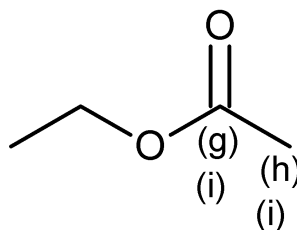


Figure 6.12: Skeletal structure of ethyl acetate-1- ^{13}C (g), ethyl acetate-2- ^{13}C (h) and ethyl acetate-1,2- ^{13}C (i).

So far the results in this chapter have concerned the impact of the hydroxyl (-OH) group on the fate of neighboring carbon atoms; here, attention is turned to an ester, another oxygenated functional group, in ethyl acetate. Three permutations of labelled ethyl acetate were tested, ethyl acetate-1- ^{13}C (g), ethyl acetate-2- ^{13}C (h) and ethyl acetate-1,2- ^{13}C (i,i), which are shown and assigned labels in Figure 6.12.

Figure 6.13 shows measured $\delta^{13}\text{C}$ data for PM samples, the fuel was enriched to a similar level in each case. Before any further processing of the data is applied, it is observable from the raw measured values of Figure 6.13 that the PM formed from ethyl acetate-1- ^{13}C , enriched at position ‘g’, has a similar isotopic signature as unenriched ethyl acetate; indicating that there is a negligible contribution to PM from the carbon bonded to two oxygen atoms.

Figure 6.14 shows the calculated percentage contributions to PM from labelled carbon atoms. The conversion rates of carbon from the labelled atoms to the PM appears to be uninfluenced by temperature in the range 1050 to 1450 °C. The calculations indicate that at 1300 °C the contribution to PM from the carbon atom at the end of the chain (h) is approximately 32%, whilst the contribution from the carbonyl group (g) is 0%.

Ethyl acetate-1,2- ^{13}C was used in a method validation experiment, the combined contribution of the carbon at positions labelled ‘i’ was found to be approximately equal that of ‘h’ alone (32%); the reader is reminded that the carbonyl carbon atom contributed a negligible amount to PM. This result is significant as the outcome is found to be the same regardless of how the experiment is carried out, and the conversion rate is uninfluenced by the identity of the neighboring carbon atom.

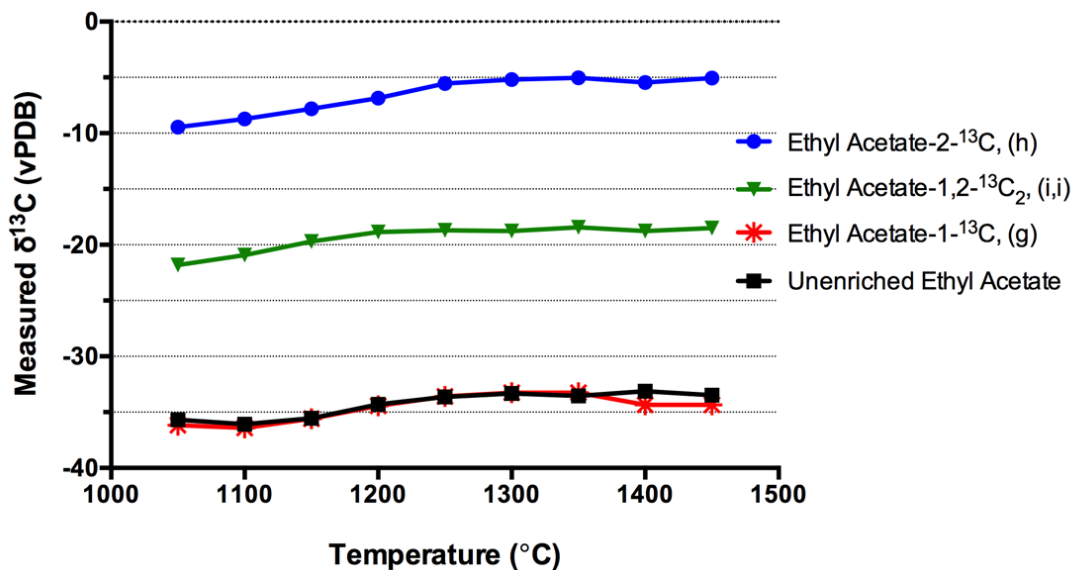


Figure 6.13: Measured $\delta^{13}\text{C}$ values for unenriched ethyl acetate, and ethyl acetate enriched with ethyl acetate-1- ^{13}C (g), ethyl acetate-2- ^{13}C (h), and ethyl acetate-1,2- $^{13}\text{C}_2$ (i,i) (enriched to -8.21, -7.86, and -6.73 $\delta^{13}\text{C}$ respectively), in the temperature range 1150 to 1450°C, at 50°C intervals.

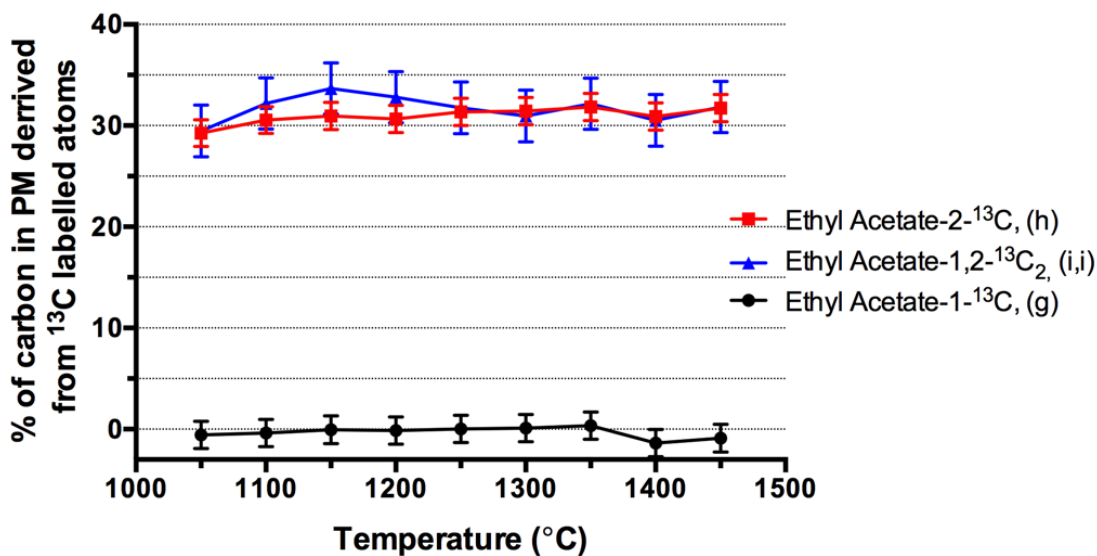


Figure 6.14: Contribution to PM from tagged groups in ethyl acetate-1- ^{13}C (g), ethyl acetate-2- ^{13}C (h), and ethyl acetate-1,2- $^{13}\text{C}_2$ (i,i). Data shows the values calculated from average measurements \pm SD.

6.3.5 Toluene

Three permutations of toluene labelling were tested, shown in Figure 6.15. These groups were specifically labelled in order to identify whether the aromatic ring in toluene contributes to PM formation to a greater extent than the methyl group that is attached to.

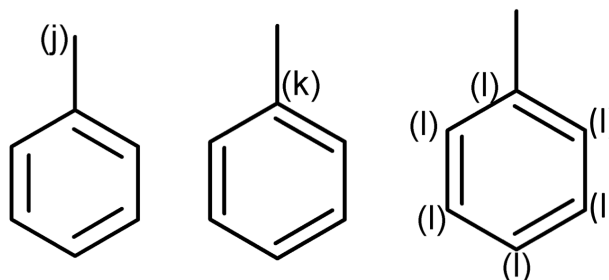


Figure 6.15: Skeletal structure for toluene showing label locations for toluene-1- ^{13}C (j), toluene- α - ^{13}C (k) and toluene-(phenyl)- $^{13}\text{C}_6$ (l).

Figure 6.16 shows the measured $\delta^{13}\text{C}$ values for PM samples generated from un-enriched toluene, and toluene enriched with ^{13}C labelled toluene at positions 'j', 'k', and 'l' respectively. The $\delta^{13}\text{C}$ results measured values show that similar levels of ^{13}C abundance are observed for all of the PM samples formed from the labelled molecules; and there is negligible change in the isotopic signature of the samples at different formation temperatures.

Figure 6.17 shows the calculated percentage contribution of PM of each of the labelled groups (on a per-carbon atom basis). The calculations indicate that each carbon atom contributed approximately 12% to the PM formed. Since toluene has 7 atoms, one would expect that if each carbon contributed equally each atom would contribute about 14.2% to the PM. Despite the small error that is apparent in the estimation, the message from the results is clear that the aromatic ring and the methyl group convert to PM formation at approximately equal rates.

The temperature (in the range 1100 to 1450°C) at which the PM was generated did not greatly affect the isotopic composition measured for the PM. Changes in the isotopic signature might have been expected at different pyrolysis temperatures, as the formation temperature could shift the molecular fragmentation patterns (e.g. rupture of the ring at higher temperatures). Experimental and modelling investigations into the pyrolysis of toluene by Colket and Seery (1994) suggested that there was minimal decomposition of toluene into phenyl and methyl fragments over this temperature range; instead, precursors of particulates and polycyclic aromatic hydrocarbons (PAHs) were predicted to form directly, incorporating the phenyl and the methyl group. However, whilst the results here appear to agree, it should be said that the measurements by EA-IRMS concerned the overall conversion of carbon atoms to PM, and inevitably, if

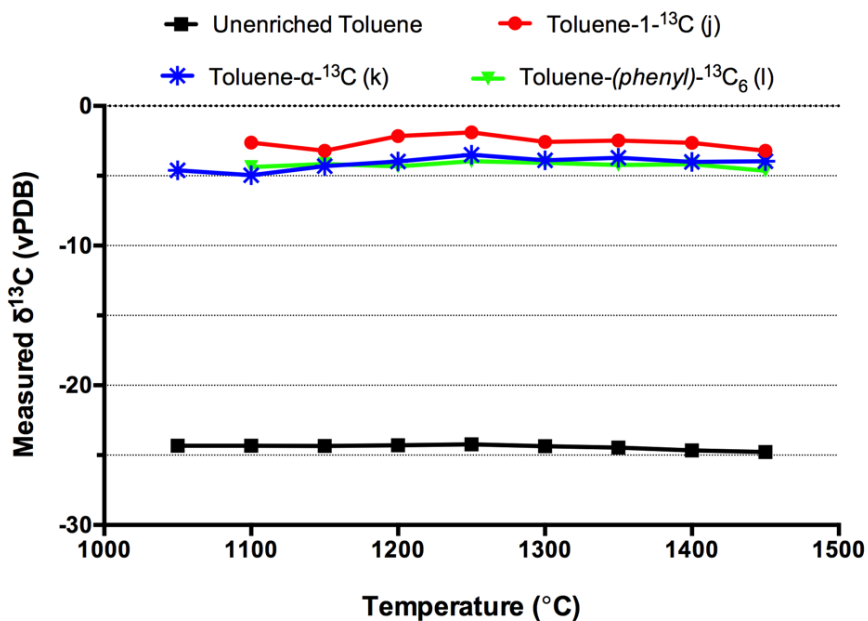


Figure 6.16: Measured $\delta^{13}\text{C}$ values for unenriched toluene, and toluene enriched with toluene-1- ^{13}C (j), toluene- α - ^{13}C (k), and toluene-(phenyl)- $^{13}\text{C}_6$ (l), enriched to -8.21, -7.86, and -6.73 $\delta^{13}\text{C}$ in the fuel respectively, in the temperature range 1150 to 1450 $^{\circ}\text{C}$, at 50 $^{\circ}\text{C}$ intervals.

fragmentation of toluene did occur, conversion to PAHs or PM from different carbon-containing fragments could have occurred at any of the different stages of PM formation.

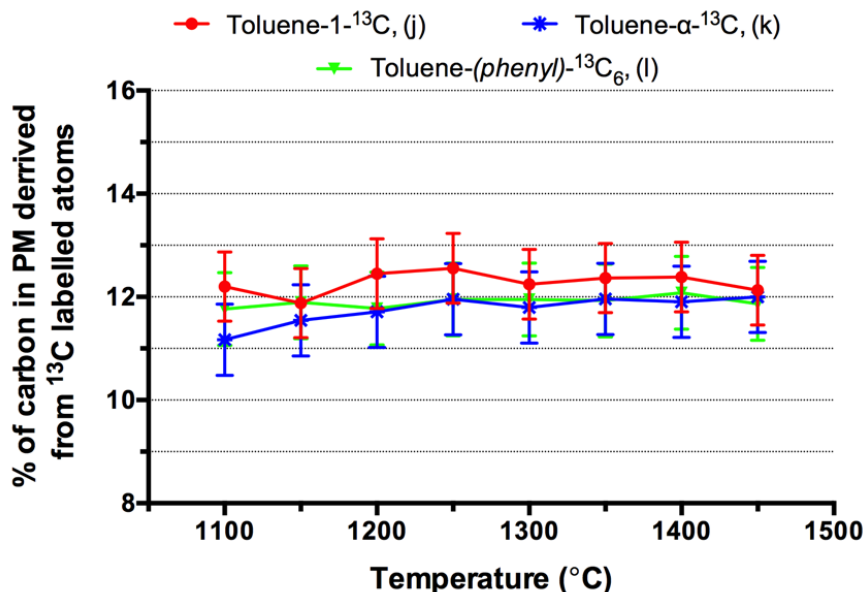


Figure 6.17: Percentage contribution to PM from labelled carbon atoms in toluene-1- ^{13}C (j), toluene- α - ^{13}C (k) and toluene-(phenyl)- $^{13}\text{C}_6$ (l). The conversion rate of carbon atoms in toluene-(phenyl)- $^{13}\text{C}_6$ is shown on a per-carbon atom basis. Data shows the calculated conversion values \pm SD.

6.3.6 Validation of methodology

In order to confirm some of the assumptions that have been made for the calculation of the conversion rates of individual carbon atoms, some experiments were carried out in order to assess the validity of these assumptions.

One of the assumptions is that the outcome of the experiments should be the same regardless of the level of ^{13}C enrichment in the fuel. Some of the experiments, discussed in previous sections, were therefore also repeated at different concentrations. Tests with ethanol-1- ^{13}C , ethyl acetate-2- ^{13}C , and toluene- α - ^{13}C were carried out at several levels of ^{13}C enrichment. Table 6.1 shows the measured values for ethanol-1- ^{13}C , ethyl acetate-2- ^{13}C , and toluene- ^{13}C at varying levels of enrichment; A straight line fit through the data (ΔF vs. ΔPM) results in R^2 regression values of $R^2 = 0.999$, $R^2 = 0.999$, and $R^2 = 0.998$ respectively. Calculated carbon conversions rates are therefore insensitive to level of enrichment used.

Another assumption is that at the temperatures used (~ 1100 to 1450°C), ^{13}C behaves in the same way as ^{12}C ; that is, a $^{13}\text{C}-^{12}\text{C}$ or $^{13}\text{C}-^{13}\text{C}$ bond should behave in the same way as a $^{12}\text{C}-^{12}\text{C}$ bond. It has been discussed previously (Section 6.3.4) that ethyl acetate has been used to validate this assumption. Ethyl acetate-1,2- $^{13}\text{C}_2$, which has a $^{13}\text{C}-^{13}\text{C}$ bond, was shown to contribute the same percentage of carbon to the PM from the two tagged carbons, as ethyl acetate-2- ^{13}C alone, which has a $^{12}\text{C}-^{13}\text{C}$ bond. This is a significant result because ethyl acetate-1- ^{13}C was shown not to contribute to PM at all, Figure 6.14, showing that the contribution from methyl carbon in acetate-2- ^{13}C was the same (32%) regardless of whether the neighboring carbon was

Table 6.1: $\delta^{13}\text{C}$ measurements of fuel and derived PM (generated at 1300 °C) for ethanol, ethyl acetate, and toluene, at various levels of enrichment.

Compound name	$\delta^{13}\text{C}$ fuel	$\delta^{13}\text{C}$ PM	ΔF	ΔPM	ΔMax	F
Ethanol						
Unenriched Ethanol	-27.833 ³	-31.191 ¹				
Ethanol-1- ^{13}C	-17.163 ³	-25.751 ¹	10.67	5.44	21.34	0.25
Ethanol-1- ^{13}C	-6.063 ³	-19.401 ¹	21.77	11.79	43.54	0.27
Ethanol-1- ^{13}C	3.103 ³	-14.151 ¹	30.93	17.04	61.86	0.28
Ethyl acetate						
Unenriched ethyl acetate	-30.252 ²	-33.331 ¹				
Ethyl Acetate-2- ^{13}C	-19.472 ²	-19.431 ¹	10.78	13.9	43.12	0.32
Ethyl Acetate-2- ^{13}C	-7.862 ²	-5.181 ¹	22.39	28.15	89.56	0.31
Toluene						
Unenriched Toluene	-24.462 ²	-24.351 ¹				
Toluene- α - ^{13}C	-12.292 ²	-15.081 ¹	12.17	9.27	73.02	0.13
Toluene- α - ^{13}C	0.322 ²	-3.891 ¹	24.78	20.46	148.68	0.14

Standard deviation applicable: ¹ $\sigma \leq 0.1$, ² $\sigma \leq 0.2$, ³ $\sigma \leq 0.3$.

^{12}C or ^{13}C . In addition, ethanol- $^{13}\text{C}_2$, where both carbon atoms were labelled, was also tested and it was verified that the level of enrichment in the fuel was the same as the level of enrichment found in the derived PM (i.e. that $\Delta\text{PM}=\Delta\text{F}$); in other words that the contribution from the two carbon atoms was found to be 100%, which showed that the ^{13}C were as likely to convert to PM as ^{12}C atoms.

For the majority of the analysis it was observed that for the PM samples derived from the unenriched fuels tested, the measured $\delta^{13}\text{C}$ value for PM was more negative (i.e. contained less ^{13}C) than the fuel from which it was formed. For example, in the case of unenriched ethanol the fuel -27.8 $\delta^{13}\text{C}$ was recorded, and -31.2 $\delta^{13}\text{C}$ was found for the derived PM formed at 1300 °C. There are a number of mechanisms that could give rise to this small shift in isotopic signature during pyrolysis:

1. A kinetic isotope effect, whereby dissociation energies of bonds are specific to the isotope participating in the bond. If a rate determining step in a series of chemical reactions involves bond breaking, it is plausible the bonds containing isotopically ‘lighter’ atoms may break easier since the vibrational frequency of such bonds tends to be higher. As a result, the ‘lighter’ isotope (i.e. containing ^{12}C) could be preferentially incorporated into the products, while ‘heavy’ isotopes would remain relatively unreacted. This process could occur during pyrolysis, and isotopically lighter molecules may fragment more readily.
2. ^{13}C might be naturally distributed unevenly in a molecule due to its formation process in nature (or synthesis). If during the pyrolysis process, one locality is converted to PM to a greater extent than the other, then the ^{13}C abundance measured in the PM will change depending on the conversion ratios and local distribution of ^{13}C .

- Evaporation is also a unidirectional process that can cause isotopic fractionation. Generally, isotopically ‘lighter’ molecules tend to have higher translational velocities; this allows them to preferentially break through the liquid surface and pass into the atmosphere (Criss, 1999). Over time the remaining liquid will become progressively enriched with the heavier, in this case ^{13}C , isotope. Only small samples of liquid are required for IRMS analysis, and there is therefore some limited potential for evaporation of the volatile liquids during the preparation of liquid samples.

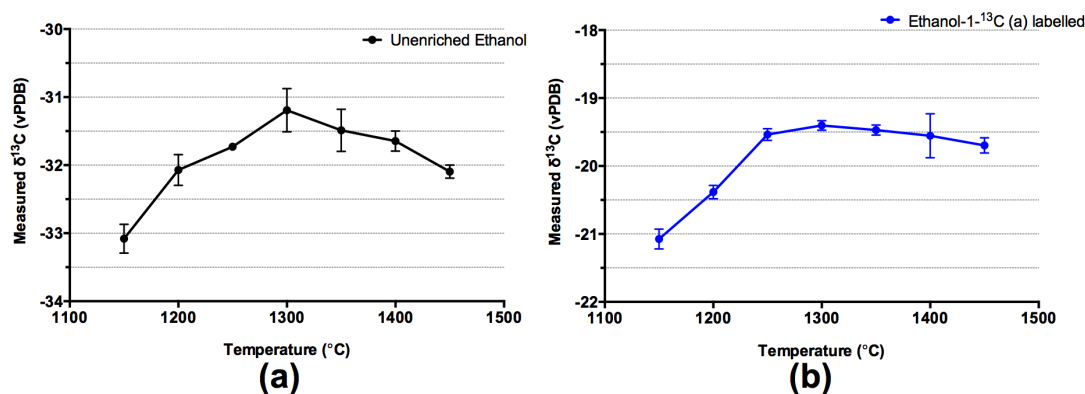


Figure 6.18: Example of behavior of raw $\delta^{13}\text{C}$ measurements, pyrolysis of unenriched ethanol (a) and ethanol enriched with ethanol-1- ^{13}C , at temperatures in the range of 1150 to 1450 $^{\circ}\text{C}$. Data shown is the average of three measurements, \pm standard deviation

If a kinetic isotope effect occurs during the pyrolysis of a hydrocarbon to any extent then one would expect that with increasing reaction temperatures increasing levels of ^{13}C would be incorporated into the PM with respect to ^{12}C , resulting in an increasing $\delta^{13}\text{C}$ for samples obtained at higher temperatures. Figure 6.18 shows that shifts in the isotopic signature of the PM formed from the unenriched ethanol is negligible in the formation temperature range 1150 to 1450 $^{\circ}\text{C}$. For example, it is seen that unenriched ethanol formed PM that had an isotopic signature of -33.08 $\delta^{13}\text{C}$ at 1150 $^{\circ}\text{C}$ and -31.19 $\delta^{13}\text{C}$ at 1300 $^{\circ}\text{C}$, a difference of just 2.16 $\delta^{13}\text{C}$ which represents a 0.216% variation in the ^{13}C rate. We can therefore conclude that kinetic isotope effects are indeed negligible in the temperature range tested, and in the literature it is generally accepted that kinetic isotope effects are minimal at temperatures upwards of about 500 $^{\circ}\text{C}$ (please refer to Section 2.4). If ^{12}C converts to PM preferentially at low temperatures, then one might expect a drift towards ^{13}C ‘heavier’ PM at higher temperatures.

If there is a natural difference in the local $\delta^{13}\text{C}$ rates within a molecule, this would have an influence on the measured values but not on the overall outcome of the experiment. Essentially the unenriched bulk of the fuel (into which labelled fuel is added) is only present as a ‘diluent’ and the only assumption is that the rate of conversion to PM is the same for identical molecules that contain either ^{12}C or ^{13}C . The calculations

Table 6.2: Measured $\delta^{13}\text{C}$ values for unenriched ethanol with varying delay between capillary transfer and capsule sealing

Sample ID	Capsule sealing delay (s)	$\delta^{13}\text{C}$ Fuel	Average	σ
S1	0	-15.69		
S2	0	-16.08		
S3	0	-15.80		
S4	0	-15.50	-15.77	0.24
S5	30	-14.97		
S6	30	-15.48		
S7	30	-15.00	-15.15	0.29
S8	60	-15.71		
S9	60	-15.74		
S10	60	-15.01		
S11	60	-14.73	-15.30	0.51

introduced in Chapter 4 to obtain the percentage contribution take account of such a shift caused by unequal ^{13}C distribution.

If evaporation of molecules containing predominantly ^{12}C occurred immediately before measurement, this could have given rise to the observed difference in the $\delta^{13}\text{C}$ rate of the PM with respect to the fuel, and could have had a large impact on the calculated results. During the sample preparation process, liquid samples were collected using a glass capillary tube that was then immediately transferred to a smooth-walled tin capsule and quickly crimped to seal the contents (the process is described in detail in Chapter 3). Fractionation by evaporation could have occurred between the point of capillary collection and it being sealed in the tin capsule. In order to identify whether fractionation occurred at the point of measurement, to an extent that could explain the difference between liquid measurements and PM measurements, an experiment was conducted whereby the time between placing the capillary into the capsule and crimping was varied (0, 30, and 60 seconds). The results, shown in Table 6.2, indicate that the measured values are insensitive to the delay in sealing the capsule. In practice, the process of transferring a capillary to a tin capsule and crimping may take between 5 and 10 seconds. This suggests that the technique for collecting the samples by capillarity was effective at limiting evaporation of the fuel during sample preparation, and therefore $^{13}\text{C}/^{12}\text{C}$ fractionation by evaporation was not the source of the difference between the fuel and PM measurements ¹.

6.4 Further discussion

It has been shown that the presence of oxygen within a molecule directly influences the conversion of neighboring carbon atoms to which it is directly attached. Therefore, it is of interest to assess how other features of oxygenated fuels influence the conversion of

¹It should be noted that some tests have been conducted with different bottles of standard lab ethanol, the isotopic signature can vary depending on the source. It has been ensured that groups of tests carried out for comparison have been conducted using only one bottle of the unenriched fuel.

carbon. For example, whether going from a primary alcohol, where the hydroxyl group is on the end of the carbon chain (e.g. 1-propanol), to a secondary alcohol where the hydroxyl group is in the middle of the chain (e.g. 2-propanol), has an impact on the conversion of the neighboring carbon atom in becoming PM. In order to assess this, it is instructive to introduce an additional parameter, $R_{relative}$, which is the relative conversion rate of the labelled carbon atoms, defined as follows:

$$R_{relative} = \frac{\Delta PM}{\Delta F} \quad (6.1)$$

Where ΔPM , and ΔF are the differences in the enrichment of the unenriched and enriched versions of the fuel and PM (defined previously in Chapter 4). $R_{relative}$, is the conversion rate of the labelled carbon atoms and allows the direct comparison of the carbon conversion rates. Another way of thinking of this parameter is as the ratio of the carbon mass fraction contributed by the labelled carbon atoms in the PM, to that of the fuel from which it was formed. For example, in the case of ethanol where the *hydroxyl* carbon (a) was labelled, the fraction of the *hydroxyl* carbon in the fuel was 0.5 (50 %), whereas the PM derived from the fuel only 27% of the carbon atoms were derived from the *hydroxyl* carbon, the conversion rate of the carbon atoms was therefore 0.54 (0.27/0.5).

Figure 6.19, shows the relative contribution of the carbon atoms directly bonded to the hydroxyl group for the alcohols tested. In the series of primary alcohols, ethanol, 1-propanol, and 1-pentanol, the length of the carbon chain does not appear to influence the conversion rate of the hydroxyl carbon atom, for example the conversion rate is 0.54, 0.49 and 0.52 respectively. However, there is an increase in the conversion rate of the hydroxyl carbon atom when going from a primary to a secondary alcohol. For example, the conversion rate of the *hydroxyl* carbon in 1-propanol is 0.49, whereas in 2-propanol it is 0.67. The *hydroxyl* carbon atom in the cyclic molecule cyclopentanol had a conversion rate of 0.79, which was the highest of all of the alcohols tested, and compared to a conversion rate of only 0.52 for the equivalent primary alcohol 1-propanol.

This result that there was a suppressed contribution to PM from the hydroxyl carbon is in alignment with the literature. Previous commentators have suggested that the 2:1 methyl-to-hydroxyl ratio of conversion of carbon atoms in the alcohol fuel to PM would be found regardless of the structure of the molecule; work by Schmieder (1985) identified 2:1 ratio during 1-butanol combustion, and Lieb and Roblee Jr (1970) found the same ratio for ethanol combustion in a diffusion flame. In this chapter, the results are in agreement with the previous work on primary alcohols, but the finding that the *hydroxyl* carbon in secondary alcohols had an increased conversion rate to PM has not been reported previously. The well-controlled conditions employed in the tube reactor experiments in this chapter make it particularly suitable for making such comparisons of the conversion rates between the different fuels.

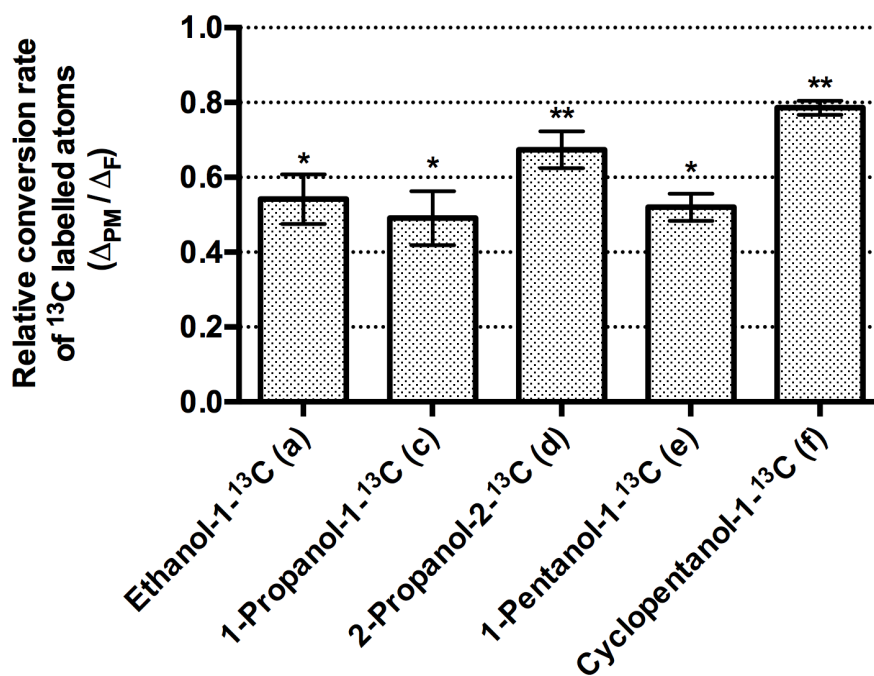


Figure 6.19: Relative conversion rate (ΔPM , and ΔF) of ^{13}C labelled atoms in various alcohol molecules calculated for PM formed from a series of alcohols, at 1300°C . Data shown is the calculated average values \pm SD (estimated using data from 3-6 measurements). (*) Indicates a primary alcohol, and (**) indicates a secondary alcohol.

6.5 Conclusions

The results presented in this chapter show that specific carbon atoms within molecules contributed to the formation of PM to different extents, depending on the local molecular structure. Oxygenated carbon atoms tend to convert to PM to a lesser extent than the average carbon atom in the molecule. Tests were conducted at different temperatures in order to identify whether shifts in the conversion rates of labelled atoms occur at different temperatures; which may result from shifts in molecular fragmentation patterns and kinetic pathways. The results from oxygen-free pyrolysis of the molecules tested in this chapter have shown insensitivity to soot formation temperature in the range tested (generally 1000 to 1450°C).

The most significant findings of the isotope tracing investigation are the following:

- The hydroxyl group reduces the contribution to the PM from the carbon atom to which it is bound in the fuel, and was observed in all alcohol molecules tested (ethanol, 1- and 2-propanol, pentanol and cyclopentanol);
- Of the alcohols tested, it was observed that the carbon atom directly bonded to the hydroxyl group in primary alcohols (ethanol, 1-propanol, 1-pentanol) converted to PM to a lesser extent than an equivalent secondary alcohol (2-propanol, cyclopentanol).

- The ester carbon in ethyl acetate (which was bound to two oxygen atoms) was not found in the PM, for all of the pyrolysis conditions investigated.
- The methyl carbon in toluene was found in the PM at approximately the same rate as the average carbon atom in that molecule.

In order to further explore how the formation of particulate from individual carbon atoms is influenced by the conditions it is formed under, the following chapter presents an investigation into the generation of particulate matter in the presence of oxygen in both a flow reactor and a diesel engine.

Chapter 7

Isotopic tracing of labelled atoms in oleic acid and methyl oleate, in a diesel engine and tube reactor

The results of the previous chapter showed the conversion rate to PM of selectively labelled carbon atoms for a range of molecules. Particulate samples were generated in a laminar flow tube reactor under pyrolysis conditions at range of temperatures. This chapter is concerned with particulate formation from the fuels oleic acid and methyl oleate, in the tube reactor and also in a direct injection compression ignition engine. The conversion of individual carbon atoms of oleic acid and methyl oleate to particulate matter is reported using the ^{13}C isotopic tracer technique.

Pyrolysis in the reactor has been carried out at 1300°C , first under oxygen-free conditions, and then at rich air-fuel equivalence ratios (λ) of 0.1, and 0.2. Samples of PM were also collected from the compression ignition engine at an intermediate engine load. In addition, emissions data from the engine and tube reactor are presented, including unburned hydrocarbons, CO, CO₂, NO_x, and also PM size and number distributions measured by a differential mobility spectrometer.

7.1 Introduction

Fatty acids such as oleic acid are often found in nature, for example oleic acid is produced by plants such as sunflowers or by olive trees in olive oil. However, more frequently, instead of the free fatty acids (FFAs), nature produces triglycerides.

The high energy density of triglycerides, relative to many other biomass sources, mean that they are a useful starting material for conversion to fuels that can be used as petroleum diesel fuel alternatives. Thermal or chemical conversion processes can be used to process triglycerides to yield oxygenate and hydrocarbon molecules. Transesterification of triglycerides with methanol, for example, produces fatty acid methyl esters, and a scheme for a typical transesterification reaction of a triglyceride (in this case yielding

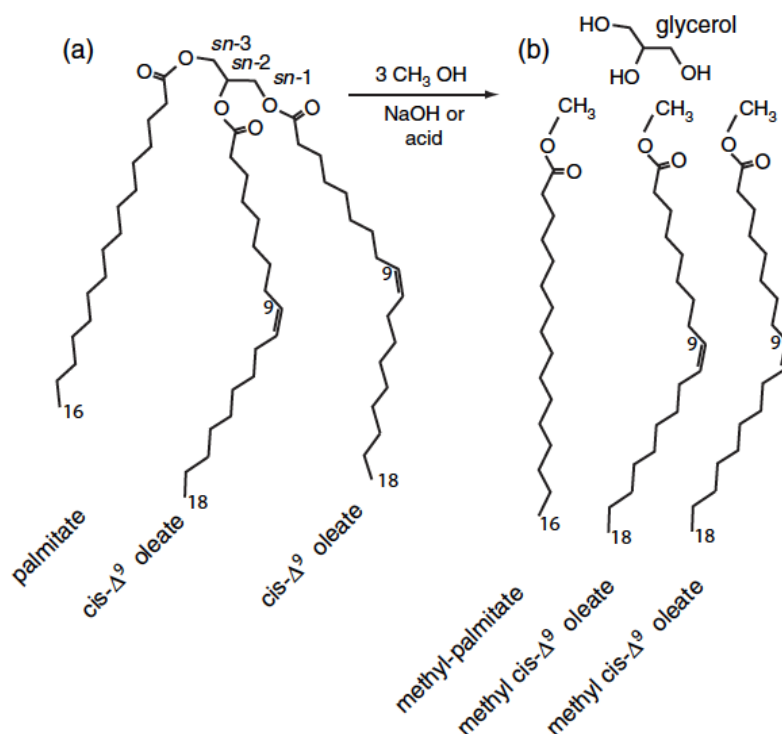


Figure 7.1: Example of a typical transesterification reaction of a triglyceride with methanol, yielding methyl esters and glycerol (Durrett et al., 2008).

methyl oleate) is shown in Figure 7.1. Fatty acid methyl esters (FAMEs) can be blended with fossil diesel fuel, or they can be used to completely substitute fossil diesel fuel in compression ignition engines. Methyl oleate (shown in Figure 7.2) is one such methyl ester, and a number of studies indicate that the combustion characteristics of methyl oleate make it suitable for use as a diesel substitute or for blending with fossil diesel fuel (Soloiu et al., 2013).

Similarly, studies have shown that free fatty acids, when processed to methyl esters are suitable for use in compression ignition engines when blended with diesel fuels or on their own. The unprocessed oleic acid (shown in Figure 7.2) is a free fatty acid (FAA), which instead of an ester group, and is found in ordinary sunflower oil at around 40% by composition, and up to 80% in a hybrid variety named ‘high oleic sunflower oil’ (Purdy, 1986). Unprocessed fatty acids such as oleic acid, and to a lesser extent triglycerides, can be combusted in a compression ignition engine without processing, but reduce engine durability and performance with increased injector nozzle coking and piston ring sticking due to the high viscosity and poor volatility of the acids, which result in poor injection system pumping efficiency and formation of large droplets in the injected spray. To overcome these issues fatty acids and triglycerides can be processed, for example, by transesterification or pyrolysis (Dhar et al., 2012). In this thesis the fatty acid oleic acid, and corresponding fatty acid methyl ester, methyl oleate, have been investigated in terms of their overall conversion to PM, and the conversion of specific carbon atoms within the two fuel molecules.

The presence of oxygen-bearing molecules in fuel reduces tailpipe particulate matter emissions, and can also improve or maintain other regulated emissions such as NO_x, CO, CO₂, and unburned hydrocarbons. Some studies show that particulate emissions decrease in a linear manner with increasing oxygen mass in the fuel, independent of the structure of the oxygenate functional group. A number of studies, however, report that the ability to reduce PM emissions is different for the various oxygenate functional groups, and the molecular structure of oxygenated groups is identified as being responsible for these differences (Buchholz et al., 2004; Mueller et al., 2003). Understanding the mechanism of how oxygen bound within a fuel reduces PM emissions is of interest for the design and processing of cleaner burning fuels; identifying how individual carbon atoms within a molecule convert to PM gives useful insights on the direct impact of local molecular structure. This knowledge could be used to inform the production and processing of future fuels, which could be designed to produce lower levels of PM and other toxic combustion emissions.

It was discussed in the literature review (Section 2.4) that there are relatively few examples of the use of isotopic tracers in combustion research. The examples in the literature, have mainly been carried out in simple systems such as a flame, or reactor, although some have been carried out in practical systems such as a diesel engine. Those that have been carried out in a diesel engine have involved tracing individual compounds or ‘sub-molecular’ parts of compounds either the fuel or engine oil to combustion products for the purpose of source apportionment, and all of the studies in the literature have invariably utilised the radioactive isotope carbon-14 (¹⁴C) (for example Buchholz et al., 2004). To the best of the author’s knowledge ¹³C has not been used before for the purpose of source apportionment of particulate samples collected from a diesel engine. The technique developed in this thesis requires only low levels of ¹³C enrichment, which means that previously prohibitively expensive isotope techniques can be performed in more cost-effective manner. This is particularly important for engine experiments which typically require large volumes of fuel. This technique, combined with the use of an ultra-low volume fuel system, such as the one used here, extends further the viability and practicality of such studies.

Particulates have been generated in a laminar flow reactor at 1300°C, under oxygen-free conditions and at rich air-fuel equivalence ratios (λ) of 0.1, and 0.2 during pyrolysis of isotope labelled oleic acid and methyl oleate. The conditions that have been employed in the reactor are, in a general sense, similar to the conditions in the core of a compression ignition engine spray, in that the conditions are oxygen-deficient and at high temperature. Concurrently, exhaust particulate matter was collected from the compression ignition research engine during combustion of isotope tagged oleic acid and methyl oleate. The results from the reactor, where conditions were laminar, premixed, homogenous, steady, and well controlled are useful for interpreting the results from the engine where the conditions were more complex, highly turbulent, heterogeneous, unsteady, and less controllable. Both the chemical and physical properties of the fuel, for

example, can impact the combustion characteristics in a compression ignition engine; in the reactor, chemical effects dominate the conversion of carbon in the fuel to pyrolysis products.

7.2 Experimental Systems and Methods

7.2.1 Fuels

In both the reactor and engine experiments, methyl oleate and oleic acid were the two single-component fuels that were tested; Table 7.1 shows some relevant properties of these two fuels, and of the reference diesel fuel.

Figure 7.2 shows the molecular locations of the ^{13}C label in oleic acid and methyl oleate. These labelled compounds are added into unenriched but otherwise identical molecules; for example, oleic acid-1- ^{13}C was added into unenriched oleic acid that nevertheless had a natural abundance of ^{13}C . Unenriched oleic acid had a certified purity >99% when it was acquired (Alfa Aesar, 31997). Unenriched oleic acid was enriched by mixing with very small amounts of labelled oleic acid-1- ^{13}C , (labelled at (a), Figure 7.2) (Aldrich, 490423), and oleic acid-8,9- ^{13}C (labelled at (b), Figure 7.2) (Aldrich, 646466). Unlabelled methyl oleate was obtained with certified purity >96% (Alfa Aesar, H31358), and labelled with methyl oleate-1- ^{13}C , 99% purity (labelled at (c), Figure 7.2) (Aldrich 605867). GC-MS analysis of the unlabelled methyl oleate showed that the balance of the molecules (<4%) were structurally similar to methyl oleate, such as methyl stearate.

The labelling experiments were designed in order to assess the following molecular features in terms of their conversion to PM (see Figure 1):

- The relative conversion rate of the carbon atom labelled in oleic acid-1- ^{13}C ('a' in Figure 7.2), to PM.
- The extent to which the tagged carbon atom in methyl oleate-1- ^{13}C ('c' Figure 7.2), is converted to PM, and identify whether this is different to the conversion of 'a' in oleic acid.
- Assess whether the double bonded carbon atoms ('b' in Figure 7.2) within oleic acid converts to PM to a greater extent than the average carbon atom in oleic acid.

Unenriched oleic acid and methyl oleate fuels were enriched with small amounts of ^{13}C labelled fuel, with molar calculations performed to calculate the volumetric quantities needed to enrich the fuel by the desired amount. For example, 110 ml of oleic acid was labelled with approximately 0.73 ml of oleic acid-1- ^{13}C (labelled at position 'a'); 110 ml was sufficient quantity for both reactor and engine tests. In order to achieve the target enrichment level, small volumes of ^{13}C labelled fuel were measured using a capillary piston pipette (Gilson, CP100). It should be noted that the actual enrichment was checked by measuring the δ value with IRMS, and the actual δ value has been used in all subsequent calculations.

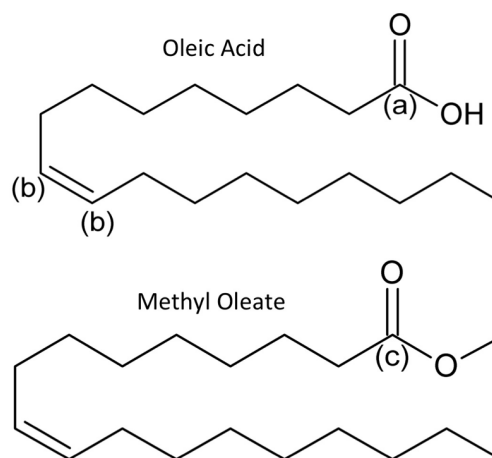


Figure 7.2: Structure and nomenclature of oleic acid and methyl oleate. Oleic Acid was ^{13}C labelled at sites: (a) oleic acid-1- ^{13}C , and (b) Oleic Acid-8,9- ^{13}C . Methyl oleate was labelled in position (c), methyl oleate-1- ^{13}C .

Table 7.1: Fuel properties.

Property	Ref. Diesel	Methyl oleate	Oleic acid
Cetane number	51.7	54	46.1
Viscosity, at 20 °C	3.42 ^a	3.73 ^a , 4.51 ^b	29.0 ^b
Flash point (°C)	66.5	163	187
Density at 20 °C (g/ml)	0.84	0.87	0.89
Degree of saturation	-	Monounsaturated	Monounsaturated
Melting point (°C)	-	-20	16
Boiling point (°C)	180 ^c , 356 ^d	218	286
Oxygen content (O:C)	0.001	0.105	0.111
Net calorific value (MJ/kg)	43.14	37	-

^a dynamic viscosity (mPa s), ^b kinematic viscosity (mm²/s),

^c initial boiling point, ^d final boiling point.

Values obtained from references (Knothe, 2005) and (Soloiu et al., 2013).

7.2.2 Engine experiments

All engine experiments, in which exhaust gas PM was collected, were conducted on a commercially available modern direct injection compression ignition automotive engine, converted and instrumented to run as a single cylinder research engine. The test engine used to conduct the tests is described in detail in Chapter 3.

The isotope tagging technique utilised in this study necessarily required high assay fuels of natural ^{13}C isotope levels, which were enriched with small quantities of ^{13}C enriched fuel; both the unenriched and enriched fuels were available only in small quantities due to their high cost. For this reason use was made of a novel low volume fuel system which allowed the engine to be operated with small volumes of sample fuel (typically 100 to 250 mL). The system utilised was based on the concept first developed by Schönborn (2009), which utilises fossil diesel as a hydraulic fluid, pressurised to fuel injection pressures by a conventional common rail fuel circuit, to pressurise test fuels for high pressure direct injection. For all experiments conducted in this chapter the low

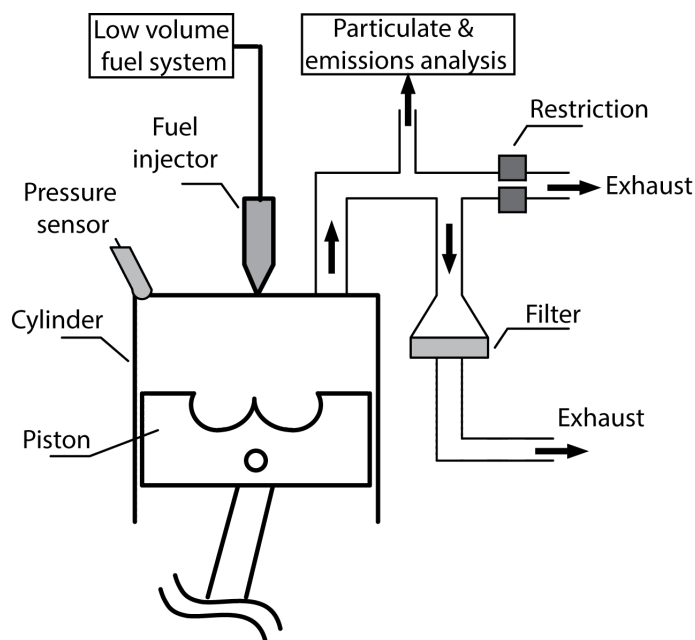


Figure 7.3: Schematic representation of the setup for particulate sample collection from the diesel engine.

volume fuel system was held at a constant temperature of 40 ± 2.5 °C, and the engine was normally aspirated with air at atmospheric temperature and pressure. All engine tests were conducted at 1200 rpm, fuel injection pressure of 450 bar and a constant start-of-fuel-injection of 5 crank angle degrees (CAD) before top-dead-centre (BTDC). For all tests, the injection duration was varied between 648 μs and 770 μs to maintain a constant engine IMEP of 4 bar at the constant speed of 1200 rpm. The engine exhaust gas composition was determined by continuous gas sampling approximately 180 mm downstream of the engine exhaust valves and analysed by an automotive gas analyser system (Horiba MEXA9100 HEGR) and a fast particulate spectrometer (Cambustion DMS 500).

7.2.3 Particulate sample collection

Samples of particulate matter from the engine exhaust gases for ^{13}C isotope analysis were collected onto glass fibre filters (Fisherbrand, Microfiber filter MF300) of 0.22 μm pore size. The engine exhaust gas flow was split and diverted through the glass fibre filter approximately 700 mm downstream of the engine exhaust valves, with the main exhaust path partially restricted to ensure sufficient exhaust gas flow through the filter. Figure 7.3 shows the exhaust sampling arrangement in schematic form. The material deposited onto the filter consisted of a non-volatile organic fraction (NVOF) and some semi-volatile material, or volatile organic fraction (VOF).

Following collection, the filters were cut in half with stainless steel scissors. One half of the filter paper was then placed into a borosilicate glass petri dish and immediately frozen, until required for analysis. The other half of the filter was baked at 300°C for

4 hours in a nitrogen atmosphere, in order to remove the VOF, leaving on the filter mostly carbonaceous particulates. This baked material is hereafter referred to as the non-volatile organic fraction (NVOF). The samples of PM containing both NVOF and VOF, and samples containing only the NVOF were both measured separately by IRMS, in order to compare the conversion rates of the labelled carbon atoms in both fractions.

7.2.4 Tube reactor

Figure 7.4 shows a schematic representation of specific configuration of the tube reactor facility used for pyrolysis experiments in this chapter. Details of the tube reactor were described in Section 3.1.4. Here, the setup consisted of a liquid feed system for metering the introduction of fuel, air and nitrogen (components 1-7), a high temperature reactor (components 8,9), and a means of collecting and analysing effluent gasses (components 10-14).

The flow rate of fuel into the reactor was fixed to a constant carbon flow rate, 21,500 ppm total hydrocarbon content on a C_1 basis, and all reactor experiments reported herein were conducted at 1300°C. The fuels were fed into the tube reactor system by means of a mechanical syringe pump feeding into the heated vaporiser. Vaporised fuels were entrained in a pre-heated carrier gas, consisting of nitrogen and varying concentrations of oxygen; nitrogen flow rates were controlled using a Bronkhorst EL-Flow series mass flow controller, and air flow rates were metered using a Bronkhorst EL-Select series model. A total flow rate of 20 L/min carrier gas was used. A fast flame ionisation detector (Cambustion, HFR400) was used to profile fuel concentration across the diameter of the reactor inlet, following the static mixer, in order to verify reactor inlet radial homogeneity. The FID response is dependent on the molecular structure of the sample, response factors were applied to the measurements and were obtained from reference Dietz (1967).

Samples of particulate were collected and stored using the conditions described in Chapter 3. A 6 mm stainless steel sample tube was positioned inside of the reactor tube 200 mm from the outlet, along the centreline of the reactor, and used to withdraw effluent gasses for analysis. Particulate size and number measurements were made using a Cambustion DMS500 differential mobility instrument, and a non-dispersive infrared gas analyser (Horiba AIA-120) was used to monitor CO and CO₂ in the effluent gas.

7.3 Results and discussion

7.3.1 Results of the isotope tracer investigation

Figure 7.5 shows the percentage of carbon in the PM that was derived from the ¹³C labelled carbon atoms for each of the following fuels tested in the flow reactor at 1300°C: oleic acid-1-¹³C (labelled at the carboxylic acid carbon, ‘a’ in Figure 7.2), oleic acid-9,10-¹³C (double bonded carbons), and methyl oleate-1-¹³C (methyl ester carbon, ‘c’ in

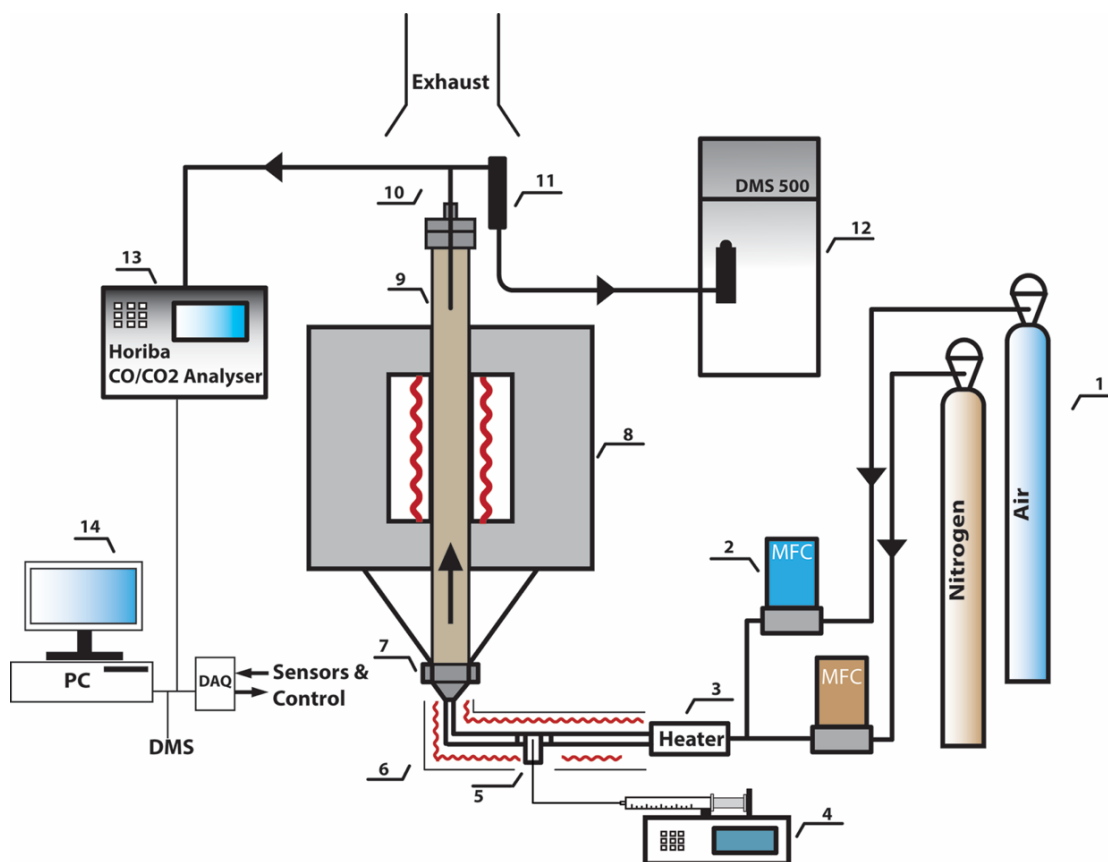


Figure 7.4: Laminar flow reactor rig. (1) Compressed air and nitrogen cylinders. (2) Mass flow controllers. (3) Process heater. (4) Syringe pump. (5) Vaporiser. (6) Heated and insulated stainless steel tube. (7) Mixer. (8) Electric oven. (9) Reactor tube. (10) Stainless steel sample tube. (11) Remote dilution cyclone. (12) Fast particulate spectrometer (13) CO and CO₂ analyser. (14) PC and data acquisition.

Figure 7.2). The measured $\delta^{13}\text{C}$ values and calculated parameters for these fuels are presented in Appendix B.

The carboxyl carbon (labelled ‘a’) in oleic acid-1-¹³C, which is attached to two oxygen atoms, was not found to contribute a significant amount of carbon to the PM formed during pyrolysis; this result was the same under oxygen-free conditions and with small amounts of air (rich equivalence ratios of $\lambda = 0.1$, and 0.2). If each of the 18 carbon atoms in oleic acid converted to particulate matter at an equal rate to PM, one would expect that each carbon atom position in the molecule would contribute 5.55% to the total PM mass. The result that the carbon atom directly bonded to two oxygen atoms in methyl oleate did not form PM in the reactor is consistent with the previous result that the equivalent carbon atom in ethyl acetate was not converted to PM formed under similar pyrolysis conditions (see Chapter 6).

From Figure 7.5 it is seen that the composition of particulate matter formed from the two labelled atoms (b-b) in oleic acid-9,10-¹³C (double bonded carbon atoms), is not significantly greater than what might be expected from that of the average carbon atom in oleic acid. The calculated composition of PM formed from a carbon atom from the

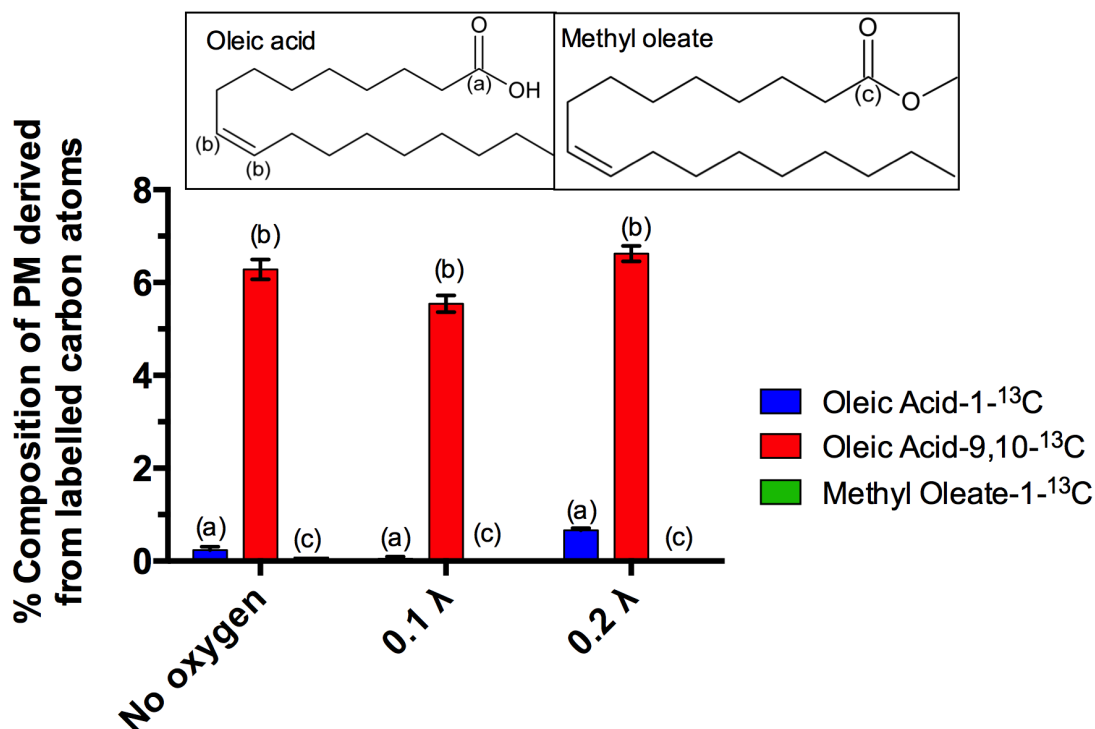


Figure 7.5: Percentage composition of PM derived from the labelled carbon atoms in oleic acid-1-¹³C ('a'), oleic acid-9,10-¹³C ('b') (shown on a per-carbon atom basis), and methyl oleate-1-¹³C ('c'), formed in a flow reactor with varying air-fuel ratios. The labels (a), (b), and (c) indicate the position of the ¹³C labelled carbon atom under investigation. Error bars show the standard deviation of 3 to 6 measurements.

double bond was not influenced and remained relatively unchanged (between 5.5 and 6.6%, for each carbon atom) by the quantity of oxygen available in the reactor.

Figure 7.6 shows the results obtained from the engine for the two molecules investigated. For each molecule, results are shown for two types of PM samples. One of them (labelled **, Figure 7.6) is the soot as collected, containing both volatile and non-volatile organic fractions (NOF + NVOF); and the other (labelled *, Figure 7.6) is for diesel soot, where volatile organic compounds are baked off by means of the oven (Section 2.2.1).

The results of the tracer experiments carried out in the diesel engine yielded similar results to those obtained in the reactor, as is apparent in Figure 7.6. The carbon atoms (a) and (c) directly bonded to the two oxygen atoms, in the case of both oleic acid and methyl oleate, were not detected in the non-volatile fraction (NVF) of the PM formed in the engine. Small amounts (about 1 to 2% levels) of the tracer were observed in the unbaked filters (NVF + VOF). This may have arisen from unburned fuel in the exhaust gas depositing on the filter. It should be noted that in the case of the particulate generated in the diesel engine, which was collected on a glass fibre filter, the particulate had absorbed on it organic species which could originate from the parent fuel and the lubricating oil or which were intermediate compounds formed during the combustion of the fuel and lubricating oil. For example, a ¹⁴C labelling investigation by Buchholz

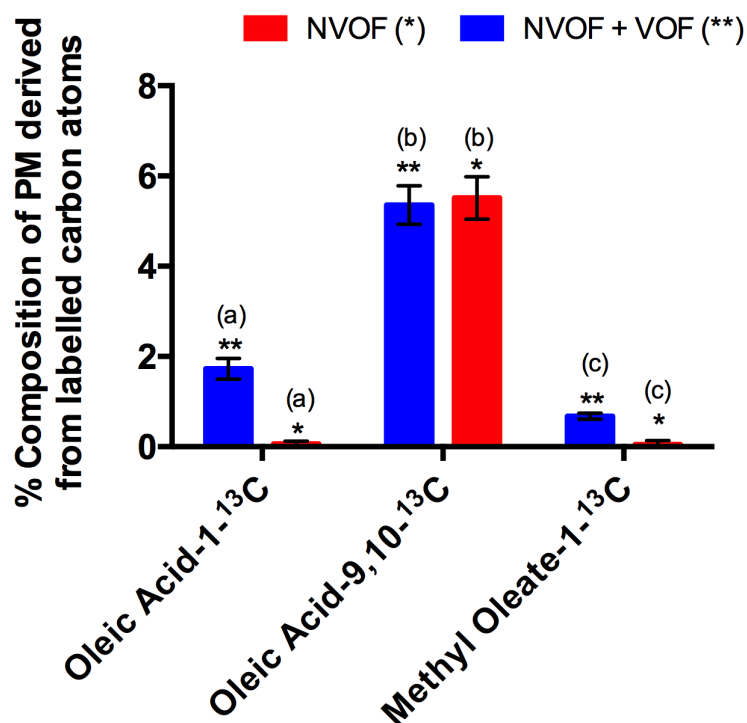


Figure 7.6: Composition of PM derived from ^{13}C labelled carbon atoms, sampled from a diesel engine exhaust gas. The labels (a), (b), and (c) indicate the position of the ^{13}C labelled carbon atom under investigation. (b) is shown on a per carbon atom basis. Error bars show the standard deviation of 3 to 6 measurements.

et al. (2003) investigated the conversion of engine oil to PM in a diesel engine ran with biodiesel; they found that less than 5 per cent of the NVF in PM arose from the engine oil. The engine oil is generally found to contribute to the VOF to a greater extent than to the NVOF of the particulate (Buchholz et al., 2003); in particulate collected from a Perkins 4-236 DI engine, 86% of the VOF was derived from the engine oil (Andrews et al., 1991). As a result, in this work it is expected that engine oil had only a small influence on the calculated conversion rates of carbon atoms from the fuel to PM NVF.

Figure 7.6 also shows that the double bonded atoms (b)-(b) in oleic acid (oleic acid-9,10- ^{13}C) were found to constitute approximately 11% (a total for the two atoms) of the PM formed from the engine, which indicates that it forms soot at about the same rate as the average carbon atom of this 18 carbon atom molecule. It is interesting to note from Figure 5 that the conversion rate of the labelled carbon atom to PM was unchanged by baking the filters. This indicates that there is no preferential incorporation of the double bonded carbon atoms into the NVF or VOF of PM, or, indeed, in the carbonaceous component of PM.

Table 7.2: Summary of physical conditions prevailing in the tube reactor and compression ignition engine.

Tube reactor	Compression ignition engine
Homogenous mixture of fuel and air	Stratified
Fuel concentration of 21,500 ppm (C1 basis)	Overall fuel concentration of $\sim 25,000$ ppm
Conducted under pyrolytic conditions, and $\lambda = 0.1$ and 0.2	Globally lean, stoichiometric in combustion regions, rich spray core
Temperature 1300°C	Calculated maximum global in-cylinder temperature 1000°C ; flame temperature $\sim 2000^{\circ}\text{C}$ (Sison et al., 2007)
Laminar	Turbulent
Residence time ~ 1 s	Duration of combustion ~ 0.008 s, residence time (fuel injection to end of exhaust stroke) ~ 0.05 s
Atmospheric pressure	Variable pressure, with peak pressure of ~ 60 Bar

7.3.2 Influence of the formation conditions on the conversion of atoms to PM

So far the results have shown the rate conversion to PM of ^{13}C labelled carbon atoms from the tube reactor and a diesel engine. It was observed that the conversion rate of the labelled atoms in both systems was very similar despite the differing physical conditions experienced by the fuel molecules in the tube reactor and diesel engine. For example, the two carbon atoms from the double bond in oleic acid (b)-(b) was found to constitute around 11% (both carbon atoms) of PM from both the reactor and the diesel engine. Table 7.2 lists some of the major differences in the formation conditions of the PM between the two different systems. This is a significant result as it shows that the relative conversion rate of individual carbon atoms to PM is conserved over a range of conditions including pressure, temperature, availability of oxygen, carbon concentration, etc.

Similarly, there were comparable levels found in the soot collected from the diesel engine of the isotope tagged carbon bonded to two oxygen atoms, in the cases of both methyl oleate and oleic acid (Figure 7.6); this suggests that soot formation was insensitive to some differences in the in-cylinder conditions present during combustion of the methyl oleate and the oleic acid. For example, Figure 7.7 shows the in-cylinder pressure and apparent net heat release rate of methyl oleate, oleic acid and the reference fossil

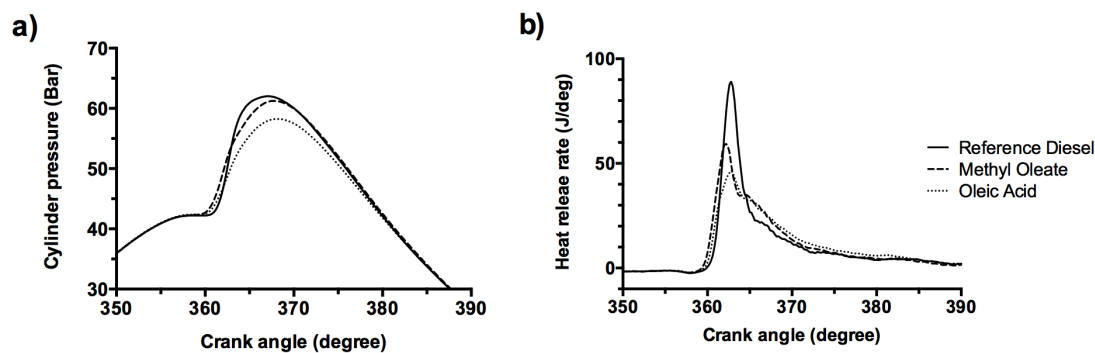


Figure 7.7: (a) In-cylinder pressure and (b) apparent heat release rates of methyl oleate, oleic acid, and reference diesel at constant injection timing.

diesel fuel; apparent from Figure 7.7(b) is the higher peak heat release rate and premixed burn fraction of methyl oleate relative to oleic acid.

7.3.3 Emissions analysis: Laminar flow reactor

Figure 7.8 shows a summary of the size and number distributions, and total mass of the particulate matter evolved from the reactor and measured by the differential mobility spectrometer. Figure 7.8(a-c) shows the aerosol size spectral measurements for diesel, methyl oleate, and oleic acid respectively, and the spectra show that the particle diameters formed from all three fuels are generally in the range of 100 to 1000 nm. The count median diameter (peak center) of the particles, shown in Figure 7.8(d), was found to be around 250 to 320 nm for all fuels and conditions tested. The presence of oxygen was found to decrease the count median particle size in all cases, for example, oxygen-free pyrolysis of methyl oleate produced particles with a count median diameter of 304 nm, compared to 246 nm for those generated at 0.2λ . The total mass of particulates formed is shown in Figure 7.8(e), and it is seen that the diesel reference fuel produced a higher mass concentration of particulates under all conditions, whilst the PM mass emissions from methyl oleate and oleic acid were essentially equal. This result was expected for the reactor-generated particulates due to the comparatively high oxygen content in the methyl oleate and oleic acid compared to that of the reference diesel; the negligible differences in the particulate composition from methyl oleate and oleic acid are not surprising, bearing in mind the similar chemical structures in terms of oxygen content and distribution, similar carbon chain length, and presence of a double bond in those molecules.

Concentrations of CO and CO₂ evolved from the reactor were monitored, and it was observed that pyrolysis of methyl oleate and oleic acid produced high concentrations of CO, and minor concentrations of CO₂. For example, pyrolysis of oleic acid produced 2110 ppm of CO and 89 ppm of CO₂. Comparatively low quantities of CO₂ were expected by means of conversion of carbon dioxide by a hydrogen atom to carbon monoxide and

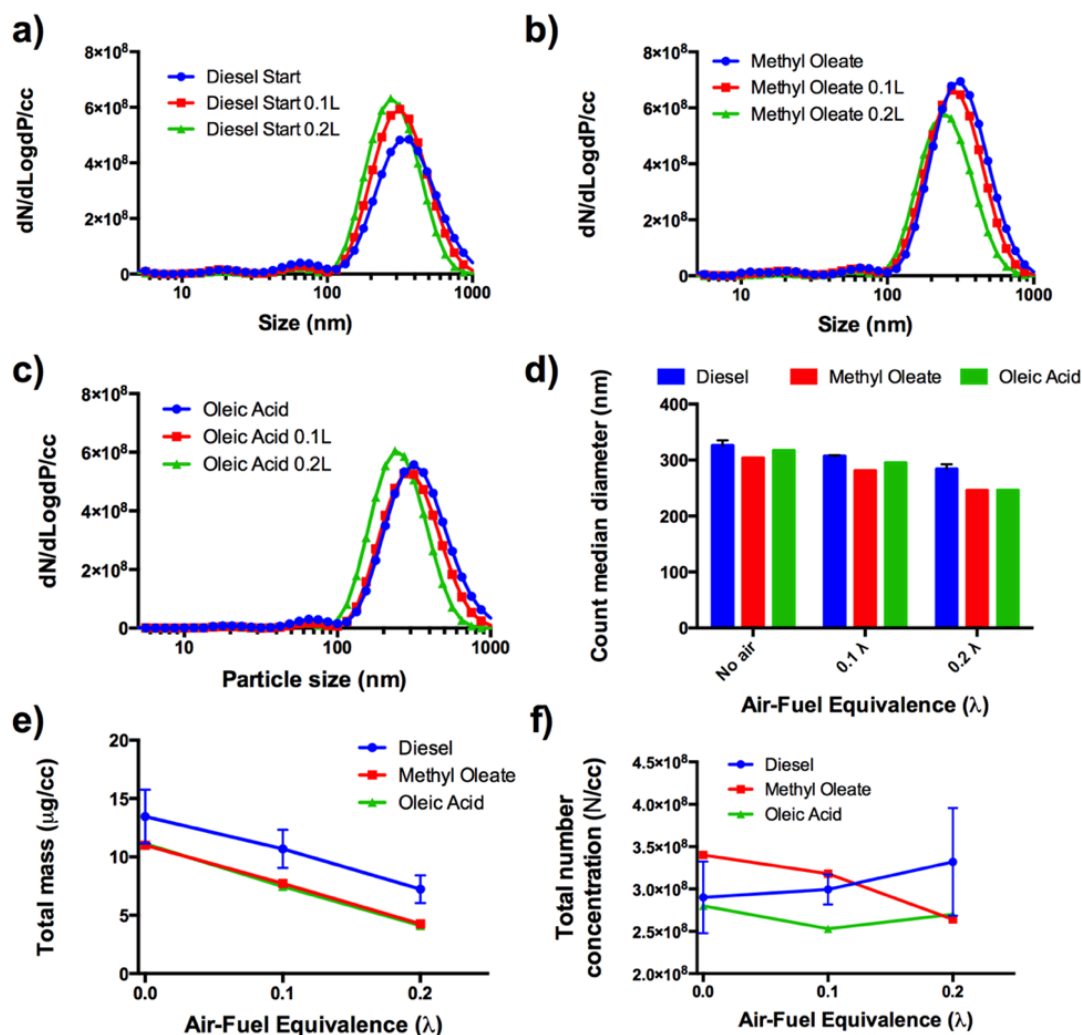


Figure 7.8: Summary of particulate size, number concentration, and total mass characteristics for the pyrolysis of diesel fuel, methyl oleate, and oleic acid in the flow reactor facility. Size and number spectrum for (a) diesel fuel, (b) methyl oleate, and (c) oleic acid. (d) Particulate count median diameter. (e) Calculated total mass concentration of PM. (f) Total number concentration of particulates (N/cc).

a hydroxyl radical, Equation (7.1) (Liu et al., 2001); the hydroxyl (OH) radical is then available to oxidise soot or unburned hydrocarbons.



7.3.4 Emissions analysis: diesel engine

Figure 7.9 shows the size and number distribution of particulates measured in the exhaust and also the total mass of particulates emitted in the engine tests of methyl oleate, oleic acid and the reference diesel. A typical bi-modal distribution of particulates is observed for each of the fuels, with oleic acid producing significantly greater peaks in the number of particles produced in the size range of 10 to 200 nm (Figure 7.9). This can

Table 7.3: CO and CO₂ concentrations (ppmv) evolved from the tube reactor pyrolysis of diesel, methyl oleate, and oleic acid.

Air-fuel ratio (λ)	Methyl oleate		Oleic acid		Diesel	
	CO	CO ₂	CO	CO ₂	CO	CO ₂
No oxygen	2743	75	2110	89	320	0
0.1	7958	402	7250	451	5698	192
0.2	12453	1069	11908	1148	10907	709

probably be attributed to the higher viscosity of the oleic acid relative to the methyl oleate and reference fossil diesel (see Table 7.1), which results in reduced fuel atomisation and efficiency of fuel and air mixing prior to the start of combustion, resulting in a greater degree of diffusion combustion in which the majority of soot formation occurs during diesel combustion. It is tentatively suggested that the dissimilar particulate profiles observed in the cases of oleic acid and methyl oleate (Figure 7.9(a)) further supports the suggestion that the in-cylinder conditions and degree of fuel conversion to soot does not impact on the fate of COO and C=C groups within a fuel molecule.

The particulate mass concentrations measured in the exhaust have been used to calculate the conversion rate of fuel to particulate, Table 7.4 shows the conversion rate to PM in terms of $\text{mg}_{pm}/\text{kg}_{fuel}$. Overall, oleic acid tended to convert to PM at a much higher rate than the reference diesel fuel, as it was described above, this was due to the high viscosity of oleic acid (see Table 7.1). Similarly, methyl oleate was shown to produce PM at a rate of less than half of that of the reference diesel fuel.

In a similar manner, specific PM yields of the carbon atoms in the locations that were isotopically labelled can be calculated. The benefit of displaying the result of the isotopic labelling experiment in this way is that the overall conversion rate of the specifically labelled carbon atoms can be compared; previously, for example in Figure 7.6, the result of the labelling experiment was shown in terms of composition of the PM which was derived from the labelled atoms. The specific yields from the labelled carbon atoms in methyl oleate and oleic acid is supplied in Table 7.5. The overall conclusions, of the labelling experiment are unchanged, to those above in Section 7.3.1. That is, the labelled carbon atoms directly bonded to two oxygen atoms in the methyl ester (methyl oleate), and fatty acid (oleic acid), were not found to convert to PM at a significant rate 0.01 and 0.03 $\text{mg}^{13}\text{C}_{pm}/\text{kg}^{13}\text{C}_{fuel}$ respectively (which corresponds to 0.001 % and 0.003 % survivability). The double bonded carbon atoms in oleic acid, did however convert to PM at a significant rate of 7.80 $\text{mg}^{13}\text{C}_{pm}/\text{kg}^{13}\text{C}_{fuel}$ (corresponding to 0.78 % survivability), which is only slightly higher than that for the oleic acid molecule overall of 5.28 $\text{mg}^{13}\text{C}_{pm}/\text{kg}^{13}\text{C}_{fuel}$.

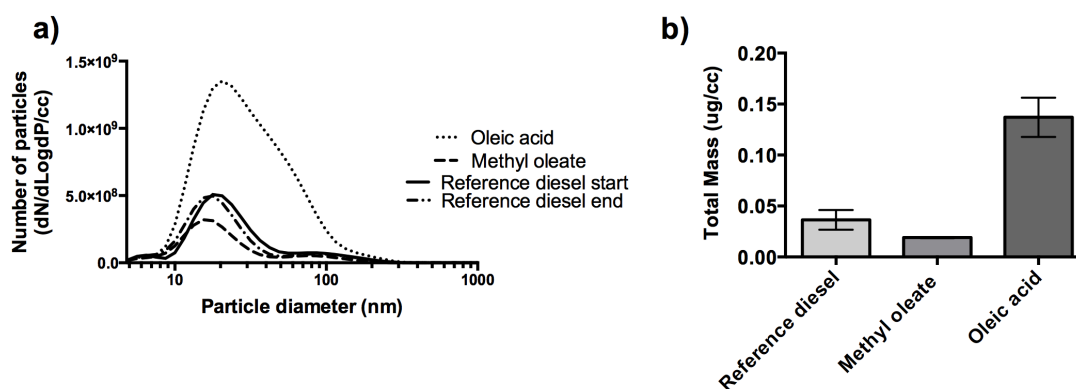
It should be noted that one disadvantage of displaying the result in terms of overall yield PM is that the engine oil contribution has not been identified, and thus the calculations of the specific yield assume that the engine oil contribution to the PM is zero; therefore, the previous way of displaying the result of the isotope labelling experiment (see Section 7.3.1) is a more accurate way of displaying the data.

Table 7.4: Calculated the conversion rate of fuel to PM in the engine, in terms of mass of PM formed per mass of fuel, using the the mass concentration of fuel into the engine (calculated), and exhaust particulate mass concentration (measured by DMS).

Fuel	Fuel conc. (g/m ³)	Soot conc. (g/m ³)	mg _{pm} /kg _{fuel}
Ref. diesel	32.1	0.036	1.13
Methyl oleate	36.2	0.019	0.52
Oleic acid	36.9	0.194	5.28

Table 7.5: Calculated the conversion rate of ¹³C labelled atoms in the fuel to PM in the engine, in terms of mass of carbon atoms derived from ¹³C labelled atoms in the PM, per mass of ¹³C atoms in the fuel.

Fuel	mg ¹³ C _{pm} /kg ¹³ C _{fuel}
Methyl oleate-1- ¹³ C	0.01
Oleic acid-1- ¹³ C	0.03
Oleic acid-9,10- ¹³ C	7.80

**Figure 7.9:** (a) diesel engine exhaust particulate number and size distributions, and (b) calculated total mass concentration of PM. Data shown = Average + SD.**Table 7.6:** CO and CO₂ evolved from the tube reactor pyrolysis of diesel, methyl oleate, and oleic acid.

Fuel	CO (ppmv)	CO ₂ (%)	O ₂ (%)	THC (ppmv)	NO _x (ppmv)
Ref. diesel end	244.80	5.42	12.74	136.18	534.29
Ref. diesel start (A)	249.51	5.61	12.83	67.87	496.64
Ref. diesel start (B)	252.67	5.63	12.75	140.04	500.65
Methyl oleate (A)	208.72	5.47	12.88	150.89	487.17
Methyl oleate (B)	217.58	5.52	12.85	164.18	510.62
Oleic acid (A)	306.94	5.57	12.69	232.61	391.02
Oleic acid (B)	312.51	5.57	12.77	288.12	397.64

Further engine emissions data (CO, CO₂, NO_x, O₂, and THC) is shown in Table 7.6. It is noteworthy that comparatively higher emissions of unburned hydrocarbons were formed from oleic acid compared to methyl oleate, which supports the finding in Figure 7.7 that a significant portion of the PM mass arose from the VOF.

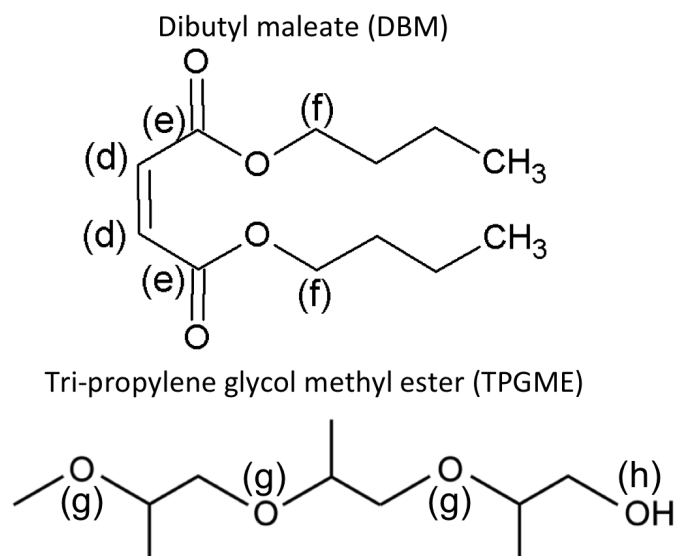


Figure 7.10: Molecular structure of dibutyl maleate (DBM) and tri-propylene glycol methyl ester (TPGME).

7.3.5 Conversion of carbon in the ester and carboxylic group to PM

The results of this study are in agreement with the results of Buchholz et al. (2004) who investigated the conversion to PM of specific carbon atoms labelled with ^{14}C in a somewhat different molecule, dibutyl maleate (DBM), shown in Figure 7.10. DBM contains a carbon-carbon double bond (d), two ester groups (e), and two 1-butyl carbon atoms (f) and each of these groups was specifically labelled with ^{14}C in turn and combusted in a diesel engine. The carbon atom directly bonded to two oxygen atoms (e) was not found in either the exhaust PM or in-cylinder deposits. The double bonded (d), and 1-butyl carbon atoms (f), in DBM was found to form PM in the exhaust at about the same rate as the average carbon atom in the molecule.

Mueller et al. (2003) studied the combustion of DBM and tri-propylene glycol methyl ester (TPGME, $\text{C}_{10}\text{H}_{22}\text{O}_4$), which contains three ether groups (g) and one hydroxyl group (h), shown in Figure 7.10. They concluded that the distribution of oxygen in TPGME was more effective at reducing PM formation than the ester group in DBM. Buchholz and Mueller suggested that the ester structure is an inefficient means of reducing PM formation, since it could produce CO_2 directly, effectively wasting an oxygen atom, which could otherwise be available to prevent another non-ester carbon atom from becoming PM. Numerical simulation by Mueller et al. of the combustion of DBM indicated that 30% of the oxygen, contained in the ester group, is unavailable for PM precursor reduction, and therefore the distribution of oxygen is not optimal. It was also suggested that the carbon-carbon double bond in DBM could form the PM precursor acetylene directly, and therefore one might expect that the contribution of the double bonded group might have been greater than that of the average carbon atom.

The experimental results presented in this paper for oleic acid, and the results of Buchholz et al. (2004) on DBM show that there is not a significantly greater contribution to PM from the doubly bonded carbon atoms. This result indicates that the chemistry of the double bond in oleic acid does not have an appreciable influence on the soot forming tendency of the molecule; this may be considered an unexpected result in light of the results in Chapter 5 which shows that unsaturated molecules have an increased tendency to form soot. The result that neither the carbon atom in the carboxylic acid or the ester group converts to PM is significant. Firstly, the result indicates that the carbon atom remains directly bonded to at least one of the oxygen atoms throughout the combustion process, which means that the carbon atom is not available for oxidation. Additionally it indicates that the distribution of oxygen within a molecule is likely to be an important factor in determining availability of oxygen in the core of a diesel spray, which is likely to have a significant impact on its ability for prevention of soot formation.

7.4 Conclusions

Selective labelling of carbon atoms in oleic acid and methyl oleate with ^{13}C has allowed the determination of the relative conversion rates of those atoms to particulates. The high-sensitivity of IRMS measurements make it suitable for determination of carbon atom conversion rates, even with low concentrations of ^{13}C enrichment, and it has been shown that ^{13}C isotope labelling can be applied to both reactor and engine studies. The following conclusions can be drawn from this study:

- The oxygenated carbon atom in oleic acid and methyl oleate is not found in the engine exhaust PM (despite dissimilar combustion phasing), or in PM formed in the reactor; this indicates that the carbon-oxygen double bond does not break during combustion or pyrolysis, thereby preventing the carbon atom conversion to PM or its precursors.
- The carbon atoms involved in the double bond in oleic acid, are found to convert to PM at approximately the same rate as would be expected from the average carbon atom in oleic acid; that is a result that was found in both engine and reactor tests.
- The results from both the engine and reactor are consistent, in that the outcome of the tracer study is the same regardless of the source of the PM.

The results in this chapter involved the combustion of two single-component fuels, oleic acid and methyl oleate, in a diesel engine. Such head-to-head studies involving single-component fuels are found in the literature (e.g. Soloiu et al., 2013; Schönborn et al., 2009b), and are useful to compare the combustion and emissions characteristics of different molecules. In the future, fuels are expected to become increasingly derived from renewable sources, which may be more uniform in composition than fossil fuels which contain variable compositions made up of numerous molecules. It is therefore of interest to identify the conversion rate of a single molecule within a multi-component

mixture to PM, and also, within that molecule identify the conversion rates of specific carbon atoms; this is the theme of the following chapter.

Chapter 8

Isotope tracing of labelled atoms in various molecules blended with heptane, in a diesel engine and tube reactor

So far, the isotope tracer investigations that have been described in the previous chapters of this thesis have been concerned with the conversion to particulate of individual carbon atoms from specific sub-molecular locations of single-component fuels. Most practical fuels are composed of many different molecules that are blended together, and a ‘typical’ diesel fuel may contain from tens to thousands of chemically distinct compounds (Wang et al., 2005). For this reason, it is of interest to identify how an individual component within a mixture of molecules contributes to the formation of particulate matter and other emissions. In this chapter a number of isotopically labelled molecules have been blended with heptane including ethanol, 1- and 2-propanol, acetone, ethyl acetate, and toluene. The fuel mixtures have been burned in a compression ignition engine, and also in a laminar flow tube reactor, and the relative conversion rate to PM of the labelled molecule or a sub-molecular structure within that molecule has been assessed.

8.1 Introduction

The production of fuels from biological feedstock has received a significant amount of attention in the literature. Ethanol has been industrially produced by fermentation for use as a gasoline substitute since the early 20th century, and among the biofuels it is produced industrially on the largest scale. Longer-chain alcohols have also been produced from biomass, for example the anaerobic bacterium *Clostridium acetobutylicum* is capable of converting large amounts of sugars into a mixture of acetone, butanol, and ethanol (ABE) naturally in the ratio of 3:6:1; and the scale of the industrial biological

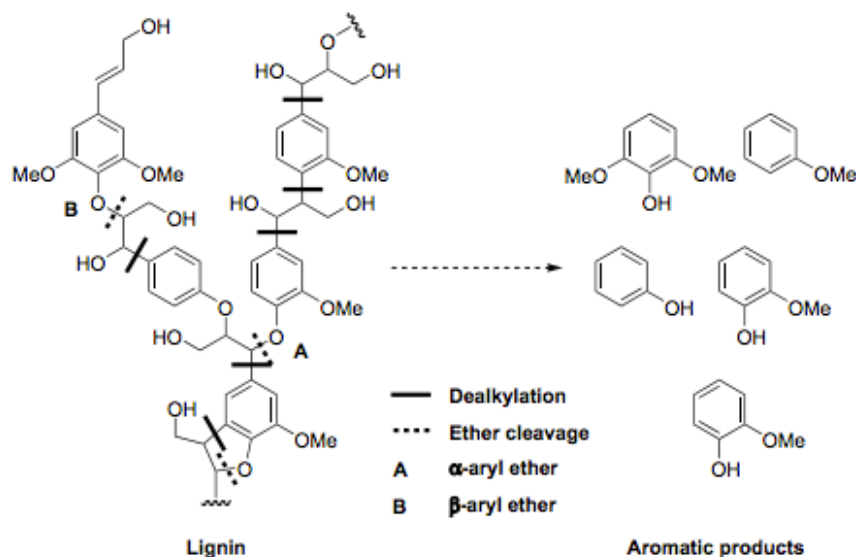


Figure 8.1: General chemical structure of lignin, and schematic for its conversion into mono-aromatic products. Reproduced from (Binder et al., 2009) with permission from Elsevier.

production of ABE is only second behind ethanol production by fermentation (Lütke-Eversloh and Bahl, 2011). As a further example Krouwel et al. (1983) demonstrated the continuous fermentation of glucose by *Clostridium beijerinckii* to produce 2-propanol, butanol and ethanol (IBE). Recently, the promise of improving the properties of fuels derived from biological feedstock has received a significant amount of attention in the literature, due to the possibility of genetically engineering organisms so to biologically produce compounds with a desired molecular structure. For example, a review by Nigam and Singh (2011) showed that there are known biological pathways to produce a number butanol isomers including 1-butanol, iso-butanol, and 2-butanol.

Both diesel and gasoline fuels typically contain significant amounts of aromatic molecules; in the EU the aromatic content of gasoline fuels is limited to 35% (v/v), whilst in diesel fuels the polycyclic aromatic hydrocarbons (PAH) limit is 8% (Directive L 140/88 E). The polycyclic aromatic compounds that are present in diesel fuels are principally naphthalene, fluorene, and phenanthrene (Williams et al., 1986). Whilst aromatic ring structures are present in current fossil fuels, and not present in lipid derived biodiesel fuel, some future bio-derived fuels could also contain significant amounts of aromatics. For example, lignin which accounts for 15-30% of wood-like biomass is a potential major source of aromatic chemicals. Figure 8.1 shows the structure of lignin, and the cleavage of the alkyl and ester linkages by acid catalysis yields phenols and methoxyphenols. Fuels can be processed so to reduce the aromatic content, and this is usually done by the catalytic hydrogenation of the aromatic ring (Choudhary and Phillips, 2011).

In the literature, toluene is the most studied of the aromatic molecules, and in

general it has been blended with alkanes (typically *n*-heptane) for the purpose of understanding fuel effects on engine knock in spark ignition engines (Herzler et al., 2007), combustion rate in HCCI engines, or the tendency of soot formation (Alexiou and Williams, 1995). In compression ignition engines, higher aromatic content is associated with poorer fuel quality due to the low cetane number and generally produces higher NO_x emissions, although there is some conflicting results in the literature regarding the tendency of aromatics to form soot in a diesel engine (Cooper and Donnis, 1996). In jet engines however the aromatic content of the fuel does produce higher particulate emissions, which correlate well with the threshold sooting index (TSI), which was introduced in Chapter 5 (Yang et al., 2007).

There is clearly an increasing possibility of engineering the design of fuel molecules by modifying biological production pathways or by post-processing the fuel to yield more desirable combustion characteristics. From the literature discussed so far it is clear that there is still a need to understand better the fundamental chemistry combustion of even some of the simplest fuels. The fuels ethanol, 1-propanol, 2-propanol, and acetone, which have been investigated in this chapter are of practical relevance due to the possibility of biologically manufacturing these molecules, or other molecules which have homologous functional group chemistry. Toluene is also of interest as an aromatic component in an otherwise paraffinic fuel; one question which does not have consensus in the literature is whether the aromatic component contributes disproportionately to particulate emissions.

Due to the low cetane number of short-chained alcohols such as ethanol and propanol they have not been used before as single-component fuels in diesel engines. A number of studies have been carried out where such molecules have been blended into heptane or diesel fuels, and combusted in compression ignition engines (Lü et al., 2006), shock tubes (Alexiou and Williams, 1995), and flow reactors (Roesler and De Tessian, 2000) to investigate how the additive molecule influences combustion and emissions. In this chapter the various fuels have been blended to a level of 10 mole percent in *n*-heptane. *n*-heptane is often used as a diesel fuel surrogate, due to its similar physical properties (e.g. vapor pressure), and combustion properties (laminar flame speed) and is frequently used in experimental and computational combustion research to emulate more complex fuels (Pitz and Mueller, 2011). *n*-heptane is a primary reference fuel for octane rating in internal combustion engines and has a cetane number of 56, which is very similar to that of conventional diesel fuel, which in the EU is around 52. Due to the large variety of different molecules present in a ‘typical’ diesel fuel, when a compound is added to a conventional diesel fuel, the added component could potentially interact with the other fuel compounds, possibly in a synergistic way, and produce higher levels soot. Due to the complex nature of diesel fuel there would be no easy way of identifying which fuel component was responsible for the synergistic behavior. The approach adopted in this work has therefore been to identify how a number of molecules convert to particulate emissions when they are added to the alkane *n*-heptane (C₇H₁₆), so as

to form a binary mixture; and, then, to measure the contribution to particulate of the compound added to the *n*-heptane.

8.2 Methods

8.2.1 Fuels

A number of oxygenated and hydrocarbon molecules were blended with heptane at 10 mole %, these were: ethanol, 1-propanol, 2-propanol, acetone, ethyl acetate, and toluene. Table 8.1 shows how a 10 percent molar concentration of the various molecules in heptane translates in terms of overall carbon content of the fuel and volume fraction of the fuel. Due to the fact that the molecules were blended with heptane, it was of interest to identify the conversion to PM of carbon in the added compound relative to that for the heptane, i.e. to determine whether, overall, the added component tends to form PM to a greater or lesser extent than the heptane alkane chain. To make this determination, a ^{13}C tracer experiment was carried out where the added component (ethanol, 1-propanol, *etc.*) was enriched with small amounts of the fuel where all of the carbon atoms were ^{13}C labelled. Furthermore, selected submolecular locations of the added fuels were also labelled with ^{13}C in order to identify the relative contribution to PM. The molecular structures and nomenclature of the ^{13}C labelled fuels tested are shown in Figure 8.2.

The selection of molecules that were blended into heptane and tested in both the flow reactor and diesel engine, allowed the following to be determined:

- The overall conversion of ethanol to PM when blended in heptane; and
- The conversion rates of the individual carbon atoms within ethanol.
- Comparison of the overall conversion of 1- and 2-propanol molecules to PM, to see if there is an effect of moving the hydroxyl group from the end on a carbon chain to the central carbon atom; and
- Assessing whether the carbon atom directly bonded to the hydroxyl group is converted to PM at a different rate for 1- and 2-propanol than the other carbon atoms of these molecules.
- Testing labelled acetone-in-heptane (shown in Group D) to identify, firstly, the overall conversion rate to PM of the acetone in the blend; and
- By comparing the result of acetone to that of 2-propanol, assess whether by going from propanol (in which oxygen is single bonded to the central carbon) to acetone (which contains a double-bonded oxygen) there is an appreciable difference in (a) the overall conversion to particulate of the molecule as a whole in the heptane blend, and (b) in the conversion rate to particulate of the carbon atom to which oxygen is bound directly.

Table 8.1: Mixture of various compounds in heptane at level of 10 mole percent.

	Mole %	Vol. % of fuel	% total fuel carbon
Ethanol	10	5.14	3.08
1-propanol	10	5.36	4.55
2-propanol	10	5.49	4.55
Acetone	10	5.29	4.55
Toluene	10	7.48	10.00

- The extent of toluene conversion to PM relative to heptane; and
- Whether there is a difference in the conversion rate of the methyl group (labelled in toluene-1- ^{13}C) and the phenyl group (labelled in toluene-*phenyl*- $^{13}\text{C}_6$).
- To identify whether the conversion rates of the labelled molecules or sub-molecular groups is different in the reactor compared to the diesel engine.
- In Chapter 6, results were obtained regarding the conversion carbon atoms in single-component fuels to PM, which was formed under pyrolysis conditions. Where there is overlap, the results obtained in this chapter will be compared to those of Chapter 6, in order to identify whether the conversion of carbon atoms to PM is influenced by the surrounding mixture. For example, in Chapter 6 it was identified that in the case of ethanol the ratio of the methyl-to-hydroxyl carbon atom conversion to PM was 68:27, and in this chapter it will be assessed whether that conversion ratio is conserved when the ethanol is blended into heptane.

8.2.2 Apparatus

Laminar flow tube reactor

All of the experiments that were carried out in this chapter using the tube reactor were conducted at a temperature of 1300 °C. Tests were conducted under pyrolysis conditions using oxygen-free nitrogen as a carrier gas fed at 20 L/min. The vaporiser and stainless steel tube to the reactor inlet was set to 200 °C. Samples of particulate were collected by thermophoretic deposition onto a borosilicate glass plate, collected at 30 mm from the reactor outlet. Following collection, the samples were stored in borosilicate glass vials at -20 °C until required for EA-IRMS analysis. For further details on the flow reactor setup refer to Chapter 3.

Diesel engine

All engine experiments in which exhaust gas PM was collected were conducted on the commercially available direct injection compression ignition engine, run as a single cylinder research engine. The engine used to conduct the tests is described in further detail in Chapter 3.

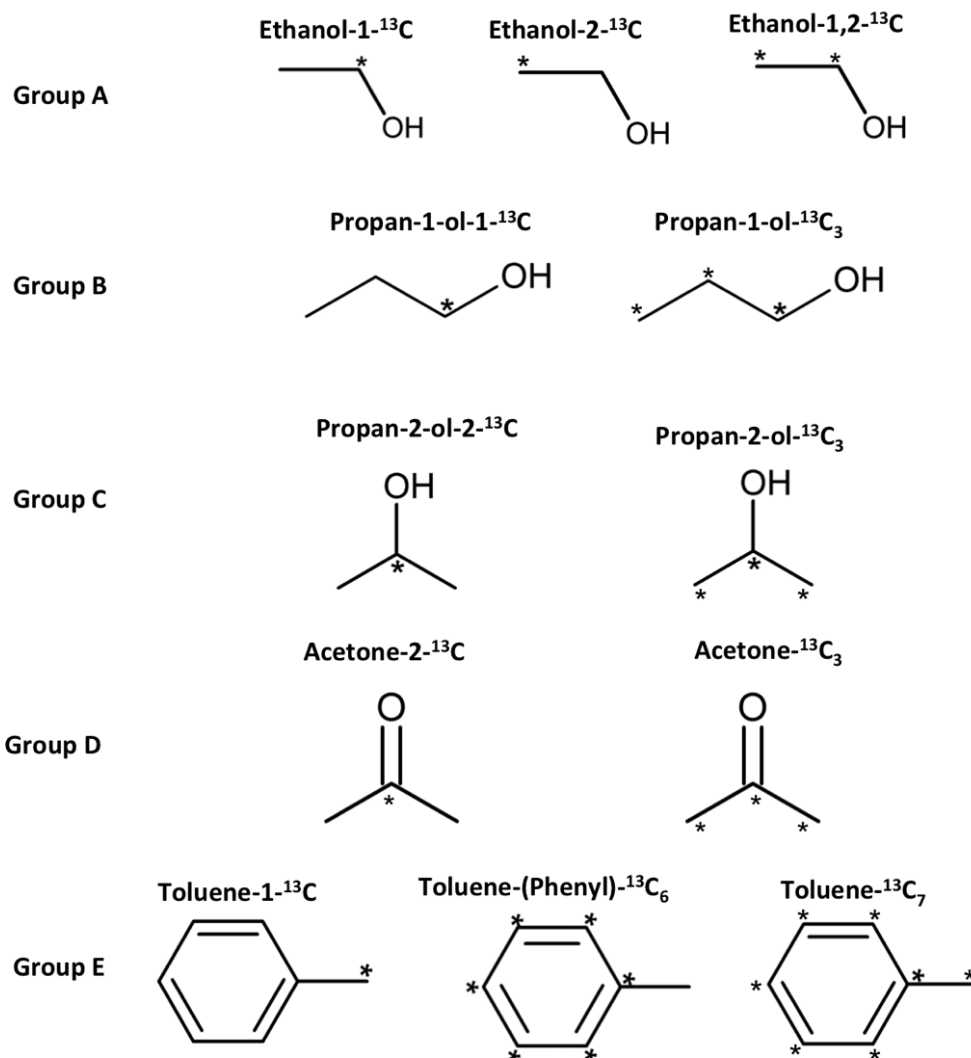


Figure 8.2: Structure and nomenclature of ¹³C labelled molecules investigated, which were blended with heptane. * = Location of ¹³C labelled atom.

For all engine experiments conducted in this chapter the low volume fuel system was utilised, with the temperature of the system being held at a constant 40 ± 2.5 °C. The engine was normally aspirated with air at atmospheric temperature and pressure. All engine tests were conducted at 1200 rpm, fuel injection pressure of 450 bar and a start-of-fuel-injection of 5 crank angle degrees (CAD) before top-dead-center (BTDC). For all tests, the injection duration was varied between 648 μ s and 770 μ s to maintain a constant engine IMEP of 4 bar. The engine exhaust gas composition was determined by continuous gas sampling approximately 180 mm downstream of the engine exhaust valves and analysed by an automotive gas analyser system (Horiba MEXA9100 HEGR) and a fast particulate spectrometer (Cambustion DMS 500).

The arrangement for collecting samples of particulate for isotopic analysis was the same as described in the previous chapter, where the exhaust was split into two

lines, in one of the lines a glass-fiber filter was placed, while in the main exhaust line a partial restriction was placed so to force sufficient flow through the other exhaust branch containing the filter, see Figure 7.3.

8.2.3 EA-IRMS analysis

Elsewhere in this thesis, for measurements of the single-component fuels, liquid samples were collected by a short length of glass capillary that was quickly sealed inside a tin capsule. The tin capsule was then submitted for analysis to the EA-IRMS by means of an autosampler carousel. A full description of the procedure of submitting the liquid samples to the EA was described in greater detail in Chapter 3. When this technique was used for the binary mixtures of fuels tested in this chapter, the technique resulted in highly variable results. This was thought to be due to the differential evaporation of the more volatile component; for example, heptane has a vapor pressure of 5.33 kPa at 20°C, and this compares to 30.6 kPa for acetone. This issue was finally resolved by a custom made modification to the EA-IRMS, which replaced the manufacturer's automatic carousel system. The isotopic measurements of the liquids measured in this chapter were carried out using an injection port that allowed the direct syringe injection of fuels into the EA, therefore greatly reducing the potential for evaporation. For further details on the design and operation of this manual injection port the reader is referred to Section 3.3.3.

The manual injection port was fitted directly above the flash combustion oven of the EA, in place of the autosampler carousel, and attached to the quartz reactor by a compression fitting. Once the injection port had been fitted to the EA, automatic leak tests were carried out and initiated from the *IsoDat* software; the instrument was then left for several hours or overnight to allow any atmospheric air contamination to be purged from the system by the helium carrier gas. Due to the time taken to switch between the autosampler and liquid injector, it was not practical to calibrate the instrument with the usual standard reference materials, which are solid samples. For this reason two 'in-house' liquid standards were made which were calibrated against the IAEA standards (discussed in Chapter 4). The two liquid standards, named standard 'A' and 'B', were determined by 10 repeat measurements to be -34.43 and -3.10 $\delta^{13}\text{C}$ ± 0.02 respectively. At the beginning and end of the batch of liquid samples to be measured, 3 of each standard 'A' and 'B' were measured. In addition, after every 10 samples measured, 2 measurements of standard 'A' were made to identify and correct for instrument drift (if applicable).

8.2.4 Analytical methods

So far in this thesis, measurements have been made of single-component hydrocarbon and oxygenate molecules. In this chapter of the thesis, measurements are presented for binary mixtures of various compounds in heptane. The move from single component fuels to binary ones requires small adjustments to the methodology, which are described

in this section. The methodology for interpreting the measured ($\delta^{13}\text{C}$) isotopic data that has been used so far has been to identify the relative conversion probability to particulate of specific carbon atom(s) in single-component fuels. Since this chapter is concerned with tracing the tracing to PM of a component molecule within a binary mixture, or tracing atoms from a specific locality within a molecule that is itself a component in a mixture, a small adaptation of the calculations that were introduced in Chapter 4 was made.

For the binary mixture, the enrichment process and measurements that are required to determine the percentage conversion of a molecule or carbon atom to particulate are the same as for the single-component fuels. Four $\delta^{13}\text{C}$ measurements were required, firstly the unenriched (native) and the corresponding enriched fuel ($\delta^{13}\text{C}_F$), and for the particulate matter derived from both of the unenriched and enriched fuels ($\delta^{13}\text{C}_{PM}$). For each fuel and derived PM, the difference in isotopic composition between the unenriched and the enriched versions called Δ_F and Δ_{PM} were (in the same way as set out before) calculated as follows:

$$\Delta_{(F)} = \delta^{13}\text{C}_F^* - \delta^{13}\text{C}_F^n \quad (8.1)$$

$$\Delta_{(PM)} = \delta^{13}\text{C}_{PM}^* - \delta^{13}\text{C}_{PM}^n \quad (8.2)$$

where the (*) refers to the enriched fuel or the PM derived from it, and the (n) refers to the unenriched (native) fuel or PM derived from it.

Δ_{max} is a parameter which was defined previously for single-component fuels as:

$$\Delta_{max} = \frac{\Delta_F}{n_{labelled}} \times n_{total} \quad (8.3)$$

where $n_{labelled}$ represents the number of carbon atoms which were labelled and n_{total} represents the total number of carbon atoms within the single-component chemical compound used as fuel. For single-component fuels the parameter Δ_{max} represents the maximum enrichment that would be reached if the added labelled compound to make the enriched mixture had (instead of $n_{labelled}$ ^{13}C atoms) all of its carbon atoms labelled with ^{13}C .

For multi-component fuels Δ_{max} is calculated in a similar way, as follows

$$\Delta_{max} = \frac{\Delta_F}{R_f \cdot n_{labelled}} \cdot \sum_{f=1}^t (R_f \cdot n_{f_{total}}) \quad (8.4)$$

where, again, $n_{labelled}$ represents the number of carbon atoms which were labelled, R_f is the molar ratio of a given component f , and t is the total number of components in the multicomponent mixture, and $n_{f_{total}}$ is the total number of carbon atoms in component f .

The final step to calculate the fraction of the PM which was derived from labelled carbon atoms ($F_{labelled}$) is the same as defined for single-component fuels, as follows

$$F_{(labelled)} = \frac{\Delta_{PM}}{\Delta_{max}} \quad (8.5)$$

The product $F_{labelled} \times 100$ gives the % contribution overall of the labelled C atom(s) to PM, taking into account all of the carbon atoms in the added compound and that of the heptane. The fraction contribution to PM of the carbon atoms that were not ^{13}C labelled could be calculated as simply $1 - F_{labelled}$.

8.3 Results

8.3.1 Emissions analysis

Before considering the results of the EA-IRMS analysis, some results are presented in this section which show an analysis of the exhaust gas stream of the diesel engine.

Figure 8.3 shows the total mass concentration of particles in the diesel engine exhaust. It is apparent that the reference diesel fuel produced a much larger total mass of particulates, whereas the heptane binary blends all produced considerably less. Considering the range of experimental error bars applicable to the measurements in Figure 8.3, it is not possible to draw firm conclusions as to the influence of the added hydrocarbon and oxygenated molecules on total particulate mass emissions.

Figure 8.4 shows the particle size distributions (PSD) of particles in the diesel engine exhaust. The PSD results are shown separately for ethanol and toluene in Figure 8.4(a), due to the fact that the remaining molecules, shown in Figure 8.4(b), were tested several months apart. Normalizing the spectra obtained over several months, for example using the reference diesel fuel was not considered appropriate. Nevertheless, the spectra shown in Figure 8.4 show PSD which are not dissimilar for the various binary mixtures tested, considering that the particles below about 40 nm in size are generally of disputable composition of either unburned fuel or oil vapor, or nascent particles.

The gaseous engine emissions, including CO, CO₂, O₂, total hydrocarbon content (THC), and NO_x are supplied in Appendix B.

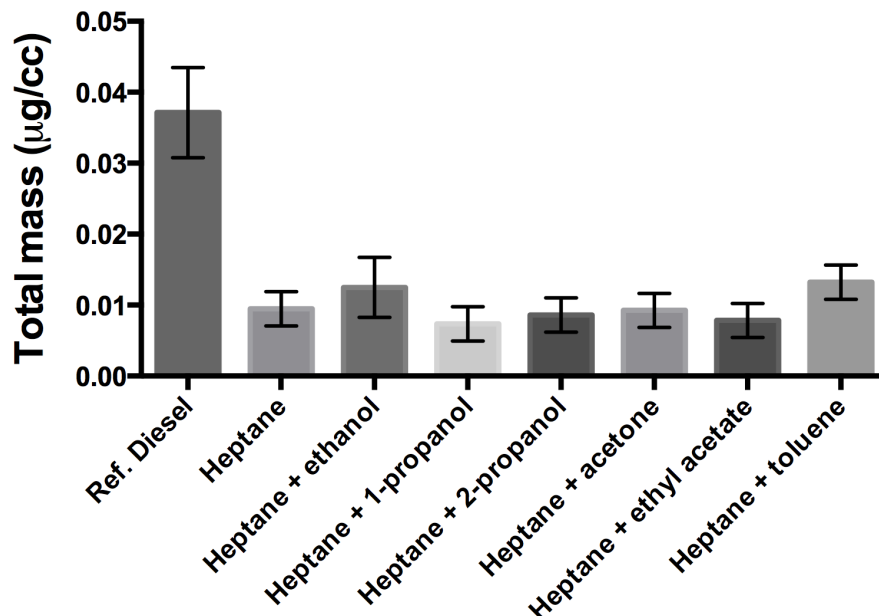


Figure 8.3: Total particulate mass emissions in the exhaust of the compression ignition engine, from heptane blended with ethanol, 1-propanol, 2-propanol, acetone, ethyl acetate, or toluene. Measurements were made by a Cambustion DMS500. Data shown is the average measurement of repeat tests, and the error bars indicate the standard deviation of 6 measurements.

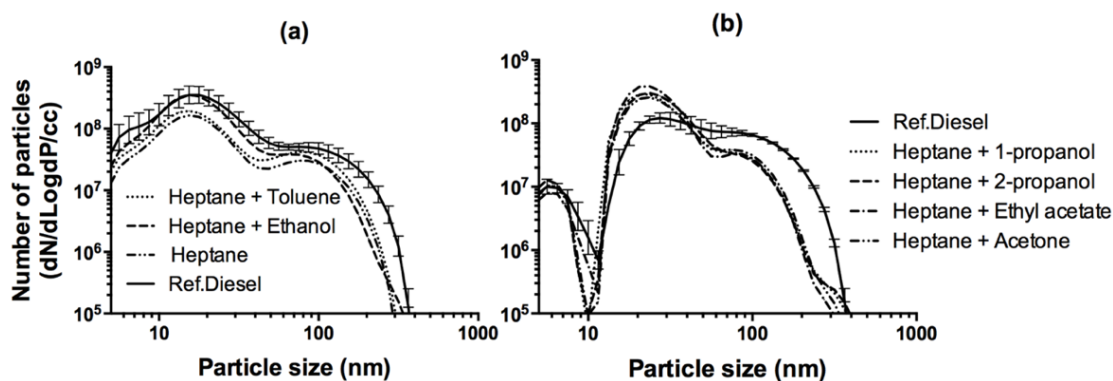


Figure 8.4: Particulate size distributions in the exhaust of the compression ignition engine, fuelled with (a) heptane blended with ethanol, or toluene, and (b) shows blends of heptane and either 1-propanol, 2-propanol, acetone, or ethyl acetate. Measurements were made by a Cambustion DMS500. Data shown is the average measurement of repeat tests, and the error bars indicate the standard deviation of 6 measurements.

8.3.2 Ethanol-in-heptane

This section deals with the formation of particulate from the ethanol-in-heptane mixtures which were tested in a flow reactor and diesel engine. Figure 8.5 shows the results of the isotope tracer study conducted in the flow reactor. Three results bars are shown, the first bar labelled ethanol-1,2- ^{13}C (ab) shows the combined contribution to PM of both ethanol carbon atoms in the binary mixture. It can be seen from Figure 8.5 that the two carbon atoms in ethanol overall contributed 2.4% of all the carbon in the particulate matter (that is, the carbon from both the ethanol and heptane). It was known that the total ethanol carbon content in the fuel was 3.08% (Table 8.1), which means that the ethanol molecule converted to PM at a lower rate than that for the heptane component. It is interesting to note that despite the presence of the oxygen-containing hydroxyl functional group in the ethanol molecule, the ethanol component overall contributes to PM at a rate of around 75%, relative to its composition in the fuel (2.4/3.08). Considering now each of the two ethanol carbon atoms separately, the hydroxyl carbon (shown by bar 'a' in Figure 8.5) is significantly less likely to convert to PM in comparison to the methyl carbon (b). The *hydroxyl* carbon atom (a) was found to constitute 0.89% of the carbon in the PM, and it is indicated in Figure 8.5 by the dotted line that the hydroxyl carbon atom (a) composed 1.54% of the carbon in the fuel. Therefore, the rate of the *hydroxyl* carbon atom in the PM was only 58% of that in

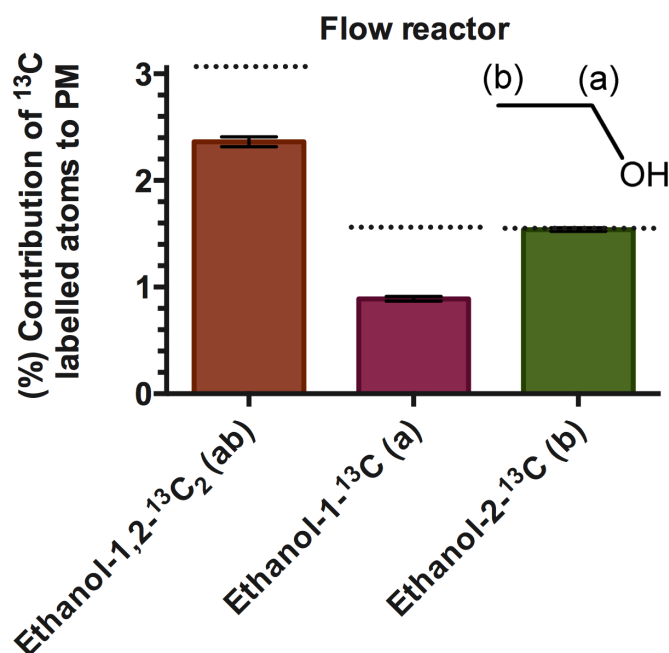


Figure 8.5: The percentage composition of the PM that was derived from the labelled carbon atoms in ethanol-1- ^{13}C , ethanol-2- ^{13}C , ethanol-1,2- $^{13}\text{C}_2$ blended into heptane, and formed under pyrolysis conditions in the laminar flow tube reactor. Data shown is the average of 3 measurements, \pm SD. The dotted line indicates the mass percentage of the carbon at the labelled position in the fuel.

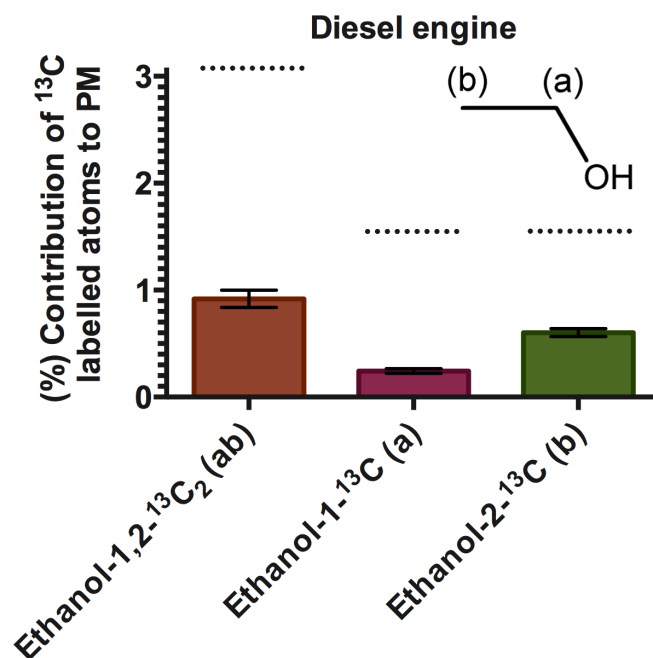


Figure 8.6: The percentage composition of the PM that was derived from the labelled carbon atoms in ethanol-1-¹³C, ethanol-2-¹³C, ethanol-1,2-¹³C₂ blended into heptane, to the PM and formed in a diesel engine. Data shown is the average of 3 measurements, ± SD. The dotted line indicates the mass percentage of the carbon at the labelled position in the fuel.

the fuel (0.89/1.54). An interesting result is that of the methyl carbon atom (b), which shows that it constitutes 1.54% of the PM, which is the same percentage mass of carbon that present at in the fuel. This means that the *methyl* carbon atom in ethanol was as likely to convert to PM as the average carbon in the heptane component. This is a significant result as it indicates that under these conditions, the presence of oxygen in the ethanol molecule only influences the hydroxyl carbon atom to which it is attached, and it does not appear to affect the carbon atom to which it is not directly attached. It appears that the methyl carbon (b) becomes available in the pool of soot precursors. The result that the hydroxyl carbon atom (a) converts to PM at a rate that is around 56% of the level in the fuel agrees roughly with the result obtained previously for ethanol as a single-component fuel, where the hydroxyl carbon (a) occurred in the PM at a rate that was 54% of the level in the fuel (Chapter 6).

Turning now to the results from the diesel engine, these are shown in Figure 8.6. It is shown that despite the two carbon atoms in the ethanol together making up 3.08% of the carbon in the fuel, the carbon in the PM that came from the ethanol (a+b) was found to only constitute 0.91% of the carbon in the particulate matter collected, that is a relative conversion rate of only 30% (PM/fuel, 0.91/3.08) (compared to 75% in the reactor). The hydroxyl carbon (a) was found to contribute 0.24% of the PM, corresponding to a conversion rate of 16%, whilst the methyl carbon (b) contributed

0.60% corresponding to a conversion rate of 39%. Considering now the relative rates at which the hydroxyl and methyl carbon atoms contributed to PM, in the engine the relative rates were 0.4:1 for the hydroxyl carbon: methyl carbon; and in the case of the reactor, the rate was 0.58:1. Therefore, in the engine the relative contribution of the hydroxyl carbon atom to PM was a little lower (0.4:1) compared to that in the reactor (0.58:1).

It is pleasing to note from Figure 8.5 that the accuracy of the method in terms of the error associated with the measurements in both the reactor and the engine appears to be relatively small (see error bars in Figure 8.5). Furthermore, the result of the experiments is the same regardless of how the labelling is carried out, that is whether the carbon atoms are labelled in turn or if both of the carbon atoms are labelled together. For example, in the results from the reactor (Figure 8.5) show that the methyl carbon (in ethanol-2-¹³C) contributed 1.53% of the carbon in the PM, while the hydroxyl carbon (ethanol-1-¹³C) contributed 0.87%, which makes the sum of the two atoms as 2.4%. In the version of the experiment where both carbon atoms were labelled simultaneously (ethanol-1,2-¹³C), it was found that the total contribution to PM was 2.36%, which considering experimental errors, is in excellent agreement with the sum of the results for the two atoms obtained from two individual experiments. There is also agreement in the results from the diesel engine (Figure 8.6) where with both atoms labelled simultaneously the contribution to PM of the labelled ethanol carbon atoms was 0.91%, while the sum of the individual carbon atom contributions to PM was 0.24% + 0.60% = 0.82%. This is further evidence for the effectiveness of the isotope tracer technique used in this work.

In the literature, comparable work was carried out by Buchholz et al. (2002), where ¹⁴C was used to trace the overall contribution of the ethanol component of ethanol-in-diesel blends to particulate matter emissions from a medium-duty direct-injection compression-ignition engine. Various amounts of ethanol were blended into fossil diesel fuel, at levels from 9% to 37% volume, with cosolvent or emulsifier added to ensure a stable mixture between the normally immiscible ethanol and diesel fuels. It was found for all tests that the carbon from the ethanol component was present to a lesser degree in the PM compared to the diesel fuel. For example, in the blend of 9% (v/v) ethanol-in-diesel, carbon from the ethanol was found to comprise 2.4 % of the overall PM, whereas it accounted for 5.7% of the carbon mass in the fuel; that is, the mass fraction of carbon derived from ethanol in the PM was 42% of the carbon mass fraction that ethanol accounted for in the fuel. By comparison, the work reported in this thesis reports a mass fraction for the PM derived from the ethanol that is only 30% of it's mass fraction in the fuel. In a 18% (v/v) ethanol-in-diesel blend, where ethanol contained 11.4% of the carbon, 2.9% of the carbon in the PM was derived from the ethanol; the PM contained a mass fraction derived from ethanol that was only 25% of the mass fraction it accounted for in the fuel. There were also differences between cosolvent and emulsified blends; indicating that the distribution of oxygen in the fuel - not jut its content- can influence PM formation. Importantly, the overall conversion rate of carbon from the

ethanol component of the fuel to PM varies depending level of ethanol in the fuel and on the surrounding fuel blends. For example, the conversion rate from fuel carbon to PM carbon of the 9% (v/v) mixture of ethanol-in-diesel was 42% (2.4/5.7), whereas the in the 18% (v/v) ethanol-in-diesel mixture was 25% (2.9/11.40). In this work an ethanol-in-heptane binary mixture was combusted in the diesel engine, and the ethanol component was found to convert at a relative rate of 30% (0.91/3.08). It should be noted from Figure 8.3 that the overall PM mass emissions are much lower for heptane than for diesel.

In this work and that by Buchholz et al., it is apparent that despite the oxygen content of the ethanol, its carbon atoms still appear to contribute a significant amount of particulate matter, albeit at a lesser rate than the surrounding non-oxygenated heptane or diesel fuel. As it was pointed out in Chapter 5, the apparent potential of ethanol, and indeed larger alcohols, to form PM is likely to be a result of the formation of unsaturated C₂ and C₃ fragments during combustion as a result of dehydration reactions.

8.3.3 1- or 2-propanol-in-heptane

The molecular structure of 1- and 2-propanol can be seen in Figure 8.7, and letters have been assigned to the various carbon atoms in the two propanol isomers to aid the description. Both 1- and 2-propanol-in-heptane blends were tested to identify the conversions of the labelled carbon atoms to PM, in the laminar flow reactor and diesel engine. Figure 8.8 shows the result of the tracer study carried out in the reactor. The first thing that is noticeable is that the overall conversion of both of the propanol isomers is suppressed with respect to the heptane component; that is, while the carbon in the fuel from the propanol component was 4.55%, the contribution from the whole molecules of 1- and 2-propanol to the PM was 3.47 and 3.79% respectively (Figure 8.8). From Figure 8.8 it is apparent that the hydroxylated carbon atom is less likely to form PM than the other two carbon atoms in both of the 1- and 2-propanol isomers. For example, in the primary alcohol 1-propanol, the hydroxyl carbon (c) contributed 0.65% of the PM; meaning that the hydroxyl carbon in 1-propanol converted to PM at a rate of only 42% (i.e. 0.65/1.52). In the equivalent secondary alcohol, 2-propanol, the hydroxyl carbon atom (e) was found to contribute 1% of the carbon of the particulate matter, equivalent to 66% of its mass fraction in the fuel (1/1.54). It should be noted that a similar result was obtained for the pyrolysis of 1- and 2-propanol as single-component fuels in Chapter 6, where the carbon atom directly bonded to oxygen in the 2-propanol converted to PM at a higher rate than the equivalent carbon atom in 1-propanol (this is discussed further below, in Section 8.4).

The PM formed from the propanol-heptane blends in the compression ignition engine, Figure 8.9, shows that carbon atoms in both 1- and 2-propanol form PM; overall only about 1% of the carbon in the PM was derived from both of the propanol isomers. In the engine, any difference between the conversion rate of the hydroxyl carbon atom from the two propanol isomers was not discernible due to the experimental errors applicable,

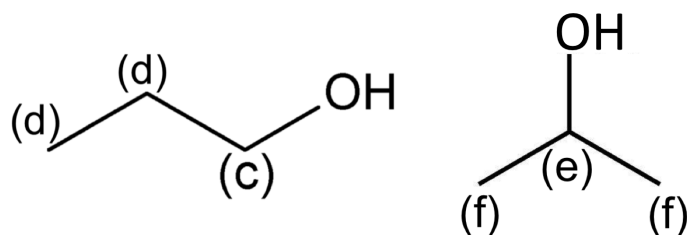


Figure 8.7: Locations of ^{13}C label in 1-propanol-1- ^{13}C 'c', 1-propanol- $^{13}\text{C}_3$ 'cdd', 1-propanol-1,3- ^{13}C 'dd', 2-propanol-2- ^{13}C 'e', 2-propanol- $^{13}\text{C}_3$ 'eff', and 2-propanol-1,3- $^{13}\text{C}_2$ 'ff'.

but the error does suggests if there is a difference it is only very small, and certainly a much smaller difference in conversion rates than that observed for the PM generated in the reactor.

Returning briefly to Figure 8.8 and 8.9, it can be seen that in both the reactor and the compression ignition engine the hydroxyl carbon atom contributes less than the methyl carbon atoms, in the case of both 1- and 2-propanol isomers. A similar result was obtained for ethanol in the previous section of this chapter. Clearly the presence of the C-O bond reduces the conversion rate of the hydroxyl carbon atom to PM, irrespective of the type of combustion system or type of alcohol.

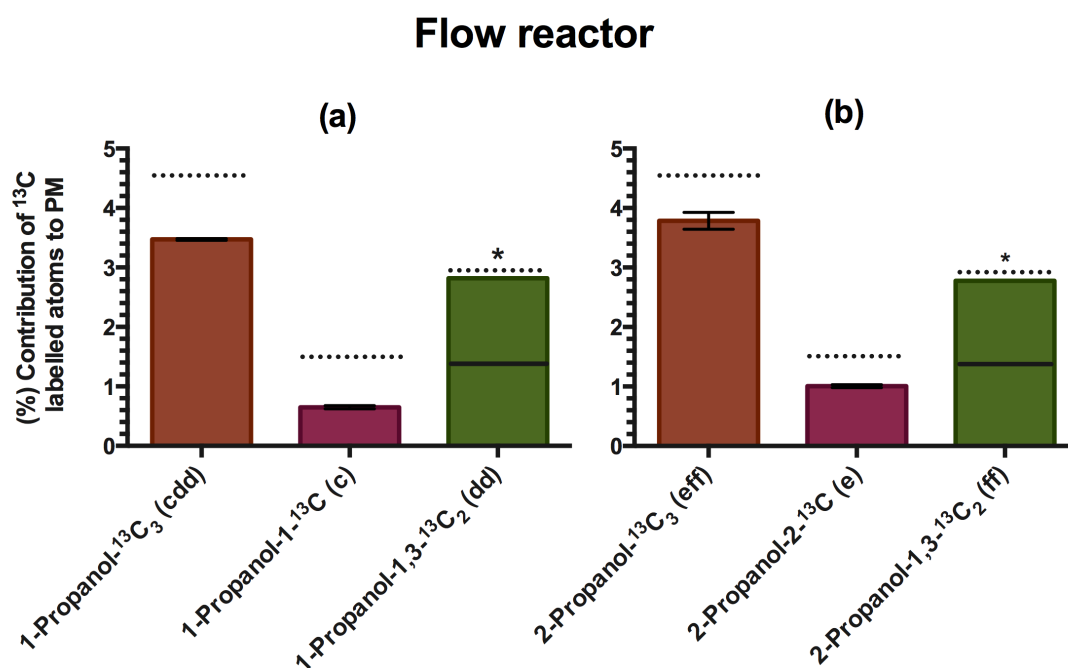


Figure 8.8: The percentage composition of the PM that was derived from the labelled carbon atoms in (a) 1-propanol-1- ^{13}C ‘c’, 1-propanol- $^{13}\text{C}_3$ ‘cdd’, 1-propanol-1,3- $^{13}\text{C}^*$ ‘dd’, and (b) 2-propanol-2- ^{13}C ‘e’, 2-propanol- $^{13}\text{C}_3$ ‘eff’, or 2-propanol-1,3- $^{13}\text{C}_2^*$ ‘ff’ blended into heptane, and formed in a tube reactor. Data shows the average 3 measurements, \pm SD. The dotted line indicates the mass percentage of the carbon at the labelled position in the fuel. * indicates that the value was calculated by subtraction, and not measured individually.

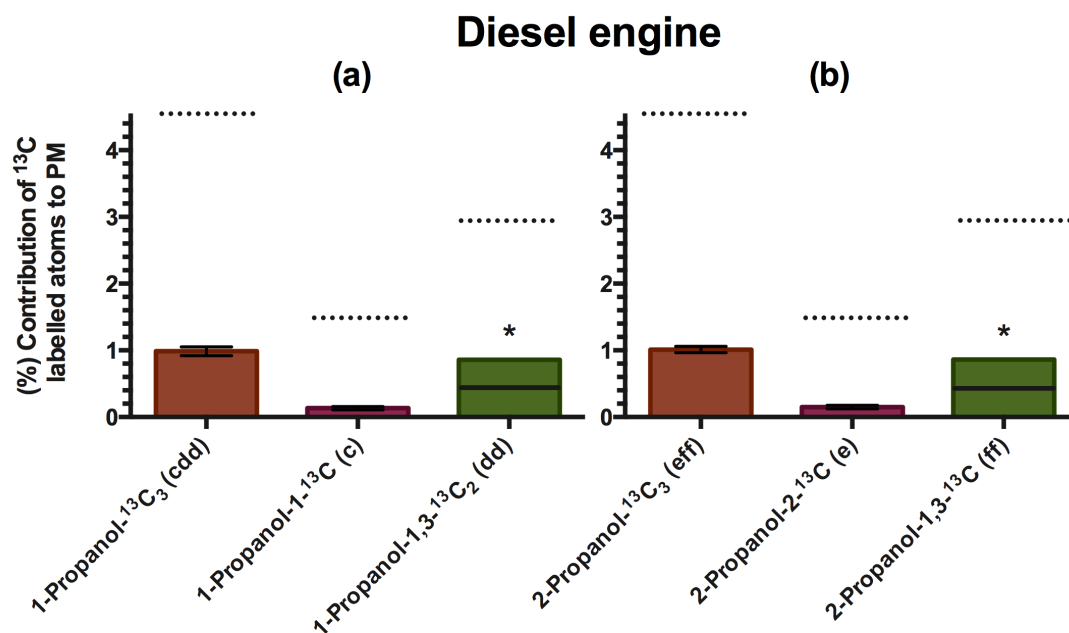


Figure 8.9: The percentage composition of the PM that was derived from the labelled carbon atoms in (a) 1-propanol-1- ^{13}C 'c', 1-propanol- $^{13}\text{C}_3$ 'cdd', 1-propanol-1,3- $^{13}\text{C}^*$ 'dd', and (b) 2-propanol-2- ^{13}C 'e', 2-propanol- $^{13}\text{C}_3$ 'eff', or 2-propanol-1,3- $^{13}\text{C}^*$ 'ff' blended into heptane, and formed in a compression-ignition engine. Data shows the average of 3 measurements, \pm SD. The dotted line indicates the mass percentage of the carbon at the labelled position in the fuel. * indicates that the value calculated by subtraction, and not measured individually.

8.3.4 Acetone-in-heptane

So far in this thesis a number of oxygenated molecules have been considered including various alcohols and esters. In this section the pyrolysis and combustion of another oxygenate, acetone, which contains a ketone moiety has been investigated. The results for the pyrolysis of acetone-in-heptane blends in the flow reactor is shown in Figure 8.10. Overall, the acetone component of the fuel accounted for 4.55% of the carbon, in the resulting particulate from that fuel only $\sim 3\%$ of the carbon was derived from acetone (labelled in acetone- $^{13}\text{C}_3$ (ghh)). Relative to the acetone in the fuel (4.55%) this corresponds to a rate in the PM of 66%, for the whole acetone molecule. It is apparent that the *carbonyl* carbon atom (g) does not convert to particulate matter. Despite the negligible contribution from the carbonyl atom (C=O), there was a significant contribution to PM from the remaining two carbon atoms (hh) in the acetone molecule. The two *methyl* carbon atoms in acetone (hh) comprised 3.08% of the carbon in the fuel, and it was calculated that the PM derived from these carbon atoms contained about the same level (3.07%); this indicates that the two methyl carbon atoms in acetone convert to particulate at about the same rate as the average carbon atom in heptane. For the reactor-generated PM, the presence of oxygen in the form of a *carbonyl* group influences the carbonyl carbon atom, but does not appear to have any affect on the likelihood of the *methyl* carbon atoms (hh) becoming available for soot formation. However, as mentioned before, the presence of the double bonded oxygen atom eliminates the possibility of the carbon which it is directly bonded to (g) becoming PM.

The results of the diesel engine tests are shown in Figure 8.11. The conversion of the acetone component of the binary fuel mixture was found to be about 1% of the overall PM. This corresponds to a conversion rate to PM for the whole acetone molecule of 22% (1/4.55). Similarly to what was seen for the PM generated in the reactor, the *carbonyl* carbon (g) did not contribute to the PM; whilst the *methyl* carbon atoms (hh) accounted for the 1% of PM derived from the acetone component. It is suggested that the oxygen stays attached to the neighboring carbon atom, forming CO, at which point it is not available for participation in reactions that result in PM formation.

Comparing the diesel engine result for acetone to that for the previous section where two propanol isomers were examined, it is seen that both of the propanol isomers as well as the acetone contributed approximately 1% of the PM formed from the diesel engine. Although it is difficult to isolate the influence of the physical effects of the fuels, this result suggests that under the conditions tested here, fuel boiling point and volatility do not significantly influence the formation of PM from the blends of acetone and propanol; acetone has a boiling point of 56 °C, and 1-propanol boils at 137 °C. It has been reported in the literature that more volatile multicomponent fuels have a tendency to form soot more readily, due to the fact that the more volatile components vaporise earlier on in the droplets lifetime, leaving the less volatile components which vaporise more slowly (Sirignano, 1983); the vaporised fuel therefore forms a less well-mixed fuel-rich primary zone, where soot formation may take place (Haynes and Wagner,

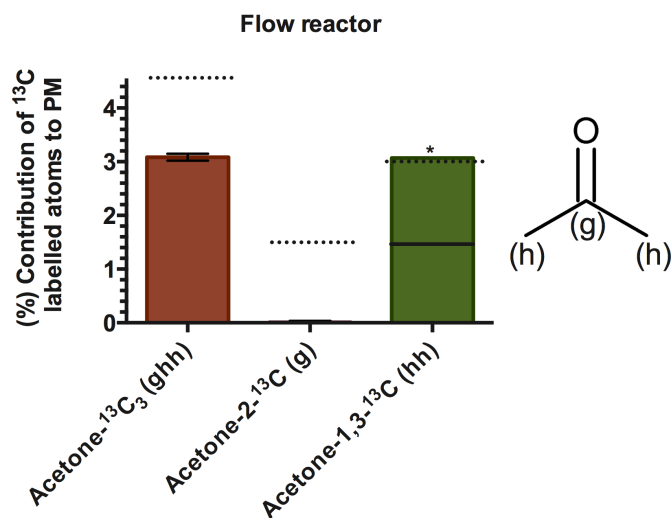


Figure 8.10: The percentage composition of the PM that was derived from the labelled carbon atoms in acetone-2- ^{13}C 'g', acetone- $^{13}\text{C}_3$ 'ghh' blended into heptane, and formed under pyrolysis conditions in the tube reactor. Data shown is the average of 3 measurements, \pm SD. The dotted line indicates the mass percentage of the carbon at the labelled position in the fuel. * indicates a value calculated by subtraction, and not measured individually.

1981).

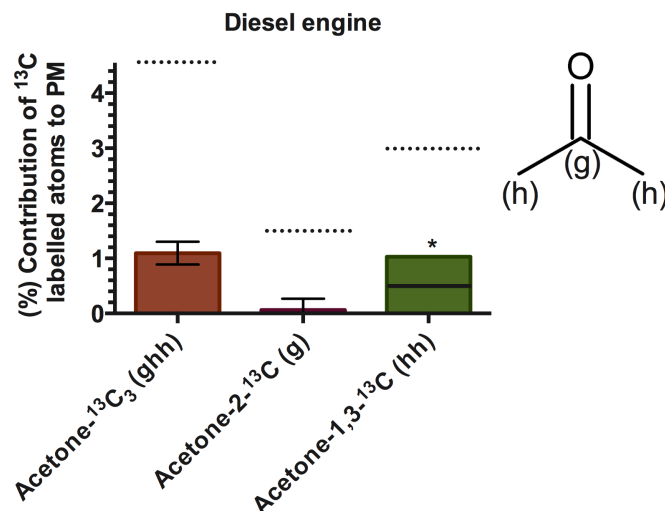


Figure 8.11: The percentage composition of the PM that was derived from the labelled carbon atoms in acetone-2-¹³C, acetone-¹³C₃ blended into heptane, and formed in a diesel engine. Data shown is the average of 3 measurements, ± SD. An estimate of the contribution of ‘hh’ is shown calculated by subtraction. The dotted line indicates the mass percentage of the carbon at the labelled position in the fuel. * indicates a value calculated by subtraction, and not measured individually.

8.3.5 Ethyl acetate-in-heptane

It was initially planned that tests would be carried out for ethyl-acetate-1-¹³C (with the ester carbon atom ¹³C labelled) and ethyl acetate-¹³C₄ (with all carbon atoms labelled), however, on the day of testing it was found that a 200 mg quantity of labelled ethyl acetate-¹³C₄ had evaporated in storage. Due to the supply long lead-times on this compound from the commercial suppliers, it was not feasible to include this compound in the test runs. However, ethyl acetate-1-¹³C was blended to 10 mole percent in heptane and was tested and in both the flow reactor and diesel engine. It was found that the ester carbon in ethyl acetate did not convert to PM in either system. Data for the ethyl acetate-1-¹³C is not shown here, however it is available in Appendix B. The result was in alignment with previous findings for single-component fuels presented in Chapter 6, which showed that the ester carbon atom in ethyl acetate did not contribute to PM under pyrolysis conditions, and in Chapter 7 where the ester carbon of methyl oleate was also not found in the PM formed in the reactor or the NVOF fraction of PM in the diesel engine.

8.3.6 Toluene-in-heptane

Figure 8.12 shows the result of the tracer study of the toluene-in-heptane blends carried out in the flow reactor. The toluene component (entire molecule labelled, toluene-¹³C₇ (jk)) comprised 10% of the carbon in the fuel, and it can be seen that carbon atoms derived from the toluene comprised 12.5% of the PM; this means that the toluene component is about 25% more likely to become PM than the heptane. The result that

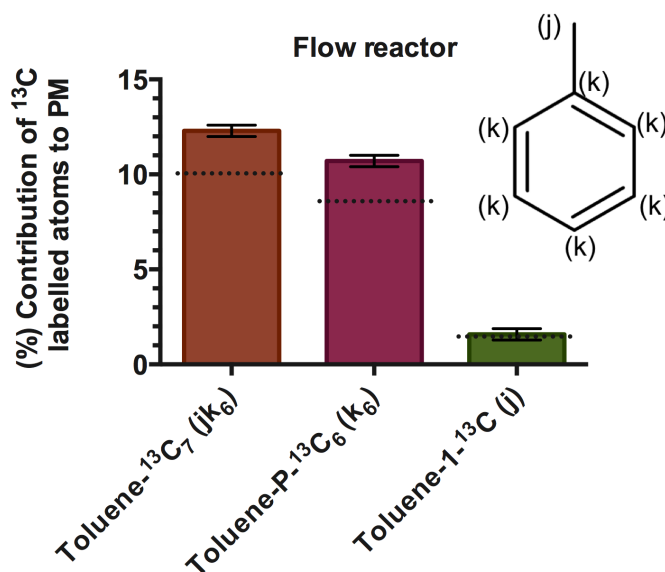


Figure 8.12: The percentage composition of the PM that was derived from the labelled carbon atoms in toluene-¹³C₇, toluene-1-¹³C, and toluene-phenyl-¹³C₆ blended into heptane, and formed in a laminar flow reactor. Data shown is the average of 3 measurements ± SD. The dotted line indicates the mass percentage of the carbon at the labelled position in the fuel.

toluene had a higher propensity to form PM was expected, as the higher sooting tendency of the toluene relative to heptane has been reported previously (Ladommatos et al., 1996). In Figure 8.12 it appears that the methyl carbon in toluene (j) contributes to PM formation at a slightly lesser rate than the phenyl ring (k), but at about the same rate compared to the average heptane atom, and at about the same rate as it was present in the fuel, indicated in Figure 8.12 by a dotted line above the bar of the methyl carbon. This result suggests that during pyrolysis demethylation of toluene occurs at least to some extent, otherwise exactly the same rate contribution to the PM would be expected for the methyl and phenyl ring. Therefore, the *methyl* carbon (j) of toluene converts to PM at about the same rate as the alkane chain of heptane, but at a reduced rate compared to the phenyl ring (k). It is tentatively suggested that the heptane and the methyl carbon atoms contribute to soot by a similar mechanism involving C₁, C₂, and C₃ carbon fragments. The phenyl ring, however, may polymerise directly to PAHs retaining its aromatic structure; indeed the literature shows that a range of C₂, C₃, as well as aromatic and polycyclic aromatic molecules are produced during shock tube pyrolysis of toluene (Colket and Seery, 1994; Haynes and Wagner, 1981). The overall result for the pyrolysis of toluene in the reactor is that the toluene component contributed more than the heptane component to soot formation; and this is in alignment with the literature, which shows that under well-controlled conditions increasing the toluene percentage in a binary mixtures of toluene-heptane results in an increased soot yield over a wide range of temperature conditions (Alexiou and Williams, 1995).

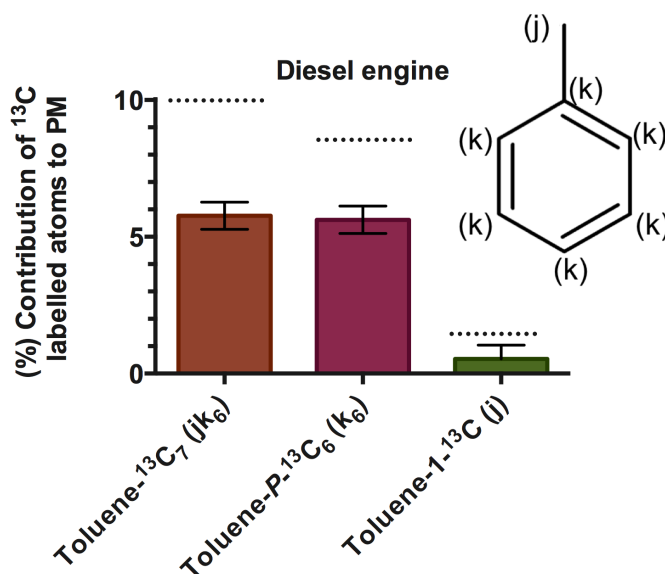


Figure 8.13: The percentage composition of the PM that was derived from the labelled carbon atoms in toluene- $^{13}\text{C}_7$, toluene-1- ^{13}C , and toluene-phenyl- $^{13}\text{C}_6$ blended into heptane, and formed in a diesel engine. Data shown is the average of 3 measurements, \pm SD. The dotted line indicates the mass percentage of the carbon at the labelled position in the fuel.

In Figure 8.13 it is seen that toluene (labelled in toluene- $^{13}\text{C}_3$ (jk)) overall forms 5.78% of the soot from the diesel engine, whereas toluene accounted for 10% of the carbon in the fuel. This result implies that in the diesel engine contributes less than heptane. Whilst it appears that toluene contributes to PM at a lower rate than heptane, which would be a surprising result, a note of caution should be added due to the inevitable contribution of the engine oil to the PM mass; this is applicable to all of the engine results and is discussed below in Section 8.4. The significant finding from the engine results is that Figure 8.13 shows that the phenyl ring (k) in toluene has an increased propensity to form PM with respect the methyl carbon atom (j). The aromatic ring contributes 5.62% of the PM, meaning that each of the six carbon atoms in the ring contributes 0.94%. The methyl group, however, contributed 0.54% of the carbon in the PM.

The above results showed that in both the reactor and in the diesel engine the methyl carbon (j) tended to contribute to PM formation at a lower rate than the phenyl ring (k). Research conducted by Lea-Langton et al. (2013) involved a ^{13}C tracer study of the pyrolysis of 9-methylphenanthrene, shown in Figure 8.14, and labelled at the methyl carbon atom. Pyrolysis of methylphenanthrene at 800°C in a flow reactor produced phenanthrene as the main pyrolysis product, indicating that dealkylation was indeed a major pyrolytic reaction. In the earlier investigation that was presented in Chapter 6, toluene was studied as a single-component fuel and it was found that there appeared to be no discernible difference in the conversion rate to PM of the methyl carbon compared to the phenyl ring. The difference in the two results is likely to be due to differences

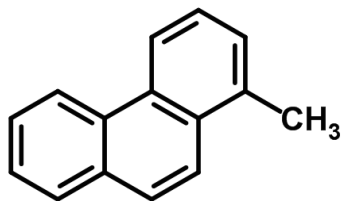


Figure 8.14: The molecular structure of methylphenanthrene.

in the intermediate pool of species which convert to PM at different rates depending whether they are aromatic or small carbon chains. Overall, however, it is clear that the fate of carbon in either the methyl group or the phenyl ring in toluene is influenced by differences in the overall fuel composition, and conversion rates may differ in multicomponent mixtures compared with those in single component fuels.

It should be noted that a previous study of toluene-in-heptane blends from 10 to 50% toluene, using the same compression ignition engine, it was found that an increasing toluene content tended to reduce the number concentration of nucleation mode particles, and had no clear influence on the total particulate mass (Hellier et al., 2013c). It was put forward that this could have been due to the reduction in the overall fuel-to-air ratio (ϕ) in the cylinder with increasing toluene content. Whilst this could explain the global sooting tendency, it does not explain why heptane should preferentially form PM.

8.4 Further discussion

In this chapter, concerning the particulate matter that was generated in the diesel engine, the engine lubricant oil inevitably would have contributed at least a small amount to the particulate emissions. For example, Hilden and Mayer (1984) found that the lubricant oil contributed between 7 to 14% of the particulate emissions formed from a number of diesel engines. More recently, Buchholz et al. (2003) identified that engine oil accounted for 4% of the PM formed in a medium-duty direct-injection diesel engine fuelled with a biodiesel fuel. The influence of the engine oil on the isotopic measurement of the particulate sample is as follows:

$$\delta^{13}C_{sample} = (\delta^{13}C_{fuel} \times x_{fuel}) + (\delta^{13}C_{oil} \times x_{oil}) \quad (8.6)$$

where the isotopic composition of the sample ($\delta^{13}C_{sample}$) is influenced by the mass fraction (x) of the PM derived from the fuel and oil components of the PM, and the isotopic composition ($\delta^{13}C$) of the fuel and oil.

In this work, the isotopic composition of the lubrication oil taken from the engine sump, which had been used for several months, was measured and found to be $-28.08 \delta^{13}C \pm 0.1$. Isotopic measurement of the fresh engine oil was carried out and found to be $-27.73 \delta^{13}C \pm 0.1$; indicating that there was not a substantial influence on the age of the oil on the isotopic composition. The small difference in the isotopic composition of

the fresh compared to the used oil in the engine sump is probably due to the presence of particulate in the oil. It is known from the isotopic measurements of the PM formed from the unenriched heptane binary mixtures that the soot in all cases was ~ -28 to -30 $\delta^{13}\text{C}$, (the actual measured values for each fuel is presented in Appendix B). Due to the similarity of the isotopic compositions of the heptane component of the fuel and the engine oil, this means that the percentage of the PM that was calculated to be derived from the labelled atoms is still a reliable measure of the overall their percentage composition of the overall PM. However, the carbon mass fraction of the oil in the PM was unknown, which means that it is not possible to speculate about the conversion of the labelled compound relative to the heptane carbon atoms. Notwithstanding the undefined contributions of the engine oil and heptane component, the most significant result that has been presented for the engine experiments was that the conversion rate to PM is different for different atoms within the labelled molecule. For example, the *carbonyl* carbon atom in acetone does not convert to PM during combustion, but the equivalent *hydroxyl* carbon atoms in both of the propanol isomers do contribute significantly to PM formation.

In order to show the comparative tendency of the carbon atoms that are directly bound to the *hydroxyl* and *carbonyl* groups, the mass fraction of carbon contributed by the tagged carbon atoms in the fuel was compared to the mass fraction of the tagged carbon atoms in the PM. For example, in the case of the ethanol-heptane binary mixture, the *hydroxyl* carbon atom accounted for 1.54% of the carbon in the fuel, the resulting PM formed in the reactor consisted of 0.89% derived from the hydroxyl carbon atom, the relative conversion rate was therefore 0.58 (0.89/1.54).

Figure 8.15 shows the relative conversion rate to PM of the carbon atom directly bonded to the oxygen for all of the oxygenated molecules as tested in the flow reactor. Firstly, it is seen that the *carbonyl* carbon atoms in acetone and ethyl acetate do not convert to PM. However, significant amounts of the oxygenated carbon atom in the alcohols (ethanol, 1-propanol and 2-propanol) were converted to the PM. For example, the *hydroxyl* carbon atom in ethanol had relative conversion rate 0.57, this compares to a rate of 0.41 and 0.64 for 1- and 2-propanol respectively. The conversion rates of the propanol isomers broadly in agreement with that observed in Chapter 6, where 1-propanol tested as a single-component was shown to convert at a relative rate of 0.49, while for 2-propanol it was 0.67. In Chapter 6 the conversion rate for ethanol tested as a single component fuel was 0.54, and here for the ethanol-in-heptane mixture the *hydroxyl* carbon formed PM at a similar rate of 0.57.

Figure 8.16 shows the relative conversion rate to PM of the oxygen bound carbon atom in the oxygenated molecules, formed in the diesel engine. Similarly to the result of the flow reactor, the *carbonyl* carbon atoms in acetone and ethyl acetate are not found in the PM formed in the diesel engine. The conversion rate of the *hydroxyl* carbon atom in the pair of propanol isomers was shown to be 0.08 and 0.1 for 1- and 2-propanol respectively. The experimental errors, indicated by the error bars in Figure 8.16, meant

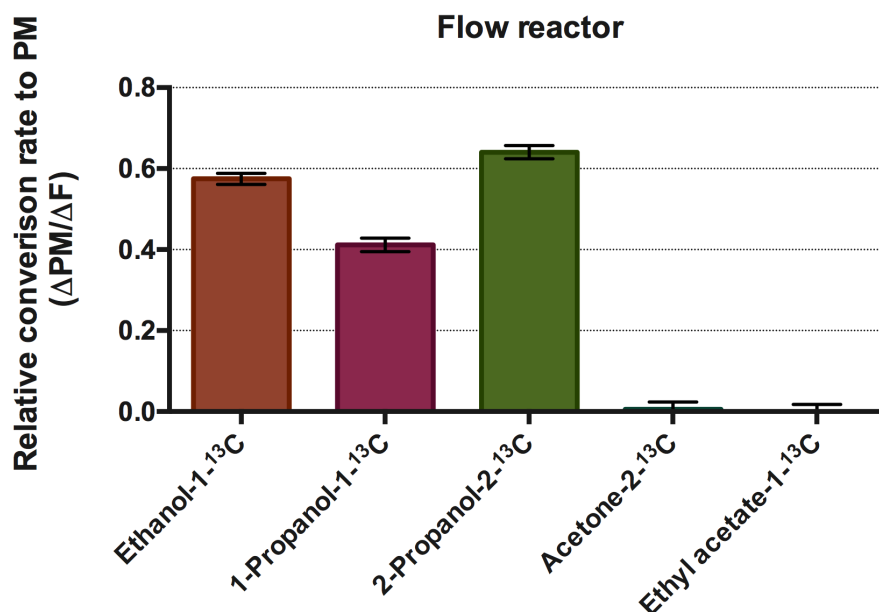


Figure 8.15: The relative conversion rates to PM formed in the flow reactor of the hydroxyl and carbonyl carbon atoms in ethanol, 1-propanol, 2-propanol, acetone, and ethyl acetate.

that no firm conclusions could be drawn as to whether there was a significant difference in the conversion rates of the *hydroxyl* carbon atoms between the two propanol isomers. In any case, any small difference there may be appears to be much smaller than that observed in the reactor. An interesting result is that of the *hydroxyl* carbon atom in ethanol appears to convert to PM at a higher rate of 0.24 compared to the equivalent carbon atoms in the propanol isomers. It is suggested that the higher rate of the hydroxy contribution to the PM for ethanol could be due to the formation of a C_2 fragment formed from the scission of the C-O bond in ethanol (Buchholz et al., 2002). It is known that C_2 species are efficient particle growth species (e.g. acetylene), the C_2 fragment may, therefore, convert to soot at a higher rate than the fragments formed from heptane pyrolysis, hence the comparatively higher conversion rate to PM from ethanol.

8.5 Conclusions

This chapter has dealt with expanding the isotope tracer technique, previously used with single-component fuels, to encompass binary mixtures of fuels, and was used to identify the contribution of a component in a mixture of molecules. The tracer technique was successfully applied to binary mixtures of various molecules in *n*-heptane, and was found to work well for the source apportionment of PM collected from the flow reactor and compression ignition engine. A number of interesting results were obtained which sheds light on the conversion of carbon atoms during combustion, and the most significant of the results presented in this chapter are as follows:

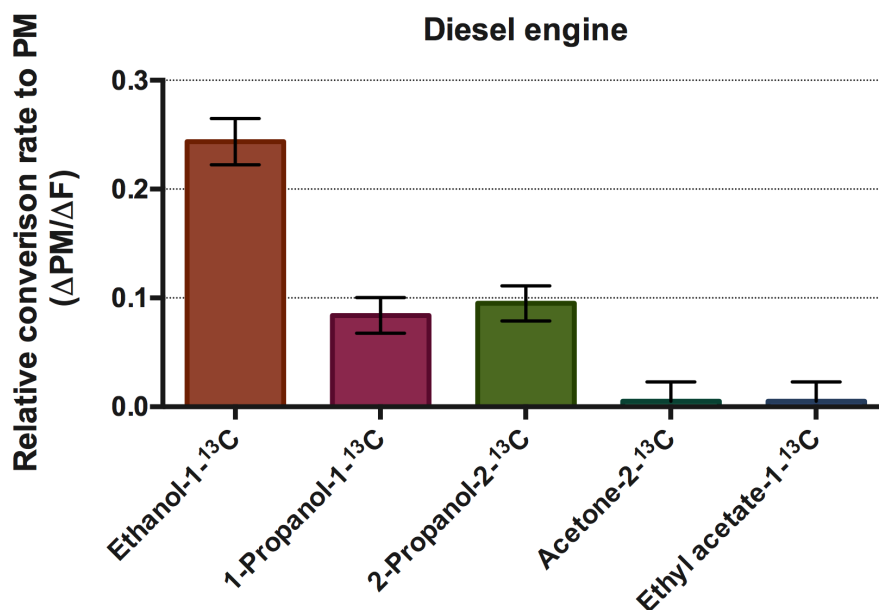


Figure 8.16: The relative conversion rates to PM formed in the diesel engine of the hydroxyl and carbonyl carbon atoms in ethanol, 1-propanol, 2-propanol, acetone, and ethyl acetate.

- The carbon atoms from the alcohols ethanol, 1-propanol, and 2-propanol were found in the all form PM during the pyrolysis and combustion in a diesel engine;
- PM produced in the flow reactor showed that the *methyl* carbon atoms in the alcohol molecules tended to form PM at about the same rate as the carbon atoms of the heptane component. This indicated that at least under pyrolysis conditions the presence of oxygen within the alcohol molecule did not directly reduce their relative likelihood of conversion to PM;
- The *hydroxyl* carbon atom in alcohols on the other hand formed PM at a reduced rate. In primary alcohols (e.g. ethanol, and 1-propanol) the PM formed in the reactor showed that the hydroxyl carbon was converted to PM at about half the rate of the average carbon atom in the mixture. In the reactor, the hydroxyl carbon atom in the secondary alcohol 2-propanol was found to contribute to soot formation at a higher rate than for the equivalent primary alcohol (1-propanol). However, the differences between the conversion rate of the hydroxyl carbon between the primary and secondary alcohols was less evident for the PM formed in the diesel engine.
- The ketone group, present in acetone, was found in to completely prevent the conversion to PM of the carbon atom it was directly bound to. This result was consistent for the PM formed in both the reactor and diesel engine.

- In the flow reactor, the two *methyl* carbon atoms in acetone formed PM at the same rate as the average heptane carbon atom. In the diesel engine the methyl carbon atoms also contributed significantly to PM formation.
- In the reactor, the average carbon atom in the toluene component of the toluene-heptane mixture formed PM at a rate 25% higher than that of the carbon atoms in the heptane component.
- The PM collected from toluene-heptane blends from both the flow reactor and diesel engine showed that the *methyl* carbon in toluene converted to PM at a lower rate compared to the phenyl ring.

Finally, as a concluding comment, it has been shown in this chapter that despite the different conditions prevailing in the in the engine and the reactor, for example, differences in the time available for soot formation, pressure and temperature, and so on, similar results were obtained for the PM formed from both the flow reactor and the diesel engine. That is, the reduced contribution from the hydroxyl group in ethanol, for example, and the increased contribution of the phenyl ring in toluene compared to the methyl carbon, are results that are consistent in both the tube reactor and diesel engine.

Chapter 9

Evaluating the use of GC/C/IRMS for the measurement of PAHs

In this final chapter of results, experimental results are presented which demonstrate the feasibility of using carbon-13 to trace carbon atoms from fuel molecules to pyrolysis-generated polycyclic aromatic hydrocarbons (PAHs). The purpose of this chapter is intended as a link to future work by demonstrating the possibility of utilising ^{13}C -tracing and IRMS to detect other species that are relevant to combustion. This technique could shed light on both the mechanisms of PAH formation, and also to identify which molecules or sub-molecular groups in the fuel tend to produce the most harmful PAHs.

9.1 Introduction

The presence of PAHs in the atmosphere is principally due to the incomplete combustion of organic fuels. PAHs and particulae matter are emitted from gasoline and to a greater extent from diesel engines; the main factors which influence the PAH emissions from diesel engines are: unburnt fuel PAH, and PAH pyrosynthesised from unburned fuel, lubrication oil PAH, and PAH in engine and engine exhaust deposits (Andrews et al., 1989). In the ambient air, low molecular weight PAHs (with two/three rings) are present individually in the vapor phase, whilst larger PAHs (> 5 rings) are predominantly found bound to the surface of soot particles. PAHs are considered to be carcinogenic, and the mutagenic potential appears to depend on the identity of the PAH (Nisbet et al., 1992). For example benzo(a)pyrene (BaP) is regarded as a particularly prolific PAH in terms of its carcinogenic potential; one study indicated that the total carcinogenic potential of BaP was accountable for between 51 to 64% of the total carcinogenic potential of all PAHs in the atmospheric air. The Environmental Protection Agency (USA), lists a number of PAH compounds that are given high-priority due to their presence in the environment and their classification as probable human carcinogens; the 16 priority PAHs

are listed in Table 9.1. It was also discussed previously in Chapter 2 that PAHs are precursors to soot formation, and their growth by the hydrogen-abstraction/ C_2H_2 addition (HACA) mechanism results in the formation of primary soot particles. Therefore, their study is important to elucidate the detailed chemical mechanisms of soot formation, and also to understand, phenomenologically, how the initial fuel influences the formation of PAHs.

In the literature, a number of systems have been used for investigating PAH formation including flow reactors (Sánchez et al., 2010, 2012a; Lea-Langton et al., 2013), jet stirred reactors (Marr et al., 1994), and diesel engines (Williams et al., 1986; Lombaert et al., 2006; Tancell et al., 1995). The quantification and speciation of soot-bound PAHs, usually carried out by GC/MS analysis, shows that both the fuel and the formation conditions influences the identity and amount of PAHs extracted from the soot surface. For example, Williams et al. (1986) investigated the relationship between the PAH composition of various diesel fuels, and the PAHs extracted from the particulate derived from those fuels when combusted in a compression ignition engine. Generally, it was found that the polycyclic aromatic compounds (PACs) found in the diesel exhaust particulate were similar to those of the fuel they were derived from, and the concentrations followed the trend of engine load. Crucially, about 0.2 to 1% of the PACs with 2 to 4 rings in the fuel survived combustion and were responsible for a substantial portion of the mutagenic compounds in the exhaust.

Sánchez et al. (2013) studied the influence of increasing inlet concentrations of acetylene in a flow reactor at 1223 K, on the EPA PAHs (see Table 9.1) formed, and present in both the vapor phase and bound to the particulate. This resulted in increasing total concentrations of PAHs, and increasing concentrations of PAHs with 2/3 rings, which tended to be present in the gas phase. A further study on the influence of temperature in the range of 800 to 1200 °C, on the pyrolysis of acetylene showed that there was maximum temperature (around 1100 °C) above which lower concentrations of PAHs were evolved from the reactor (Sánchez et al., 2010). Due to the fact that the PAHs of interest span a range of molecular weights and boiling points (Table 9.1), generally only the lighter PAHs (naphthalene and acenaphthylene) are typically found in the gas state, whilst the majority of the larger 16 PAHs are found bound to the surface of the soot particles (Sánchez et al., 2012b). In this present work only the PAHs bound to the surface of the soot particles have been extracted and analysed.

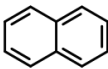
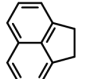
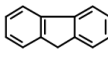
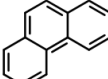
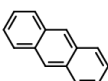
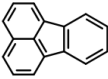
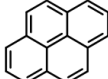
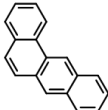
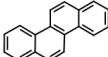
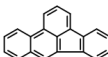
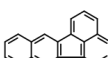
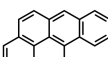
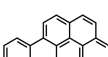
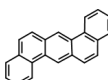

Firstly, this chapter presents results of the GC/MS analysis of PAHs which were extracted from particulate matter by means of solvent extraction, where the particulate was generated by the pyrolysis of ethane and ethylene in the tube reactor at two temperatures, 1150 and 1250 °C. This initial work was conducted using GC/MS in order to simply characterise the PAHs formed in the tube reactor, and to ensure that using the established experimental procedures reported in the literature for sample collection, soxhlet extraction, sample concentration, and GC/MS analysis were suitable for the experimental system used in this work. Once the technique had been carried

out successfully using GC/MS analysis, the technique was developed for GC/C/IRMS analysis (gas chromatography combustion isotope ratio mass spectrometry). In previous chapters of this thesis, site-specifically labelled carbon-13 atoms were traced from the fuel to the particulate matter produced under pyrolysis conditions, and samples of PM were analysed by EA/IRMS (elemental analysis isotope ratio mass spectrometry) which is a bulk analysis technique that gives the average isotopic composition of the entire sample. The GC/C/IRMS has been used to measure the isotopic signature of individual PAHs which have been extracted from the surface of particulate into a solvent, the gas chromatography part of the analysis is used to separate the individual PAH molecules so that they can be measured individually by IRMS.

Previous methods have been reported for tracing ^{13}C site-specifically labelled PAHs (Lea-Langton et al., 2013), or deuterated PAHs (Lombaert et al., 2006) in the fuel to PAH molecules in the resulting particulate matter, using GC/MS as the detection method. One notable advantage of using GC/MS analysis is that the mass spectrum of the fragmented PAHs, which is an output of GC/MS analysis, may be used to determine the precise fragment of the PAH molecule in which the ^{13}C resides. Due to the fact that the GC/C/IRMS technique involves the combustion of each of the PAHs in turn to CO_2 , the measurement technique reports the isotopic composition for the whole PAH molecule and not the individual fragments, as in GC/MS. However, the sensitivity of the GC/MS is much lower than that of IRMS, which means that without using higher levels of isotopic enrichment the use of GC/MS may be restricted to tracing certain components, such as PAHs; PAHs are efficiently traced from the fuel to PM using GC/MS principally due to their ‘survivability’ during combustion. In this chapter particulate was generated from ^{13}C labelled ethanol (tested as a single-component) in the flow reactor, and then GC/C/IRMS was used in order to detect the EPA-16 PAHs which were extracted from the particulate into the solvent dichloromethane (DCM).

In the literature there are many different methodologies available for the GC/MS analysis of PAHs. Despite the apparent simplicity of extending the established methodology for GC/MS analysis to include GC/C/IRMS, there are several differences between the two analysis methods which could complicate the process for GC/C/IRMS. The main difference is due to the fact that there are several additional components and fittings required to interface the GC to the combustion reactor and the IRMS instrument, which causes the broadening of the GC peaks. In practice, the peak broadening could mean that without sufficient compound separation, there may be peak overlap between the compounds of interest, which could make the isotopic signature of specific compounds difficult to resolve. The further details of the GC/MS instrument were provided in Section 3.4.3, and the principles of the GC/C/IRMS instrument is provided below in Section 9.2.3.

Table 9.1: Structures, names, and molecular weights of the 16-EPA-PAHs.

Structure	Name	Molecular formula	MW (g/mol)
	Napthalene	C ₁₀ H ₈	128.19
	Acenaphthene	C ₁₂ H ₈	152.20
	Fluorene	C ₁₃ H ₁₀	166.23
	Phenanthrene	C ₁₄ H ₁₀	178.23
	Anthracene	C ₁₄ H ₁₀	178.23
	Fluoranthene	C ₁₆ H ₁₀	202.26
	Pyrene	C ₁₆ H ₁₀	202.25
	Benz(a)anthracene	C ₁₈ H ₁₂	228.28
	Chrysene	C ₁₈ H ₁₂	228.28
	Benzo(b)fluoranthene	C ₂₀ H ₁₂	252.32
	Benzo(k)fluoranthene	C ₂₀ H ₁₂	252.32
	Benzo(a)pyrene	C ₂₀ H ₁₂	252.31
	Indeno(1,2,3-cd)pyrene	C ₂₂ H ₁₂	276.32
	Dibenzo(a,h)anthracene	C ₂₂ H ₁₄	278.35
	benzo(g,h,i)perylene	C ₂₂ H ₁₂	276.34

9.2 Methods

9.2.1 Generation of particulates and sample collection

Particulate matter has been generated using the laminar flow reactor rig described in Chapter 3. All of the experiments described in this chapter have been conducted under pyrolysis conditions, using oxygen-free nitrogen as a carrier gas at a fixed rate of 20 L/min, and the vaporiser was set to 150 °C for all experiments. The samples of particulate for GC/MS analysis were generated from ethane and ethylene at inlet concentrations of 5,000 ppmv. The sample of particulate collected for GC/C/IRMS analysis was generated from ethanol pyrolysis, at an inlet concentration of 5,000 ppmv.

Samples of particulate matter were withdrawn from within the reactor tube at 300 mm from the outlet by a stainless steel sampling probe using a vacuum pump drawing the sample gas at 5 L/min. The particulate was collected onto a glass-fiber filter (Fisherbrand, Microfiber filter MF300) which was positioned in a quick-release filter housing; an image of the setup used for collecting particulate onto a filter is shown in Appendix A. At each condition about 300 mg of particulate matter sample was collected for analysis; three filters were collected and weighed using a micro-balance, each filter contained around 100 mg. Immediately following collection the 60 mm diameter filters were placed in a petri dish and stored at -20 °C until they were required for soxhlet extraction.

9.2.2 Soxhlet extraction

Soxhlet extraction is a common technique used to extract the PAHs that are bound to the surface of soot particles into a solvent. Soxhlet extraction involves repeatedly soaking the sample in fresh solvent, thereby avoiding transfer equilibrium from limiting the extraction efficiency.

The filter loaded with the particulate matter sample was folded and placed into a borosilicate glass extraction thimble (Whatman, 2814-300), and the thimble was then positioned inside the soxhlet extractor. A 250 mL volume of HPLC-grade dichloromethane was used as the solvent for the extraction. The extraction was carried out for 24 hours, with a cycle time of 15 minutes (for a total of 96 cycles); this optimised method was reported previously by Sánchez et al. (2013). An image of the soxhlet extraction apparatus is shown in Appendix A.

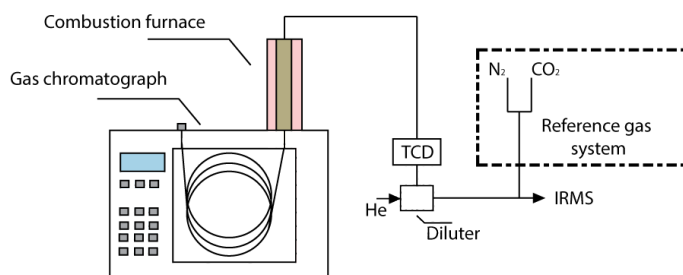
Following soxhlet extraction the solvent containing the extracted PAHs was concentrated by rotary evaporation, followed by micro-concentration under a nitrogen stream to a final volume of 5 mL.

9.2.3 GC/C/IRMS

In this work a Agilent 6890N GC was connected via a conflo IV to a Thermo Finnigan Delta V IRMS, and was used to conduct the GC/C/IRMS analysis described in this chapter. The first stage in the analysis is gas chromatography (GC), involving the

Table 9.2: Chromatographic Conditions.

GC	Agilent 6890N
Sampler	Agilent 7683B,
Syringe	(Agilent 5188-5246) 5.0 μL
Injection	1.0 μL splitless injection, 5 ng each component on column
Carrier	Helium 45 cm/s, constant flow
Inlet	Pulsed splitless; 300 °C, 40 psi until 0.2 min
purge flow	30 mL/min at 0.75 min
Column	Agilent DB-5 Ultra Inert 30 m x 0.25 mm x 0.25 μm
Oven	55 °C (1 min) to 320 °C (25 °C/min), hold 3 min

**Figure 9.1:** Setup of the GC-IRMS instrument.

separation of compounds based on their mobility through a chromatography column (as described in Chapter 3); the chromatographic conditions employed in the GC for the analysis are shown in Table 9.2. Following GC the separated sample was then passed to the micro-combustion reactor (set to 950 °C) where the samples were in turn combusted to CO_2 as they eluted from the GC column. Following combustion to CO_2 the samples were passed to the IRMS instrument for analysis.

There are number of differences in the components that interface the GC to the IRMS, which means that the analysis by GC/C/IRMS results in spectra which have peak shapes that are usually broader than those by GC/MS. Depending on how well compounds are separated by the chromatography there can be considerable overlap between neighboring spectral peaks for GC/C/IRMS. The ‘band-broadening’ usually occurs at components for interfacing the GC to the micro-combustion reactor and the IRMS, where the cross-sectional area of the line increases. For example, attached to the GC column immediately before the combustion furnace a backflush valve is usually fitted in order to divert the solvent before the combustion furnace so to prevent the solvent from being oxidised to CO_2 . Furthermore, the combustion reactor was fitted with an alumina reactor tube with diameter of ~ 0.5 mm i.d., which was larger than that of the GC column, which may also have been point where band broadening may have occurred.

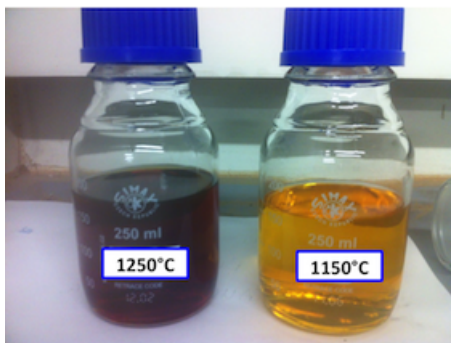


Figure 9.2: Appearance of the soluble extract of PM formed from ethane pyrolysis at 1250 °C (left) and 1150 °C (right).

9.3 Results

9.3.1 Result and discussion of the GC/MS analysis

GC/MS analysis was carried out on the solvent extracted solution from both ethane and ethylene at the temperatures 1150 and 1250 °C. Figure 9.2 shows the appearance of the soxhlet extracted compounds in dichloromethane (which is otherwise colorless), as extracted from the PM formed from ethane at 1150 and 1250 °C. Likewise, Figure 9.3 shows the GC/MS spectra for the PAHs extracted from the PM formed pyrolysis of ethane at the two temperatures. It generally appears that at the higher temperature of 1250 °C higher peak levels of PAHs were formed, for example, the anthracene peak (which has a retention time of ~34 min) was ~3 times larger at 1250 than for 1150 °C.

Figure 9.4 shows GC/MS chromatograms for PAHs extracted from the PM formed from ethylene at the two temperatures tested. It appears that in contrast to the result from ethane, the peak PAH concentrations for the majority of PAHs detected appear to be lower at the higher temperature of 1250 °C. For example, the abundance of anthracene (retention time ~34 min) extracted from PM formed at a temperature of 1150 °C is twice the level of that formed at the higher temperature of 1250 °C.

Sánchez et al. (2010) reported results regarding the PAHs formed from the pyrolysis of acetylene at temperatures in the range of 800 to 1200 °C. Sánchez et al. found that at increasing pyrolysis temperatures the amount of the smaller PAHs (smaller than anthracene) tended to decrease with temperature, whilst the larger PAHs reached a maximum at 1000 °C, and decreased thereafter. It was suggested by Sánchez et al. and also Font et al. (2003) that the maximum yield of PAHs at lower temperatures may be attributed to the competition between the formation and destruction pathways of PAHs at low and high temperatures respectively.

Another reason for the observed decrease in PAHs at higher temperatures, is likely to be due to the fact that at higher temperatures more of the initial fuel is converted to soot. The higher conversion of carbon to soot means that there is, therefore, lower concentrations of gaseous hydrocarbon species, including PAHs. In Chapter 5 particles

formed from ethane and ethylene were characterised in terms of their size and number distributions, formed at temperatures in the range of 1000 to 1400 °C. It was shown that high number concentrations of small diameter nascent particles tended to be formed at lower temperatures ~ 1100 °C, but at higher temperatures (> 2000 °C) much lower concentrations of larger diameter agglomerated particles were formed. Therefore, due to the particle agglomeration and higher conversion rates of fuel to PM, the particles could overall have less surface area available for the adsorption of PAHs, and thereby solvent extraction inevitably results in lower PAH yields. It is therefore suggested that future work in this area, where PAHs are extracted from PM should also consider the number and size distributions of the particulates; this is especially relevant in systems such as a flow reactors, where the formation conditions can result in large differences in particle morphology.

The results in this section show that lower levels of PAHs were produced from ethylene at the higher formation temperature, and it appears that the results are in alignment with the findings of Sánchez et al. (2010), and the logic discussed above regarding the reduction of PAHs at higher temperatures. Ethane is known to have a lower sooting tendency than that of ethylene, had probably not yet reached its peak temperature for PAH formation.

The objective of this initial work was to verify the effectiveness of the established methodology for extracting and analysing PAHs for the PM formed from the reactor. The results have shown that well-defined chromatographic peaks of PAHs were detected by GC/MS analysis, and that PAHs were present at concentrations that were practical for detection, the established method required no modifications for GC/MS analysis, and was extended to GC/C/IRMS in the following section.

9.3.2 Result and discussion of the GC/C/IRMS analysis

Figure 9.5 shows the GC/C/IRMS spectrum of a standard mix of 16 PAHs (with each PAH at a level of 200 $\mu\text{g}/\text{ml}$) measured by GC/C/IRMS. The chromatogram shows that there were 12 distinct peaks of roughly similar amplitude detected; indicating that some of the PAHs that had a similar structure had eluted together. For example, two compounds were likely to have coeluted in the broad peak detected at 986 seconds. Despite the apparent overlap of some of the peaks, there was good separation for the majority of the compounds under the GC conditions employed, for the purpose of determining the isotopic composition of the PAHs the GC/C/IRMS spectrum (Figure 9.5) was considered to be of good quality. However, inevitably the isotopic composition of the PAHs that coeluted would have to be reported as a group.

Figure 9.6 shows the GC/C/IRMS chromatogram of the PAHs extracted from the PM formed from ethanol. Many of the same PAHs were detected as were present in the standard mix (Figure 9.5), for example detectable concentrations of naphthalene and anthracene were recovered from the PM (detected at ~ 560 and 1150 seconds respectively).

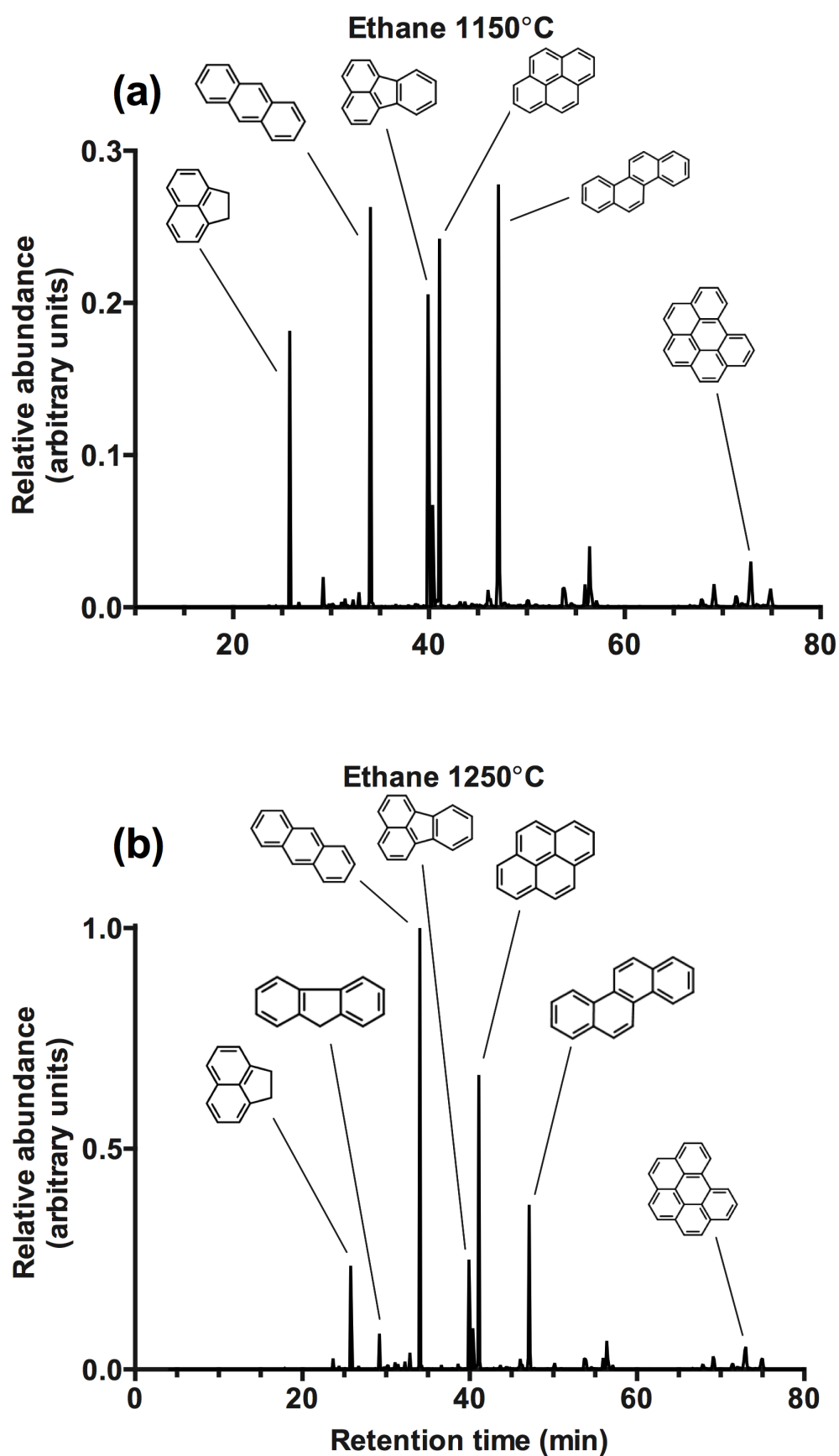


Figure 9.3: GC/MS spectra of PAHs extracted from samples of PM collected from the pyrolysis of ethane in the flow reactor, at (a) 1150°C and (b) 1250°C.

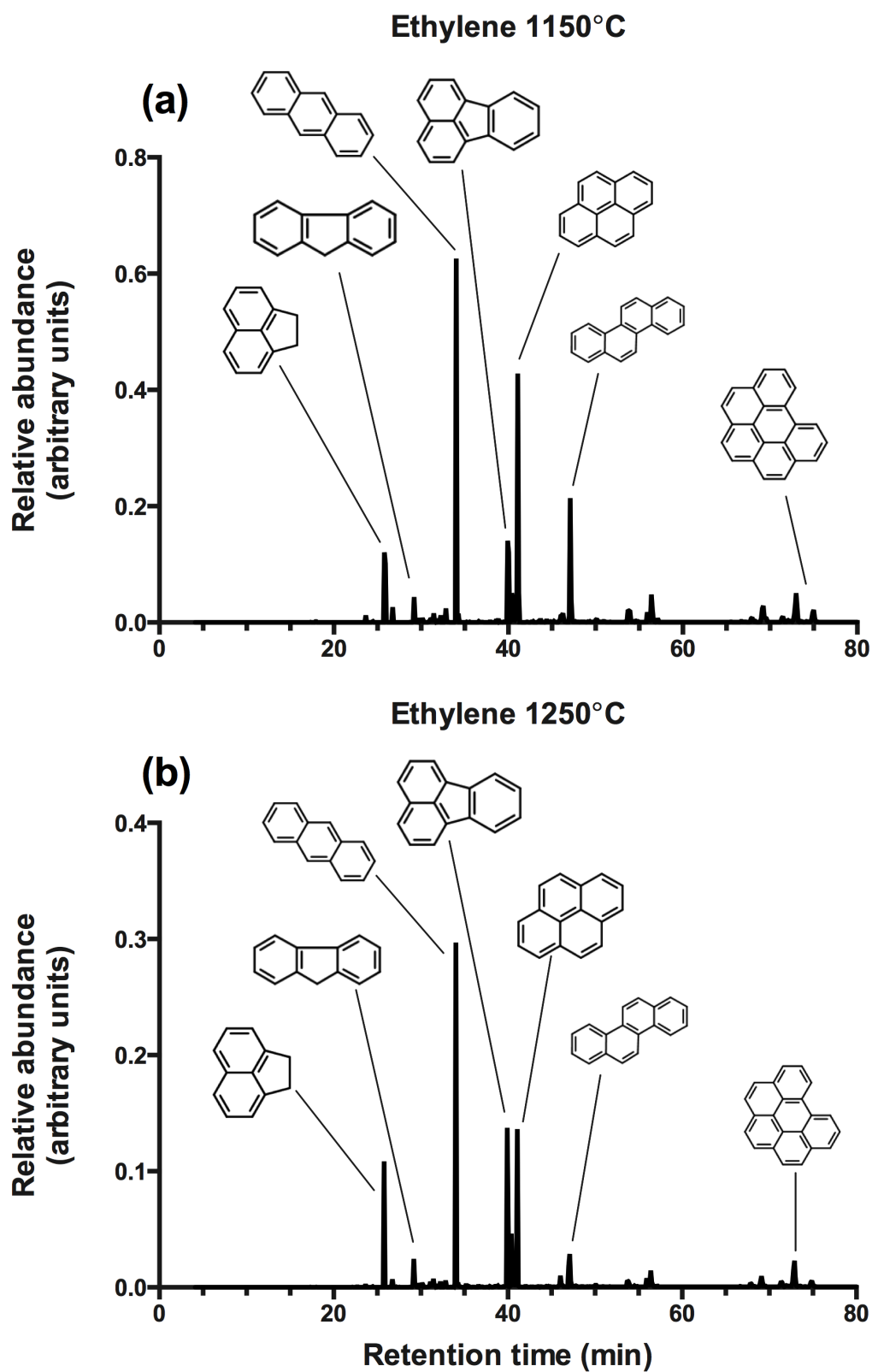


Figure 9.4: GC/MS spectra of PAHs extracted from samples of PM collected from the pyrolysis of ethylene in the flow reactor, at (a) 1150 °C and (b) 1250 °C.

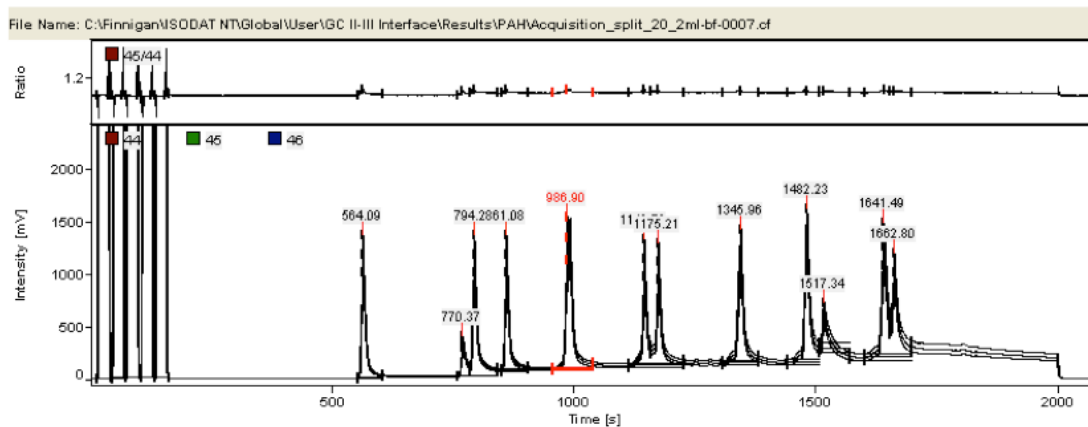


Figure 9.5: GC/C/IRMS spectrum of a standard mix of 16 PAHs (47930-U Supelco), showing response of the mass 44 detector.

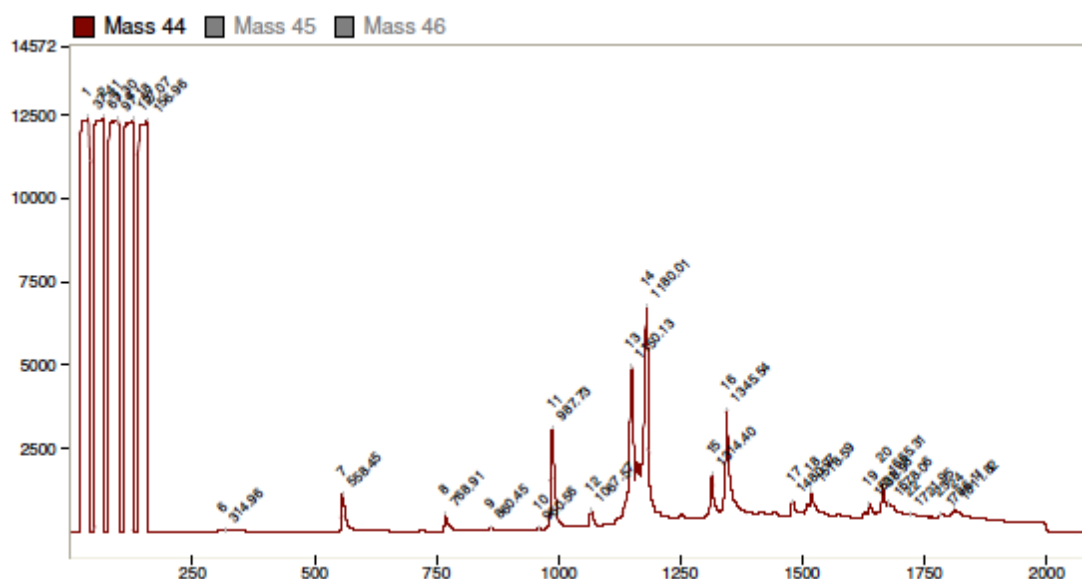


Figure 9.6: GC/C/IRMS spectrum of PAHs extracted from the PM generated from the pyrolysis of ethanol at 1150 °C.

Similarly to the chromatogram for the standard PAH mix, well-defined peaks were observed that were suitable for the determination of the isotopic composition ($\delta^{13}\text{C}$). In addition, it was observed that the spectrum for ethanol, and the spectra shown in the previous section for ethane and ethylene, that the compounds detected were principally the 16 PAHs of interest; in other words, out of the 1000s of possible polycyclic aromatic compounds (PACs) (a class of compound that includes PAHs) which could have been present in the PM, it was mainly the 16-PAH which were present.

9.4 Conclusions

The main result shown in this chapter is that GC/C/IRMS appears to be a suitable method for the isotopic analysis of combustion-generated PAHs. The spectra from both the GC/MS and GC/C/IRMS show that many of the EPA 16-priority PAHs are present in the particulate collected from the reactor, formed from the fuels ethane, ethylene and ethanol. The successful application of GC/C/IRMS analysis of a standard mix of PAHs and also combustion-generated PAHs demonstrated the feasibility of using IRMS for determining the isotopic composition of PAHs; GC/C/IRMS could therefore be used as a technique for efficiently carrying out isotope tracer analysis in flames or engines in which PAHs are the compound of interest.

Additionally, the results of the GC/MS analysis ethane and ethylene appeared to agree with the literature that there was a peak temperature for the recovery of PAHs, above which the PAH yield reduced. Significantly, when interpreted with the results of Chapter 5 which showed the size and number distributions of particles formed from ethane and ethylene, it was put forward that an important factor in the recovery of PAHs was the morphology of the particles. Therefore, it is strongly recommended that future work carried out on PAHs recovered from PM should also seek to characterise the size and number distributions of the PM.

Chapter 10

Conclusions

In this thesis a range of unique experimental results have been obtained that have concerned the influence of fuel molecular structure on the formation of particulate matter under various conditions. In this chapter the most significant findings of the thesis are summarised, and their impact on the relevant scientific area is outlined. On the basis of the conclusions, recommendations for future work are made.

10.1 Summary of conclusions

It was concluded in the literature review that there were relatively few examples of the use of isotopes for the purpose of tracking specific atoms of a molecule through combustion to particulate emissions, and the majority of those in the literature had utilised the radioactive isotope ^{14}C . Despite the apparent usefulness of such techniques for better understanding chemical processes during combustion, it was thought that one of the main obstacles that had probably prevented the wider use of isotope tracing was the lack of a cost-effective methodology.

To examine how the chemistry of a compound influences its tendency to form particulate matter, a laminar flow tube reactor was designed and commissioned that allowed high-temperature pyrolysis of a range of liquid and gaseous fuels up to $\sim 1700^\circ\text{C}$ under homogenous and well-defined inlet conditions. Fuels were also tested in a modern direct-injection compression ignition engine. The following sections outline the most significant results that were obtained in each chapter of this thesis.

10.1.1 Influence of molecular structure on the particulate matter formed during pyrolysis of C_1 to C_5 Fuels

In Chapter 5 a range of C_1 to C_5 hydrocarbon and oxygenated molecules were tested in the flow reactor in order to assess the overall propensities of the molecules to form PM. The following noteworthy results were observed:

- C_2 and C_3 fuels tended to form PM under pyrolysis conditions in the order: alcohol < alkane < alkene.

- Increasing pyrolysis temperature in the range of 1000 to 1400°C resulted in increasing particulate yield.
- Pyrolysis of the isomers 1- and 2-propanol, showed that 2-propanol tended to yield higher particulate mass concentrations, which was particularly evident at the higher temperatures tested; and
- Cyclopentanol, which contains a 5-member ring structure, formed significantly higher mass concentrations of particulate matter than the corresponding straight-chained equivalent 1-pentanol, at all temperatures tested.
- Structural isomerism, in the molecules *n*-butane and *i*-butane, was not found to influence the number and size distributions or the total mass concentration of particulate formed in the reactor.

10.1.2 The conversion of labelled carbon atoms from single-component fuels to PM

In Chapter 6 the first results of the isotope labelling experiments were presented, and several experiments were carried out to validate the isotope technique. Specifically, the result for ethyl acetate showed that the outcome of the labelling experiment was the same regardless of the presence of the ^{13}C isotope. In other words, the presence of ^{13}C did not appear to affect the particulate forming reactions and this was confirmed by the bonds ^{12}C - ^{12}C , ^{13}C - ^{12}C , or ^{13}C - ^{13}C behaving in the same way during high-temperature pyrolysis. Also, the outcome of the tracing experiment was uninfluenced by the level of ^{13}C enrichment in the fuel, which meant that low levels of ^{13}C could be used. In addition to the development of the technique, a number of insights into the behavior of carbon atoms from specific localities within single-component fuel molecules was reported, and the results included the following findings:

- Carbon atoms which were directly bound to a hydroxyl functional group were found to have a reduced tendency to form PM compared to carbon atoms in the alkyl chain; the discussion of the results put forward the hypothesis that the lower particulate conversion rate was because of retention of the C–O bond, and subsequent formation of carbon monoxide (CO).
- The contribution of the *hydroxyl* carbon atom to PM of a secondary alcohol was greater than that of the hydroxyl carbon atom in the corresponding primary alcohols.
- The ester group in ethyl acetate prevented the formation of PM from the *carbonyl* carbon atom, which was not detected in the PM.
- For toluene, it was found that the *methyl* carbon atom and each of the six phenyl ring carbon atoms converted to PM at the same rate.

10.1.3 The conversion of oleic acid and methyl oleate to particulate matter in a flow reactor and diesel engine

In Chapter 7 a number of results were presented, including the conversion rates of specific carbon atoms for the molecules methyl oleate and oleic acid. The labelling experiment, which was at first applied to pyrolysis generated PM in the homogenous reactor, was then adapted and carried out for particulate matter collected from a diesel engine. The following conclusions were drawn:

- In the compression ignition engine, oleic acid formed a far higher total *mass* of particulates compared to methyl oleate and reference diesel, and much higher particulate *number* concentrations; this was attributed to the high viscosity of oleic acid compared to that of methyl oleate, which resulted in reduced mixing of fuel and air prior to combustion; but
- In the flow reactor under homogenous conditions, the reference diesel formed much higher concentrations of PM by mass than either of the two oxygenated molecules.
- In both the diesel engine and the laminar flow reactor it was found that the *carbonyl* carbon atom in the carboxylic acid functional group of oleic acid, and also the *carbonyl* carbon atom in the ester methyl oleate, did not convert to PM during combustion.
- Surprisingly, the double bonded carbon atoms in the oleic acid alkyl chain did not contribute to PM at a significantly greater rate than the ‘average’ carbon atom in the alkyl chain of the molecule during pyrolysis.
- It was showed that similar results were obtained in both the tube reactor and diesel engine, despite the differences in the formation conditions, such as: temperature, pressure, residence time, fuel concentration, presence of oxygen, and so on.

10.1.4 Conversion of labelled carbon atoms in binary mixtures of various hydrocarbon and oxygenate molecules in heptane

In Chapter 8 the combustion and pyrolysis of binary mixtures of various compounds added to heptane was carried out in the flow reactor and diesel engine. A number of notable results were obtained, as follows:

- Samples of PM collected from the pyrolysis reactor showed that for oxygenated compounds (e.g. ethanol, the isomers of propanol, and acetone) the carbon atoms which were not directly attached to the oxygen group tended to convert to PM at the same rate as the heptane atoms; indicating that the presence of oxygen within a molecule does not have an appreciable impact on the fate of neighboring carbon atoms.

- The carbon atoms which were directly bonded to oxygen, on the other hand, contributed to PM formation in varying amounts, but always to a lesser degree than carbon atoms that were not directly bonded to oxygen. In the reactor, the *hydroxyl* carbon atom in primary alcohols contributed to PM to a lesser extent than the equivalent *hydroxyl* carbon atoms in secondary alcohols; however, in the diesel engine, there was no discernible difference in the contribution to PM of the hydroxyl carbon atoms between the two isomers.
- In the toluene-heptane binary mixture, the methyl carbon atom of toluene was shown to form PM at a lower rate than the phenyl ring carbon atoms in both the reactor and the diesel engine. This is in contrast to the finding in Chapter 6, where toluene was tested as a single-component fuel, indicating that complex interactions between the fuels takes place, influencing the conversion of carbon atoms to PM.

10.2 A summary of the suitability of carbon-13 as a tracer for combustion research

One of the main developments that this thesis has reported is the efficient application of isotopic ^{13}C for use as a tracer in combustion and pyrolysis processes. The use of low levels ^{13}C enrichment and the highly sensitive measurements by isotope ratio mass spectrometry (IRMS), as described in this work, has opened-up the possibility of the technique being more widely used for combustion research. Calculations to determine the percentage conversion of the labelled component of a molecule to the particulate matter were developed and set out in Chapter 4; and, in principle, these calculations can also be applied to identify the relative conversion rate of any labelled reactant undergoing a high temperature reaction, to a given product species.

It was found in this thesis that even at low levels of ^{13}C enrichment an adequate level of resolution was achieved for determining the percentage composition of the PM derived from specific carbon atoms. Naturally, to improve the resolution of the measurements the most obvious route would be to increase the level of ^{13}C enrichment in the initial fuel. The level of enrichment used in this thesis was about $30 \delta^{13}\text{C}$, in the range of about $-30 \delta^{13}\text{C}$ to about $0 \delta^{13}\text{C}$, which was still in the natural abundance range, and for measurements in the natural range of isotopic abundance the IRMS instrument was shown to give a highly linear response. For measurements of samples with an isotopic composition outside the natural abundance range, this may not be the case, and it is recommended that reference materials covering the range of measurements is used rather than relying on extrapolation. The International Atomic Energy Agency (IAEA) supplies the ^{13}C isotopic standards of sodium bicarbonate ‘A’ and ‘B’ of $\delta^{13}\text{C}$ 93.3 and 466.0 respectively, and these are recommended for use as standards if higher levels of ^{13}C enrichment are required (<http://nucleus.iaea.org/rpst/Documents/IAEA-303.pdf>. Accessed: 30/02/2015).

Given the alternative technique and experimental results put forward in this thesis, and the relatively small number of labelling experiments that have been reported in the literature, there is a large potential for isotope labelling being used as a diagnostic technique in combustion and other reactions, and could provide a fruitful new area of research. It is expected that this work will be of value to the combustion community and could lead to the development of better kinetic models, by providing experimental data against which suggested chemical mechanisms could be validated. Also, in the longer term, it is anticipated that this work will aid the design of fuels which produce less PM, through modification of molecules to reduce conversion to soot. Some specific potential avenues for research are specified in the following section.

10.3 Recommendations for future work

This work has opened-up a range of possibilities for deploying ^{13}C as tracer. As it has been discussed above, a range of functional groups including primary and secondary alcohols, acids, ketones, esters, and aromatics have been tested. The first recommendation is for the testing of a number of other relevant functional groups, for instance aldehydes, tertiary alcohols, and the influence of isomerisation (e.g. *cis/trans*).

The focus of the work presented here has principally been on the the formation of particulate emissions. However the labelling technique could also be expanded to any number of other stable intermediate or product species, for example PAHs (as demonstrated in Chapter 9), which are of particular importance due to their mutagenic and carcinogenic properties.

One of the areas which the ^{13}C labelling technique could be used is to develop group additivity based estimates of sooting tendency. In the literature group additivity methods have been proposed to estimate the sooting tendency of single component fuels or fuel blends (e.g. Barrientos et al., 2013; Pepiot-Desjardins et al., 2008). The group additivity method was initially developed in order to estimate thermodynamic properties of molecules for which data was not available (Benson and Buss, 1958), and is based upon the division of compounds into smaller units where each unit has a numerical contribution to the property being estimated. Clearly the ^{13}C labelling technique, as set out in this thesis, which shows the direct contribution of individual sub-molecular groups, could be used to validate the theoretical basis of such models and develop further their predictive ability. To do this a large matrix of compounds would need to be tested. It should also be pointed out that one of the findings of this thesis was that the relative contributions to PM of different functional groups within a molecule appear to vary, depending on whether the molecule was consumed singly or in a binary mixture with heptane. For example, in Chapter 8 it was found that in a binary mixture of toluene and heptane, the methyl carbon of toluene formed comparatively less soot than the ring structure; in Chapter 6 however, pyrolysis of toluene as a single-component showed that the methyl carbon formed soot at an equal rate to the carbon atoms in the phenyl ring.

This result indicates that there is likely to be complex interactions that additivity-based models cannot currently predict, but isotope tracing could shed light on the interactions which could then be incorporated into the models.

A further recommendation is to identify the extent of the engine oil contribution to the PM under a range of engine running conditions. Due to the differences in the particle size distribution and total particulate mass concentrations observed between different fuels, it would also be of interest to explore whether the engine oil contribution to PM is influenced by the composition of the fuel being burned. Some previous studies on the engine oil contribution have been carried out utilising ^{14}C as a tracer (including, Buchholz et al., 2003; Hilden and Mayer, 1984). There does however seem to be a number of difficulties that might be encountered when expanding the technique to ^{13}C . The first point to make is that due to the fact that the contribution to PM from the oil is generally quite small, the overall level of ^{13}C enrichment would need to be increased in order to achieve sufficient resolution, due to the ‘dilution’ effect of the fuel-derived PM. In addition, due to the fact that several litres of engine oil are usually required to lubricate the engine sump, this would require the enrichment of several litres of oil, therefore requiring much larger volumes of costly ^{13}C labelled compound than has typically been used in this thesis. Finally, due to the diversity of the hydrocarbon molecules present in motor oil, a molecule in the oil would have to be selected for labelling that behaves in a way that is representative of the overall oil mixture. On balance, it is suggested that the method put forward by Buchholz et al. (2003) which exploits the natural variation in ^{14}C abundance (described in Chapter 2) is probably the most convenient and cost-effective way to identify the extent of lubrication oil contribution to particulate emissions.

10.3.1 Claims of originality

To the best of the author’s knowledge, the flow reactor which was used for fuel pyrolysis is thought to be of a unique design. The major advantage of using this system, compared to a wick-fed diffusion flame for example, is that the inlet conditions and temperature history of fuels undergoing pyrolysis were well-defined. As stated above, this is thought to be the first time that ^{13}C has been used as a tracer from fuel to PM in the way described in this thesis. Furthermore, also unique are the experimental results which show the percentage contribution to PM of individual carbon atoms in a range of molecules. Finally, the manual injector which was designed for syringe injection of volatile binary fuels into the IRMS elemental analyser is an original design.

To date, the work described in this thesis has resulted in the publication of three peer-reviewed journal papers:

- A. Eveleigh; N. Ladommatos; R. Balachandran; A. Marca, Conversion of oxygenated and hydrocarbon molecules to particulate matter using stable isotopes as tracers, *Combustion and Flame* 161 (11) (2014) 2966-2974.

-
- A. Eveleigh; N. Ladommatos; P. Hellier; A-L. Jourdan, An investigation into the conversion of specific carbon atoms in oleic acid and methyl oleate to particulate matter in a diesel engine and laminar flow reactor, *Fuel* 153 (0) (2015) 604-611.
 - A. Eveleigh; N. Ladommatos; R. Balachandran; Gas and Particulate Matter Products Formed in a Laminar Flow Reactor: Pyrolysis of Single-Component C₂ Fuels, *Energy Procedia*, *article in press*.

Appendix A

Supplementary mechanical drawings and images

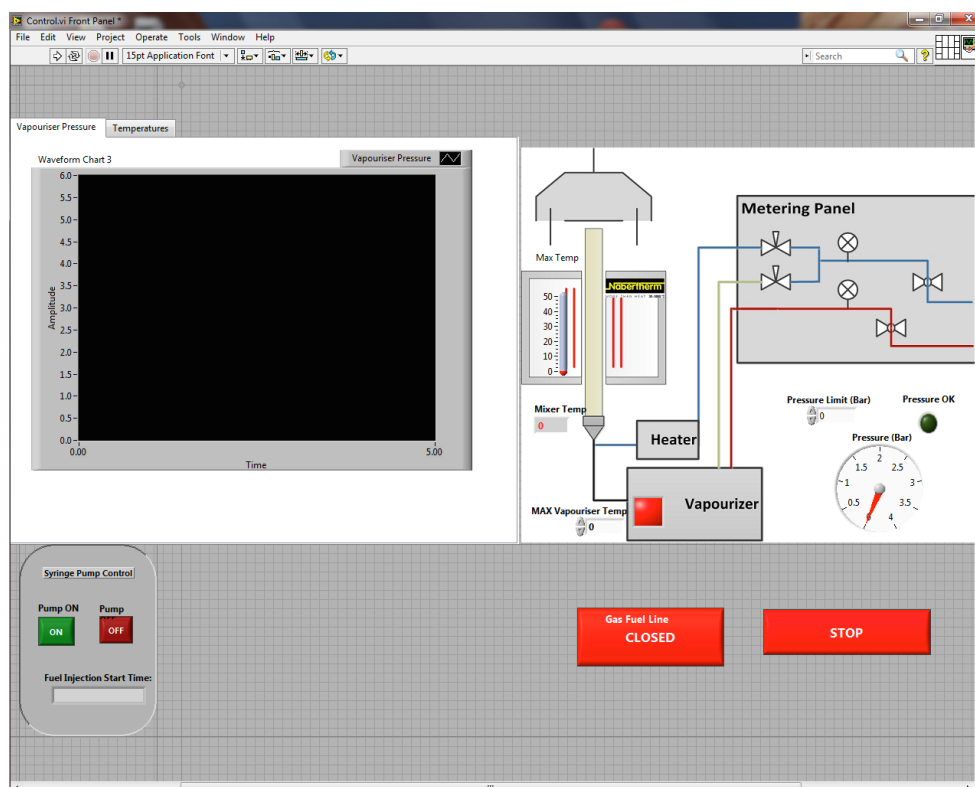


Figure A.1: Screenshot of the user interface used to monitor and control the laminar flow tube reactor (written in NI LabView).



Figure A.2: Image of the laminar flow reactor facility.

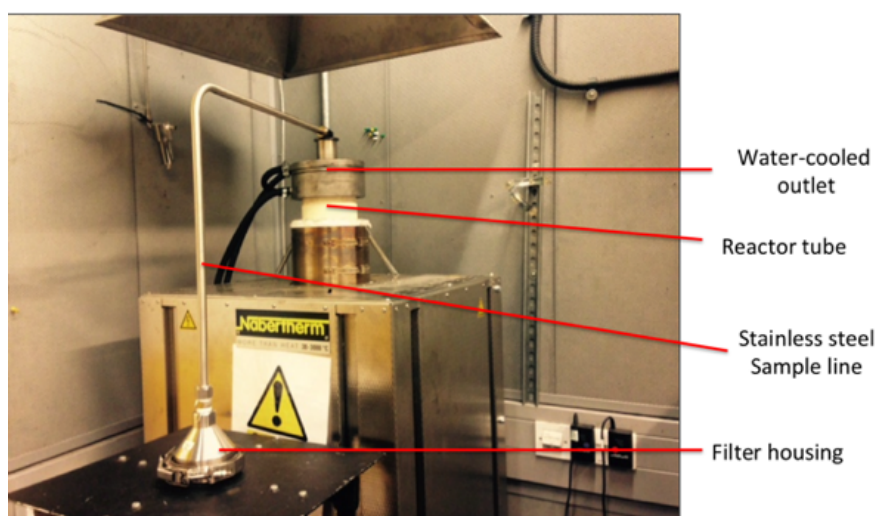


Figure A.3: Outlet of the flow reactor with assembly for collecting particulate matter onto a filter.

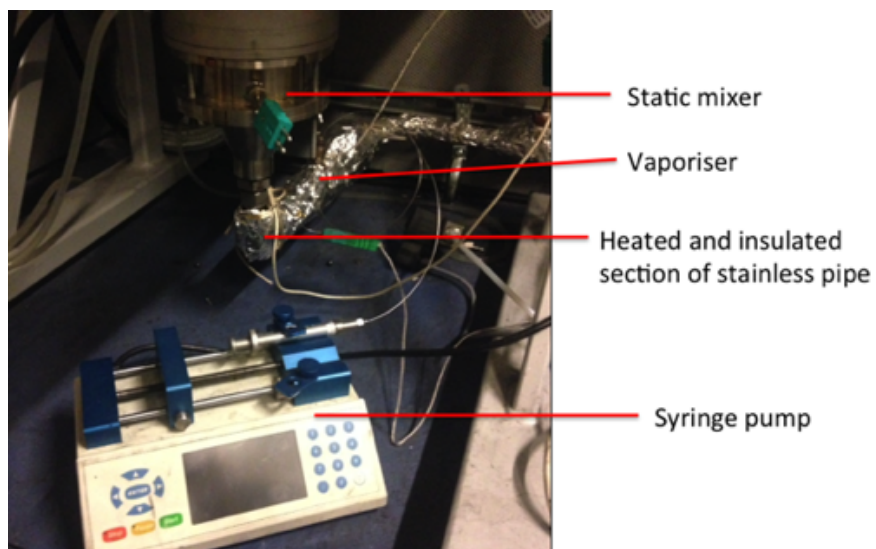


Figure A.4: Fuel vaporiser and inlet to the reactor.

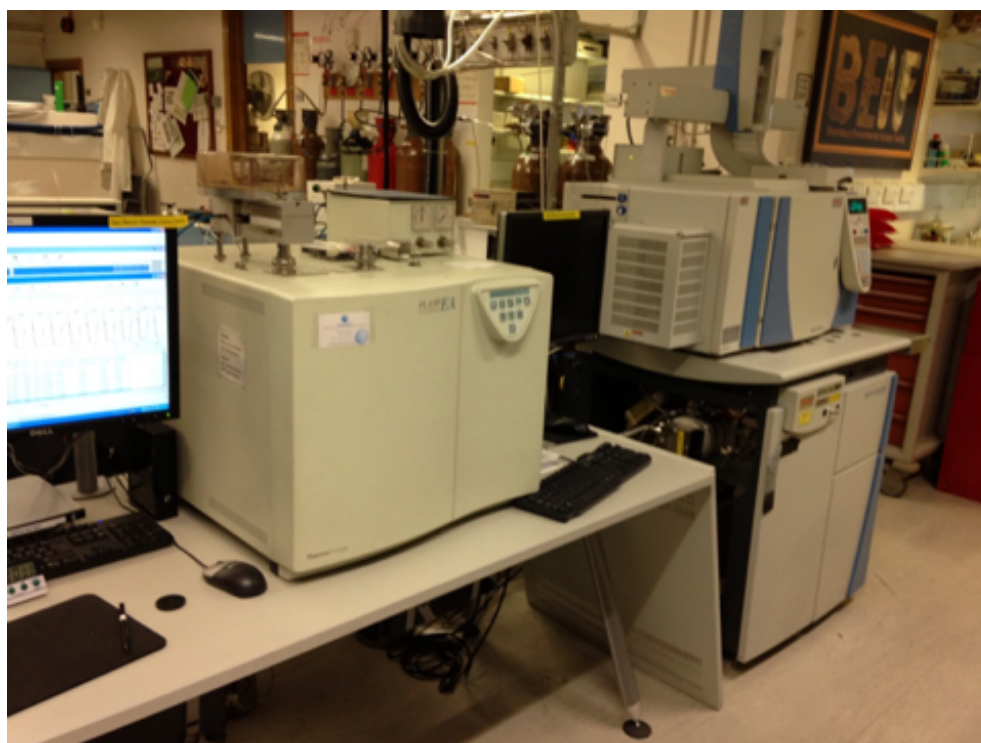


Figure A.5: Image of the EA-IRMS analysis equipment installed in the Bloomsbury Environmental Isotope Facility (BEIF). Consisting of a Thermo Flash EA, 1112 series elemental analyser, coupled to Thermo Finnigan, Delta V IRMS.



Figure A.6: Operation of the liquid/gas injection port, installed onto the EA-IRMS.

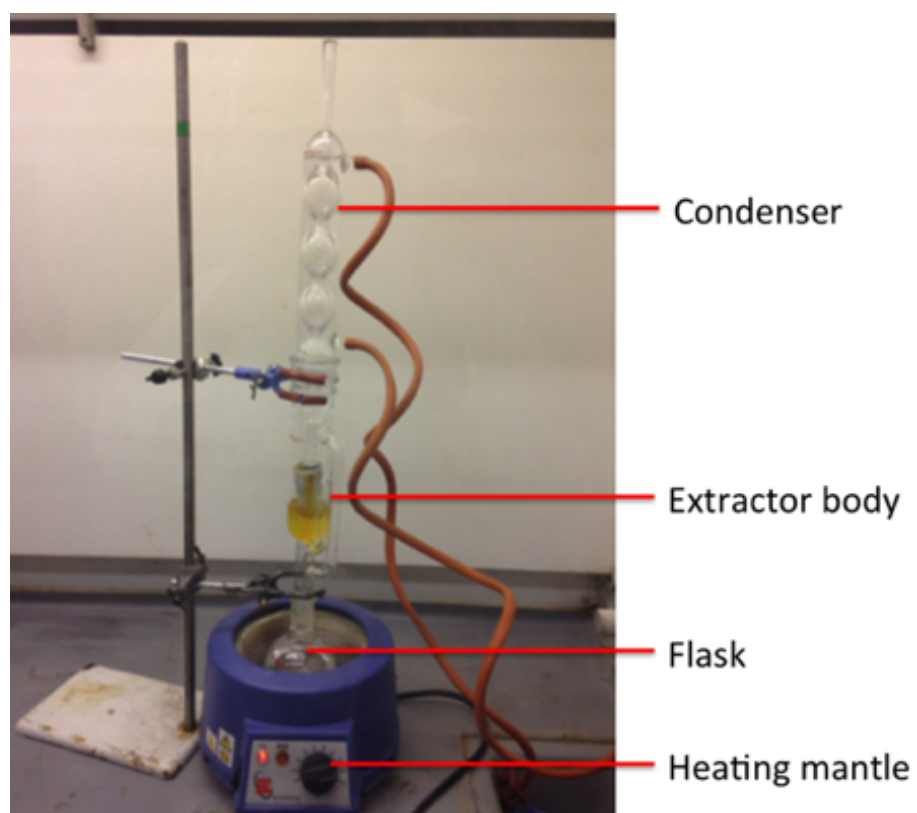
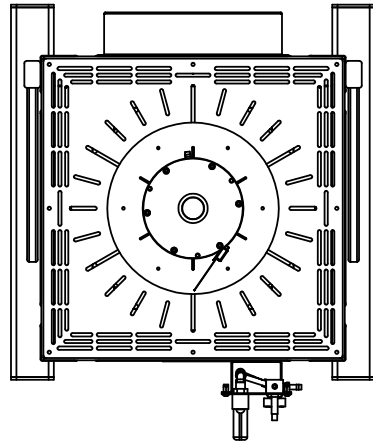
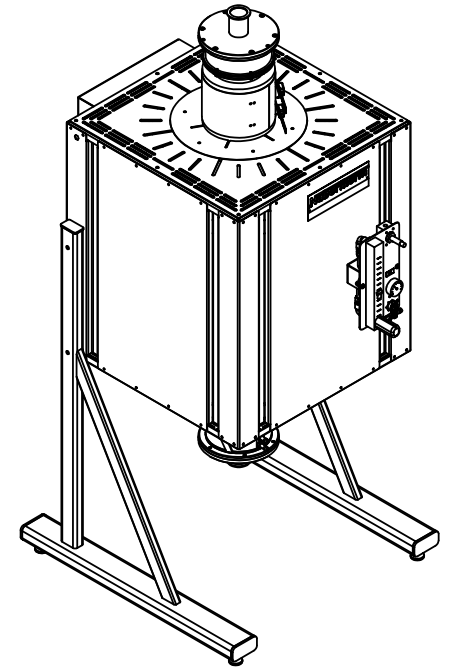
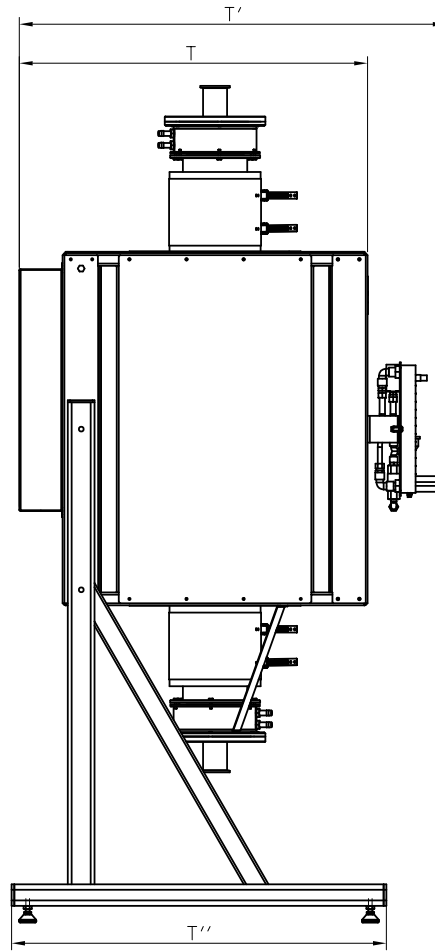
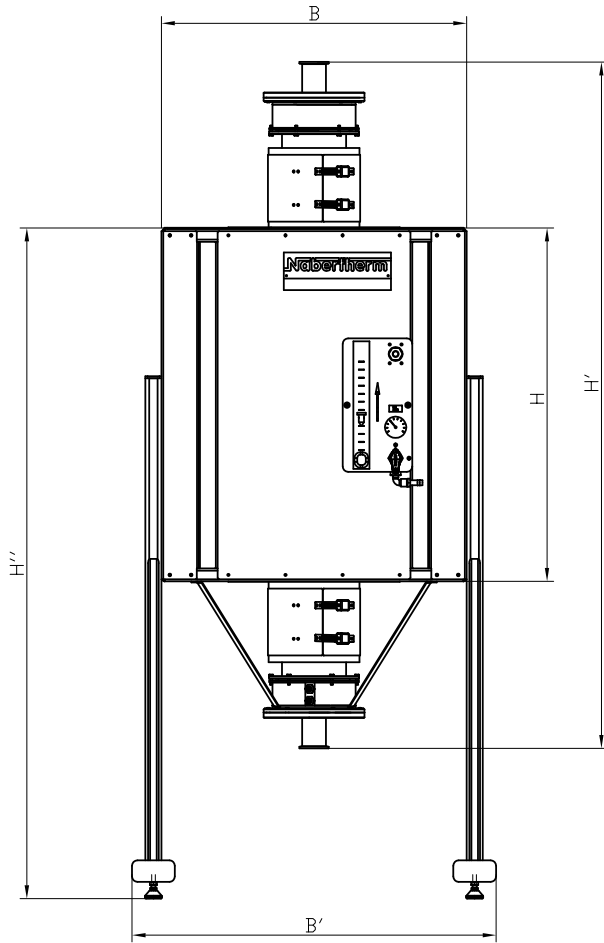


Figure A.7: Setup for soxhlet extraction.

Technische Änderungen vorbehalten! Weitergabe, sowie Vervielfältigung dieser Unterlage, Verwertung und Mitteilung ihres Inhalts nicht gestattet!



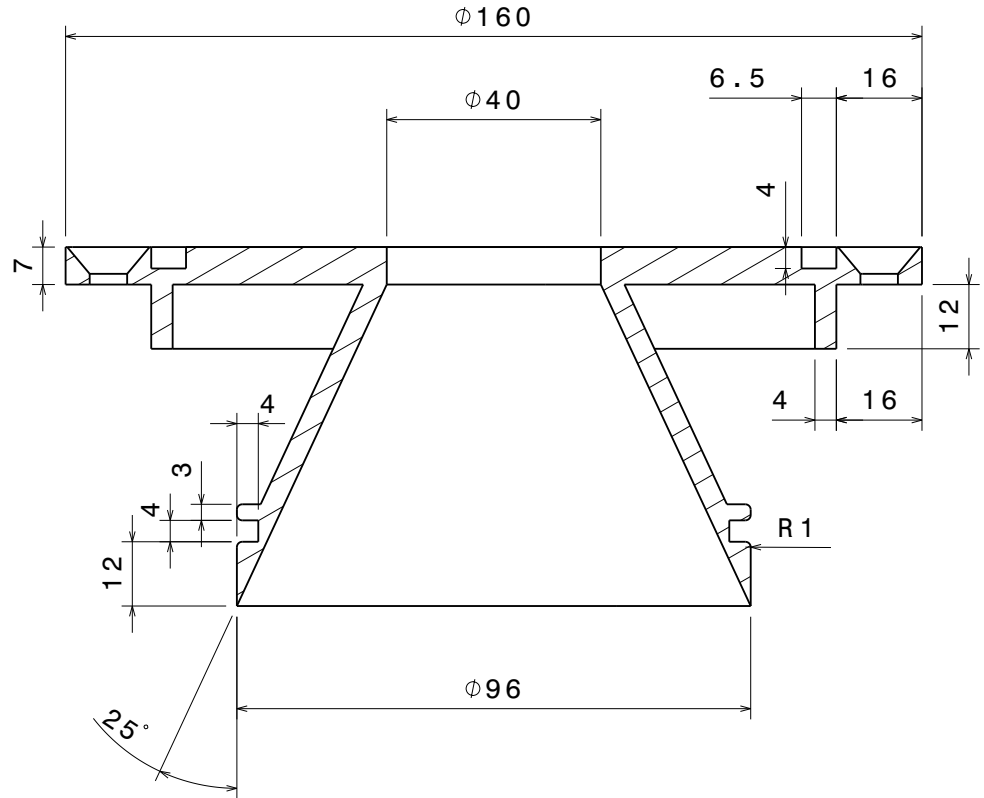
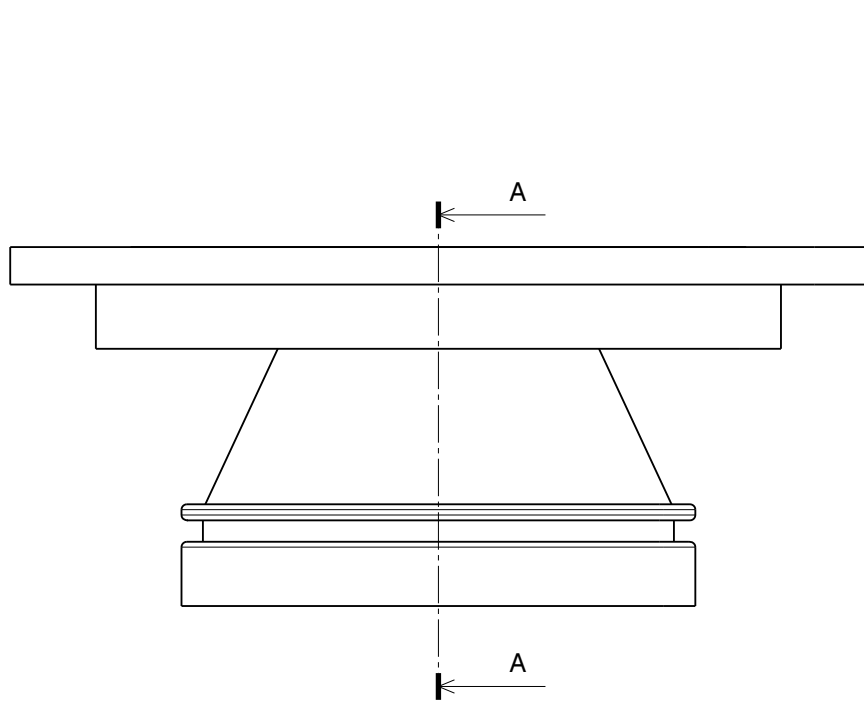
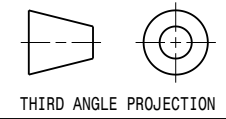
Modell	beh. Länge [mm]	H [mm]	H' [mm]	H'' [mm]	B [mm]	B' [mm]	T [mm]	T' [mm]	T'' [mm]
RHTV 120-150	150	510	1130	1100	570	680	650	800	700
RHTV 120-300	300	660	1280	1250	570	680	650	800	700
RHTV 120-600	600	960	1580	1550	570	680	650	800	700

X' gilt für Öfen mit Begasung und Vakuumflanschen

X'' gilt für Öfen mit Vertikalgestell


Verantwortlicher: F + E		Allgemein- toleranz ISO 2768-m		Maßstab 1:10	
Originalablage:		Datum		Fa. Nabertherm 28865 Lilienthal	
		Bearb.	08.01.2007	Name	D. Meyer
		Gepr.	08.01.2007		W. Bartilla
		Ers. f.		RHTV 120-.../...	
		Ers. d.		Maßblatt	
				Nabertherm	
Zust.	Änderung	Datum	Name	Blatt 1 von 1	
				DIN A3 DWG	

Outlet Cone - Front View



Front view
Scale: 1:1

Section view A-A
Scale: 1:1

Title		Outlet Cone		Date	30/10/2012	Drawn by	Aaron Eveleigh				
Dwg. No.		1 of 2		eveleigh.a@gmail.com							
Matl.		Stainless Steel									
Heat Treat.		N/A									
Surface Finish		N/A									
Scale	1:1	Size	A3					Sheet	1 of 1	Qty per Assembly	1
3. GENERAL FINISH $\sqrt{3}$ REMOVE BURRS & LIGHTLY BREAK SHARP EDGES											

GENERAL TOLERANCES:	
LINEAR AND RADIAL	0.00 ±0.05 0.0 ±0.2 0 ±0.5
ANGULAR	±1°

NOTES: UNLESS OTHERWISE STATED	
1.	ALL DIMENSIONS ARE IN MILLIMETRES (mm)
2.	THREADS: ISO COARSE TO CLASS 6H/6g U.O.S
3.	GENERAL FINISH $\sqrt{3}$ REMOVE BURRS & LIGHTLY BREAK SHARP EDGES
4.	DO NOT SCALE

1 2 3 4 5 6 7 8

A

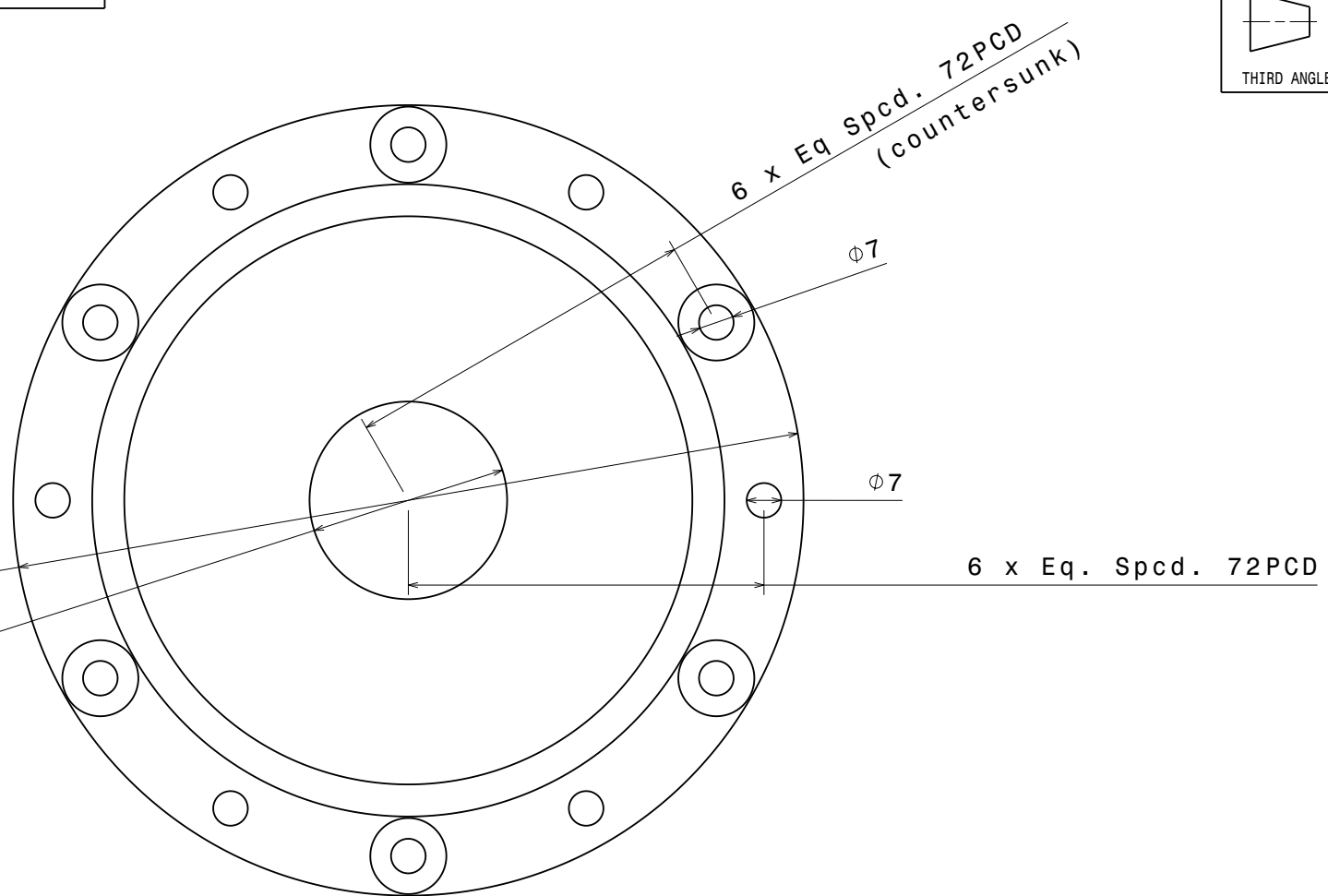
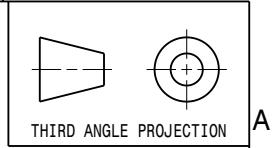
B

C

D

E

Outlet Cone- Top View



Top view
Scale: 1:1

Title		Outlet Cone		Date	30/10/2012	Drawn by	Aaron Eveleigh
Dwg. No.		2 of 2					
Matl.		Stainless Steel					
Heat Treat.		N/A					
Surface Finish		N/A					
Scale	1:1	Size	A3	Sheet	1 of 1	Qty per Assembly	1

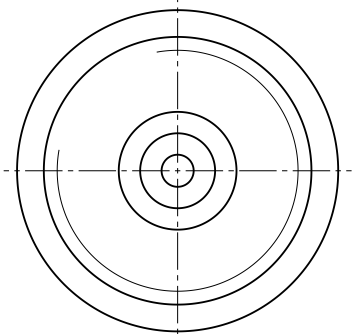
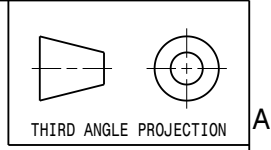
GENERAL TOLERANCES:

LINEAR AND RADIAL	0.00 ±0.05 0.0 ±0.2 0 ±0.5
ANGULAR	±1°

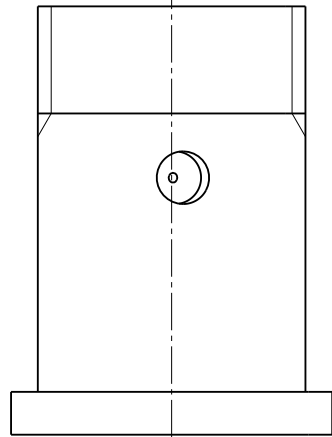
NOTES: UNLESS OTHERWISE STATED

- ALL DIMENSIONS ARE IN MILLIMETRES (mm)
- THREADS: ISO COARSE TO CLASS 6H/6g U.O.S
- GENERAL FINISH $\sqrt{}$ REMOVE BURRS & LIGHTLY BREAK SHARP EDGES
- DO NOT SCALE

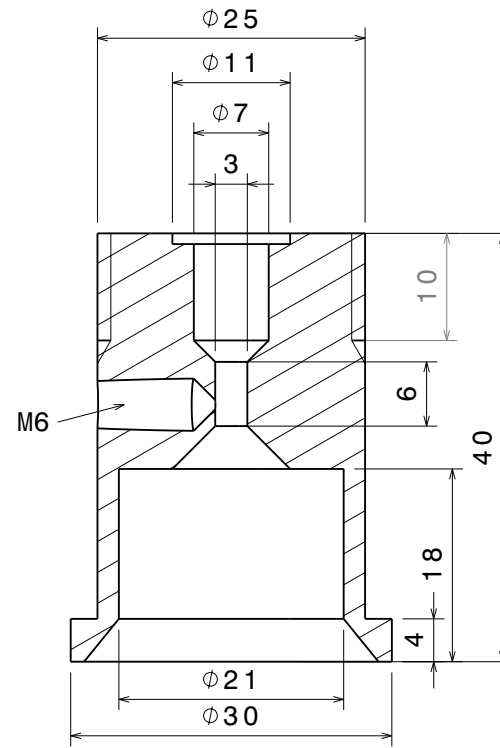
EA- Injector block and lid



Top view
Scale: 2:1



Front view
Scale: 2:1



Section view A-A
Scale: 2:1

Title				Injector block		Date	22/08/14	Drawn by	Aaron Eveleigh
Dwg. No.				1 of 2		Department of Mechanical Engineering University College London Torrington Place London WC1E 7JE			
Matl.				Stainless steel (316)		aaron.eveleigh.10@ucl.ac.uk www.mecheng.ucl.ac.uk			
Heat Treat.				N/A					
Surface Finish				N/A					
Scale	1:1	Size	A3	Sheet	1 of 2	Qty per Assembly	1		

GENERAL TOLERANCES:	
LINEAR AND RADIAL	0.00 ±0.05 0.0 ±0.2 0 ±0.5
ANGULAR	±1°

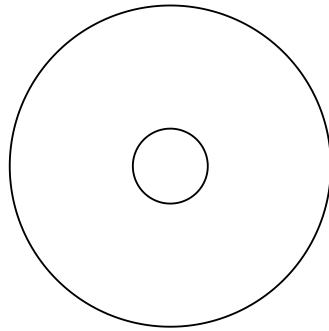
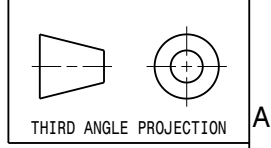
NOTES: UNLESS OTHERWISE STATED	
1.	ALL DIMENSIONS ARE IN MILLIMETRES (mm)
2.	THREADS: ISO COARSE TO CLASS 6H/6g U.O.S
3.	GENERAL FINISH $\sqrt{3}$ REMOVE BURRS & LIGHTLY BREAK SHARP EDGES
4.	DO NOT SCALE

A
B
C
D
E

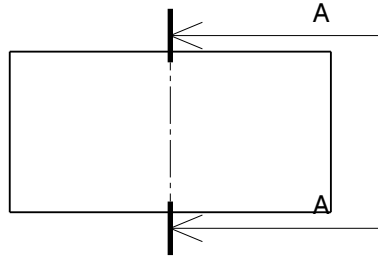
A
B
C
D
E

1 2 3 4 5 6 7 8

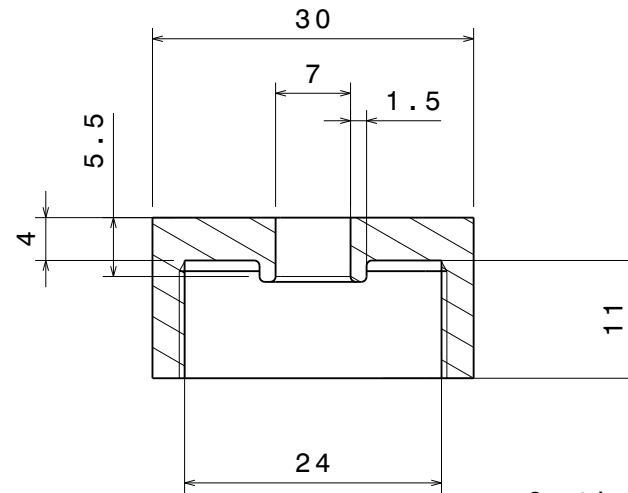
EA- Injector block and lid



Top view
Scale: 2:1



Front view
Scale: 2:1



Section view A-A
Scale: 2:1

Note: Knurling applied to external surface of lid.

Title		Injector lid			Date	22/08/14	Drawn by	Aaron Eveleigh
Dwg. No.		2 of 2			Department of Mechanical Engineering University College London Torrington Place London WC1E 7JE			
Matl.		Stainless steel (316)			aaron.eveleigh.10@ucl.ac.uk www.mecheng.ucl.ac.uk			
Heat Treat.		N/A			Scale 1:1			
Surface Finish		N/A			Size A3			
Scale		1:1			Sheet 2 of 2			
Qty per Assembly		1						

GENERAL TOLERANCES:	
LINEAR AND RADIAL	0.00 ±0.05 0.0 ±0.2 0 ±0.5
ANGULAR	±1°

NOTES: UNLESS OTHERWISE STATED	
1.	ALL DIMENSIONS ARE IN MILLIMETRES (mm)
2.	THREADS: ISO COARSE TO CLASS 6H/6g U.O.S
3.	GENERAL FINISH $\sqrt{3}$ REMOVE BURRS & LIGHTLY BREAK SHARP EDGES
4.	DO NOT SCALE

Appendix B

Supplementary experimental data

Table B.1: Measured $\delta^{13}\text{C}$ values, and calculated parameters for PM formed in a laminar flow reactor at 1300°C.

Fuel ID	Lambda (λ)	$\delta^{13}\text{C}$ Fuel	σ	$\delta^{13}\text{C}$ PM	σ	$\Delta(\text{F})$	$\Delta(\text{PM})$	Δ_{max}	F	%
Oleic acid native	0	-31.66	0.08	-34.65	0.01	27.17	1.16	489.09	0.00	0.24
Oleic acid-1- ^{13}C	0	-4.49	0.16	-33.49	0.09	12.65	14.30	113.84	0.13	12.56
Oleic acid-9,10- ^{13}C	0	-19.01	0.26	-20.34	0.13	31.16	28.45	31.16	0.91	91.28
Oleic acid $^{13}\text{C}18$	0	-0.50	0.38	-6.20	0.12					
Methyl oleate native	0	-32.06	0.23	-34.94	0.05					
Methyl oleate 1- ^{13}C	0	-7.69	0.40	-34.60	0.08	24.37	0.35	463.12	0.00	0.07
Oleic acid native	0.1	-31.66	0.08	-30.80	0.06					
Oleic acid-1- ^{13}C	0.1	-4.49	0.16	-30.57	0.02	27.17	0.24	489.09	0.00	0.05
Oleic acid-9,10- ^{13}C	0.1	-19.01	0.26	-18.18	0.05	12.65	12.62	113.84	0.11	11.09
Oleic acid- $^{13}\text{C}18$	0.1	-0.50	0.38	-2.43	0.07	31.16	28.37	31.16	0.91	91.04
Methyl oleate native	0.1	-32.06	0.23	-32.39	0.02					
Methyl oleate-1- ^{13}C	0.1	-7.69	0.40	-32.96	0.25	24.37	-0.57	463.12	0.00	-0.12
Oleic acid native	0.2	-31.66	0.08	-27.24	0.06					
Oleic acid-1- ^{13}C	0.2	-4.49	0.16	-27.57	0.01	27.17	3.23	489.09	0.01	0.66
Oleic acid-9,10- ^{13}C	0.2	-19.01	0.26	-15.72	0.02	12.65	15.08	113.84	0.13	13.25
Oleic acid $^{13}\text{C}18$	0.2	-0.50	0.38	1.03	0.15	31.16	28.26	31.16	0.91	90.70
Methyl oleate native	0.2	-32.06	0.23	-29.67	0.02					
Methyl oleate-1- ^{13}C	0.2	-7.69	0.40	-29.76	0.10	24.37	-0.09	463.12	0.00	-0.02

Table B.2: Measured $\delta^{13}\text{C}$ values, and calculated parameters for PM formed in a diesel engine.

Fuel type	$\delta^{13}\text{C}$ Fuel	$\delta^{13}\text{C}$ PM	Δ_F	Δ_{PM}	Δ_{max}	F	%
Oleic acid native (B1)	-31.66	-28.92	-	-	-	-	-
Oleic acid-9,10- $^{13}\text{C}2$ (B1)	-19.01	-16.73	12.65	12.20	113.84	0.11	10.71
Oleic acid- $^{13}\text{C}18$ (B1)	-0.50	-1.70	31.16	27.23	31.16	0.87	87.37
Oleic acid native (B2)	-31.37	-28.59	-	-	-	-	-
Oleic acid-1- ^{13}C (B2)	-3.54	-19.93	27.83	8.66	500.86	0.02	1.73
Oleic acid native Baked (B1)	-31.66	-28.51	-	-	-	-	-
Oleic acid-9,10- $^{13}\text{C}2$ Baked (B1)	-19.01	-15.95	12.65	12.56	113.84	0.11	11.03
Oleic acid- $^{13}\text{C}18$ Baked (B1)	-0.50	-1.03	31.16	27.48	31.16	0.88	88.18
Oleic acid native Baked (B2)	-31.37	-28.89	-	-	-	-	-
Oleic acid-1- ^{13}C Baked (B2)	-3.54	-28.58	27.83	0.31	500.86	0.00	0.06
Methyl oleate native	-32.06	-28.76	-	-	-	-	-
Methyl oleate-1- ^{13}C	-7.69	-25.62	24.37	3.14	463.12	0.01	0.68
Methyl oleate native Baked	-32.06	-29.12	-	-	-	-	-
Methyl oleate-1- ^{13}C Baked	-7.69	-28.88	24.37	0.24	463.12	0.00	0.05

Table B.3: Measured $\delta^{13}\text{C}$ values, and calculated parameters for PM formed from binary mixtures of ethanol-in-heptane, in the flow reactor and diesel engine.

Fuel type	$\delta^{13}\text{C}_{Fuel}$	σ	$\delta^{13}\text{C}_{PM}$	σ	ΔF	ΔPM	$\Delta PM/\Delta F$	F	%	σ
Flow reactor										
(Liq)Heptane+Ethanol10Mol%	-27.2	0.14	-	-	-	-	-	-	-	-
Heptane+Ethanol10MOL%	-	-	-31.25	0.1	-	-	-	-	-	-
Heptane+Ethanol10MOL% +Ethanol-1,2- ¹³ C ₂	2.88	0.1	-8.33	0.1	30.08	22.92	0.76	0.024	2.362	1.465
Heptane+Ethanol10MOL% +Ethanol-1- ¹³ C	5.38	0.1	-12.52	0.1	32.58	18.73	0.570	8.999	0.89	1.362
Heptane+Ethanol10MOL% +Ethanol-1- ¹³ C	5.38	0.1	-12.73	0.1	32.58	18.53	0.570	0.01	0.881	1.362
Heptane+Ethanol10MOL% +Ethanol-1- ¹³ C	5.38	0.1	-12.62	0.1	32.58	18.63	0.570	0.01	0.886	1.362
Heptane+Ethanol10MOL% +Ethanol-2- ¹³ C	6.29	0.01	2.27	0.1	33.49	33.520	1	0.01	1.54	1.065
Diesel engine										
(E)Heptane+Ethanol10MOL%	-	-	-25.37	0.1	-	-	-	-	-	-
(E)Heptane+Ethanol10MOL% +Ethanol-1,2- ¹³ C ₂	2.88	0.1	-17.14	0.81	30.08	8.23	0.27	0.01	0.86	1.15
(E)Heptane+Ethanol10MOL% +Ethanol-1,2- ¹³ C ₂ (2)	2.88	0.1	-16.04	0.81	30.08	9.33	0.31	0.01	0.975	1.15
(E)Heptane+Ethanol10MOL% +Ethanol-1- ¹³ C	5.38	0.1	-19.97	0.81	32.58	5.4	0.17	0.01	0.259	1.16
(E)Heptane+Ethanol10MOL% +Ethanol-1- ¹³ C (1)	5.38	0.1	-20.6	0.81	32.58	4.78	0.15	2E-3	0.23	1.156
(E)Heptane+Ethanol10MOL% +Ethanol-2- ¹³ C (2)	6.29	0.01	-13.29	0.81	33.49	12.09	0.36	0.01	0.56	1.07
(E)Heptane+Ethanol10MOL% +Ethanol-2- ¹³ C (3)	6.29	0.01	-12.11	0.81	33.49	13.26	0.4	0.01	0.62	1.07
(E)Heptane+Ethanol10MOL% +Ethanol-2- ¹³ C	6.29	0.01	-11.73	0.81	33.49	13.65	0.41	0.01	0.63	1.07

Table B.4: Measured $\delta^{13}\text{C}$ values, and calculated parameters for PM formed from binary mixtures of 1-propanol or 2-propanol-in-heptane, in the flow reactor and diesel engine.

Fuel type	$\delta^{13}\text{C}_{Fuel}$	σ	$\delta^{13}\text{C}_{PM}$	σ	ΔF	Δ_{PM}	$\Delta_{PM}/\Delta F$	F	%	σ
Flow reactor										
Heptane+1-propanol10%	-34.18	0.03	-37.61	0.13	28.51	21.53	0.76	0.03	3.47	0.07
Heptane+1-propanol10% +1-propanol- $^{13}\text{C}_3$	-5.67	0.11	-16.07	0.13	32.94	13.57	0.41	0.01	0.65	0.03
Heptane+1Propanol10% +1-propanol- ^{13}C	-1.24	0.25	-24.04	0.13	29.06	24.01	0.83	0.04	3.79	0.14
Heptane+2Propanol10%	-34.08	0.03	-36.16	0.13	32.05	20.53	0.64	0.01	1.01	0.03
Heptane+2Propanol10% +2propanol- $^{13}\text{C}_3$	-5.02	0.58	-12.16	0.13						
Heptane+2Propanol10% +2propanol-2- ^{13}C	-2.03	0.22	-15.64	0.13						
Diesel engine										
(E)Heptane+1-propanol10%Mol	-34.18	0.03	-28.04	0.13	28.51	5.97	0.21	0.01	0.99	0.07
(E)Heptane+1-propanol10%Mol +1-propanol- $^{13}\text{C}_3$	-5.67	0.11	-22.07	0.13	32.94	2.87	0.09	0.00	0.14	0.03
(E)Heptane+1-propanol10%Mol +1-propanol-1- ^{13}C	-1.24	0.25	-25.17	0.13	29.06	6.23	0.21	0.01	1.01	0.05
(E)Heptane+2-propanol10%Mol	-34.08	0.03	-27.96	0.13	32.05	3.05	0.10	0.00	0.15	0.03
(E)Heptane+2-propanol10%Mol +2-propanol- $^{13}\text{C}_3$	-5.02	0.58	-21.73	0.13						
(E)Heptane+2-propanol10%Mol +2-propanol-2- ^{13}C	-2.03	0.22	-24.91	0.13						

Table B.5: Measured $\delta^{13}\text{C}$ values, and calculated parameters for PM formed from binary mixtures of acetone-in-heptane, in the flow reactor and diesel engine .

Fuel type	$\delta^{13}\text{C}_{Fuel}$	σ	$\delta^{13}\text{C}_{PM}$	σ	Δ_F	Δ_{PM}	Δ_{PM}/Δ_F	F	%	σ
Flow reactor										
Heptane+Acetone10%	-25.62	0.07	-29.12	0.13	24.71	16.51	0.67	0.03	3.08	0.07
heptane+acetone10% +Acetone- $^{13}\text{C}_3$	-0.91	0.00	-12.61	0.13	24.71	16.51	0.67	0.03	3.08	0.07
Heptane+acetone10% +Acetone-2- ^{13}C	0.89	0.14	-28.99	0.13	26.51	0.13	0.01	0.00	0.01	0.03
Diesel engine										
(E)Heptane+Acetone10%Mol	-25.62	0.07	-25.69	0.50	24.71	5.75	0.23	0.01	1.10	0.21
(E)Heptane+Acetone10%Mol +Acetone- $^{13}\text{C}_3$	-0.91	0.00	-19.94	0.50	24.71	5.75	0.23	0.01	1.10	0.21
(E)Heptane+Acetone10%Mol +Acetone-2- ^{13}C	0.89	0.14	-25.34	0.50	26.51	0.35	0.01	0.00	0.06	0.21

Table B.6: Measured $\delta^{13}\text{C}$ values, and calculated parameters for PM formed from binary mixtures of ethyl acetate-in-heptane, in the flow reactor and diesel engine.

Fuel type	$\delta^{13}\text{C}_{Fuel}$	σ	$\delta^{13}\text{C}_{PM}$	σ	Δ_F	Δ_{PM}	Δ_{PM}/Δ_F	F	%	σ
Flow reactor										
Heptane+EthylAcetate10%	-25.86	0.04	-29.07	0.13						
Heptane+EthylAcetate10% +Ethyl acetete-1-13C	1.08	0.01	-29.22	0.13	26.94	-0.16	-0.01	0.00	-0.01	0.50
Diesel engine										
(E)Heptane+EA10%Mol	-25.86	0.04	-25.82	0.13						
(E)Heptane+EA10%Mol +Ethyl acetete-1-13C	1.08	0.01	-25.80	0.13	26.94	0.02	0.00	0.00	0.00	0.50

Table B.7: Measured $\delta^{13}\text{C}$ values, and calculated parameters for PM formed from binary mixtures of toluene-in-heptane, in the flow reactor and diesel engine.

Fuel type	$\delta^{13}\text{C}_{Fuel}$	σ	$\delta^{13}\text{C}_{PM}$	σ	Δ_F	Δ_{PM}	Δ_{PM}/Δ_F	F	%	σ
Heptane+Toluene10MOL%	-28.38	0.04	-31.60	0.13	25.34	32.43	1.28	0.11	10.71	0.12
Heptane+Toluene10MOL% +Toluene- $^{13}\text{C}_6$	-3.03	0.02	0.83	0.13	25.34	32.43	1.28	0.11	10.71	0.12
Heptane+Toluene10MOL% +Toluene-1- ^{13}C	-3.17	0.09	-3.56	0.13	25.21	28.05	1.11	0.02	1.59	0.14
Diesel engine										
(E)Heptane+Toluene10mol%	-28.38	0.04	-25.29	0.20	25.06	13.81	0.55	0.06	5.77	0.19
(E)Heptane+Toluene10mol% +Toluene- $^{13}\text{C}_7$	-3.31	0.08	-11.48	0.20	25.06	13.81	0.55	0.06	5.77	0.19
(E)Heptane+Toluene10mol% +Toluene-1- ^{13}C	-3.17	0.09	-15.78	0.20	25.21	9.51	0.38	0.01	0.54	0.19
(E)Heptane+Toluene10mol% +Toluene-p- $^{13}\text{C}_6$	-3.03	0.02	-9.19	0.20	25.34	16.10	0.64	0.06	5.62	0.19

Table B.8: Engine exhaust emissions, as measured by the Horiba MEXA9100 HEGR instrument.

Fuel	CO (ppm)	SD	CO₂ (%)	SD	O₂ (%)	SD	THC (ppm)	SD	NOx (ppm)	SD
Reference diesel	283.92	7.70	5.50	0.03	13.18	0.09	78.04	33.45	546.41	12.34
Heptane	287.59		5.15		13.21		513.65		568.96	
Heptane + acetone	269.32	10.60	5.07	0.02	13.32	0.01	245.28	6.13	570.61	4.69
Heptane + ethyl acetate	261.40	3.94	5.14	0.05	13.36	0.02	237.31	5.91	571.97	5.09
Heptane + 1-propanol	278.47	1.85	5.14	0.03	13.23	0.06	311.17	6.63	578.93	8.34
Heptane + 2-propanol	274.87	4.76	5.12	0.02	13.22	0.03	299.44	7.08	573.50	6.06
Heptane + ethanol	278.35	9.52	5.12	0.03	13.33	0.05	266.03	7.09	593.95	6.79
Heptane + toluene	288.99	4.32	5.20	0.02	13.29	0.04	506.83	12.45	605.34	6.04

Bibliography

2010. Euro 5 and euro 6 standards: reduction of pollutant emissions from light vehicles.
2012. Co2 emissions from fuel combustion highlights. Technical report, International Energy Agency.
- Abbass, M., G. Andrews, P. Williams, K. Bartle, I. Davies, and L. Tanui
1988. Diesel particulate emissions: pyrosynthesis of pah from hexadecane. *SAE Technical Paper 880345*.
- Abu-Zaid, M.
2004. Performance of single cylinder, direct injection diesel engine using water fuel emulsions. *Energy Conversion and Management*, 45(5):697–705.
- Adamson, I. Y. R., H. Frieditis, and R. Vincent
1999. Pulmonary toxicity of an atmospheric particulate sample is due to the soluble fraction. *Toxicology and Applied Pharmacology*, 157(1):43–50.
- Alexiou, A. and A. Williams
1995. Soot formation in shock-tube pyrolysis of toluene-n-heptane and toluene-isooctane mixtures. *Fuel*, 74(2).
- Anderson, J., B. Giechaskiel, R. Munoz-Bueno, and P. Dilara
2007. Particle measurement programme (pmp) light-duty inter-laboratory correlation exercise final report. <http://www.unece.org/fileadmin/DAM/trans/doc/2007/wp29grpe/PMP-2007-18-02e.pdf>.
- Andreae, M. and A. Gelencsér
2006. Black carbon or brown carbon? the nature of light-absorbing carbonaceous aerosols. *Atmospheric Chemistry and Physics*, 6(10):3131–3148.
- Andrews, G. E., M. K. Abbass, S. A. Haleem, Y. Shen, P. T. Williams, and K. D. Bartle
1991. The determination of the lubricating oil fraction of diesel particulates. *Journal of Aerosol Science*, 22, Supplement 1:S459–S462.

- Andrews, G. E., M. K. Abbass, P. T. Williams, and K. D. Bartle
1989. Factors influencing the composition of the organic fraction of diesel particulates. *Journal of Aerosol Science*, 20(8):1373–1376.
- Andrews, G. E., R. Ishaq, J. Farrar-Khan, Y. Shen, and P. Williams
1998. The influence of speciated diesel fuel composition on speciated particulate soot emissions. *SAE Technical Paper 980527*.
- Aronowitz, D., D. W. Naegeli, and I. Glassman
1977. Kinetics of the pyrolysis of methanol. *The Journal of Physical Chemistry*, 81(25):2555–2559.
- Barnaud, F., P. Schmelzle, and P. Schulz
2000. AquazoleTM: An original emulsified water-diesel fuel for heavy-duty applications. *SAE Technical Paper 2000-01-1861*.
- Barrientos, E. J., M. Lapuerta, and A. Boehman
2013. Group additivity in soot formation for the example of c-5 oxygenated hydrocarbon fuels. *Combustion and Flame*, 160(8):1484–1498.
- Bartok, W. and A. F. Sarofim
1991. Fossil fuel combustion: a source book.
- Benson, S. W. and J. H. Buss
1958. Additivity rules for the estimation of molecular properties. thermodynamic properties. *The Journal of Chemical Physics*, 29(3):546–572.
- Binder, J. B., M. J. Gray, J. F. White, Z. C. Zhang, and J. E. Holladay
2009. Reactions of lignin model compounds in ionic liquids. *Biomass and Bioenergy*, 33(9):1122–1130.
- Böhm, H., H. Jander, and D. Tanke
1998. PAH growth and soot formation in the pyrolysis of acetylene and benzene at high temperatures and pressures: Modeling and experiment. *Symposium (International) on Combustion*, 27(1):1605–1612.
- Bolton, J. L., M. A. Trush, T. M. Penning, G. Dryhurst, and T. J. Monks
2000. Role of quinones in toxicology. *Chemical Research in Toxicology*, 13(3):135–160.
Cited By (since 1996):802 Export Date: 6 October 2014.
- Bond, T. C., S. J. Doherty, D. W. Fahey, P. M. Forster, T. Berntsen, B. J. DeAngelo, M. G. Flanner, S. Ghan, B. Kärcher, D. Koch, S. Kinne, Y. Kondo, P. K. Quinn, M. C. Sarofim, M. G. Schultz, M. Schulz, C. Venkataraman, H. Zhang, S. Zhang, N. Bellouin, S. K. Guttikunda, P. K. Hopke, M. Z. Jacobson, J. W. Kaiser, Z. Klimont, U. Lohmann, J. P. Schwarz, D. Shindell, T. Storelvmo, S. G. Warren, and C. S. Zender
2013. Bounding the role of black carbon in the climate system: A scientific assessment. *Journal of Geophysical Research: Atmospheres*, 118(11):5380–5552.

- Botero, M. L., S. Mosbach, and M. Kraft
2014. Sooting tendency of paraffin components of diesel and gasoline in diffusion flames. *Fuel*, 126(0):8–15.
- Bowman, C. T.
1975. Kinetics of pollutant formation and destruction in combustion. *Progress in Energy and Combustion Science*, 1(1):33–45.
- Bryce, D., N. Ladommatos, Z. Xiao, H. Zhao, et al.
1999. Investigating the effect of oxygenated and aromatic compounds in fuel by comparing laser soot measurements in laminar diffusion flames with diesel-engine emissions. *Journal of the Institute of Energy*, 72(156):150–156.
- Buchholz, B. A., A. Cheng, and R. Dibble
2002. Isotopic tracing of bio-derived carbon from ethanol-in-diesel blends in the emissions of a diesel engine. *SAE Technical Reports 2002-01-1704*, Pp. 37–46.
- Buchholz, B. A., R. W. Dibble, D. Rich, and A. Cheng
2003. Quantifying the contribution of lubrication oil carbon to particulate emissions from a diesel engine. *SAE Technical Paper 2003-01-1987*.
- Buchholz, B. A., C. J. Mueller, A. Upatnieks, G. C. Martin, W. J. Pitz, and C. K. Westbrook
2004. Using carbon-14 isotope tracing to investigate molecular structure effects of the oxygenate dibutyl maleate on soot emissions from a di diesel engine. *SAE Transactions 2004-01-1849*.
- Busby Jr, W. F., H. Smith, C. L. Crespi, B. W. Penman, and A. L. Lafleur
1997. Mutagenicity of the atmospheric transformation products 2-nitrofluoranthene and 2-nitrodibenzopyranone in salmonella and human cell forward mutation assays. *Mutation Research/Genetic Toxicology and Environmental Mutagenesis*, 389(2–3):261–270.
- Calcote, H. and D. Manos
1983. Effect of molecular structure on incipient soot formation. *Combustion and Flame*, 49(1–3).
- Celnik, M., A. Raj, R. West, R. Patterson, and M. Kraft
2008. Aromatic site description of soot particles. *Combustion and Flame*, 155(1–2):161–180.
- CFR
2007. Code of federal regulations title 40, protection of environment, part 1065—engine testing.

- Cheng, A., R. W. Dibble, and B. A. Buchholz
2002. The effect of oxygenates on diesel engine particulate matter. *SAE Technical Paper 2002-01-1705*.
- Cheng, A. S.-T.
2002. *Effects of oxygenates blended with diesel fuel on particulate matter emissions from a compression-ignition engine*. PhD thesis, University of Berkeley.
- Choi, M., A. Hamins, G. W. Mulholland, and T. Kashiwagi
1994. Simultaneous optical measurement of soot volume fraction and temperature in premixed flames. *Combustion and flame*, 99(1):174–186.
- Choudhary, T. V. and C. B. Phillips
2011. Renewable fuels via catalytic hydrodeoxygenation. *Applied Catalysis A: General*, 397(1–2):1–12.
- Coda Zabetta, E., M. Hupa, and S. Niemi
2006. Bio-derived fuels may ease the regeneration of diesel particulate traps. *Fuel*, 85(17–18):2666–2670.
- Cole, J. A., J. D. Bittner, J. P. Longwell, and J. B. Howard
1984. Formation mechanisms of aromatic compounds in aliphatic flames. *Combustion and Flame*, 56(1):51–70.
- Colket, M. B. and D. J. Seery
1994. Reaction mechanisms for toluene pyrolysis. *Symposium (International) on Combustion*, 25(1):883–891.
- Colombo, B. and B. Tosi
1982. Sampler for analytical detection systems.
- Cooper, B. H. and B. B. L. Donnis
1996. Aromatic saturation of distillates: an overview. *Applied Catalysis A: General*, 137(2):203–223.
- Corso, T. and J. Brenna
1997. High-precision position-specific isotope analysis. *Proceedings of the National Academy of Sciences*, 94(4):1049–1053.
- Corso, T. N. and J. T. Brenna
1999. On-line pyrolysis of hydrocarbons coupled to high-precision carbon isotope ratio analysis. *Analytica Chimica Acta*, 397(1–3):217–224.
- Corso, T. N., B. A. Lewis, and J. T. Brenna
1998. Reduction of fatty acid methyl esters to fatty alcohols to improve volatility for isotopic analysis without extraneous carbon. *Analytical Chemistry*, 70(18):3752–3756.

Craig, H.

1957. Isotopic standards for carbon and oxygen and correction factors for mass-spectrometric analysis of carbon dioxide. *Geochimica et Cosmochimica Acta*, 12(1–2):133–149.

Criss, R.

1999. *Principles of Stable Isotope Distribution*. Oxford University Press, USA.

Curran, H. J., P. Gaffuri, W. J. Pitz, and C. K. Westbrook

1998. A comprehensive modeling study of n-heptane oxidation. *Combustion and Flame*, 114(1–2):149–177.

Dagaut, P., S. M. Sarathy, and M. J. Thomson

2009. A chemical kinetic study of n-butanol oxidation at elevated pressure in a jet stirred reactor. *Proceedings of the Combustion Institute*, 32(1):229–237.

Davidson, C. I., R. F. Phalen, and P. A. Solomon

2005. Airborne particulate matter and human health: A review. *Aerosol Science and Technology*, 39(8):737–749.

de Groot, P.

2008. *Handbook of Stable Isotope Analytical Techniques*. Elsevier Science.

Dec, J. E.

1997. A conceptual model of di diesel combustion based on laser-sheet imaging. *SAE Technical Paper 970873*, 2013:09–13.

Dhar, A., R. Kevin, and A. K. Agarwal

2012. Production of biodiesel from high-ffa neem oil and its performance, emission and combustion characterization in a single cylinder dici engine. *Fuel Processing Technology*, 97(0):118–129.

Dietz, W. A.

1967. Response factors for gas chromatographic analyses. *Journal of Chromatographic Science*, 5(2):68–71.

Dockery, D. W., C. A. Pope, X. Xu, J. D. Spengler, J. H. Ware, M. E. Fay, B. G. Ferris, and F. E. Speizer

1993. An association between air pollution and mortality in six u.s. cities. *New England Journal of Medicine*, 329(24):1753–1759.

Donaldson, K., X. Li, and W. MacNee

1998. Ultrafine (nanometre) particle mediated lung injury. *Journal of Aerosol Science*, 29(5):553–560.

Durrett, T. P., C. Benning, and J. Ohlrogge

2008. Plant triacylglycerols as feedstocks for the production of biofuels. *The Plant Journal*, 54(4):593–607.

Endo

2003. Mutagenicity of size-fractionated airborne particles collected with andersen low pressure impactor.

Esarte, C., Á. Millera, R. Bilbao, and M. U. Alzueta

2009. Gas and soot products formed in the pyrolysis of acetylene-ethanol blends under flow reactor conditions. *Fuel Processing Technology*, 90(4).

Eveleigh, A., N. Ladommatos, R. Balachandran, and A. Marca

2014. Conversion of oxygenated and hydrocarbon molecules to particulate matter using stable isotopes as tracers. *Combustion and Flame*, 161(11):2966–2974.

Ferguson, R. E.

1957. An isotopic tracer study of carbon formation in hydrocarbon flames. *Combustion and Flame*, 1(4):431–437.

Fiala, J., B. Denby, J. Horálek, P. Kurfürst, P. de Smet, F. de Leeuw, and A. Lükewille

2009. Spatial assessment of pm10 and ozone concentrations in europe (2005). Report, EEA Technical report.

Font, R., I. Aracil, A. Fullana, I. Martn-Gullón, and J. A. Conesa

2003. Semivolatile compounds in pyrolysis of polyethylene. *Journal of Analytical and Applied Pyrolysis*, 68–69(0):599–611.

Frampton, M. W., M. J. Utell, W. Zareba, G. Oberdörster, C. Cox, L.-S. Huang, P. E.

Morrow, F. E.-H. Lee, D. Chalupa, L. M. Frasier, D. M. Speers, and J. Stewart
2004. Effects of exposure to ultrafine carbon particles in healthy subjects and subjects with asthma. *Research report (Health Effects Institute)*, (126):1–47; discussion 49–63.

Frassoldati, A., A. Cuoci, T. Faravelli, U. Niemann, E. Ranzi, R. Seiser, and K. Seshadri

2010. An experimental and kinetic modeling study of n-propanol and iso-propanol combustion. *Combustion and Flame*, 157(1):2–16.

Frenklach, M.

1989. On the driving force of pah production. *Symposium (International) on Combustion*, 22(1):1075–1082.

Frenklach, M.

2002. Reaction mechanism of soot formation in flames. *Physical Chemistry Chemical Physics*, 4(11).

Frenklach, M., M. K. Ramachandra, and R. A. Matula

1985. Soot formation in shock-tube oxidation of hydrocarbons. *Symposium (International) on Combustion*, 20(1):871–878.

Frenklach, M. and H. Wang

1991. Detailed modeling of soot particle nucleation and growth. *Symposium (International) on Combustion*, 23(1).

- Gan, S., H. K. Ng, and K. M. Pang
2011. Homogeneous charge compression ignition (hcci) combustion: Implementation and effects on pollutants in direct injection diesel engines. *Applied Energy*, 88(3):559–567.
- Gill, R. J. and D. B. Olson
1984. Estimation of soot thresholds for fuel mixtures. *Combustion Science and Technology*, 40(5-6):307–315.
- Gowers, A., B. Miller, and J. Stedman
2014. *Estimating local mortality burdens associated with particulate air pollution*.
- Graham, D. Y. and P. D. Klein
2000. Accurate diagnosis of helicobacter pylori: 13c-urea breath test. *Gastroenterology Clinics of North America*, 29(4).
- Gu, X., Z. Huang, J. Cai, J. Gong, X. Wu, and C.-f. Lee
2012. Emission characteristics of a spark-ignition engine fuelled with gasoline-n-butanol blends in combination with egr. *Fuel*, 93:611–617.
- Gülder, Ö. L., B. Glavinčevski, and M. F. Baksh
1990. Fuel molecular structure and flame temperature effects on soot formation in gas turbine combustors. *Journal of Engineering for Gas Turbines and Power*, 112(1):52–59.
- Hansen, A. C., Q. Zhang, and P. W. L. Lyne
2005. Ethanol–diesel fuel blends –a review. *Bioresource Technology*, 96(3):277–285.
- Harrison, R. M.
1996. Airbourne particulate matter in the united kingdom, third report of the quality of urban air review group. *The University of Birmingham, Edgbaston, England*.
- Harrison, R. M. and J. Yin
2000. Particulate matter in the atmosphere: which particle properties are important for its effects on health? *Science of The Total Environment*, 249(1–3):85–101.
- Haynes, B. and H. Wagner
1981. Soot formation. *Progress in Energy and Combustion Science*, 7(4).
- Heeb, N. V., P. Schmid, M. Kohler, E. Gujer, M. Zennegg, D. Wenger, A. Wichser, A. Ulrich, U. Gfeller, P. Honegger, K. Zeyer, L. Emmenegger, J.-L. Petermann, J. Czerwinski, T. Mosimann, M. Kasper, and A. Mayer
2008. Secondary effects of catalytic diesel particulate filters: Conversion of pahs versus formation of nitro-pahs. *Environmental Science & Technology*, 42(10):3773–3779.
- Hellier, P., L. Al-Haj, M. Talibi, S. Purton, and N. Ladommatos
2013a. Combustion and emissions characterization of terpenes with a view to their biological production in cyanobacteria. *Fuel*, 111(0):670–688.

- Hellier, P., N. Ladommatos, R. Allan, S. Filip, and J. Rogerson
2013b. The importance of double bond position and cis–trans isomerisation in diesel combustion and emissions. *Fuel*, 105:477–489.
- Hellier, P., N. Ladommatos, R. Allan, and J. Rogerson
2011. Influence of fatty acid ester alcohol moiety molecular structure on diesel combustion and emission. *Energy Fuels*.
- Hellier, P., N. Ladommatos, R. Allan, and J. Rogerson
2013c. Combustion and emissions characteristics of toluene/n-heptane and 1-octene/n-octane binary mixtures in a direct injection compression ignition engine. *Combustion and Flame*, 160(10):2141–2158.
- Hellier, P. R.
2013. *The molecular structure of future fuels*. Thesis.
- Herdman, J. D. and J. H. Miller
2008. Intermolecular potential calculations for polynuclear aromatic hydrocarbon clusters. *The Journal of Physical Chemistry A*, 112(28):6249–6256.
- Herzler, J., M. Fikri, K. Hitzbleck, R. Starke, C. Schulz, P. Roth, and G. T. Kalghatgi
2007. Shock-tube study of the autoignition of n-heptane/toluene/air mixtures at intermediate temperatures and high pressures. *Combustion and Flame*, 149(1–2):25–31.
- Heywood, J. B.
1988. *Internal combustion engine fundamentals*, volume 930. Mcgraw-hill New York.
- Higgins, B. and D. Siebers
2001. Measurement of the flame lift-off location on di diesel sprays using oh chemiluminescence. Report, SAE Technical Paper 2001-01-0918.
- Hilden, D. L. and W. J. Mayer
1984. The contribution of engine oil to particulate exhaust emissions from light-duty, diesel-powered vehicles. Report, SAE Technical Paper 841395.
- Homan, H. S. and W. K. Robbins
1986. A carbon-14 tracer study of the relative fractions of various fuel carbons in soot. *Combustion and Flame*, 63(1–2):177–190.
- Hunt, R. A.
1953. Relation of smoke point to molecular structure. *Industrial & Engineering Chemistry*, 45(3):602–606.
- IARC
2013. Agents classified by the iarc monographs, volumes 1 to 109.

ICCT

2012. http://www.theicct.org/sites/default/files/publications/ICCT_LDVcostsreport_2012.pdf.

Jensen, C. M. and D. W. Lee

2000. Dry-ice bath based on ethylene glycol mixtures. *Journal of Chemical Education*, 77(5):629.

Jess, A.

2010. What might be the energy demand and energy mix to reconcile the world's pursuit of welfare and happiness with the necessity to preserve the integrity of the biosphere? *Energy Policy*, 38(8):4663–4678.

Johnson, M. V., S. S. Goldsborough, Z. Serinyel, P. O'Toole, E. Larkin, G. O'Malley, and H. J. Curran

2009. A shock tube study of n- and iso-propanol ignition. *Energy & Fuels*, 23(12):5886–5898.

Jones, H., G. McTaggart-Cowan, S. Rogak, W. Bushe, S. Munshi, and B. Buchholz

2005. Source apportionment of particulate matter from a diesel pilot-ignited natural gas fuelled heavy duty di engine. Report, SAE Technical Paper 2005-01-2149.

Jouwsma, W.

1993. Marketing and design in flow sensing. *Sensors and Actuators A: Physical*, 37–38(0):274–279.

Kajimoto, T., E. Yamada, M. Shinoda, N. Desmira, K. Kitagawa, and A. K. Gupta

2013. Analysis of flame structure by isotope shift-planar laser induced fluorescence spectrometry of trace oh and od radicals. *Microchemical Journal*, 106(0):334–339.

Kamimoto, T. and M.-h. Bae

1988. High combustion temperature for the reduction of particulate in diesel engines. *SAE Technical Paper 880423*.

Kasper, T., P. Oßwald, U. Struckmeier, K. Kohse-Höinghaus, C. A. Taatjes, J. Wang, T. A. Cool, M. E. Law, A. Morel, and P. R. Westmoreland

2009. Combustion chemistry of the propanol isomers — investigated by electron ionization and vuv-photoionization molecular-beam mass spectrometry. *Combustion and Flame*, 156(6):1181–1201.

Kass, M. D., J. F. Thomas, J. M. Storey, N. Domingo, J. Wade, and G. Kenreck

2001. Emissions from a 5.9 liter diesel engine fueled with ethanol diesel blends. *SAE Technical Paper 2001-01-2018*.

- Katoh, A., K. Kitagawa, and A. K. Gupta
2006a. Examination of methane-hydrogen mixture flame using isotope shift/plif spectroscopy. In *Collection of Technical Papers - 44th AIAA Aerospace Sciences Meeting*, volume 6, Pp. 4407–4413.
- Katoh, A., H. Oyama, K. Kitagawa, and A. K. Gupta
2006b. Visualization of oh radical distribution in a methane-hydrogen mixture flame by isotope shift/planar laser induced fluorescence spectroscopy. *Combustion Science and Technology*, 178(12):2061–2074.
- Katoh, A., M. Shinoda, K. Kitagawa, and A. K. Gupta
2006c. Visualization of steam addition effect on oh distribution in a flame by isotope shift/planar laser-induced fluorescence (is/plif) spectroscopy. *Journal of Engineering for Gas Turbines and Power*, 128(1):8–12.
- Kawanaka, Y., E. Matsumoto, K. Sakamoto, N. Wang, and S.-J. Yun
2004. Size distributions of mutagenic compounds and mutagenicity in atmospheric particulate matter collected with a low-pressure cascade impactor. *Atmospheric Environment*, 38(14):2125–2132.
- Kittelson, D. B.
1998. Engines and nanoparticles: a review. *Journal of Aerosol Science*, 29(5–6):575–588.
- Kittelson, D. B., J. Reinertsen, and J. Michalski
1991. Further studies of electrostatic collection and agglomeration of diesel particles. Report, SAE Technical Paper 910329.
- Knothe, G.
2005. Dependence of biodiesel fuel properties on the structure of fatty acid alkyl esters. *Fuel Processing Technology*, 86(10):1059–1070.
- Koebel, M., M. Elsener, and M. Kleemann
2000. Urea-scr: a promising technique to reduce nox emissions from automotive diesel engines. *Catalysis today*, 59(3):335–345.
- Krouwel, P., W. Groot, N. Kossen, and W. Van der Laan
1983. Continuous isopropanol-butanol-ethanol fermentation by immobilized clostridium beijerinckii cells in a packed bed fermenter. *Enzyme and Microbial Technology*, 5(1):46–54
- Ladommatos, N., P. Rubenstein, and P. Bennett
1996. Some effects of molecular structure of single hydrocarbons on sooting tendency. *Fuel*, 75(2).

- Ladommatos, N., P. Rubenstein, K. Harrison, Z. Xiao, and H. Zhao
1997. The effect of aromatic hydrocarbons on soot formation in laminar diffusion flames and in a diesel engine. *Journal of the Institute of Energy*, 70(484):84–94.
- Lavoie, G. A., J. B. Heywood, and J. C. Keck
1970. Experimental and theoretical study of nitric oxide formation in internal combustion engines. *Combustion Science and Technology*, 1(4):313–326.
- Lea-Langton, A., H. Li, and G. E. Andrews
2008. Comparison of particulate pah emissions for diesel, biodiesel and cooking oil using a heavy duty di diesel engine.
- Lea-Langton, A. R., A. B. Ross, K. D. Bartle, G. E. Andrews, J. M. Jones, H. Li, M. Pourkashanian, and A. Williams
2013. Low temperature pah formation in diesel combustion. *Journal of Analytical and Applied Pyrolysis*, 103(0):119–125.
- Leach, F., R. Stone, and D. Richardson
2013. The influence of fuel properties on particulate number emissions from a direct injection spark ignition engine. Report, SAE Technical Paper 2013-01-1558.
- Li, J., A. Kazakov, and F. L. Dryer
2001. Ethanol pyrolysis experiments in a variable pressure flow reactor. *International Journal of Chemical Kinetics*, 33(12):859–867.
- Li, L. and P. B. Sunderland
2012. An improved method of smoke point normalization. *Combustion Science and Technology*, 184(6):829–841.
- Lieb, D. F. and L. H. S. Roblee Jr
1970. A radioisotopic tracer study of carbon formation in ethanol-air diffusion flames. *Combustion and Flame*, 14(3):285–296.
- Liu, F., H. Guo, G. J. Smallwood, and Ö. L. Gülder
2001. The chemical effects of carbon dioxide as an additive in an ethylene diffusion flame: implications for soot and nox formation. *Combustion and Flame*, 125(1–2):778–787.
- Lombaert, K., L. Le Moyne, J. T. De Maleissye, and J. Amouroux
2006. Experimental study of pah in engine soot by isotopic tracing. *Combustion science and technology*, 178(4):707–728.
- Lü, X., Y. Hou, L. Zu, and Z. Huang
2006. Experimental study on the auto-ignition and combustion characteristics in the homogeneous charge compression ignition (hcci) combustion operation with ethanol/n-heptane blend fuels by port injection. *Fuel*, 85(17–18):2622–2631.

- Lütke-Eversloh, T. and H. Bahl
2011. Metabolic engineering of *clostridium acetobutylicum*: recent advances to improve butanol production. *Current Opinion in Biotechnology*, 22(5):634–647.
- Marr, J., L. Giovane, J. Longwell, J. Howard, and A. Lafleur
1994. Soot and tar production in a jet-stirred/plug-flow reactor system: high and low C_2H_2 concentration environments. *Combustion science and technology*, 101(1-6):301–309 0010–2202.
- Matter, U. and K. Siegmann
1997. The influence of particle filter and fuel additives on turbo diesel engine exhaust. *Journal of Aerosol Science*, 28, Supplement 1(0):S51–S52.
- Matti Maricq, M.
2007. Chemical characterization of particulate emissions from diesel engines: A review. *Journal of Aerosol Science*, 38(11):1079–1118.
- Mayer, W. J., D. C. Lechman, and D. L. Hilden
1980. The contribution of engine oil to diesel exhaust particulate emissions. *SAE Technical Paper 800256*.
- McCormick, R. L., J. D. Ross, and M. S. Graboski
1997. Effect of several oxygenates on regulated emissions from heavy-duty diesel engines. *Environmental Science & Technology*, 31(4):1144–1150.
- Miller, J. A. and C. F. Melius
1992. Kinetic and thermodynamic issues in the formation of aromatic compounds in flames of aliphatic fuels. *Combustion and Flame*, 91(1).
- Miyamoto, N., H. Ogawa, T. Arima, and K. Miyakawa
1996. Improvement of diesel combustion and emissions with addition of various oxygenated agents to diesel fuels. *SAE Technical Paper 962115*.
- Miyamoto, N., H. Ogawa, N. M. Nurun, K. Obata, and T. Arima
1998. Smokeless, low nox, high thermal efficiency, and low noise diesel combustion with oxygenated agents as main fuel. *SAE technical paper 980506*.
- Miyamoto, N., H. Ogawa, M. Shibuya, K. Arai, and O. Esmilaire
1994. Influence of the molecular structure of hydrocarbon fuels on diesel exhaust emissions. *SAE Technical Paper 940676*.
- Mueller, C. J., W. J. Pitz, L. M. Pickett, G. C. Martin, D. L. Siebers, and C. K. Westbrook
2003. *Effects of oxygenates on soot processes in DI diesel engines: Experiments and numerical simulations*, volume 112. New York, NY, ETATS-UNIS: Society of Automotive Engineers.

- Nakakita, K., S. Takasu, H. Ban, T. Ogawa, H. Naruse, Y. Tsukasaki, and L. I. Yeh
1998. Effect of hydrocarbon molecular structure on diesel exhaust emissions part 1: Comparison of combustion and exhaust emission characteristics among representative diesel fuels. *SAE Technical Paper 982494*.
- Neeft, J. P. A., M. Makkee, and J. A. Moulijn
1996. Diesel particulate emission control. *Fuel Processing Technology*, 47(1):1–69.
- Neoh, K. G., J. B. Howard, and A. F. Sarofim
1985. Effect of oxidation on the physical structure of soot. *Symposium (International) on Combustion*, 20(1):951–957.
- Nier, A. O.
1947. A mass spectrometer for isotope and gas analysis. *Review of Scientific Instruments*, 18(6):398–411.
- Nigam, P. S. and A. Singh
2011. Production of liquid biofuels from renewable resources. *Progress in Energy and Combustion Science*, 37(1):52–68.
- Nikula, K., M. Snipes, E. Barr, W. Griffith, R. Henderson, and J. Mauderly
1995. Comparative pulmonary toxicities and carcinogenicities of chronically inhaled diesel exhaust and carbon black in F344 rats. *Toxicological Sciences*, 25(1):80–94
- Nisbet, I., C. LaGoy, and P. K.
1992. Toxic equivalency factors (TEFs) for polycyclic aromatic hydrocarbons (PAHs). *Regulatory Toxicology and Pharmacology*, 16(3).
- Noorani, K. E., B. Akih-Kumgeh, and J. M. Bergthorson
2010a. Comparative high temperature shock tube ignition of C1-C4 primary alcohols. *Energy & Fuels*, 24(11):5834–5843.
- Noorani, K. E., B. Akih-Kumgeh, and J. M. Bergthorson
2010b. Comparative high temperature shock tube ignition of C1-C4 primary alcohols. *Energy & Fuels*, 24(11):5834–5843.
- Norton, T. S. and F. L. Dryer
1990. The flow reactor oxidation of C1–C4 alcohols and MTBE. In *Symposium (International) on Combustion*, volume 23, Pp. 179–185. Elsevier.
- Oberdörster, G., J. Finkelstein, C. Johnston, R. Gelein, C. Cox, R. Baggs, and A. Elder
2000. Acute pulmonary effects of ultrafine particles in rats and mice. *Research report (Health Effects Institute)*, (96):5–74; disc. 75–86.
- Oberdörster, G., Z. Sharp, V. Atudorei, A. Elder, R. Gelein, W. Kreyling, and C. Cox
2004. Translocation of inhaled ultrafine particles to the brain. *Inhalation Toxicology*, 16(6-7):437–445.

- Oehlschlaeger, M. A., D. F. Davidson, and R. K. Hanson
2004. High-temperature thermal decomposition of isobutane and n-butane behind shock waves. *The Journal of Physical Chemistry A*, 108(19):4247–4253.
- Oßwald, P., K. Kohse-Höinghaus, U. Struckmeier, T. Zeuch, L. Seidel, L. Leon, and F. Mauss
2011. Combustion chemistry of the butane isomers in premixed low-pressure flames.
- Peg, M., M. Ruiz, A. Millera, R. Bilbao, and M. U. Alzueta
2007. Ethanol pyrolysis and formation of soot. *THIRD EUROPEAN COMBUSTION MEETING ECM*.
- Pepiot-Desjardins, P., H. Pitsch, R. Malhotra, S. R. Kirby, and A. L. Boehman
2008. Structural group analysis for soot reduction tendency of oxygenated fuels. *Combustion and Flame*, 154(1–2):191–205.
- Pitz, W. J. and C. J. Mueller
2011. Recent progress in the development of diesel surrogate fuels. *Progress in Energy and Combustion Science*, 37(3):330–350.
- Pope, C. A., M. J. Thun, M. M. Namboodiri, D. W. Dockery, J. S. Evans, F. E. Speizer, and C. W. Heath
1995. Particulate air pollution as a predictor of mortality in a prospective study of u.s. adults. *American Journal of Respiratory and Critical Care Medicine*, 151(3):669–674.
- Purdy, R.
1986. High oleic sunflower: Physical and chemical characteristics. *Journal of the American Oil Chemists' Society*, 63(8):1062–1066.
- Radiocarbon
2014. List of known ¹⁴C laboratories. <http://www.radiocarbon.org/Info/Labs.pdf>.
- Richter, H. and J. Howard
2000. Formation of polycyclic aromatic hydrocarbons and their growth to soot—a review of chemical reaction pathways. *Progress in Energy and Combustion Science*, 26(4–6).
- Roesler, J., S. Martinot, C. McEnally, L. Pfefferle, J. Delfau, and C. Vovelle
2003. Investigating the role of methane on the growth of aromatic hydrocarbons and soot in fundamental combustion processes. *Combustion and Flame*, 134(3).
- Roesler, J. F.
1998. An experimental and two-dimensional modeling investigation of combustion chemistry in a laminar non-plug-flow reactor. *Symposium (International) on Combustion*, 27(1):287–293.

- Roesler, J. F. and M. A. De Tissan
2000. Aromatics and soot growth enhancement by methane addition to fuel-rich n-heptane combustion in a flow reactor. *Combustion Science and Technology*, 161(1):245–268.
- Rogers, G., G. Rogers, and Y. Mayhew
1992. *Engineering Thermodynamics: Work and Heat Transfer*. Longman Scientific & Technical.
- Rosillo-Calle, F. and A. Walter
2006. Global market for bioethanol: historical trends and future prospects. *Energy for Sustainable Development*, 10(1):20–32.
- Ruiz, M., A. Callejas, A. Millera, M. Alzueta, and R. Bilbao
2007a. Soot formation from c2h2 and c2h4 pyrolysis at different temperatures. *Journal of Analytical and Applied Pyrolysis*, 79(1–2).
- Ruiz, M., R. de Villoria, A. Millera, M. Alzueta, and R. Bilbao
2007b. Influence of the temperature on the properties of the soot formed from c2h2 pyrolysis. *Chemical Engineering Journal*, 127(1–3).
- Ruiz, M., R. Guzmán de Villoria, Á. Millera, M. U. Alzueta, and R. Bilbao
2007c. Influence of different operation conditions on soot formation from c2h2 pyrolysis. *Industrial & Engineering Chemistry Research*, 46(23).
- Sánchez, N., A. Callejas, A. Millera, R. Bilbao, and M. Alzueta
2010. Determination of polycyclic aromatic hydrocarbons (pah) adsorbed on soot formed in pyrolysis of acetylene at different temperatures. *Chemical Engineering Transactions*, 22.
- Sánchez, N. E., A. Callejas, A. Millera, R. Bilbao, and M. U. Alzueta
2012a. Formation of pah and soot during acetylene pyrolysis at different gas residence times and reaction temperatures. *Energy*, 43(1):30–36.
- Sánchez, N. E., A. Callejas, Á. Millera, R. Bilbao, and M. U. Alzueta
2012b. Polycyclic aromatic hydrocarbon (pah) and soot formation in the pyrolysis of acetylene and ethylene: Effect of the reaction temperature. *Energy & Fuels*, 26(8):4823–4829.
- Sánchez, N. E., J. Salafranca, A. Callejas, Á. Millera, R. Bilbao, and M. U. Alzueta
2013. Quantification of polycyclic aromatic hydrocarbons (pahs) found in gas and particle phases from pyrolytic processes using gas chromatography–mass spectrometry (gc–ms). *Fuel*, 107:246–253.
- Sang, O. Y.
2003. Biofuel production from catalytic cracking of palm oil. *Energy Sources*, 25(9):859–869.

- Santrock, J. and J. M. Hayes
1987. Adaptation of the unterzaucher procedure for determination of oxygen-18 in organic substances. *Analytical Chemistry*, 59(1):119–127.
- Sarathy, S. M., P. Oßwald, N. Hansen, and K. Kohse-Höinghaus
2014. Alcohol combustion chemistry. *Progress in Energy and Combustion Science*, 44(0):40–102.
- Schaus, J., P. McPartlin, R. Cole, R. Poola, and R. Sekar
2000. Effect of ethanol fuel additive on diesel emissions. Technical report, Argonne National Laboratory for Illinois Department of Commerce.
- Schmieder, R. W.
1985. Radiotracer studies of soot formation in diffusion flames. *Symposium (International) on Combustion*, 20(1):1025–1033.
- Schönborn, A.
2009. Influence of the molecular structure of biofuels on combustion in a compression ignition engine. *Mechanical Engineering*, PhD.
- Schönborn, A., N. Ladommatos, J. Williams, R. Allan, and J. Rogerson
2009a. The influence of molecular structure of fatty acid monoalkyl esters on diesel combustion. *Combustion and Flame*, 156(7):1396–1412.
- Schönborn, A., N. Ladommatos, J. Williams, R. Allan, and J. Rogerson
2009b. The influence of molecular structure of fatty acid monoalkyl esters on diesel combustion. *Combustion and Flame*, 156(7):1396–1412.
- Shafiee, S. and E. Topal
2009. When will fossil fuel reserves be diminished? *Energy Policy*, 37(1):181–189.
- Shukla, B. and M. Koshi
2010. A highly efficient growth mechanism of polycyclic aromatic hydrocarbons. *Physical Chemistry Chemical Physics*, 12(10):2427–2437.
- Shukla, B. and M. Koshi
2011. Comparative study on the growth mechanisms of pahs. *Combustion and Flame*, 158(2):369–375.
- Shukla, B., A. Miyoshi, and M. Koshi
2010. Role of methyl radicals in the growth of pahs. *Journal of the American Society for Mass Spectrometry*, 21(4):534–544.
- Siebers, D. and B. Higgins
2001. Flame lift-off on direct-injection diesel sprays under quiescent conditions. *SAE Technical Paper 2001-01-0530*.

Simon, G.

1986. Diesel fuel comprising cerium and manganese additives for improved trap regenerability.

Sirignano, W. A.

1983. Fuel droplet vaporization and spray combustion theory. *Progress in Energy and Combustion Science*, 9(4):291–322.

Sison, K., N. Ladommatos, H. Song, and H. Zhao

2007. Soot generation of diesel fuels with substantial amounts of oxygen-bearing compounds added. *Fuel*, 86(3):345–352.

Skjøth-Rasmussen, M. S., P. Glarborg, M. Østberg, J. T. Johannessen, H. Livbjerg, A. D. Jensen, and T. S. Christensen

2004. Formation of polycyclic aromatic hydrocarbons and soot in fuel-rich oxidation of methane in a laminar flow reactor. *Combustion and Flame*, 136(1–2):91–128.

Soloiu, V., J. Weaver, H. Ochieng, M. Duggan, S. Davoud, B. Vlcek, C. Jenkins, and C. Butts

2013. Experimental study of combustion and emissions characteristics of methyl oleate, as a surrogate for biodiesel, in a direct injection diesel engine. *SAE Technical Paper 2013-01-1142*.

Song, J., M. Alam, A. Boehman, and U. Kim

2006. Examination of the oxidation behavior of biodiesel soot. *Combustion and Flame*, 146(4):589–604.

Song, K. H., Y. Lee, and T. A. Litzinger

2000. Effects of emulsified fuels on soot evolution in an optically-accessible diesel engine. *SAE Technical Paper 2000-01-2794*.

Sorek, H. and J. E. Anderson

1986. C14 study of relative fuel-to-soot carbon conversion in premixed flames. *Combustion Science and Technology*, 49(3-4):201–204.

Sorek, H., J. E. Anderson, W. O. Siegl, and K. Otto

1984. Radioisotopic study of methanol-to-soot conversion in methanol-hydrocarbon diffusion flames. *Combustion Science and Technology*, 41(3-4):203–209.

Stein, S. E. and A. Fahr

1985. High-temperature stabilities of hydrocarbons. *The Journal of Physical Chemistry*, 89(17):3714–3725.

Symonds, J. P., K. S. J. Reavell, J. S. Olfert, B. W. Campbell, and S. J. Swift

2007. Diesel soot mass calculation in real-time with a differential mobility spectrometer. *Journal of Aerosol Science*, 38(1):52–68.

- Takatori, Y., Y. Mandokoro, K. Akihama, K. Nakakita, Y. Tsukasaki, S. Iguchi, L. I. Yeh, and A. M. Dean
1998. Effect of hydrocarbon molecular structure on diesel exhaust emissions part 2: effect of branched and ring structures of paraffins on benzene and soot formation. *SAE Technical Paper 890421*.
- Tancell, P. J., M. M. Rhead, R. D. Pemberton, and J. Braven
1995. Survival of polycyclic aromatic hydrocarbons during diesel combustion. *Environmental Science & Technology*, 29(11):2871–2876.
- Togbé, C., A. Mzé-Ahmed, and P. Dagaut
2010. Kinetics of oxidation of 2-butanol and isobutanol in a jet-stirred reactor: Experimental study and modeling investigation. *Energy & Fuels*, 24(9):5244–5256.
- Tree, D. R. and K. I. Svensson
2007. Soot processes in compression ignition engines. *Progress in Energy and Combustion Science*, 33(3).
- Tsurutani, K., Y. Takei, Y. Fujimoto, J. Matsudaira, and M. Kumamoto
1995. The effects of fuel properties and oxygenates on diesel exhaust emissions. *SAE Technical Paper 952349*.
- Vandooren, J., L. Thill, M. Musick, and P. Van Tiggelen
1998. Depletion of soot precursors by co2 addition to rich hydrocarbon flames. In *20th Task Leaders Meeting of the IEA implementing agreement “Energy Conservation and Emission Reduction in Combustion*, Pp. 118–137.
- Veloo, P. S. and F. N. Egolfopoulos
2011. Studies of n-propanol, iso-propanol, and propane flames. *Combustion and Flame*, 158(3):501–510.
- Vogel, C. F. A., E. Sciallo, P. Wong, P. Kuzmicky, N. Kado, and F. Matsumura
2005. Induction of proinflammatory cytokines and c-reactive protein in human macrophage cell line u937 exposed to air pollution particulates. *Environmental health perspectives*, Pp. 1536–1541.
- Wang, F. C.-Y., K. Qian, and L. A. Green
2005. Gcms of diesel: A two-dimensional separation approach. *Analytical Chemistry*, 77(9):2777–2785.
- Wang, H.
2011. Formation of nascent soot and other condensed-phase materials in flames. *Proceedings of the Combustion Institute*, 33(1):41–67.
- Wang, Y., A. Raj, and S. H. Chung
2013. A pah growth mechanism and synergistic effect on pah formation in counterflow diffusion flames. *Combustion and Flame*, 160(9):1667–1676.

- Watson, R. J., M. L. Botero, C. J. Ness, N. M. Morgan, and M. Kraft
2013. An improved methodology for determining threshold sooting indices from smoke point lamps. *Fuel*, 111(0):120–130.
- Westbrook, C. K., W. J. Pitz, and H. J. Curran
2006. Chemical kinetic modeling study of the effects of oxygenated hydrocarbons on soot emissions from diesel engines. *The Journal of Physical Chemistry A*, 110(21):6912–6922.
- Williams, P. T., K. D. Bartle, and G. E. Andrews
1986. The relation between polycyclic aromatic compounds in diesel fuels and exhaust particulates. *Fuel*, 65(8):1150–1158.
- Yang, Y., A. L. Boehman, and R. J. Santoro
2007. A study of jet fuel sooting tendency using the threshold sooting index (tsi) model. *Combustion and Flame*, 149(1–2):191–205.
- Yasunaga, K., T. Mikajiri, S. M. Sarathy, T. Koike, F. Gillespie, T. Nagy, J. M. Simmie, and H. J. Curran
2012. A shock tube and chemical kinetic modeling study of the pyrolysis and oxidation of butanols. *Combustion and Flame*, 159(6):2009–2027.
- Yoon, S. S., D. H. Anh, and S. H. Chung
2008. Synergistic effect of mixing dimethyl ether with methane, ethane, propane, and ethylene fuels on polycyclic aromatic hydrocarbon and soot formation. *Combustion and Flame*, 154(3):368–377.
- Zang, L.-Y., K. Stone, and W. A. Pryor
1995. Detection of free radicals in aqueous extracts of cigarette tar by electron spin resonance. *Free Radical Biology and Medicine*, 19(2):161–167.
- Zecca, A. and L. Chiari
2010. Fossil-fuel constraints on global warming. *Energy Policy*, 38(1):1–3.
- Zhang, J., Y. Nazarenko, L. Zhang, L. Calderon, K.-B. Lee, E. Garfunkel, S. Schwander, T. D. Tetley, K. F. Chung, A. E. Porter, M. Ryan, H. Kipen, P. J. Liroy, and G. Mainelis
2013a. Impacts of a nanosized ceria additive on diesel engine emissions of particulate and gaseous pollutants. *Environmental Science & Technology*, 47(22):13077–13085.
- Zhang, Y., S. Tao, H. Shen, and J. Ma
2009. Inhalation exposure to ambient polycyclic aromatic hydrocarbons and lung cancer risk of chinese population. *Proceedings of the National Academy of Sciences*, 106(50):21063–21067.
- Zhang, Y., W. Yuan, J. Cai, L. Zhang, F. Qi, and Y. Li
2013b. Product identification and mass spectrometric analysis of nbutane and ibutane pyrolysis at low pressure. *Chinese Journal of Chemical Physics*, 26(2):151–156.

- Zielinska, B., J. Sagebiel, J. D. McDonald, K. Whitney, and D. R. Lawson
2004. Emission rates and comparative chemical composition from selected in-use diesel and gasoline-fueled vehicles. *Journal of the Air & Waste Management Association*, 54(9):1138–1150.